

Glass Panel under Shear Loading - Use of Glass Envelopes in Building Stabilization

THÈSE N° 4185 (2008)

PRÉSENTÉE LE 24 MARS 2008

À LA FACULTE ENVIRONNEMENT NATUREL, ARCHITECTURAL ET CONSTRUIT
LABORATOIRE DE LA CONSTRUCTION MÉTALLIQUE
PROGRAMME DOCTORAL EN STRUCTURES

ÉCOLE POLYTECHNIQUE FÉDÉRALE DE LAUSANNE

POUR L'OBTENTION DU GRADE DE DOCTEUR ÈS SCIENCES

PAR

Danijel MOCIBOB

M.Sc. in computational engineering, Ruhr-Universität Bochum, Allemagne
et de nationalité croate

acceptée sur proposition du jury:

Prof. Y. Weinand, président du jury
Prof. J.-P. Lebet, directeur de thèse
Prof. J. Belis, rapporteur
Prof. P. Cruz, rapporteur
Prof. I. Devanthéry-Lamunière, rapporteur



ÉCOLE POLYTECHNIQUE
FÉDÉRALE DE LAUSANNE

Suisse
2008

Abstract

The latest trends in contemporary architecture are fully transparent pavilions: a single storey building free of any steel or concrete frame, where glass panels are used as unique vertical structural elements to support the roof and as wind bracing to stabilize and stiffen the building. In this application, individual glass panel is supported on two sides (roof and foundation) and subjected to in-plane shear force (lateral wind), out-of-plane distributed load (perpendicular wind) and in-plane compression force (self weight of the roof, snow). While several studies on glass plate behaviour under distributed load and column buckling exist, shear buckling of two sides supported glass panel has not been investigated yet. Therefore, research on this topic gives original and innovative importance to both theoretical (glass panel under shear loading) and practical (use of glass envelope for building stabilization) applications.

Two structural concepts are developed:

- **point support concept** - the glass panel is attached to the substructure by bolted connections at corners
- **linear support concept** - the glass panel is glued to the substructure by two shorter sides.

The local behaviour of the connection devices and the global behaviour of the glass panel under in-plane shear force are studied by means of experimental investigations, numerical modelling and parametric analyses.

Experimental investigation and numerical simulation of connection devices was conducted in order to better understand the behaviour of different types of glass/substructure bolted (for point support) and glued (for linear support) connections. Deformation, stress distribution and local influence on the surrounding glass were analyzed. From these studies, the most suitable connection device for load introduction was chosen and implemented in the glass panel.

Tests on full size glass panels were conducted in order to estimate the shear buckling behaviour of a glass panel. Also the influence of different boundary conditions (point and linear) and load interaction (in-plane shear force with out-of-plane distributed load and in-plane compression force) on global glass panel behaviour were analyzed. The specimen deformation, the stress distribution and the failure mode have been analyzed.

Advanced numerical models of point and linear supported glass panel were implemented using the Finite Element Code Ansys. Elastic buckling analysis was used to determine the critical shear buckling force, shear buckling coefficient and shear buckling mode shape, further used as the initial geometrical imperfection. By means of nonlinear buckling analyses the global glass panel behaviour was studied analysing glass panel deformations, stresses distribution and support reactions. The influence of initial imperfection shape was investigated as well as the interaction of in-plane shear force with out-of-plane distributed load and in-plane compression force. The models were validated by comparing their results with experimental measurements.

The parametric study was carried out to identify the most important parameters, evaluating their influence on shear buckling behaviour. The influence of the glass panel and connection device geometrical/material properties on critical shear force, global deformation, stress distribution and support reaction could be determined.

A simple method for preliminary design of glass panels subjected to in-plane shear force was proposed by developing formulas, graphs and curves for determining the glass panel shear buckling resistance. Finally, this study led to some recommendations for practical use of glass panels in fully-transparent pavilions as structural elements.

Keywords: Fully transparent pavilions, structural glass, glass panel, point support, linear support, shear buckling, in-plane shear force, critical shear buckling force, elastic buckling analyses, non linear buckling analyses

Résumé

Ces dernières années, l'architecture contemporaine s'est orientée vers la conception de pavillons en verre entièrement transparents. Il s'agit de structures à un étage, sans système porteur en acier ou en béton, seuls des panneaux de verre permettent de reprendre les charges verticales de toiture et servent de contreventement afin d'assurer la stabilité et la rigidité de la structure. Ce travail de thèse porte sur l'étude de ces panneaux de verre, appuyés sur deux côtés (en toiture et au niveau des fondations) soumis à différents types de sollicitations: cisaillement dans le plan (vent latéral), charge répartie sur la surface du verre (vent perpendiculaire) et compression dans le plan (poids propre de toiture, neige). Bien que plusieurs recherches se soient penchées sur l'étude du comportement de panneaux de verre soumis à des charges réparties ainsi que sur l'étude de leur stabilité, aucune d'entre elles n'avait jusqu'alors abordé l'étude du voilement par cisaillement de panneaux appuyés sur deux côtés. En effet, ce domaine de recherche présente un intérêt novateur et original aussi bien du point de vue théorique (panneau de verre sous charge de cisaillement) que pratique (utilisation de façades vitrées comme éléments de stabilisation).

Deux types de conceptions structurales ont été développés dans cette thèse :

- **la conception avec appuis ponctuels** - le panneau de verre est fixé à la sous-structure au moyen d'assemblages boulonnés dans les angles,
- **la conception avec appuis linéaires** - le panneau de verre est collé à la sous-structure sur deux côtés.

Le comportement local de la connexion et le comportement global du panneau de verre cisailé dans son plan ont été étudiés au moyen d'investigations expérimentales, de modèles numériques et d'analyses paramétriques.

L'investigation expérimentale et les simulations numériques des moyens d'assemblage ont été effectuées afin de comprendre le comportement des différents types d'assemblages boulonnés (appui ponctuel) ou d'assemblages collés (appui linéaire). Les déformations, la distribution des contraintes et l'influence locale sur le verre ont été analysées. A partir de ces considérations, on a pu déterminer le moyen d'assemblage le mieux adapté à l'introduction des forces afin de l'expérimenter sur des panneaux de verre.

Des essais sur des panneaux en vraie grandeur ont été effectués afin d'estimer le comportement du verre soumis au voilement par cisaillement. L'influence de différentes conditions de bord (appuis ponctuels ou linéaires) et l'interaction de différents types de chargement (cisaillement dans le plan combiné à une charge répartie perpendiculaire ainsi qu'à une force de compression dans le plan) ont alors été analysés sur ces panneaux. Les déplacements, la distribution des contraintes et le mode de rupture ont été examinés en particulier.

Les modélisations numériques des panneaux de verre ont été réalisées au moyen du logiciel Eléments Finis ANSYS. L'analyse du voilement élastique a permis de déterminer la charge critique de voilement en cisaillement, le coefficient de voilement en cisaillement et le mode de voilement en cisaillement. La déformation sous ce mode a été introduite par la suite comme imperfection géométrique initiale. Puis, grâce à des analyses non linéaires de voilement, le comportement global du panneau a pu être étudié (déplacements, distribution des contraintes et réactions d'appui). L'influence de la forme des imperfections initiales ainsi que l'interaction des types de chargement décrits ci-dessus ont été recherchés. Le modèle numérique a finalement été validé par comparaison avec les mesures expérimentales.

Une étude paramétrique a alors été menée afin de mettre en évidence les paramètres déterminants et d'évaluer leur influence sur le voilement en cisaillement. L'influence du type de panneau de verre ainsi que l'influence de la géométrie et du matériau des moyens d'assemblage sur la charge critique de voilement en cisaillement, sur la déformation globale, sur la distribution des contraintes et sur les réactions d'appui, a également pu être déterminée.

Sur cette base, une méthode simplifiée de prédimensionnement de panneaux de verre, soumis au cisaillement dans leur plan, a été proposée. Cette méthode, se présentant sous la forme de formules, de graphiques et de courbes, permet de déterminer la résistance au voilement de ces panneaux. Finalement, cette étude propose certaines recommandations à l'usage des ingénieurs praticiens pour la conception des pavillons entièrement vitrés, dont le vitrage pourra servir de structure porteuse.

Mots-clés: pavillons entièrement transparents, verre structural, panneaux de verre, appui ponctuel, appui linéaire, voilement en cisaillement, cisaillement dans le plan, charge critique de voilement (en cisaillement), analyse du voilement élastique, analyses non linéaires de voilement.

Zusammenfassung

Die neuesten Trends in der zeitgenössischen Architektur sind vollständig transparent Pavillons: ein einstöckiges Gebäude frei von Stahl- oder Betonrahmen, in dem alleinig Glasscheiben für den vertikalen Lastabtrag der Dachlasten, für die Aufnahme der Windlasten und zur Aussteifung berücksichtigt werden. Die einzelne Glasscheibe wird hierbei zweiseitig gelagert (Dach und Fundament) und in drei Richtungen belastet: infolge Flächenlasten senkrecht zur Scheibe durch frontalen Wind, infolge Schub in der horizontalen Scheibenebene durch seitlichen Wind, und infolge Druckkräfte in der vertikalen Scheibenebene durch das Eigengewicht des Daches und Schnee. Während einige Untersuchungen von Glasscheiben unter Flächenlasten und Knicken bestehen, wurde das Schubknickverhalten von zweiseitig gelagerten Platten bisher nicht untersucht. Daher ist die Forschung von diesem Thema von origineller und innovativer Bedeutung bezüglich theoretischer (Glasscheiben unter Schubbelastungen) und praktischer Anwendung (Verwendung von Glasscheiben als tragende Gebäudehülle).

Zwei Lagerungskonzepte werden entwickelt:

Deux types de conceptions structurales ont été développés dans cette thèse :

- **Punktuelle Lagerung** - die Glasscheibe wird durch Schraubenverbindung an den Ecken am Dach und in den Fundamenten befestigt
- **Linienförmige Lagerung** - die Glasscheibe wird linienförmig an das Dach und in die Fundamente geklebt

Das lokale Verhalten der Befestigungsanschlüsse und das globale Verhalten der Glasscheibe unter Schubkräften in Scheibenebene werden experimentell und mit Hilfe von numerische Modellierung und Parameterstudien untersucht.

Experimentelle Untersuchung und numerische Simulation der Befestigungsanschlüsse wurden durchgeführt, um besser das Verhalten unterschiedlicher Lagerungskonzepte zu verstehen (punktuelle Schraubverbindungen und linienförmige Klebeverbindung). Verformungen, Spannungsverteilungen und lokaler Einfluss auf das Glas im Verbindungsbereich wurden analysiert. Der bestgeeignetes Befestigungsanschluss wurde schliesslich gewählt und für die weiteren Untersuchungen an den Glasscheiben verwendet.

Tests an Glasscheiben in Originalgrösse wurden durchgeführt, um das Schubknickverhalten der Glasscheiben zu bestimmen. Auch der Einfluss der verschiedenen Lagerungskonzepte (punktuell und linear) und die Interaktion der Lasteinwirkungen (Flächenlasten senkrecht zur Scheibe, Schub in horizontalen Scheibenebene, Druckkräfte in vertikalen Scheibenebene) auf das globale Tragverhalten der Glasscheibe wurde analysiert. Verformungen, Spannungsverteilungen und der Versagensmodus wurden analysiert.

Numerische Modelle von punktueller und linienförmiger Lagerung wurden mit Hilfe des Finite Elemente Programmes Ansys implementiert. Elastische Knickanalysen wurden verwendet, um die kritische Knickkraft, den Knickkoeffizienten und den Knickmodus zu bestimmen, im Weiteren als die anfängliche geometrische Imperfektion verwendet. Das Verhalten der Glasscheibe, Glasverformungen, Spannungsverteilungen und Auflagerreaktionen wurden mit Hilfe nichtlinearen Knickanalysen analysiert. Der Einfluss der Imperfektion wurde untersucht, sowie die Interaktion von Flächenlasten senkrecht zur Scheibe und Druckkräfte in vertikalen Scheibenebene. Die Modelle wurden anhand der experimentellen Messergebnisse validiert.

Parameterstudien wurden durchgeführt um die massgeblichen Einflussparameter für das Schubknicken zu bestimmen. Der Einfluss der Geometrie und die Materialeigenschaften der Glasscheiben und der Verbindungsmittel auf die kritische Schublast, die globale Verformung, die Spannungsverteilung und die Auflagerreaktionen wurde ermittelt.

Eine einfache Methode zum Design von Glasscheiben unter Schub in Scheibenebene wurde vorgestellt; sie beinhaltet Formeln, Grafiken und Kurven zur Bestimmung der Schubknicklast. Diese Studie ermöglichte die Formulierung von Empfehlungen für die praktische Anwendung von Glasscheiben an volltransparenten Pavillons als tragende Gebäudehülle.

Schlagwörter: Volltransparente Pavillons, Glas als tragendes Element, Glasscheiben, punktuelle Lagerung, linienförmige Lagerung, Schubknicken, Schubkräfte in Scheibenebene, kritische Schubknicklast, elastische Knickanalyse, nichtlineare Knickanalyse.

ACKNOWLEDGEMENTS

Over the past four years I have received support and encouragement from many people, professionally and personally. Here, I would like to acknowledge them.

To begin with, I would like to express my gratitude to Prof. Dr. Manfred A. Hirt who provides me with the opportunity to do my doctoral studies in the Steel Structures Laboratory (ICOM) of the Swiss Federal Institute of Technology in Lausanne (EPFL). I am deeply grateful to Mr. Michel Crisinel, the scientific supervisor of my thesis, for his continuous support and excellent guidance during my research, for being patient with me, and for his humour and good mood. He helped me not only to discover the structural use of glass, but also to discover the Swiss culture, tradition, language, songs and food. It was a great pleasure to work and spend time together. More than a supervisor, he and his family became my unforgettable friends. I would like to thank Prof. Dr. Jean-Paul Lebet, the director of my thesis, and Prof. Dr. Alain Nussbaumer for their advices and useful comments.

I would like to thank the Swiss National Science Foundation for funding this project, and furthermore Félix Construction SA, SADEV Architectural Glass Systems, Hilti (Suisse) SA, Pilkington (Suisse) SA, Verres Industriels SA Moutier and Glass Trösch AG for their generous donations of the experimental materials and the fabrication of my test specimens.

I would like to express my gratitude to the members of the advisory committee who followed my work and gave constructive suggestion for my thesis: Dr. Rudolph Hess, Dr. Andreas Luible, Rodolphe Luscher and Urs Kern. Thanks to the members of my thesis jury whose comments I have gratefully appreciated: Prof. Dr. Yves Weinand (chairman), Prof. Dr. Inès Lamunière, Prof. Dr. Jean-Paul Lebet, Prof. Dr. Jan Belis and Prof. Dr. Paulo Cruz. Also thanks to the people whose ideas and advices help me significantly: Dr. Mauro Overend, Dr. Matthias Haldimann, Mr. Philippe Paraire, Mrs. Claire Fleury and Mr. Cédric Zürcher.

I would like to thank all the members of ICOM over the past four years. Particularly, I would like to thank my two officemates: Dr. Michel Thomann, helping me to adopt in Swiss lifestyle by giving me useful advices on research, sport and entertainment; and Dr. Luis Borges who was always there when I needed him (from serious discussions up to celebrations). Thanks to Mrs. Esther von Arx for helping me with the administrative work and Mr. Claudio Leonardi for the help with graphics and design. I would like to also thank also other members of ICOM for their good company and support: Tamar, Laurence, Claire, Rahel, Thierry, Dimitrios, Thomas, Scott. The experimental investigations were accomplished with the dedicated assistance of the following technicians, to whom I am extremely grateful: Sylvain Demierre, Gilles Guignet, Francois Perrin, Roland Gysler, Hansjakob Reist, Patrice Gallay and Gérald Rouge. Thanks for the help that I received from the student assistants Hugues, Odile and Claudia.

I want to acknowledge the encouragement and help of Prof. Dr. Mehmed Čaušević from the University of Rijeka who filled me with the optimism and enthusiasm to pursue my Doctoral degree.

Many thanks to all the friends, with whom I spent a good part of the last few years in Switzerland: Mario, Bernard, Marko, Erika, Dragan, Ana V., Goran, Danko, Ana R., Zorica, Branka, Andrea, Neven, Anamarija, Irena, Igor, Federica, Juan, Kristijan, Evgeny, Maxim, Gianluca, Vesna, Milica, Paolo, Marcelo, colleagues from Basketball Club de Morges and Chanson de Morrens. A special thanks to many friends from Croatia, who even from far, supported me on a daily basis: Jasmin, Gordana, Aleksandar, Alen, Davor, Vlasta, Emi, Oliver, Kristijan, Ines, Eugen, Hrvoje, Ivan, Albert, Vedran and Krešimir, as well as friends from Bochum: Mark, Hrvoje, Tanja, Milica, Ksenija, Rusmir, Nataša, Wisdom and Babu.

During these years, my family gave me tremendous support that was crucial for keeping me going forward at each and every moment. To my mother Ružica, father Milovan and sister Gabrijela I am eternally grateful for your unconditional encouragement, affection and love.

CONTENTS

ABSTRACT	I
AKNOWLEDGMENTS	VII
CONTENTS	IX
NOMENCLATURE	XIII
1 INTRODUCTION	1
1.1 BACKGROUND AND MOTIVATION	1
1.2 OBJECTIVES	3
1.3 ORGANISATION OF THE THESIS	3
2 LITERATURE REVIEW	5
2.1 INTRODUCTION	5
2.2 MECHANICAL OVERVIEW OF STRUCTURAL GLASS	6
2.2.1 Glass in buildings	6
2.2.2 Glass panel under in-plane force	10
2.2.3 Connection devices	12
2.3 ARCHITECTURAL OVERVIEW ON STRUCTURAL GLASS	14
2.3.1 Glass in building	14
2.3.2 Glass pavilions	16
2.3.3 Fully-transparent glass pavilions	18
2.4 CONCLUSION	23
3 STRUCTURAL CONCEPTS	25
3.1 INTRODUCTION	25
3.2 BUILDING STABILIZATION	26
3.2.1 Actions on glass panel	27
3.3 POINT SUPPORTED CONCEPT	28
3.3.1 Standard point supported glass panel	28
3.3.2 Boundary conditions and actions on point supported glass panel	29
3.4 LINEAR SUPPORTED CONCEPT	30
3.4.1 Standard linear supported glass panel	30
3.4.2 Boundary conditions and actions on linear supported glass panels	31
3.5 SUMMARY AND CONCLUSIONS	32

4	EXPERIMENTAL INVESTIGATION	33
4.1	INTRODUCTION	33
4.2	POINT SUPPORTED CONNECTION TESTS.....	34
4.2.1	Specimen description.....	34
4.2.2	Test set-up and test instrumentation	37
4.2.3	Test results	38
4.3	POINT SUPPORTED PANEL TEST	43
4.3.1	Specimen description.....	43
4.3.2	Testing frame and load introduction devices	44
4.3.3	Test set-up.....	45
4.3.4	Test instrumentation	46
4.3.5	Test results	47
4.4	LINEAR SUPPORT CONNECTION TEST	50
4.4.1	Specimen description.....	50
4.4.2	Test set-up and test instrumentation	52
4.4.3	Test results	52
4.5	LINEAR SUPPORTED PANEL TEST	55
4.5.1	Specimen description.....	55
4.5.2	Testing frame and load introduction devices	56
4.5.3	Test set-up.....	56
4.5.4	Test instrumentation	56
4.5.5	Test results	57
4.6	SUMMARY AND CONCLUSIONS	61
5	MODELLING	63
5.1	INTRODUCTION	63
5.2	POINT SUPPORTED CONNECTION MODEL	64
5.2.1	Analytical bases and existing solution.....	64
5.2.2	Numerical model	67
5.2.3	Validation of the point supported connection model.....	72
5.3	POINT SUPPORTED PANEL MODEL	74
5.3.1	Point support structural model.....	74
5.3.2	Analytical bases and existing solution.....	75
5.3.3	Numerical modelling	80
5.3.4	Validation of the point supported glass panel model.....	88
5.4	LINEAR SUPPORTED CONNECTION MODEL	90
5.4.1	Analytical bases	90
5.4.2	Numerical modelling	93
5.4.3	Validation of the linear supported connection model	95
5.5	LINEAR SUPPORTED GLASS PANEL MODEL.....	96
5.5.1	Linear support structural model.....	96
5.5.2	Analytical bases and existing solutions	97
5.5.3	Numerical modelling	98
5.5.4	Validation of the linear supported glass panel model.....	105
5.6	SUMMARY AND CONCLUSIONS	106

6	PARAMETRIC STUDY	109
6.1	INTRODUCTION.....	109
6.2	POINT SUPPORTED PANEL PARAMETRIC STUDY	110
6.2.1	Parameter influences on V_{cr} values	111
6.2.2	Parameter influence on $V-w_{max}$ behaviour.....	112
6.2.3	Parameter influence on $V-u$ behaviour.....	113
6.2.4	Parameter influence on $V-\sigma_{1,max}$ behaviour	114
6.2.5	Parameter influence on $V- R$ behaviour	115
6.3	LINEAR SUPPORTED PANEL PARAMETRIC STUDY	116
6.3.1	Parameter influence on V_{cr} values.....	117
6.3.2	Parameter influence on $V-w_{max}$ behaviour.....	118
6.3.3	Parameter influence on $V-u$ behaviour.....	119
6.3.4	Parameter influence on $V- \sigma_{1,max}$ behaviour	120
6.3.5	Parameter influence on $V-R$ behaviour	121
6.4	SUMMARY AND CONCLUSION	122
7	DESIGN PROPOSAL AND PRACTICAL RECOMMENDATIONS.....	125
7.1	INTRODUCTION.....	125
7.2	SHEAR BUCKLING RESISTANCE	126
7.3	DESIGN PROPOSAL	129
7.3.1	Determination of loads and actions	129
7.3.2	Structural analyses.....	130
7.3.3	Determination of strength.....	131
7.3.4	Verification.....	134
7.3.5	Serviceability limit state	134
7.4	PRACTICAL RECOMMENDATION.....	135
7.4.1	Glass panel	135
7.4.2	Point supported connection devices	136
7.4.3	Linear supported connection devices	137
7.5	SUMMARY AND CONCLUSIONS	138
8	CONCLUSION AND FUTURE WORK.....	139
8.1	SUMMARY AND RESULTS RELATED TO THE OBJECTIVES.....	139
8.2	MAIN CONCLUSIONS.....	141
8.3	FUTURE WORK	143
	REFERENCES	145
	CURRICULUM VITAE	151

NOMENCLATURE

Latin letters

a	glass panel height	[mm]
A_{net}	net area	[mm ²]
b	glass panel width	[mm]
c	hole-edge distance	[mm]
c_A	adhesive width	[mm]
C_e	exposure coefficient	[-]
c_{pe}	aerodynamic factor for external pressure	[-]
c_{pi}	aerodynamic factor for internal pressure	[-]
C_t	thermal coefficient	[-]
d	hole diameter	[mm]
D	flexural stiffness	[Nmm]
d_b	bolt diameter	[mm]
D_c	flexural bending stiffness of the core (negligible)	[Nmm]
D_{lam}	flexural rigidity for the sandwich	[Nmm]
D_i	flexural stiffness of the faces around their individual neutral axes	[Nmm]
D_o	flexural stiffness of the faces around the middle axis	[Nmm]
d_s	seating block width	[mm]
E	modulus of Elasticity of glass	[N/mm ²]
E_A	modulus of Elasticity of the adhesive	[N/mm ²]
F	force	[N]
F_c	compression force	[N]
F_e	maximum elastic force	[N]
F_{failure}	force at the failure	[N]
F_t	tension force	[N]
G	shear modulus of glass	[N/mm ²]
G_A	shear modulus of the adhesive	[N/mm ²]
$G_{A,e}$	elastic adhesive shear modulus	[N/mm ²]
$G_{A,p}$	plastic adhesive shear modulus	[N/mm ²]
G_{PVB}	shear modulus of the PVB interlayer	[N/mm ²]
H	width of the plate	[mm]
HK	Knoop hardness	[GPa]
l_A	length of the adhesive	[mm]
k_τ	shear buckling coefficient of the monolithic glass	[-]
$k_{\tau,\text{lam}}$	shear buckling coefficient of the laminated glass panel	[-]
k'_τ	modified shear buckling coefficient of the monolithic glass	[-]
$k'_{\tau,\text{lam}}$	modified shear buckling coefficient of the laminated glass	[-]
K_t	stress concentration factor	[-]
N	in-plane normal force	[N]
q	out-of-plane distributed load	[N/mm ²]
$q_k(z)$	characteristic value of the wind load	[kN/m ²]
R	support reactions	[N]
s	characteristic snow load on the roof s	[kN/m ²]
s_k	characteristic value of a snow load on the ground	[kN/m ²]
t	glass panel thickness	[mm]
t_A	adhesive thickness	[mm]
t_g	thickness of the individual glass sheet	[mm]
T_g	transition temperature	[°C]
T_l	liquid temperature	[°C]
t_{PVB}	thickness of the PVB interlayer	[mm]
u	in-plane displacement of the glass panel	[mm]
u_{failure}	in-plane specimen displacement at failure	[mm]

u_d	allowable displacement	[mm]
V	in-plane shear force	[N]
$V_{b,Rk}$	characteristic shear buckling resistance	[N]
$V_{failure}$	failure shear force	[N]
V_{Ed}	design value of the shear force	[mm]
V_{Rk}	characteristic shear strength	[mm]
w	out-of-plane deflection of the glass panel	[mm]
w_d	allowable deflection	[mm]
w_e	wind pressure acting on the outer surface of the structure	[mm]
w_i	wind pressure acting on the inner surface of the structure	[mm]
w_{max}	maximum out-of plane deflection	[mm]
w_o	the initial imperfection	[mm]
w_t	total pressure acting on a structure	[mm]

Greek letters

α	geometric ratio	[-]
$\bar{\alpha}$	Ayrton-Pery coefficient	[-]
α_T	coefficient of thermal expansion	[K ⁻¹]
β	angle at which the reaction force R acts on the hole	[-]
β_A	adhesive coefficient	[-]
δ	specimen displacement	[mm]
δ_A	adhesive displacement	[mm]
$\delta_{A,e}$	displacement at the point of the maximum elastic force	[mm]
δ_g	relative displacement between the glass and the supports	[mm]
δ_h	horizontal glass displacement	[mm]
δ_l	longitudinal specimen displacement	[mm]
$\delta_{M,F}$	mortar displacement at the point of maximum force	[mm]
$\delta_{l,failure}$	longitudinal specimen displacement at failure	[mm]
ΔR	clearness between the glass hole and the bolt	[mm]
ρ	density	[kg/m ³]
$\bar{\lambda}$	non-dimensional shear plate slenderness	[-]
μ_i	roof snow load shape coefficient	[-]
σ_{adm}	admissible stress at the edge of the glass hole	[N/mm ²]
σ_{max}	maximum stress	[N/mm ²]
σ_{nom}	reference nominal stress	[N/mm ²]
σ_r	radial stress	[N/mm ²]
σ_{res}	residual stress	[N/mm ²]
σ_Φ	tangential stress	[N/mm ²]
$\sigma_{l,max}$	maximum principal tension stress	[N/mm ²]
τ_A	shear stresses in the adhesive	[N/mm ²]
τ_{adm}^{short}	admissible shear stress under short-term loading	[N/mm ²]
τ_{cr}	critical shear stress	[N/mm ²]
τ_p	plastic shear stress	[N/mm ²]
τ_{Rk}	characteristic shear strength of the glass panel	[N/mm ²]
$\tau_{r\Phi}$	shear stress	[N/mm ²]
τ_{xy}	shear stresses	[N/mm ²]
ν	Poisson's ratio of glass	[-]
ν_A	Poisson's ratio of the adhesive	[-]
γ_A	shear strain of the the adhesive	[-]
γ_e	elastic shear strain	[-]
γ_M	shear resistance factor	[-]
γ_p	plastic shear strain	[-]
χ	shear buckling reduction factor	[-]

Abbreviations

IGU	insulated glass unit
AR	axial rigid test
ER	eccentric rigid test
EP	eccentric pinned test
CF	cohesive failure
AF	adhesive failure
MF	mortar failure
TNS	tension in net section
ST	glass failure due to splitting tension
2S	two side connections
3S	three side connections

Terminology

Annealed glass: glass without internal stresses caused by heat treatment.

Critical shear buckling force: the smallest shear load at which the equilibrium of the structure fails to be stable as the load is slowly increased from zero.

Elastic buckling analysis: buckling analysis on an ideal linear elastic structure used to predict the theoretical buckling strength (critical load).

Float glass: transparent glass with flat, parallel surface formed on the surface of a bath of molten tin. The term generally refers to the annealed float glass.

Fully tempered glass: made from annealed glass by a thermal tempering process. Fully tempered glass is a type of a safety glass that has the increased strength and will usually shatter in small pieces when broken. It is used when strength, thermal resistance and safety are important considerations.

Fully transparent pavilion: a pavilion free of any steel or concrete frames, where glass panels have a load bearing function, carry all the imposed loads and stabilize the building.

Glass: molecularly cooled liquid - solid which combines transparency with hardness and resistance consisting of geometrically irregular configuration of silica and oxygen atoms with alkaline parts in between. It is a brittle material that breaks into sharp shards.

Glass pavilion: a covered structure with surrounding walls made of glass elements. The load bearing structure can be made of a metal or a concrete frame, as well as of shear walls hidden in the structure. The glass panel has the function to divide the internal space from the external world.

Glazing: collective elements of a building comprising glass, frame and fixing.

Heat strengthened glass: glass that has been tempered to induce surface residual stresses, but at a lower temperature and with a lower cooling rate than fully tempered glass. It has lower residual stresses than a fully tempered glass. Upon breaking, it breaks into large sharp pieces, smaller than those of the annealed glass, but bigger than those of a fully tempered glass.

Inherent strength: part of the tensile strength that is not due to a compressive residual stress but to the resistance of the material itself.

In-plane normal force: uniaxial tension or compression load acting in the panel axis.

In-plane shear force: shear load acting in the panel axis.

Insulating glass unit: piece of a glazing consisting of two or more layers of glass separated by a spacer along the edge and sealed to create a dead air space or a vacuum between the layers in order to provide thermal insulation. The dead air space is often filled with an inert gas (argon or krypton).

Interlayer: a thin layer between two sheets of glass, a transparent, tough plastic sheeting material (PVB for instance), that is capable of retaining the fragments after fracture.

Initial imperfection: a real geometrical imperfection of the unloaded glass panel causing out-of-plane deflection when glass is subjected to the in-plane load.

Laminated glass: two or more sheets of glass bonded together by an adhesive.

Monolithic glass: a single sheet of glass.

Out-of-plane distributed load: a uniform lateral load acting perpendicular to the surface.

Non-linear buckling analysis: a buckling analysis on a real structure including the initial imperfections, plastic behaviour and a large displacement theory response. It is used to track the post-buckling performance of the structure.

Pavilion: a free-standing, single floor structure whose architecture makes it a place of pleasure.

PVB: polyvinyl butyral is a viscoelastic resin made of a vinyl acetate monomer as the main raw material. It provides a strong binding, an optical clarity, adhesion to surfaces, toughness and flexibility. The PVB is the most commonly used interlayer material for laminated glass.

Residual stress: the residual compressive surface stress that arises from the tempering process.

Shear buckling: a failure mode characterized by a sudden failure of a structural member subjected to shear stresses, where the actual shear stresses at failure are greater than the ultimate shear stresses the material is capable of withstanding.

Soda-lime-silica glass: type of glass commonly used in glazing.

Splitting tension: a failure mode that occurs when the glass is subjected to in-plane concentrated compression force. Due to Poisson's ratio, perpendicular to the compression field the tension stresses take place. These tension stresses try to split the glass and cause glass failure.

Strength: the maximum stress required to overcome the cohesion of a material. Strength is considered in terms of compressive strength, tensile strength, and shear strength, namely, the limit states of compressive stress, tension stress and shear stress respectively.

Structural design: iterative process of selecting a structural element that meets a set of performance requirements that depend on the specific application. Common requirements for structural glass elements relate to aspects such as deformation, vibration, usability, aesthetics, acoustic or optical performance and a load bearing capacity.

Viscosity: measure of the resistance of a fluid to deformation under shear stress. Viscosity describes a fluid's internal resistance to flow and may be thought of as a measure of fluid friction.

1 INTRODUCTION

1.1 BACKGROUND AND MOTIVATION

When it was completed in 1949, Philip Johnson's Glass House in New Canaan (USA) was a revolutionary achievement. The transparent pavilion was an architectural experiment in forms, materials, ideas and radical departure from houses of that time (Fig. 1.1). Indeed, the light roof is supported by a very thin metal frame, strong enough to carry all superposed loads, horizontal and vertical, but light enough to permit the unsurpassed view inside the house. Transparent glass walls are used as a physical barrier between the surrounded nature and interior living space. At the same period (1951), architect Ludwig Mies van der Rohe designed Farnsworth House in Plano (USA). With two distinctly expressed horizontal slabs, the roof and the floor, sandwich an open living space enclosed by clear floor-to-ceiling glass panels (Fig. 1.2). The house seems to float weightlessly above the ground.



Figure 1.1 – Glass House, New Canaan (USA)

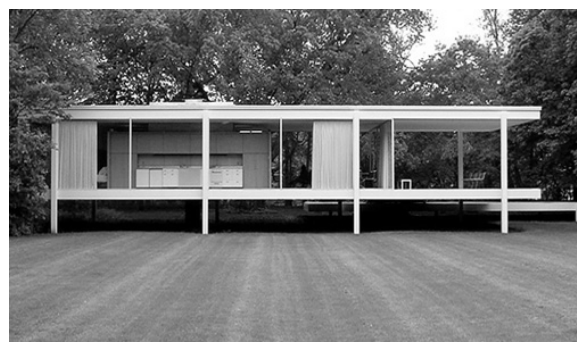


Figure 1.2 – Farnsworth House, Plano (USA)

Inspired by the work of Johnson and van der Rohe, many further architects attempted to design transparent pavilions driven by the idea of minimizing the load bearing structure and increasing the clearness, achieving the impression of building lightness. Following this trend, at the end of the last century, grew the idea of removing completely the load bearing structural frame and using the glass wall, not only as space barrier and building envelope, but also in a structural manner as primary element capable to carry and transfer the imposed loads. The concept of *fully-transparent pavilion* was born in 1991 with the Rheinbach Glass Museum in Rheinbach (Germany), designed by Juergen Marquardt. Glass walls, that form the façade, work as supporting columns for the steel roof and as lateral wind bracing achieved by the rigid fixing in the floor slab (Fig. 1.3)



Figure 1.3 – Rheinbach glass museum, Rheinbach (D)



Figure 1.4 – Novartis campus entrance, Basel (CH)

Recently, more and more fully-transparent pavilions are built in Europe, as Novartis campus entrance building in Basel (Fig. 1.4) for instance. At the same time the lack of knowledge and experience in structural behaviour of glass for this kind of applications, obliges the design by testing, making the procedure time consuming and high costly.

Glass panels, being the unique vertical structural elements in fully-transparent pavilions, have to support and transfer all imposed loads from the roof to the foundation as well as to stabilize and stiffen the building. In this application, an individual glass panel (hatched in Figure 1.5) is subjected to in-plane shear force (lateral wind), out-of-plane distributed load (perpendicular wind) and in plane compression force (self weight of the roof, snow). While large experiences in glass plate behaviour under uniform out-of-plane bending exist as well as norms and standards dealing with design, the knowledge on glass behaviour under in-plane force is very limited and with constrained applications.

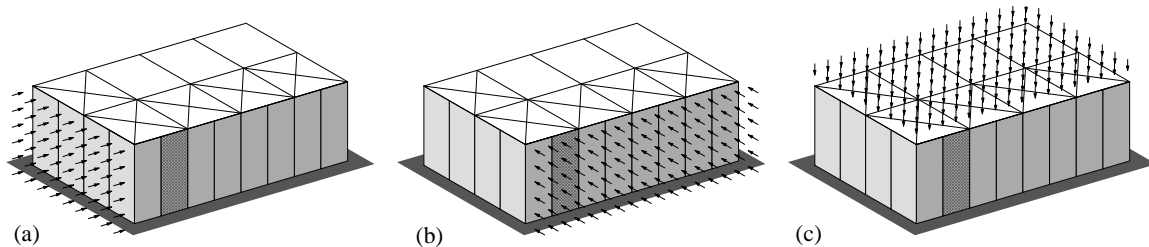


Figure 1.5 – Load on individual glass panel in fully transparent pavilion
(a) in-plane shear force (b) out-of-plane distributed load (c) in plane compression force

Recently, few researches have been undertaken to improve the understanding of the glass panel subjected to in-plane loading. First investigation on stability problem of glass elements was done by [Liess 2001] studying column buckling. [Luiblé 2004] did experimental, analytical and numerical investigation on column buckling, plate buckling and lateral torsional buckling. Lateral torsional buckling of glass panels was also deeply investigated by [Belis et al. 2003]. [Englhardt 2008] studied the glass plate buckling behaviour under concentrated in-plane load. [Wellershoff 2005] did a research on glass panel circumferentially glued to the steel frame subjected to in-plane shear (shear buckling). [Huveners et al 2007] studied the use of in-plane glass stiffness to stabilize a steel frame in a façade.

In fully-transparent pavilions, the top side of glass panel is attached to the roof; the bottom side is supported by the foundation while the lateral edges are support-free. At present, no research on two sides supported panels subjected to in-plane shear force exists; neither for glass, neither for other materials, making the shear buckling behaviour of glass panel with such boundary conditions unknown (Fig. 1.6). Therefore, research on this topic has original and innovative importance for both theoretical (glass panel under shear loading) and practical (use of glass envelope for building stabilisation) applications.

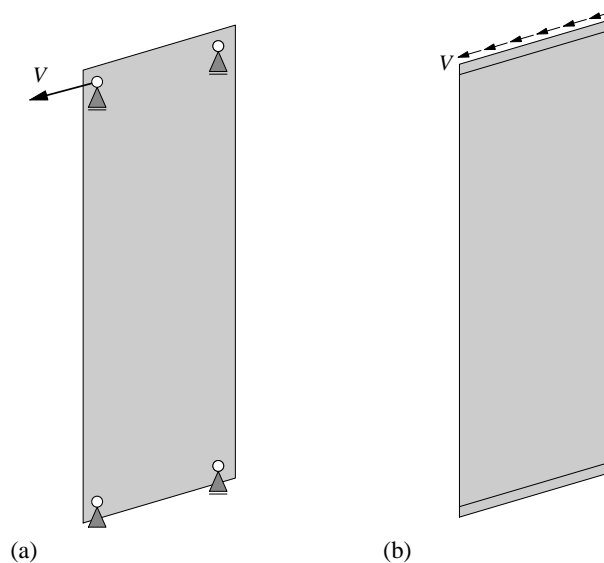


Figure 1.6 – Two sides supported glass panel under in-plane shear force V
(a) point supports at corners (b) linear supports at the edges

1.2 OBJECTIVES

This thesis is an investigation on glass panel behaviour under in-plane shear force with application on fully transparent pavilions. The objectives are the following:

Objective 1: To evaluate the current knowledge and trends

- Investigate the existing knowledge on glass panels under in-plane loading.
- Recognise architectural trends in structural use of glass, focusing on fully-transparent pavilions.

Objective 2: To develop the structural concepts

- Identify the main functions of glass panel in fully transparent pavilion.
- Develop connection devices able to insure uniform load transfer between glass and substructure.
- Develop glass panel structural concepts utilizable as structural element in fully transparent pavilion
- Determine the actions and the load path in the glass panels.

Objective 3: To analyse the structural concepts

- Perform experimental investigations on connection devices to study their local behaviour.
- Find the most suitable connection devices and implement it in full-size glass panel. Test it to study the shear buckling behaviour of glass panels.
- Define a hypothesis and develop numerical models of the structural concepts.
- Compare and verify the numerical results with experimental results.
- Perform the parametric study on a validated model to identify the influence of different parameters.

Objective 4: Provide the design proposals and recommendations

- Propose a design method for preliminary design of glass panels under in-plane shear force.
- Give some practical recommendations for glass panel applications in fully-transparent pavilions.

1.3 ORGANISATION OF THE THESIS

The thesis is divided in 8 chapters. Organisation chart is schematically represented in Figure 1.7.

Chapter 2 summarises the literature review on mechanical behaviour of glass utilised in the building, focusing on glass panel buckling and in-plane load transfer between the glass and substructure. Furthermore, an overview on glass architectural use in buildings is given from its first application as simple windows up to nowadays esthetical, structural and environmental achievements, focusing on fully-transparent pavilions. The architectural tendency for transparent structures is recognised and potential utilization of a glass panel as a load-carrying element subjected to in-plane shear force is predicted.

Chapter 3 describes the development of two structural concepts which consist of glass panel, connection devices and substructures. The requirements and functions of the structural glass panel in fully-transparent pavilions are determined. In the **point supported concept** the glass panel is attached to the substructure by bolted connections at the corners, while in **linear supported concept** the glass panel is glued to the substructure by two shorter sides. The actions on the glass panel are determined.

Chapter 4 describes the specimens and the testing procedure. The results of experimental investigations on local behaviour of glass/substructure connection are given. The most suitable connection devices for point support and linear support concepts are identified. Furthermore, the global behaviour of glass panel is investigated in order to estimate the shear behaviour and the

influence of different boundary conditions (point and linear) and load interaction (in-plane shear force with out-of-plane distributed load and in-plane compression force).

Chapter 5 describes the numerical model of connection devices developed for studying the deformation, the stress distribution and the local influence on surrounding glass area. By means of numerical models, considering the global deformation of the glass panel, the shear buckling behaviour, the stress distribution and the support reactions are investigated. The models are with experiments.

Chapter 6 presents the parametrical study carried out with numerical models in order to identify the most important parameters, evaluating their influence on the glass panel shear buckling behaviour. The geometrical/material parameters are chosen and their influence on the critical shear force, the global deformation and the stress distribution and supports reaction described.

Chapter 7 collects the results of the previous chapters and incorporates them in a preliminary design method for dimensioning of glass panel under in-plane shear force for both developed concepts. Developed formulas, graphs, curves and design procedure are explained. Some recommendations for the practical use of glass panels as primary structural elements for building stabilisation are proposed.

Chapter 8 summarises the work of this thesis. Principal results, main conclusions and suggestions for future work are given.

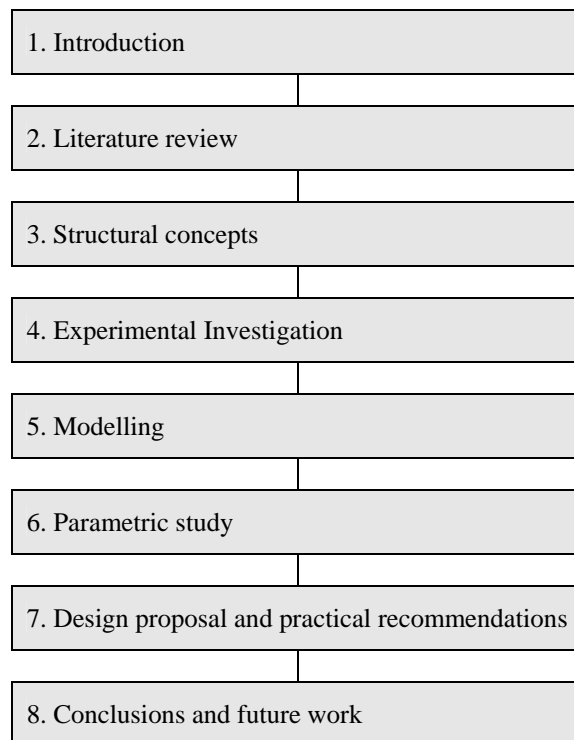


Figure 1.7 - Organization of the thesis

2 LITERATURE REVIEW

2.1 INTRODUCTION

This Chapter summarizes the literature review on mechanical behaviour of glass utilised in the building, focusing on glass panel buckling and in-plane load transfer between the glass and the substructure. Furthermore, the literature review on utilization of glass in buildings is given from its first application as simple windows up to its utilization in contemporary architecture with its esthetical, structural and environmental achievements. Organization of Chapter 2 is illustrated in Figure 2.1.

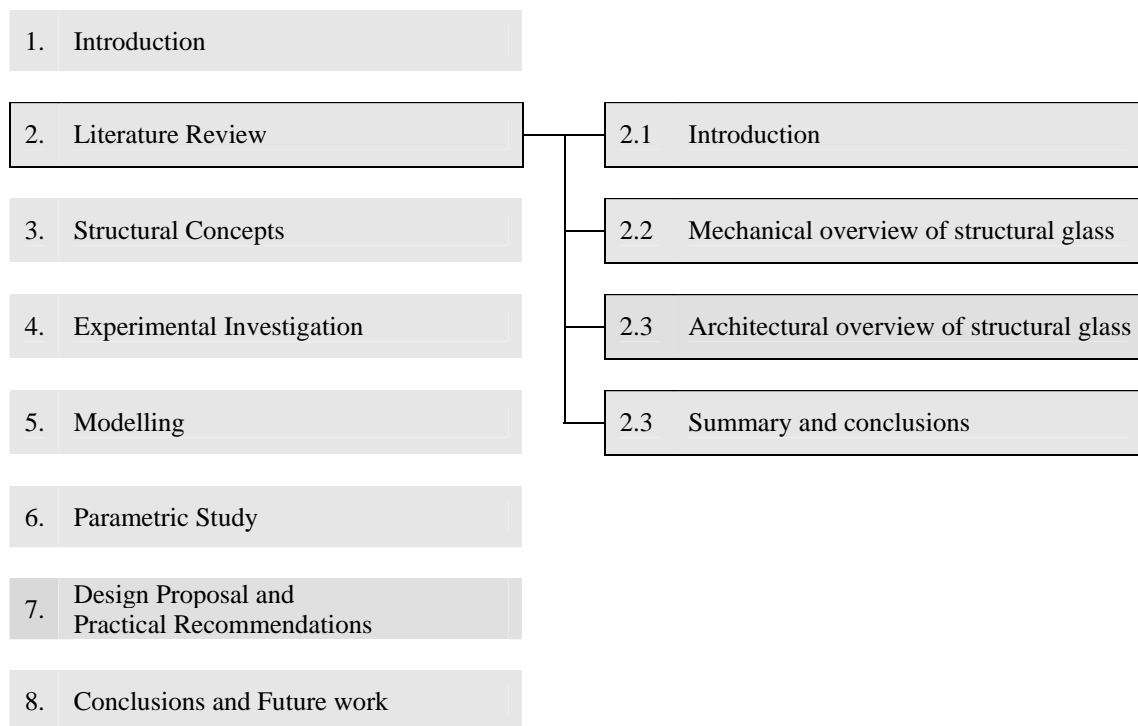


Figure 2.1 - Organization chart of Chapter 2

Mechanical overview of structural glass. This section defines the types, products, chemical compositions and mechanical properties of glass utilized in a building. The existing researches of in-plane loaded glass panels with special focus on shear buckling are listed and described. Moreover, relevant studies on in-plane load transfer by point and linear connection devices between glass and substructure are mentioned.

Architectural overview of structural glass. This section gives a historical overview on glass utilization in buildings from middle ages to nowadays. The glass production development, its technical improvement and application in the architecture through the history is illustrated with description of a representative example for each period. Summary of single storey pavilions with glass envelopes are given. Finally, examples of fully transparent glass pavilions, where glass envelopes are used as a structural element, are presented paying special attention to connection devices and the load transfer between the main structure and the glass façade.

Summary and conclusions. At the end of the Chapter the summary and main conclusions are given. They will be utilized for developing structural concepts of a glass panel in fully transparent pavilions.

2.2 MECHANICAL OVERVIEW OF STRUCTURAL GLASS

2.2.1 Glass in buildings

2.2.1.1 Glass types

Glass is a molecularly cooled liquid – a solid which combines transparency with hardness and resistance. It is formed when liquid is rapidly cooled from its molten state through its glass transition temperature T_g into the solid state without crystallization. The glass consists of a geometrically irregular configuration of silica and oxygen atoms with alkaline parts between them.

Soda-lime-silica glass

Soda-lime-silica glass (SLS) is a type of glass commonly used in glazing. It is prepared by melting the raw material (soda, lime, silica, aluminium and small quantities of fining agents) in a glass furnace from 1600°C to 1800°. The temperature is only limited by the quality of the furnace superstructure material and by the glass composition. For lowering the price of the raw materials, pure chemicals are not used, but relatively inexpensive minerals such as trona, sand and feldspar. Soda-lime glass is divided into glass used for windows (called float glass) and glass for containers (called container glass). The chemical composition and mechanical properties of the soda-lime-silica glass are presented in Table 2.2

Table 2.2. – Chemical composition and mechanical properties of soda-lime-silica glass

Chemical composition			Mechanical properties		
Silica sand	SiO ₂	73 %	Transition temperature	T_g [°C]	564
Lime	CaO	9 %	Liquid temperature	T_l [°C]	1000
Soda	Na ₂ O	14 %	Coefficient of thermal expansion	α_T [K ⁻¹]	9·10 ⁻⁶
Magnesia	MgO	4 %	Density	ρ [kg/m ³]	2500
Alumina	Al ₂ O ₃	0.15 %	Young's modulus	E [MPa]	70000
Potassium Oxide	K ₂ O	0.03	Shear modulus	G [MPa]	28000
Titanium Dioxide	TiO ₂	0.02	Poisson's ratio	ν [-]	0.23
Ferric Oxide	Fe ₂ O ₃	0.1	Knoop hardness	HK [GPa]	6.0

Float glass

Float glass is produced by the process invented by Sir Alastair Pilkington in 1953. The molten glass is poured onto a molten tin bath. The glass floats on the tin and levels out as it spreads along the bath, giving a smooth face to both sides. The glass cools and slowly solidifies as it travels over the molten tin and leaves the tin bath in a continuous ribbon. The glass is then annealed by cooling in an oven called a *lehr*. The finished product has almost perfect parallel surfaces. A very small amount of the tin is embedded into the glass on the side it touched, which can have influence on the surface when it is glued [Lotz 1995] causing some surface defects that reduce the strength [Sedlacek et al. 1999]. The tin side is easier to make into a mirror and is also softer and easier to scratch. Float glass is produced in standard metric nominal thicknesses of 2, 3, 4, 5, 6, 8, 10, 12, 15, 19 and 25 mm. Molten glass floating on tin in a nitrogen/hydrogen atmosphere will be spread out to a thickness of about 6 mm and stop the spreading due to surface tension. Thinner glasses are made by stretching the glass while it floats on the tin and cools. Thicker glasses are pushed back and not permitted to expand as they cool on the tin.

Annealed glass

Annealed glass is glass without internal stresses caused by heat treatment. Annealing is a process of slowly cooling glass to relieve internal stresses after it was formed. If glass is not annealed, it will retain many of the thermal stresses caused by quenching and significantly decrease the overall strength of the glass. Glass becomes annealed if it is heated above the transition point, then allowed to cool slowly, without being quenched. Float glass is annealed during the process of manufacture. Annealed glass breaks into large, jagged shards that can cause serious injury (Fig. 2.3) [Laufs et al. 2003]. Thus, monolithic annealed glass is considered a hazard in architectural applications. Some building codes restrict the use of annealed glass in areas where a high risk of breakage and injury exists.

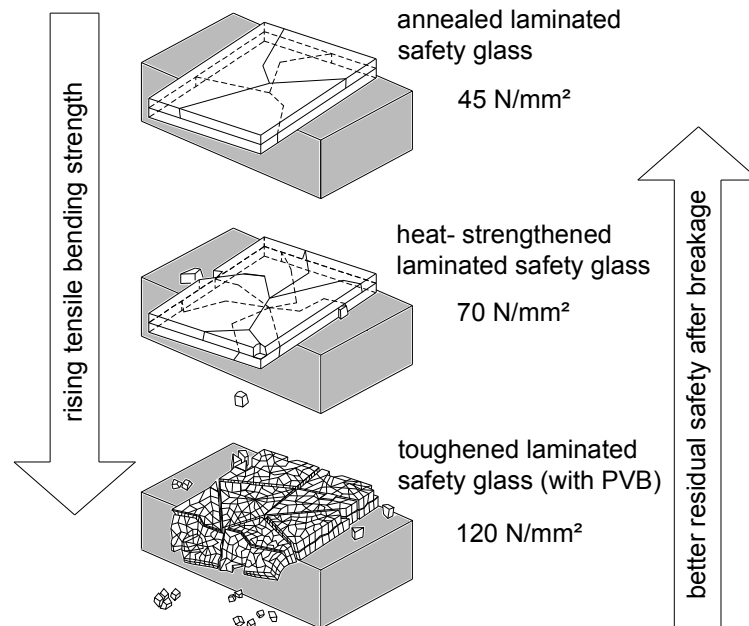


Figure 2.3 - Standard glass types with their corresponding breakage patterns (laminated with PVB) and 5%-fractile characteristic tensile bending stress values (with 95% probability level) according to [prEN 13474-1]

Fully tempered glass

The first patent on fully tempered glass was held by chemist Rudolf A. Seiden, in Austria. Fully tempered glass is a type of *safety glass* that has increased strength (between 80-150 MPa) and will usually shatter in small, pieces when broken (hence the name safety glass). It is used when strength, thermal resistance and safety are important considerations. Fully tempered glass is made from annealed glass by a thermal tempering process. The glass is placed onto a roller table, taking it through a furnace that heats it to above its transition temperature. The glass is then rapidly cooled with draughts of air such that the inner portion of the glass remains free to flow for a short time. Fully tempered glass must be cut to size and pressed to shape before tempering, as well as the polishing of the edges and drilling holes, because if once tempered it cannot be re-worked. Due to the balanced stresses in the glass, damage to the glass after tempering will result in the glass shattering into large pieces. Using fully tempered glass can cause a safety risk in some situations due to the tendency of the glass to shatter completely upon hard impact rather than leaving shards in the windows. Fully tempered glass can fracture spontaneously due to nickel sulphide inclusions. When single panes of fully tempered glass are used overhead, such failures can have dangerous consequences. The problem can be overcome by heat-soaking the glass after the tempering process to discover impurities, or by using an additional lower laminated glass as a safety bearing layer, which can additionally improve thermal insulation qualities and allow access onto the glass roof for cleaning.

Numerical modelling of the tempering process is possible [Laufs 2000], [Schneider 2001], [Bernard et al. 2002]. The residual stress distribution in central regions of the fully tempered glass plate is parabolic in shape. Due to reason that internal stresses should be in equilibrium, the magnitude of the surface compression is twice that of the mid-plane tension so the sum of the residual tensile and compressive stresses is zero. At the edges, corners and at holes, the residual stress distribution is distorted (Fig 2.4).

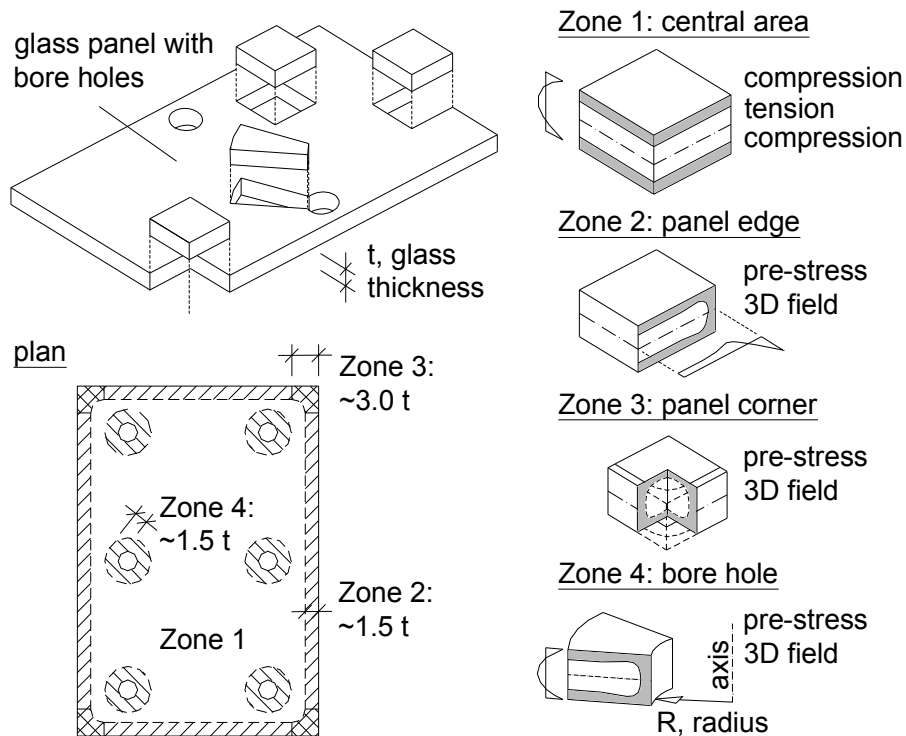


Figure 2.4 – Residual stress distribution in fully tempered glass

The residual stress varies near glass edges, boreholes and corners [Laufs 2000]. The externally applied forces must first neutralise the residual stresses before any tensile stress can be applied. The tensile strength of fully tempered glass is higher than that of annealed glass, but other physical properties remain unchanged. Furthermore, if a crack is driven through the compressive layer into the central tension region, there is enough tensile strain energy available to make the crack propagate violently through the glass.

Heat-strengthened glass

Heat-strengthened glass (also called partly tempered glass) is glass that has been tempered to induce surface residual stresses, but at a lower temperature and with a lower cooling rate than fully tempered glass. Due to it, the heat-strengthened glass has lower residual stresses than fully tempered glass. Its strength is an intermediate between the annealed and the fully tempered glass strength. On breaking, heat-strengthened glass breaks into large sharp pieces, smaller than those found on breaking annealed glass, but bigger than those on fully tempered glass. Used in laminated glass element, the large fracture patterns result in a remaining resistance of the failed element. Glasses thicker than 12 mm can not be heat-strengthened by using the normal tempering process.

Chemically strengthened glass

Chemically strengthened glass has a very high strength. The glass is chemically strengthened by submerging it in a bath containing a potassium salt (potassium nitrate) at 450 °C. This causes sodium ions in the glass surface to be replaced by potassium ions from the bath. These potassium ions are

larger than the sodium ions and they block the gaps left by the smaller sodium ions when they migrate to the potassium nitrate. This replacement of ions causes the surface of the glass to be in a state of compression and the core in compensating tension. The surface compression of chemically strengthened glass may reach up to 690 N/mm^2 . Chemical strengthening process does not use extreme variations of temperature and therefore chemically strengthened glass has little or no bow or warp, optical distortion or strain pattern. Chemically strengthened glass may be cut after strengthening, but loses its added strength within the region of approximately 20 mm of the cut. When the surface of a chemically strengthened glass is deeply scratched, this area loses its additional strength. When broken, it still shatters in long pointed splinters similar to annealed glass. For this reason, it is not considered a safety glass and must be laminated if a safety glass is required.

2.2.1.2 Glass products

Monolithic glass

Monolithic glass corresponds to one sheet of glass (Fig. 2.5(a))

Laminated glass

Laminated glass (Fig. 2.5(b)) was invented in 1903 by the French chemist Eduard Benedictus. It is a type of safety glass which consists of more glass sheets bonded together by a transparent interlayer. The interlayer is sandwiched by the glass sheets, heated at 140° and pressed up to 14 bars to expel air inclusions and form the bond. The most commonly used interlayer is PVB (polyvinyl butyral) with a thickness of multiples of 0.38mm. In case of breakage, the interlayer holds the fragments together, prevents the glass from breaking up into large sharp pieces and continues to provide residual resistance. The PVB interlayer gives a sound insulation due to the damping effect, and partly blocks the transmitted UV light. Laminated glass is used where there is a possibility of human impact, where the glass could fall if shattered and to ensure the resistance after breakage (shop-fronts, balconies, stair-railings, roof glazing etc.)

Insulated glazing

On Insulated Glass Unit IGU (Fig. 2.5(c)) is a set of two or more sheets of glass hermetically sealed to form a single glazed unit with space between each sheet. Its function is to improve the thermal performance of glass when used in architectural applications. The space between the sheets may be filled with air or gas, like argon or krypton, which would prevent condensation and improve insulating performance. A 16mm space is often considered the optimum thickness, although this depends on many factors such as the size of the window, the temperature difference between the two panes and whether it is vertical. The most commonly found IGUs are double glazed, made with two layers of glass. IGUs with three layers or more are sometimes used in very cold climates. Insulated glass assemblies must be manufactured to the proper size in a workshop with special equipment.

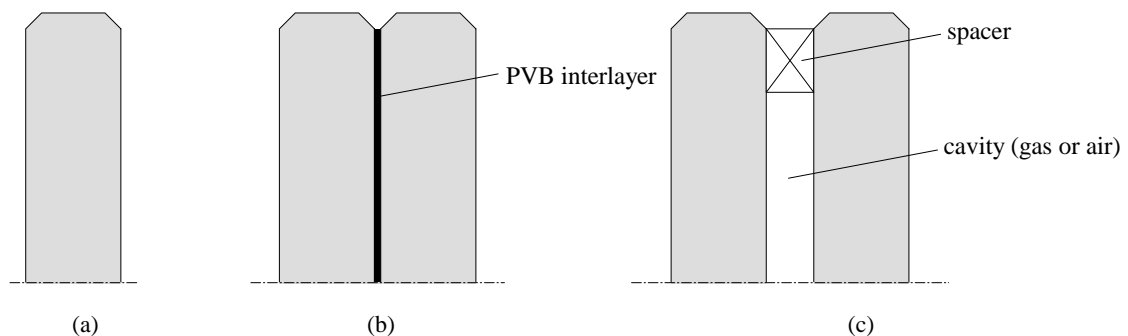


Figure 2.5 – Glass products (a) monolithic glass (b) laminated glass (c) insulating glass

2.2.2 Glass panel under in-plane force

Plate-buckling is a phenomenon that occurs in thin plates supported on four sides when subjected to normal in-plane compressive forces. Due to initial geometrical imperfection, the plate under in-plane load will deform out-of-plane. The plate will return to the initial position when the force does not act any more. It is valid only when the applied force is smaller than the critical plate-buckling force. If the applied force is higher, the plate will remain in the deformed position forming buckles. Particular case of plate-buckling is shear plate-buckling (shear buckling in further text) where a plate is subjected to in-plane shear force.

The basis of plate buckling was given by Euler in 1744 developing the bifurcation theory. From that time many researchers have studied buckling phenomena in thin plates for different materials, boundary conditions and load directions. However, this was not the case for glass plates. Only recently a few authors have studied the simplest cases of buckling behaviour of glass panel under in-plane compression and in-plane shear force.

[Luible 2004] studied the plate-buckling behaviour of monolithic and laminated safety glass circumferentially supported at four edges and subjected to normal compressive forces, by means of plate buckling tests, analytical and numerical models (Figure 2.6.a). It was shown that glass panels have a large post critical load carrying capacity [Luible et al. 2005]. The main influences on the buckling resistance of a load carrying glass element were found to be the glass thickness, the initial deformation, the tensile resistance of the glass surface and the composite action due to the PVB interlayer in laminated safety glass. One of the main differences as compared with steel is that the tensile strength limits the buckling strength. The initial fracture occurs always on the glass surface under tensile strength. The ultimate breaking stress of glass is not a material property, but depends on the residual compressive surface stress due to the tempering process, the degree of damage of the glass surface and the load duration. Plate-buckling coefficients were developed using the plate theory (for monolithic glass) and sandwich theory (for laminated glass). As a final result, a design method to calculate the glass panel load bearing capacity under normal compressive force was proposed.

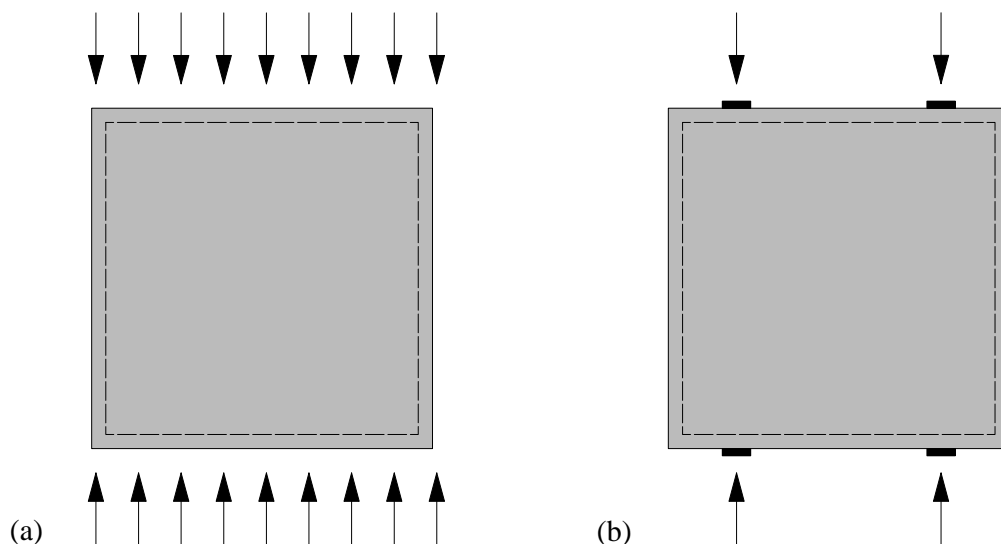


Figure 2.6 – Glass panel under in-plane compression force
(a) over the hole edge (b) as concentrated forces introduced by setting blocks

[Englhardt 2008] studied and compared the plane buckling behaviour for uniaxial in-plane loading over the hole edges and with a pair of concentrated force introduced by setting blocks (Fig 2.7(b)). For glass plates with loading over the whole length, the load distribution is nearly constant for load values below the critical buckling load, while for a loading by settings block, the concentrated distribution of the pressure stresses occur at the longitudinal edges causing higher values of critical buckling load.

The design values for the plate buckling of both systems were determined based on plate buckling calculations of steel structure. The buckling values, buckling reduction factor and interaction curves for the different loading systems were defined.

[Wellershoff 2006] studied the utilization of glass panels in space grid structures to cover large public areas without any columns developing a system of space grid structures with plane glass elements where common wind bracing made of rods or prestressed steel cables are omitted. The stiffening force is transmitted by a glass panel activated as shear panel which stabilises the structure. The glass panels are glued to the grid members along the four edges and subjected to in-plane shear force (Fig. 2.7(a)). The shear buckling of glass was studied analytically, numerically and experimentally. The stiffness of the adhesive utilised to glue the glass panel to the grid influenced the stress flow in the glass panel. Three areas with higher surface stress concentration were identified: along the tensile diagonal, in the line of maximal buckle bending and in the anchorage points of the diagonal tension field. The principle stress theory was used (commonly used for brittle materials like glass). The developed verification rules are similar to the known verification rules for steel elements, but with different reduction factor.

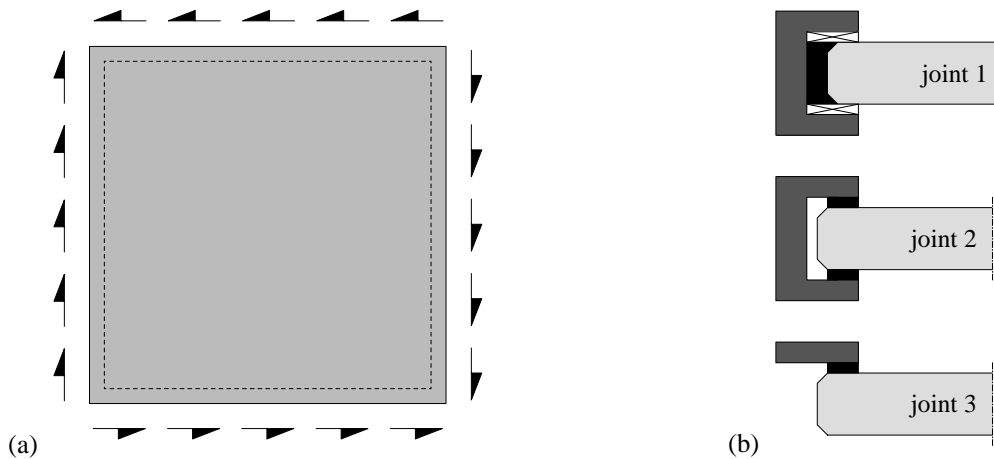


Figure 2.7 – Glass panel under in-plane shear force
(a) supported by four edges (b) different joint type between glass panel and framework

[Huveners et al. 2005] and [Huveners et al. 2007] studied the experimental and analytical use of in-plane stiffness of glass panel to stabilize a steel framework in a façade. The glass panel was circumferentially structurally bonded with adhesive to the framework (Fig. 2.7(a)). Three systems of annealed glass with two different adhesives were tested under in-plane shear loading (Fig. 2.7(b)). Joint type 1 is polyurethane joint on end, joint type 2 is a two-sided epoxy joint and joint type 3 is a one-sided epoxy joint. Joint 2 demonstrated larger stiffness than joint type 3 and joint type 1. Analytically, joint type 1 was modelled as one strut model with effective width of one-third of the compressed diagonal while joint type 2 and 3 were modelled as shear walls. Systems 1 and 2 demonstrated post-critical behaviour while this was not the case for joint type 3. It was found that the joint type and adhesive determine the stress distribution in the pane and the horizontal displacement of the framework. Both criteria were considered important for stabilizing buildings: the stress distribution for determining the critical tensile stress (safety) and the displacement for serviceability.

2.2.3 Connection devices

2.2.3.1 Point supports

Point supports (also called point fixing, bolted connections) are a commonly used connection type in glazing systems (Fig. 2.8) [Laufs et al. 2001], [Schittich et al. 2001]. The in-plane load is transferred from bolts to the glass panel by contact - the compression contact force acts on the glass hole surface causing stress concentration. In steel construction, this stress concentration can be reduced by local plastification, which is not the case in glass, being a brittle material. Due to the high difference between modulus of elasticity of glass and steel bolts, the failure on the glass/steel contact will occur at a very low level of load and therefore should be avoided. Liner material must be placed between the bolt and the glass such as plastic, aluminium or injected mortar, to avoid high stress concentration and to distribute the force more uniformly over contact area. The highest influences on stress concentration have a support type, geometry of the connection system and glass, the quality of glass edge treatment, liner material, load eccentricity and clearness between glass and bolt.

There is a considerable number of papers, studying stress distribution around the hole in aluminium and steel plates due to extensive use of bolted connections in the aerospace industry. However, there are only few researches on stress distribution around the glass hole.

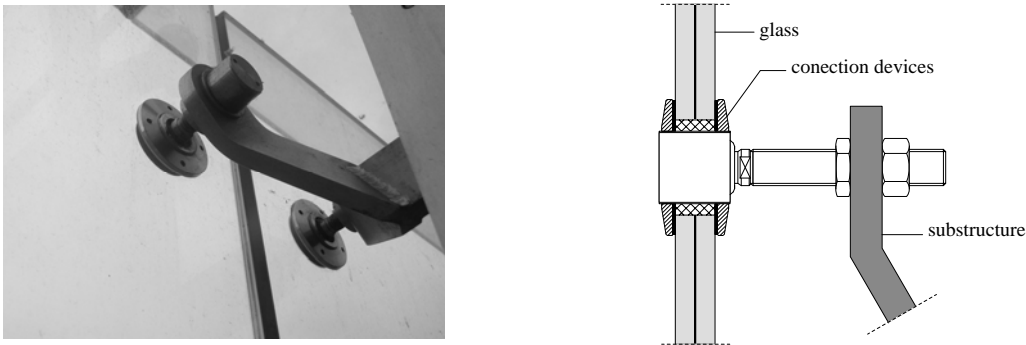


Figure 2.8 – Point support

[Overend 2002] performed numerical and experimental investigations on double bolted connections in glass panels under in-plane loading. Analyses and experiments showed that as the coefficient of friction between the bolt and the glass is reduced, the point of maximum stress shifts towards 90° from the line of action of the load. The brass liner material between a bolt and glass produced stiffer connections, while PTFE (polytetrafluoroethylene) liner material produced flexible connections. This difference did not affect the connection strength considerably, but the PTFE liner reduced hard spots and premature failure.

[Maniatis 2006] investigated the load-bearing capacity of bolted connections in glass panels under in-plane loads based on contact mechanism of Hertz theory, deriving advanced solutions of a contact between a bolt and a conforming hole in an infinite and a finite panel. Analytical, numerical and experimental investigations were conducted, with intensive parametrical study. It was found that different liner materials had slight influence on the stress distribution around the glass hole. Increasing the clearance between a bolt and a hole, the stress on the hole surface increased while the location of maximal principal tensile stresses changed from the perpendicular point of the load direction. Moving the load from an axial to an eccentric position, the maximum stress concentration moved from the mid-plane to the glass surface. The stress drastically increased with decreasing of the ratio of hole diameter to panel width, as well as with increasing the glass thickness.

2.2.3.2 Linear supports

In a linear support system, glass is connected at least on two opposite sides to a continuous substructure which is then fixed to the main building structure (Figure 2.9) [Laufs et al. 2001],

[Schittich et al. 2001]. The glass panel is glued to the substructure by adhesive. The European guidelines [EOTA 1999] developed the technical approval for bounded façades (SSGS – Structural Sealant Glazing System) and allowed the use of structural silicone sealant for linear supported glazing only. The structural silicon sealant can be glued to surfaces other than glass, such as aluminium or stainless steel, but not to pure or painted mild steel or standard polyester powder coated materials. Structural silicon sealant is UV-stable and compatible with PVB and resin interlayers. However, the adhesive technology has not been fully exploited for structural glass application by now. Lately, there have been several studies trying to analyse new adhesives types and their potential use for glazing.



Figure 2.9 – Linear support

[Blandini 2005] analysed several type of adhesives (epoxy, acrylic and polyurethane) by series of experimental, analytical and numerical investigations on tensile, shear and bending behaviour of adhesives under variable temperature and load durations. The *Yeoh* mathematical model, demonstrating the best fitting with laboratory results, was used to simulate the adhesive behaviour. At standard temperature (+23°), all adhesives demonstrate non-linear elasto-plastic behaviour while extreme high temperatures (+80°C) drastically decrease strength of the tested adhesives. In some cases, high temperature causes adhesive failure without applying the load. Extremely negative temperatures (-20°) drastically decrease the strength causing brittle failure. Only adhesive DP490 exhibited acceptable behaviour under all conditions, but the collected information was not sufficient to define its thermo-mechanical behaviour, so further investigations are required.

[Wellershoff et al. 2005] studied the behaviour of adhesives in linear overlapping supports under variable loads and different environmental conditions (UV-radiation, humidity and higher temperatures). Polyurethane, acrylic and silicon adhesives were tested in compliance with the aging and loading conditions of the European Technical Approval for Structural Sealant Glazing Systems [EOTA 1999]. In normal conditions, polyurethane and acrylic adhesives are much stiffer than the structural silicone. The acrylic adhesive showed substantial aging effects due to UV-radiation and immersion in water. With rising temperature, polyurethane and acrylic adhesives show decreasing of stiffness due to the melting point of one component at their transition temperature, while silicon remained stable.

[Overend 2002] performed double-lap adhesive tests in order to identify the best performing adhesive and compare the results with double bolted connections. The double-lap adhesive specimen failed at high loads in the order of 3 times the failure load of the bolted specimens. All specimens tested resulted in glass failure. In double-lap adhesive specimens, the deflections tended to increase rapidly close to failure, and in some cases a limited amount of strain softening was observed. The initial stiffness of the adhesive joints was much greater than the initial stiffness of the bolted connections. This is due to a lack of tolerances in the adhesive assemblies. The elongation at failure of the double-lap adhesive joints was in the order of 1/3 than that of the bolted connections.

[Weller 2007] investigated the behaviour (experimentally and theoretically) of adhesively bonded joints, with the adhesive applied in points, lines or areas. He demonstrated that adhesively bonded joints are possible, but the requirements for a technical approval for glass structures with adhesively bonded joints is high because there is only small experience in practise.

2.3 ARCHITECTURAL OVERVIEW ON STRUCTURAL GLASS

2.3.1 Glass in building

Glass as a building material has been inspiring architects from ancient times. Historically, the relationship between glass and architecture was imposed by load-bearing capacity of the structural element which determined the width of window openings. Nowadays, architects use glass to create the transparent building envelope as well as transparent load bearing walls and canopies. In the future glass function may be multivalent - combining transparency with structural implementation and high performance environmental control.

Glass started to be used in construction almost two thousand years ago after the discovery of the blown glass which led to production of thin transparent sheets strong enough to be utilized as windows. With this development, a new concept in architecture became possible. The first application was in Gothic cathedrals where the stone frames construct arched windows filled with coloured glass. By introducing light to spacious Gothic cathedrals the architectural task to achieve transparency and luminosity of the building began [Slessor 1998].

With the industrial revolution and manufacturing and engineering inventions in the nineteenth century, new materials started to be frequently employed in building construction. The improved production technology provided larger glass panels of uniform thickness in sizes of up to 1m. The introduction of the structural frame made of iron, steel and reinforced concrete offered the possibilities of creating lightweight structural frames to form vast spaces covered with glass and filled with natural light. Structural frame and glass technology generated new architectural typologies - conservatories, arcades, glazed rail sheds and exhibition buildings. Early examples were the Palm House conservatories in Kew (1848) designed by Turner and Burton; the Crystal Palace exhibition halls in London (1851) designed by Paxton (Fig. 2.10) and the Great Railway sheds in London designed by Pancras and Paddington. The shopping streets were covered by glazed roof structures to protect customers from the weather. Examples are the Galleria Vittorio Emanuele in Milan (1861) designed by Mengoni (Fig. 2.11); Waterloo terminal in London (1993) designed by Nicholas Grimshaw and glass Orangery in Prague designed by Eva Jiricna (1998), with frameless glass panel suspended from a steel structure. [Dawson 1999].

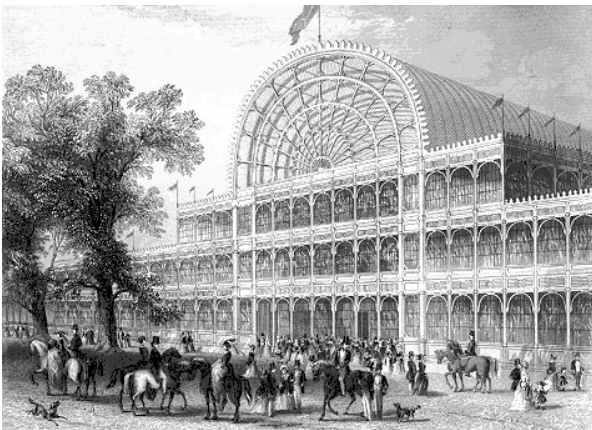


Figure 2.10 - Crystal Palace exhibition hall, London (UK)



Figure 2.11 – Galleria Vittorio Emanuele, Milan (I)

In the 1930s, the fully tempered glass was invented, which enabled the manufacturing of glass sheet and plate four to six times as strong as annealed glass. Fully tempered glass was for the first time utilised as building envelope in the façade of Willis Corroon building, designed by Norman Foster in 1975. The facade is made of 12mm fully tempered curved glass panels with coated surfaces suspended from the roof by bolted clamping strips and stiffened by glass fins. The only visible connections are fittings at the corners of the glass panes. The combination of a steel structure and glass has improved contemporary tendency of lightness and transparency.

Nowadays, the concept of transparency has more and more impact on architectural imagination. By combining glazing with new lightweight material (aluminium, composite etc.) innovative possibilities in architecture are achievable, developing new cladding materials and glass fixings. In 1980, the architect Adrien Fainsilber and structural engineers Martin Francis and Peter Rice utilized for the first time the bolted connection in glazing creating a series of large transparent enclosures for the Science Museum at the Park de La Villette, Paris (Fig. 2.12). They designed a four-way connector which penetrates the glass through holes drilled at the corners. A system of spherical bearings and string supports connects the glass wall to a cable truss system [Rice et al. 1995].

Architect Richard Hywel Evans designed the headquarters of Cellular Operations, Swindon, UK, in 2000 where a 9m high glass vault curves over two floors of open-plan office space. The facade is formed of glass panes with different angles. The glass entrance wall in Kempinsky Hotel in Munich designed by Schlaich Bergermann and Partner is composed of panels attached at their corners to a cable-net structure to be almost invisible and flexible enough to move up to one meter under wind load [IStrucE 1999]. An arts complex in Philadelphia, USA, designed by architect Rafael Vinoly and structural engineer Dewhurst Macfarlane, takes this idea one step further in search for ultimate transparency; the centre has a glass roof enclosed at its ends by a glass curtain suspended only from vertical cables.



Figure 2.12 – Parc de La Villette, Paris (F)



Figure 2.13 – Glass museum, Kingswinford (UK)

A further stage was reached when mechanical properties of the glass and its carrying capacity started to be exploited by using it as a primary load bearing structure. In the past, the glass was designed to endure very low stresses, but as structural engineers began to understand its characteristics and the methods of laminating became more sophisticated, the use of glass as a load bearing element became an irresistible temptation. The entrance canopy to KP Foods at Billingham in Teeside designed by architects BAAD and structural engineer Techniker is a glass canopy supported at each end by three glass panels, arranged in a Y-shape in top view to give support and lateral stability. Each panel consists of laminated fully tempered glass; the canopy rests on stainless steel fins bonded into laminate between the panes.

A system of laminated glass beams and glass columns was developed by structural engineer Dewhurst Macfarlane and Design Antenna (1995) to create a glass entrance to Glass Museum in Kingswinford, UK (Fig. 2.13). The glass elements required incredible precision in manufacture - joints between glass roof panels had to meet along an only 30mm wide glass beam. In 1995 Macfarlane produced a 10m cantilevered glass canopy for a subway entrance in the Tokyo International Forum, Japan, designed by architect Rafael Vinoly [Dawson 1999]. A glass beam was made from a series of glass blades connected at their ends and at their mid-points to form a rigid cantilever. The bolted connection was used and the loads are evenly distributed by a metal piece fitted into the bolt-hole.

Future step in façade engineering is the improvement of glass influence on building internal environment, conserving the natural energy of the building. The environmentally engineered glass

wall should regulate the transmission of light and heat, prevent the building condensation and provide an acoustic barrier. The window has developed from a simple glazing into an architectural skin capable of variable functions. With the improvement of low-emissivity coatings, photochromics, electrochromics and thermochromics, so called double-skin facade has become a key element in environmental control. The first concept of a double-skin building façade with multiple environmental functions dates from the early 1930s, when Le Corbusier attempted to create the neutralising wall for the Cité de la Refuge in Paris. Sixty years later, Norman Foster designed a modern, high performance version of a neutralising wall, building the first double skin glass façade for the Business Intelligence Centre at Duisburg in 1993. The aim was to modify light and heat transmission and deliver natural ventilation to the building [Campagno 1995].

New developed glass facades use self-regulating thermal protection and solar control measures to adapt to changing light and weather conditions in a dynamic way. In this way, they meet the needs of building users, while reducing energy consumption levels. It is obvious that glass and its assistant technologies will be fatherly developing, improving the material's capabilities, buildings aesthetics and environmental building control [Wigginton 1996].

2.3.2 Glass pavilions

The term pavilion refers to a free-standing structure whose architecture makes it an object of pleasure. Typically, the pavilions are small single floor buildings connected with relaxation and pleasure in its intended use. Glass pavilions can be defined as covered structures with surrounding walls made of glass elements. The load bearing structure can be made of metal or concrete frame, as well as of shear walls hidden in the structure. In glass pavilions, the glass panel has the function of dividing the internal space from the external world.

The first glass pavilion, known as Glass House, was designed by the architect Philip Johnson's in New Canaan (USA) in 1949 as his residence (Fig. 2.14). This transparent pavilion, masterpiece in the use of glass, was a revolutionary achievement for that time due to architectural experiment with forms, materials and ideas that radically differed from houses of the time. The brick floor is above the ground. The roof, made of steel beams and lightweight slab, is supported by steel columns which carry the vertical load imposed by the self weight of the roof and the snow and stabilize the pavilion. The walls of the pavilion are made of glass panels which allow a free view inside the house. Transparent glass walls are only used as a physical barrier between the surrounding nature and the interior living space. Some of the glass panels have the possibility to slide, opening the space and allowing the interaction of house and nature. The interior is open with the space divided by cabinets; a brick cylinder contains the bathroom and is the only object, except glass panels, connecting the floor and the ceiling.



Figure 2.14 – Glass House, New Canaan (USA)



Figure 2.15 - Farnsworth House, Plano (USA)

Almost in the same period (1945-1951), architect Ludwig Mies van der Rohe designed and constructed the Farnsworth House in Plano (USA) as a one-room weekend retreat (Fig. 2.15). Two parallel horizontal slabs were constructed. The first lower slab, made of concrete, forms the floor while the second, made of steel frame, forms the roof. The house is elevated above the ground by eight H-shape steel columns which are attached to the sides of the floor and ceiling slabs. The slab ends extend beyond the column supports, creating cantilevers. The space between the two slabs forms the open living space surrounded by transparent floor-to-ceiling glass panels. The third floating slab, an attached terrace, acts as a transition between the living area and the ground.

Glass House and Farnsworth House are widely recognized as masterpieces in use of glass in the modern architecture. Later, they inspired many architects in designing transparent pavilions driven by the idea of minimizing the load bearing structure, increasing the pavilion transparency and achieving the impression of a floating weightless roof.

Architects Inès Lamunière and Patrick Devanthery designed the Edouard Fleuret Library pavilion at University of Lausanne (Switzerland) in 2000 (Fig. 2.16). It consists of long rectangular and uncluttered single floor building, stretched between two prestressed concrete slabs that form the ground and roof covering. Four vertical load-bearing concrete walls are located in the middle of the building. The concrete slab is cantilevered from the supporting walls. The free-standing perimeter between two slabs is composed entirely of glass, creating a connection with the natural environment. Window frames and curtains give the pavilion a feeling of preciousness and an impression of levitation. The library is also known to be environmental friendly using modern technology for natural ventilation and temperature regulation – the vertical lames along the façade allow the air circulation inside the pavilion due to differential pressure between east and west [Smith 2007].



Figure 2.16 – Edouard Fleuret Library, Lausanne (CH)

Figure 2.17 - Toledo Glass Pavilion, Toledo (USA)

Toledo Museum's Glass Pavilion in Toledo (US, 2000-2006) designed by SAANA architects combines the most advanced structural, material, environmental and aesthetic knowledge creating an elegant building that could not have been realized a generation earlier (Fig. 2.17). This is a single storey pavilion where the interior curved glass walls form the galleries. Between the galleries, there are cavities used for ventilation and heating. The structure combines steel framing in the roof and concrete in the floor. The steel roof, consisting of rigidly connected beams can be compared to a flat plate. The concrete floor is made up of shallow and wide slabs. Round bar columns have pinned connections at the top. Vertical steel plate serves as both column and shear panel for vertical and lateral support. During glass panel fabrication process, the raw glass was shaped into the exact sizes needed for the construction of the Glass Pavilion. Since there are no right-angled corners on the exterior of the building, much of the glass was rounded to fit the corner areas. The mechanical ventilation system uses the cavity space as a temperature buffer, reusing the cooled air of the galleries to cool the hot shops and recycling the heat generated by glass ovens to heat the cavity in winter through coils embedded in the topping slab.

The glass pavilion designed by architect Danilo Mondada in 2000 was built as an annex of the Fondation de l'Hermitage Museum in Lausanne (Switzerland) and presents the new museum entrance and library (Fig 2.18). The pavilion façade is made entirely of glass panel inserted between the two slabs. The lower slab made of concrete floats 40cm above the ground. The steel columns hidden behind the glass envelope bear the vertical load of the roof and stabilize the pavilion with rigid connections. The structure of the roof is made of steel beams with wooden panel in between covered with zinc. The roof is cantilevered further on the envelope to reduce the sunshine on the glazing during summer. The insulating glass and the lames are utilised to reduce the insulation and extreme temperature inside the pavilion.



Figure 2.18 –Hermitage Museum, Lausanne (CH)



Figure 2.19 – Leonardo Glass Cube, Bad Driburg (D)

The latest example of glass pavilion is Leonardo Glass Cube in Bad Driburg (Germany) designed by the architects 3delux and inaugurated in 2007 (Fig. 2.19). The integrative design concept combines architecture, interior design and landscape design into a complex aesthetic entity. Inside the pavilion, the curved white wall creates an open space. Between the curved wall and the glass façade, a hall provides space for meetings and events. The glass facade allows interplaying with the surrounding landscape.

Several other examples of recently designed and constructed glass pavilions exist around the world. Their similarities lay in the intention to make the pavilion as transparent as possible, to build steel structural frame strong enough to carry the imposed load, but at the same time are fine enough not to disturb the clearness and transparency of the structure. Further improvement in the transparency of glass pavilions can be found in so called fully-transparent glass pavilions, where glass envelope is employed as primary structural element capable of carrying and supporting the entire structure.

2.3.3 Fully-transparent glass pavilions

When glass panels in a glass pavilion have a load bearing function and support all imposed load applied to the building and when the pavilion is free of any steel or concrete vertical structural element, the name of fully transparent glass pavilion is used. In the architectural and structural challenge to design the glass pavilion as transparent as possible, the idea of removing all visible vertical elements and to use glass panel envelope in structural manner to carry vertical load and to stabilize the pavilion, was firstly born in the end of 1990s. Due to lack of knowledge in structural use of glass, as well as lack of analytical or empirical solutions for glass panel behaviour under in-plane force, the construction of fully transparent glass pavilions was accompanied by expensive full scale prototype laboratory testing and time consuming numerical modelling. A few examples of constructed fully-transparent glass pavilion are presented in this paragraph.

Rheinbach glass museum pavilion, Rheinbach (Germany)

The new pavilion of the technical college in Rheinbach was built in 1999 as space for seminars and congresses and as a “walk-in showcase” for exhibitions (Fig. 2.20). It was designed by architect Juergen Marquardt and structurally calculated by Ludwig Ingenieure. The experimental investigation on full-scale glass panel specimens was made by RWTH Aachen [Wellershoff et al 2003], [Wellershoff et al 2002]. The eight rectangular glass cubes made of large sized glass panes form the facade and has the function to display cabinets and act as supporting columns for the roof of nearly 500 square meters. The grid roof, with a size of 32.5 x 15m (IPE 360 steel section), rests on glass supports of approximately 3.80m in height and 1.25m in width. The roof appears to float over the exhibition area. Cantilevered out on all sides, the large steel girder grid provides shading in summer when the central area of the pavilion is turned into a glazed lecture hall.

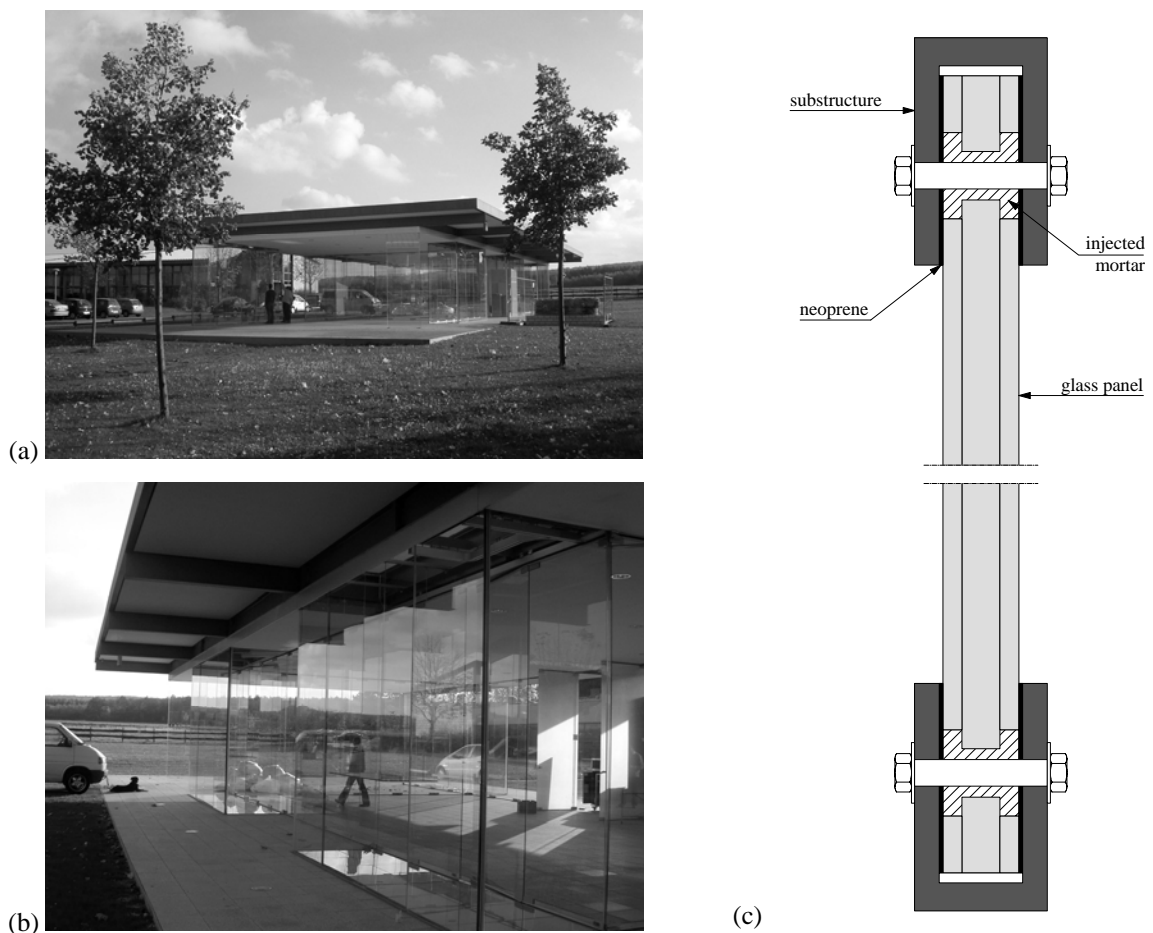


Figure 2.20 – Rheinbach glass museum pavilion, Rheinbach (Germany)

(a) pavilion view (b) façade element (c) connection details

The glass walls consist of two protective outer layers of heat strengthened safety glass (10mm each) and a load-bearing intermediate layer of toughened glass (19mm). The PVB interlayer of 1.52 mm is utilised to laminate the panel. The connection detail between glass panel and substructure is illustrated in Figure 2.20(c). The substructure and connection are hidden in the roof and foundation, giving the impression that glass panels grow from the ground and disappear in the roof. The connection between glass panels and substructure is bolted. The empty spaces between glass and bolt are filled with injected mortar. Neoprene is placed to avoid the contact of glass panel and substructures. The loads are transmitted from the roof to the glass panel and later to the foundation through the connection, while longitudinal and lateral bracings are achieved by the rigid connection of the glass panels in the floor slab.

Novartis campus entrance pavilion, Basel (Switzerland)

The fully transparent glass pavilion presenting the Novartis campus entrance building designed by the architect Marco Serra and structural engineer E. Basler + Partner was constructed in Basel in 2006 (Fig. 2.23). It is a single story pavilion of 4.50m in height, built on a large underground parking garage. The rectangular floor plan is limited by four glass walls. The walls consist of insulating glass. The interior panel, made of laminated glass, is assumed to be the structural element. The glass panels are stiffened every 1.7 m with short transversal and double-webbed glass stiffeners. The glass walls carry a glass fibre reinforced polymer sandwich roof. The roof structure has cantilevers on all four sides to protect the glass walls from direct solar radiation. The glass walls are held in their position by the roof which acts as a horizontal disc. The roof is supported at each intersection point of glass walls and stiffeners. Each support point consists of two concentrated steel supports on glass walls on each side of the stiffeners and a prestressed steel rod between the two webs of the glass stiffeners, anchored to the foundations to prevent an uplift of the roof.

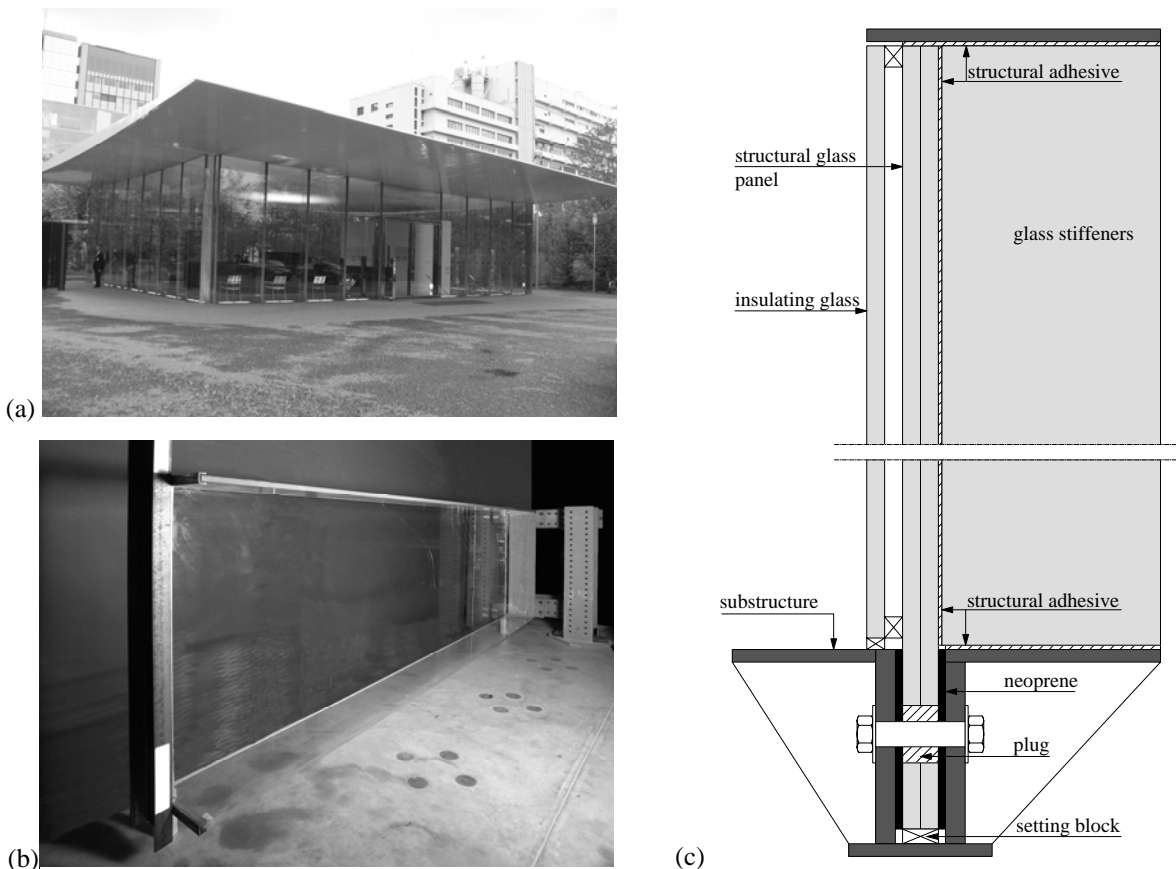


Figure 2.21 – Novartis campus entrance pavilion, Basel (Switzerland) (a) pavilion view
(b) facade element (in horizontal position) during experimental investigation (c) connection details

The external glass panel consists of 10 mm fully tempered glass, while the internal glass panel, designed to be structural, is made of heat strengthened laminated panel (two glass sheets) of 2x12 mm in thickness. Three layered laminated glass stiffeners have a thickness of 3x10 mm. The glass is connected by bolts to the bottom substructure (Fig. 2.21(c)). Each glass hole is filled with two cylindrical plugs, one for each layer of laminated glass. Afterwards, the two plugs are drilled with the same diameter as the bolts which are used to connect the glass panel with the substructure. The glass panel is connected to upper substructure by structural silicon along the glass edge. Three layered glass stiffeners are glued to the main glass panel by structural silicon, as well. The substructures are bolted and hidden in the foundation and roof.

Café Lichtblick, Innsbruck (Austria)

On the top of the Town Hall in Innsbruck, the architect Dominique Perrault designed the Café Lichtblick (Fig. 2.22). The site with 360 degree views on the Austrian Alps inspired the architect to build a pavilion with structural glass panels without vertically visual supports. Due to circumferential plan view of the pavilion, the curved laminated glass panels were used as the unique structural member supporting the roof. The glass ‘walls’ are designed to be opened as sliding doors up to 50 % (still holding the weight of the roof). The lightweight roof is made of textile membrane tensioned by circumferential steel beams welded to the glass panel substructure. The structural design was done by engineering firm Bollinger und Grohmann. The pavilion was completed in 2005.

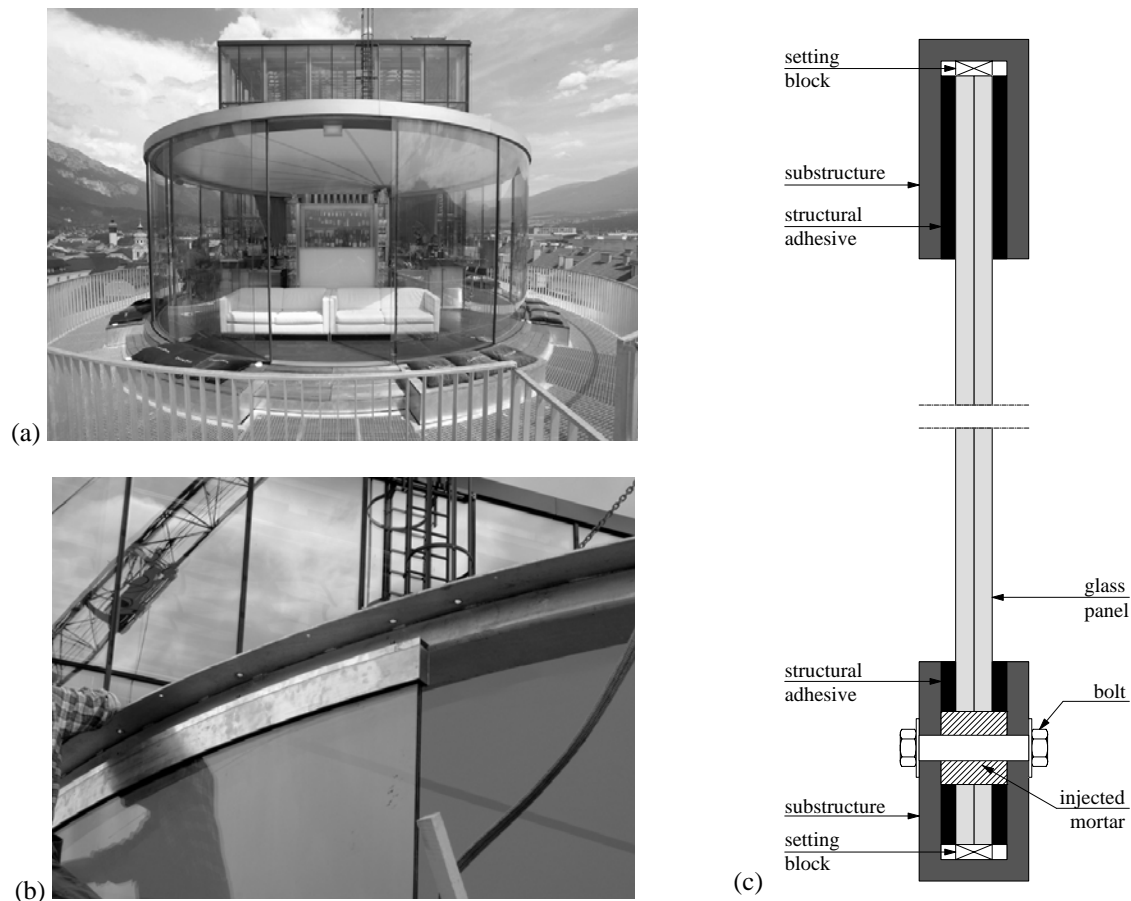


Figure 2.22 - Café Lichtblick, Innsbruck (Austria)

(a) pavilion view (b) façade element with substructure (c) connection details

Two layered laminated glass panels were used. Each glass panel has a thickness of 10 mm with PVB interlayer of 1.52 mm. For this application, heat strengthened glass was chosen. The bottom glass panel was attached to the substructure by bolted connection. The space between glass hole (diameter 40 mm) and bolt (M16) was filled by injected mortar Hilti HIT HY 50 [Hilti 2003]. Additionally, the glass panel was glued to the aluminium substructure by structural adhesive DC 983 [Dow Corning 2007]. The setting blocks were made of EPDM (50 shore). Top connection of glass panels and substructure differs from the bottom one. Here the glass panel is only glued to the aluminium substructure by structural adhesive (DC 983) along the glass edge without any bolted connection. Again, the setting blocks are made of EPDM (50 shore). The connection details are shown in Figure 2.22(c).

Talus du Temple, Avallon (France)

Architect Dirk Jan Postel and engineer Rob Nijse designed a small pavilion on the top of the existing stone landing, the only remains of the railway bridge dismantled in 20th century [Nijse 2003]. The pavilion was built in Avallon in France between 2000 and 2001. Inspired by the beautiful 360° view on the river Serein, the constructors opted for glass walls all around (Fig. 2.23). The glass panels are supposed not only to carry the weight of the roof but also to provide stability for the structure. For this purpose, bolts connected to fix the walls to the rest of the structure were chosen. The project won the Benedictus Award 2003 for outstanding innovations in laminated glass.

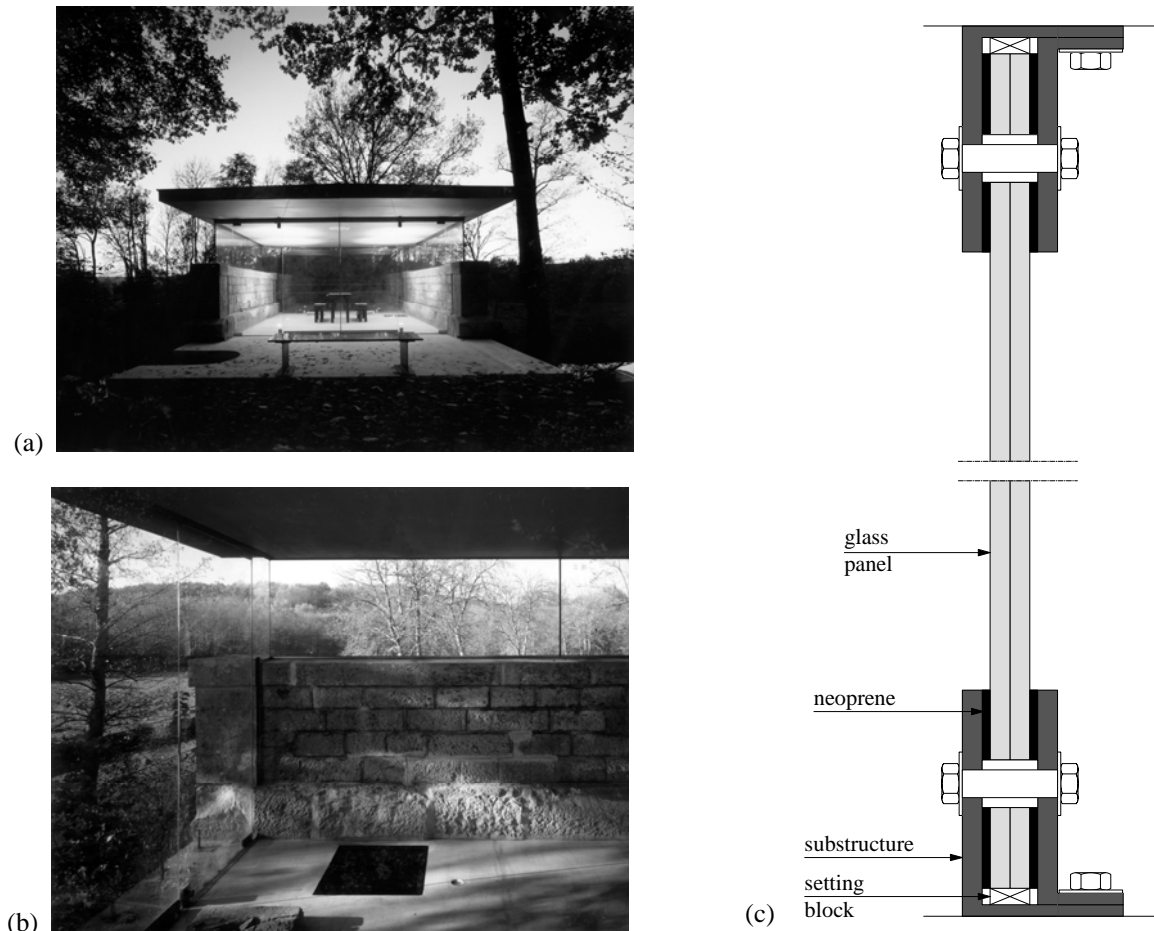


Figure 2.23 – Talus du Temple, Avallon (France)
(a) pavilion view (b) façade element (c) connection details

The pavilion's cantilevered roof is supported just by two panels of laminated glass. The roof was constructed separately then lowered carefully onto the glass to evenly distribute the load. The walls are made of laminated fully tempered glass panel (2x10 mm thick). The fixed parts are connected by bolts to a steel angle mounted on the ground and on the roof. On the front and back façade hinged glass doors are installed. The roof is made of a wooden box clad by copper plates, prefabricated on the ground below and then lifted over the freestanding glass walls and slowly lowered onto them. The detail of the connection between glass panel and substructure is illustrated in Figure 2.2(c). The connection is made by bolts. To avoid the direct contact between the bolts and glass, as well as steel angle and glass panel, neoprene was utilised. The setting blocks are made of PMMA (Polyethylene methacrylate). The angles are attached to the roof and foundation by bolts.

2.4 SUMMARY AND CONCLUSIONS

In Chapter 2 overviews on mechanical behaviour and architectural utilisation of structural glass were conducted.

Mechanical overviews of structural glass focused on research on plate buckling and shear buckling of the glass panel as well as on in-plane load transfer between glass and substructure.

The existing research shows that glass plates under in-plane compression and in-plane shear load behave in similar manner: in both cases the glass panels deflect out-of plane and both demonstrate the post-buckling reserve caused by the membrane effect. For this reason it is often assumed that shear buckling is a special sub-case of plate buckling. Existing research of plate buckling and shear buckling of glass panel deal with simple cases of four side supported glass panels, based on known thin-plate theories. Load introduction systems and connection types highly influence the buckling behaviour. No research on shear buckling behaviour of point supported glass panel or glass panel supported only on two sides was found.

Several researches insist on in-plane load transfer by bolt, all dealing with in-plane tension forces which try to break the glass plate perpendicular to the force direction. Stress concentration at glass hole is found to be the main problem and cause of glass failure. Consequently, the system and the material that can reduce this stress concentration are the main topics of those researches. However, no research on in-plane transfer of compression forces from the bolt to the glass exists.

Nowadays, many researchers and manufacturers work on development of the new adhesive and their implementation in glass connection. They want to discover a stiff adhesive stable through time and under all environmental conditions. According to [EOTA 1999], by now, only silicon sealant is allowed in the glazing

From **architectural overview of structural glass** was concluded that the latest trend in contemporary architecture are fully-transparent pavilions: a single storey building free of any steel or concrete frame, where glass panels are used as unique vertical structural elements to support the roof and as wind bracing to stabilize and stiffen the building. From the examples of recently constructed fully transparent pavilions, the structural system and load transfer path through different kind of connections devices are recognised. However, due to lack of knowledge in structural use of glass, as well as lack of analytical or empirical solutions for glass panel behaviour under in-plane force, the construction of fully-transparent glass pavilions was accompanied with expensive, full-scale prototype laboratory testing and time consuming numerical modelling.

3 STRUCTURAL CONCEPTS

3.1 INTRODUCTION

From the literature review in Chapter 2, the architectural tendency for transparent structures is recognized and potential utilization of glass panel as carrying element subjected to in-plane shear force is predicted. From there, the idea of implementing the glass panel as primary structural element in fully transparent pavilions has been growing. In this Chapter, two structural concepts are developed. They consisting of glass panel, connection devices and substructures. These structural concepts will be further investigated experimentally (Chapter 4) and numerically (Chapter 5). Organization of Chapter 3 is illustrated in Figure 3.1.

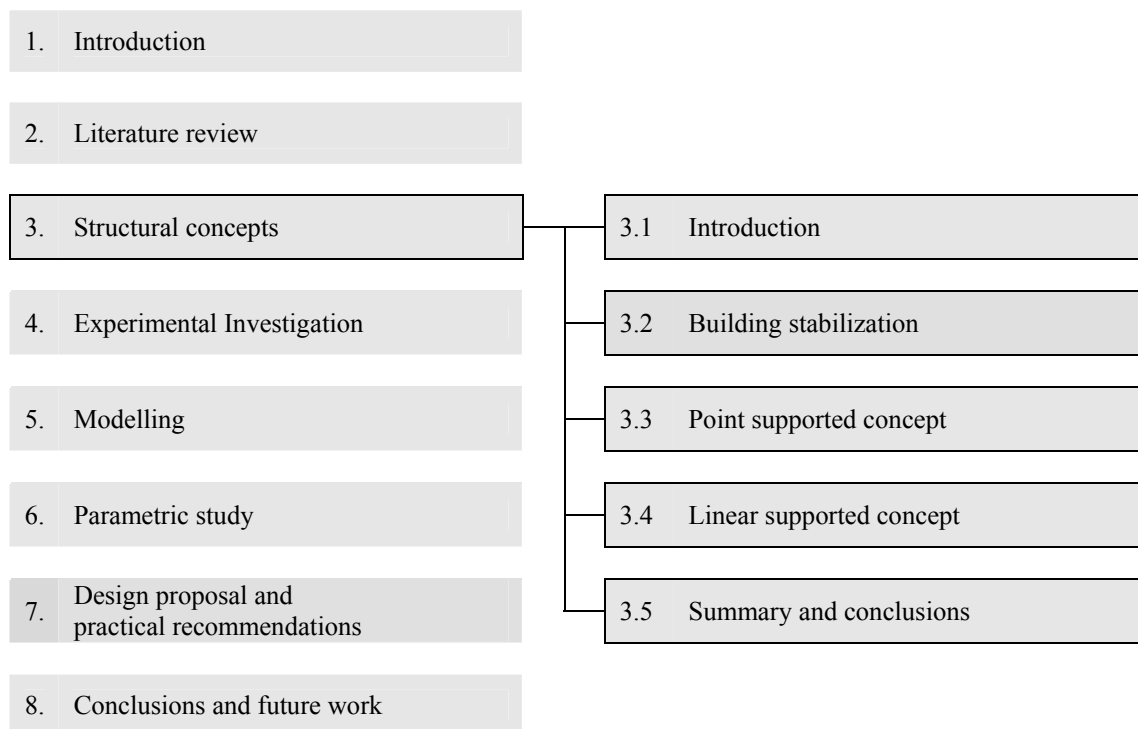


Figure 3.1 - Organization chart of Chapter 3

Building stabilization. This section defines the building stabilization system, its basic requirements and functions with emphasis on fully transparent pavilions. The force acting on the glass panel is determined.

Point supported concept. This section describes the first structural concept developed in this work. The glass panel is connected to the substructure by point supports (bolted connections) on the corners. The geometrical and mechanical property of *standard point supported glass panel* is defined, as well as boundary conditions and support reactions for each loading case.

Linear supported concept. In this section the second structural concept is developed. The glass panel is linearly connected to the substructure by adhesives on its two shortest edges. Additional setting blocks are used to transfer the permanent load. The geometrical and mechanical property of *standard linear supported glass panel*, boundary conditions and support reaction for different load cases are defined.

Summary and conclusions. At the end of the Chapter the summary and main conclusions are given. They will be utilized as a basis for further investigation.

3.2 BUILDING STABILIZATION

A pavilion is stable if stabilization system is rigid (non deformable) in three spatial direction. Consequently, the load bearing surfaces should be arranged in a way to make a three-dimensional system. The pavilion roof presents the rigid plate used for horizontal stabilization. In the classical steel frame pavilion, the longitudinal and transversal stabilization is obtained by series of wind bracing implemented in the façade (Fig. 3.2(a)), rigid frame or shear walls (diaphragm). The idea of this research is to replace the classical stabilization system by glass panels and activating them as shear walls. Through the glass panels, the shear force will be transferred from the roof to the foundation, stabilizing the pavilion in longitudinal and transversal directions (Fig. 3.2(b)). Glass panels should be capable to rigidify the pavilion, to resist the forces and to assure the load transfer [Hirt 2006.1].

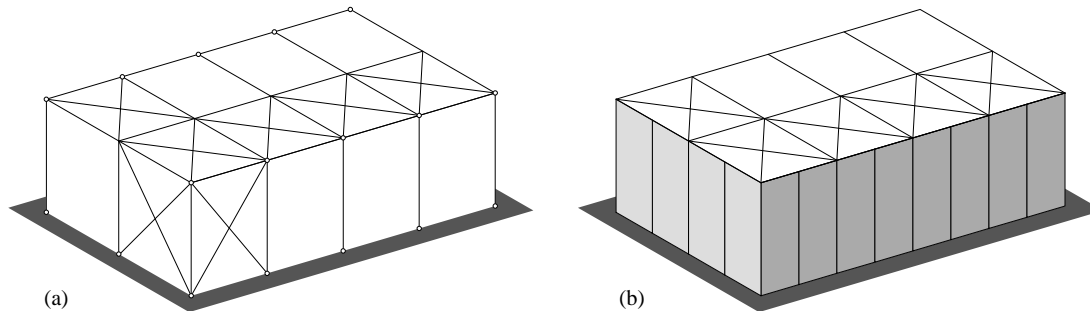


Figure 3.2 – Stabilization system in the pavilion (a) wind bracing (b) glass panel

Pavilions, using glass panel as stabilization system, can be divided in:

- **Transparent pavilions:** the pavilion is made of pinned steel frames and the glass panel has the only function to stabilize the pavilion transversally and longitudinally. Shear forces are taken by the glass panels while the vertical forces are carried by the steel frames.
- **Fully-transparent pavilions:** glass panels are the unique vertical elements in the pavilion; their function is to stabilize the pavilion as well as to carry all imposed vertical forces.

The primary functions and requirements that the stabilization system should fulfil are the following:

- **Force transfer:** all the forces acting on the structure should be transferred to the foundation and the force equilibrium at each point of the structure should be insured. The force transfer between the glass panels and the substructure should be guaranteed by connection devices. Glass, being a brittle material sensitive to stress concentration and contact with material of different hardness, adequate connection devices assuring smooth load path should be used.
- **Limitation of the deformation:** the deformation of the structure should be limited due to serviceability limit state. Additionally, the deformation can have a disadvantageous effect on the stability (effect of second order). The horizontal deformation of the pavilion is the sum of the glass panel deformation and the deformation of the connection devices.
- **Stabilization of the structure:** horizontally, the pavilion is stabilized by the roof surface. The vertical (longitudinal and transversal) stabilizations must be achieved by utilizing glass panel. The connection between roof and glass panels as well as between glass panels and foundation should create a support necessary to stabilize the entire structure.

As mentioned before, the roof in the pavilion should be rigid in horizontal direction to fulfil the primary stabilization function. Additionally, for fully transparent pavilion application, the roof must be rigid in the vertical direction also, forming the so called shear floor (in earthquake engineering term defining the roof and foundation infinitely rigid) because of the following favourable effects:

- The membrane effect and post-buckling behaviour in the glass panel can be achieved only if the roof is vertically rigid (Fig. 3.3(a)). In this case the tension and compression takes place diagonally (Section 3.3 and 3.4). Having soft roof which deforms vertically (Fig. 3.3(b)), the glass panel is not capable of creating tension diagonally and consequently neither a membrane effect nor post-buckling behaviour can be achieved. Therefore, the load carrying capacity of the glass panel is higher while the glass panel deformation is smaller in case of a rigid roof.

- In the case of openings in the façade or in case of breakage of one or more glass panels, a rigid roof allows a more homogeneous load repartition between the remaining glass panels (Fig. 3.3(c)) than a soft roof (Figure 3.3.d). The glass panel deformation is smaller within the rigid roof system giving higher residual safety to the system.

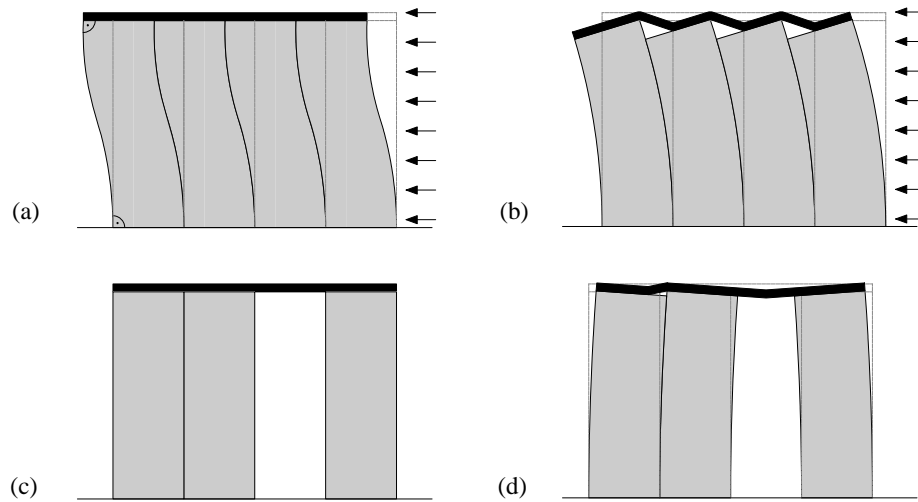


Figure 3.3 – Glass panel deformation (a) lateral load - rigid roof (b) lateral load - soft roof (c) façade openings or glass breakage - rigid roof (d) façade openings or glass breakage - soft roof

3.2.1 Actions on glass panel

An individual glass panel in a fully transparent pavilion (scratched glass panel in Fig. 3.4) can be subjected to the following actions [EN 1991]:

- In-plane shear force V due to wind in longitudinal direction (Fig. 3.4.(a))
- Out-of-plane bending force q due to wind in transversal direction (Fig. 3.4.(b))
- In-plane normal force N due to gravity loads of the roof, including its own weight (Fig. 3.4.(c))

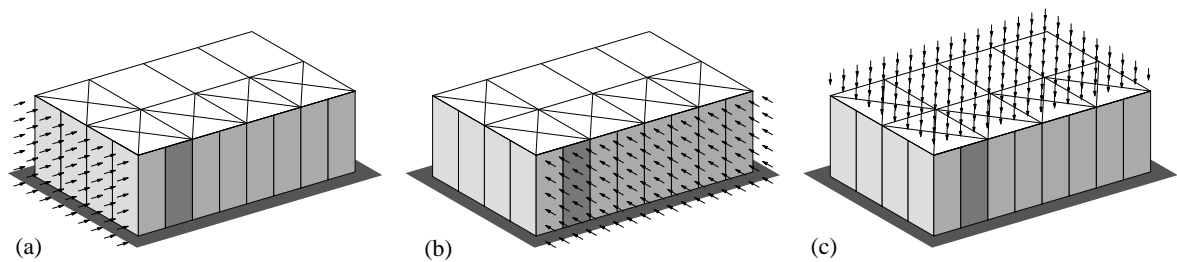


Figure 3.4 – Actions (a) in-plane shear force V (b) out-of-plane distributed load q (c) in-plane normal force N

The roofs of fully transparent pavilions are usually made of lightweight material such as steel, aluminium, fibre reinforced polymers or wood, while the pavilion foundation is usually made of concrete. The thermal expansion coefficients of these materials are slightly different from the thermal expansion coefficient of the glass (Table 3.5). Therefore, the temperature effect should be taken into consideration. Two solutions are possible: the glass panel resists the additionally imposed load due to different thermal expansion between the structural elements or that a constructive solution in the connection devices is made in order to avoid the additionally imposed load from the thermal expansions.

Table 3.5 – Thermal expansion coefficient α_T

Thermal expansion coefficient	Glass	Steel	Aluminium	Stainless steel	Concrete	GFRP
$\alpha_T \cdot 10^{-6} [K^{-1}]$	9	12	23	17	12	21~23

3.3 POINT SUPPORTED CONCEPT

The first concept developed in this work is a system of glass panel pointy connected to the substructure by bolts at four corners.

3.2.2 Standard point supported glass panel

In the following paragraph, a *standard point supported glass panel* is defined by the following geometrical and mechanical properties (Table 3.6, Fig. 3.7):

Table 3.6 – Geometrical and mechanical properties of a standard point supported glass panel

Geometrical properties			Material properties		
glass panel height	a [mm]	3500	glass modulus of elasticity	E [N/mm ²]	70'000
glass panel width	b [mm]	1200	glass Poisson's ratio	ν [-]	0.23
glass panel thickness	t [mm]	8/1.52/8	PVB shear modulus	G_{PVB} [N/mm ²]	0.50
hole-edge distance	c [mm]	100			
hole diameter	d [mm]	42			

The details of the connection devices between a glass panel and a substructure are illustrated in Figure 3.7(b). The steel pin and bolt are placed in the middle of the glass hole and they are fixed to the glass panel by steel cylinder. Between steel cylinder and glass panel the gasket made of POM is placed to avoid direct contact between glass and steel cylinder. The mortar is injected through the hole in the steel cylinder to fill the space between the pin and the hole. The connection device is attached to the substructure which is later connected to the roof and foundation.

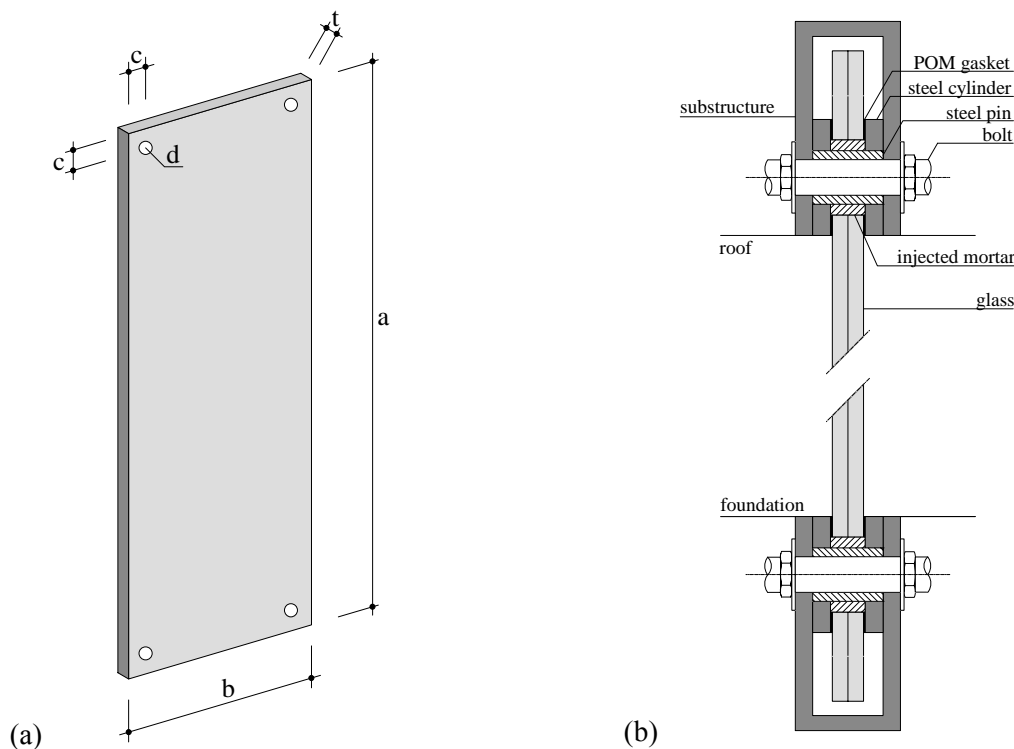


Figure 3.7 – Point support concept (a) glass panel (b) connection devices

Standard point supported glass panel is a base on which experimental and numerical investigation of shear buckling behaviour of point supported glass panel will be conducted.

3.2.3 Boundary conditions and actions on point supported glass panel

The glass panels in fully transparent pavilions can be subjected to in-plane shear force V , out-of-plane distributed load q and in-plane compression forces N (§3.2.1, Fig 3.4).

To avoid the load induced by different thermal expansions of glass and substructure the constructive solution is utilised. Thermal expansions of glass panels are not restrained in vertical direction because in fully transparent pavilions these are the unique vertical elements. On the other hand, in horizontal direction, the thermal expansion of the glass panel is restrained due to the foundation and the roof. Therefore, the support at point 3 is fixed in all directions, while other supports are free in horizontal direction allowing the expansion of the glass without introducing an additional load. Figure 3.8(a) shows the boundary conditions of point supported glass panels.

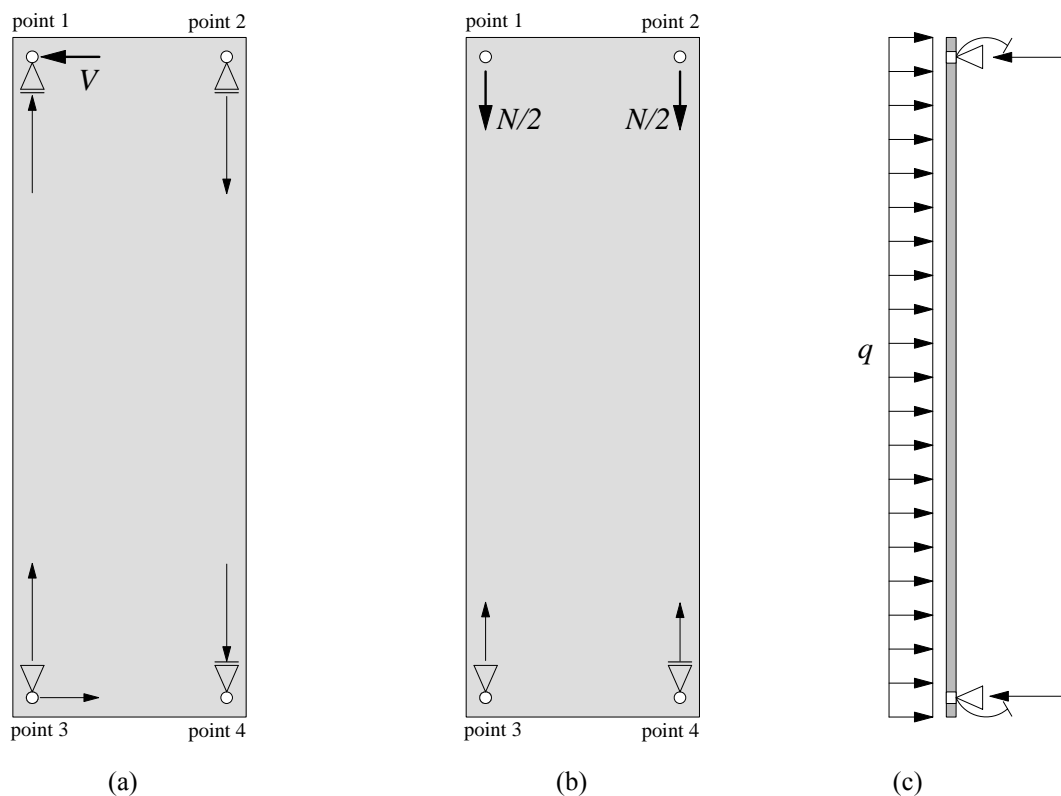


Figure 3.8 – Boundary conditions and support reactions for a point supported concept subjected to (a) in-plane shear force V (b) in-plane normal compression force N (c) out-of-plane distributed load q

The in-plane shear load V is introduced as a concentrated force at point 1 (Fig. 3.8(a)). The horizontal reaction occurs in the opposite direction of the introduced force at point 3. To keep the system in equilibrium, a pair of vertical reactions exists. The maximum reactions (resultant of vertical and horizontal reactions) take place at point 1 (tensile reaction) and at point 3 (compression reaction).

The in-plane normal force N is applied vertically as concentrated force through the point 1 and point 2 (Fig. 3.8(b)). The vertical reaction at point 3 and point 4 keep the system in equilibrium. In case of a very light roof and an open pavilion, the upward wind effect attempts to lift the roof and, consequently, introduce a tensile normal force in the glass pane.

The out-of-plane distributed load q acts perpendicular to the glass panel surface (Fig. 3.8(c)). Rotations around the supports are not allowed (rigid connection) and therefore reaction moments and forces take place.

3.3 LINEAR SUPPORTED CONCEPT

The second concept developed in this work is a system of glass panel linearly connected along its two short edges to the substructure by adhesives. Due to the fact that actual regulations do not allow adhesives to carry permanent loads, the setting blocks are added.

3.3.1 Standard linear supported glass panel

Geometrical and mechanical properties defining *standard linear supported glass panel* are chosen to be the following (Table 3.9, Fig. 3.10(a)):

Table 3.9 – Geometrical and mechanical properties of standard linear supported glass panel

Geometrical properties			Material properties		
glass panel height	a [mm]	3500	glass modulus of elasticity	E [N/mm ²]	70'000
glass panel width	b [mm]	1200	glass Poisson's ratio	ν [-]	0.23
glass panel thickness	t [mm]	8/1.52/8	PVB shear modulus	G_{PVB} [N/mm ²]	0.50
adhesive width	c_A [mm]	40			
adhesive thickness	t_A [mm]	9.5			
setting block width	d_A [mm]	100			
setting position	$b/5$ [mm]	240			

Figure 3.10(b) shows the connection detail of glass panel and its substructure (made of stainless steel to be compatible with the adhesive). The spacers are placed to keep the adhesive geometry constant during the drying period. The substructure is attached to the roof and the foundation by bolts, welding or other techniques that are not subject of this research.

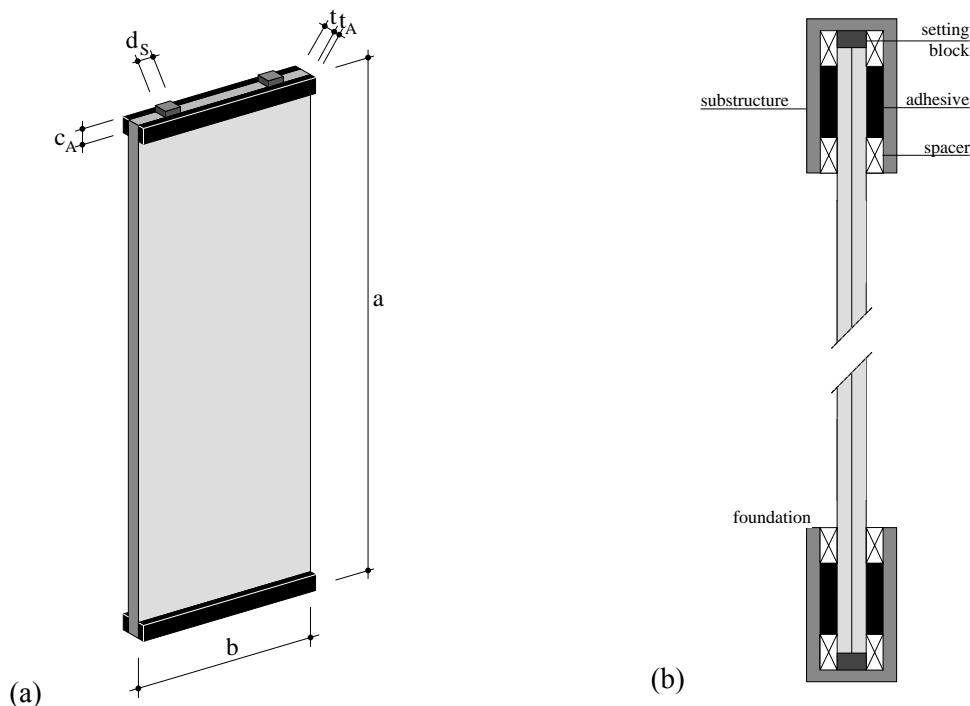


Figure 3.10 – Linear supported concept (a) glass panel (b) connection details

On standard linear supported glass panel the experimental and numerical investigation of shear buckling behaviour of linear supported glass panels will be performed.

3.3.2 Boundary conditions and actions on linear supported glass panels

The glass panels in fully transparent pavilions can be subjected to in-plane shear force V , out-of-plane distributed load q and in-plane compression forces N (§3.2.1, Fig 3.4). Figure 3.11 shows the boundary conditions and support reactions of linear supported glass panel for different load cases.

The in-plane shear force V is introduced into glass through the adhesive on top edge. A horizontal reaction takes place in the adhesive at the bottom edge. The vertical reactions keep the system in equilibrium. The setting blocks support the compression reaction (not being able to support tension reaction), while the adhesive supports the vertical tensile reaction (triangular distribution is assumed on half of the adhesive width) (Fig. 3.11(a)).

The in-plane compression force N is applied vertically through the upper setting blocks (Fig. 3.11(b)). The vertical reactions at the lower setting blocks keep the system in equilibrium. In case of light roof and open pavilion where the elevation of the roof can occur; a tensile reaction should be carried by the adhesive.

The out-of-plane distributed load q acts perpendicularly to the glass panel surface (Fig. 3.11(c)).

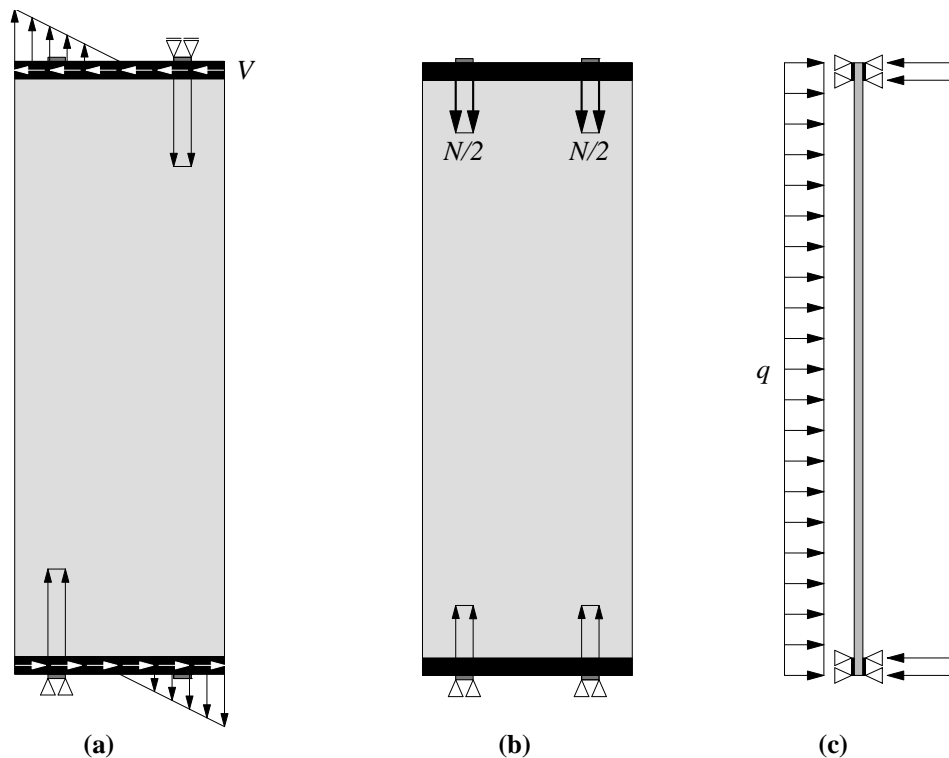


Figure 3.11 - Boundary conditions and support reactions for a linear supported concept subjected to (a) in-plane shear force V (b) in-plane normal compression force N (c) out-of-plane distributed load q

As the adhesive a structural silicon sealant will be utilized. It is a highly deformable elastic material that can be stretched to large deformations. As a consequence, the adhesive can compensate the differential deformation between thermal expansions of glass panel and roof or foundation.

3.4 SUMMARY AND CONCLUSIONS

This Chapter defines structural concepts on which shear buckling behaviour of glass panel will be studied and investigates a potential utilization of glazing in building stabilization.

The description of the building stabilization system and its primary functions are explained. The loads and actions on fully-transparent pavilions are determined. Based on these facts, two structural concepts were developed:

In the **Point support concept** the glass panel is attached to the substructure by bolted connections at the corners. Substructure is connected to the pavilion roof and *the* foundation. The geometrical and material properties of *standard point supported glass panel* are defined as well as the boundary conditions and support reactions for each of the load cases.

In the **Linear support concept** the glass panel is linearly connected to the substructure by adhesives on its two shortest edges. Setting blocks are used to transfer the permanent loads. The geometrical properties of *standard linear supported glass panel* are defined, in addition to boundary conditions and support reactions for different load cases.

The shear buckling behaviour of these two developed structural concepts will be studied in the following chapters by means of experimental investigation, numerical simulation and parametric study. First, the local behaviour of point support and linear support connection devices will be investigated. The most suitable connections will be implemented in full-size glass panels. Afterwards, the global behaviour of point supported and linear supported glass panels will be studied.

4 EXPERIMENTAL INVESTIGATION

4.1 INTRODUCTION

A set of experimental investigations was performed to study the local behaviour of the glass/substructure connection and identify the most suitable connection devices for point support and linear support concepts. To study the global behaviour of glass panel under in-plane shear force V , full size glass panels were tested with different boundary conditions and under different load cases. This Chapter describes the specimens and the testing procedure, giving the main results for each group of tests. Figure 4.1 presents the organization of Chapter 4.

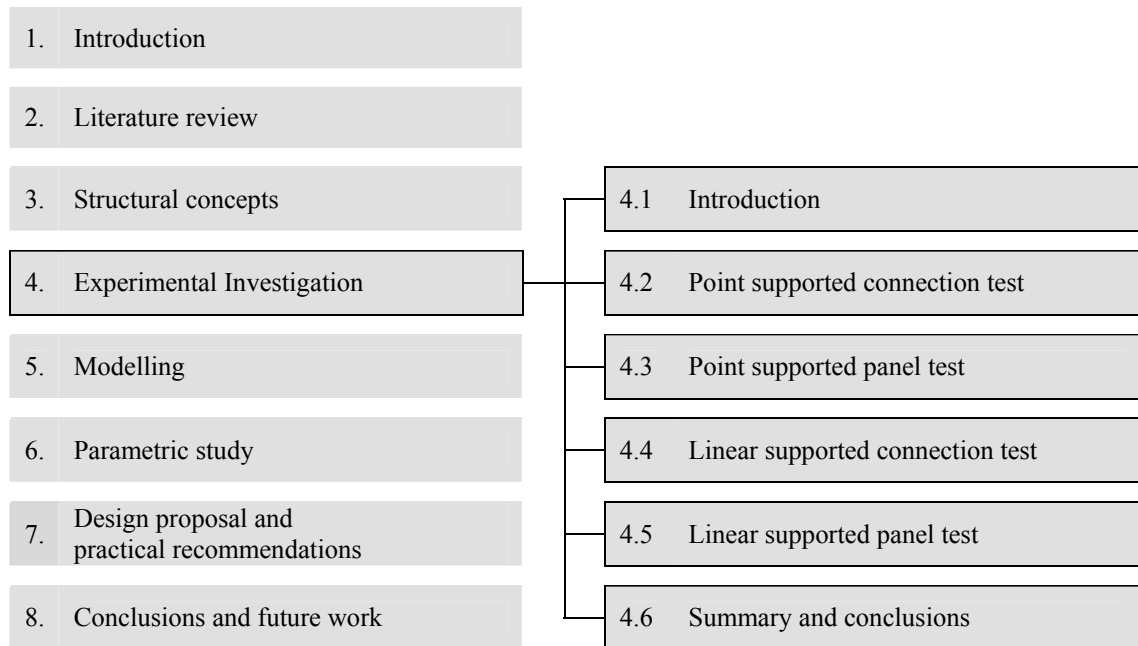


Figure 4.1 - Organization chart of Chapter 4

Point supported connection tests. This section describes three types of glass/substructure bolted connection devices that were developed and tested. They vary by load introduction path (axial and eccentric), connection systems (rigid and pinned), load directions (compression and tension), glass plate thicknesses (monolithic and laminated), and bolts diameters (M16 or M20).

Point supported panel tests. This section deals with the experimental investigation on shear buckling behaviour of point supported glass panels. From the point supported connection test, the most suitable connection devices were chosen to build three full-scale specimens. They were tested under different load cases: in-plane shear force V , interaction of out-of-plane distributed load q + in-plane shear force V and interaction of in-plane normal compression force N + in-plane shear force V .

Linear supported connection tests. To study the adhesive behaviour, two types of glass/substructure glued connections devices were developed. They varied by the number of glued sides (two sides and three sides) and load direction (longitudinal and transversal shear). Additional tests to study the potential use of mortar as setting block for load introduction were developed.

Linear supported panel tests. In this section the experimental investigation on shear buckling behaviour of linear supported glass panels are described. From previous tests, the most suitable glued connection type was chosen to build three full-scale specimens. They were tested under different load cases: in-plane shear force V , interaction of out-of-plane distributed load q + in-plane shear force V and interaction of in-plane normal compression force N + in-plane shear force V .

Summary and conclusions. The summary and the conclusions are written in the end of this Chapter.

4.2 POINT SUPPORTED CONNECTION TESTS

The objective of this test is to study the behaviour of different types of glass/substructure bolted connection devices on a small size specimen focusing on:

- longitudinal displacement of the specimen,
- horizontal displacement of the glass plate,
- stress distribution in the glass plate around the hole,
- specimen failure modes.

4.2.1 Specimen description

The specimen consisted of heat strengthened glass plate, measuring 200x500 mm with two holes (\varnothing 42mm) and bolted connection devices [Mocibob et al. 2007]. Mortar Hilti HIT HY 50 [HILTY 2003] was injected into glass hole. Regarding the connection devices three test types were developed:

- **Axial rigid test, AR:** the force F in glass plate was introduced axially in its centre line. The connection between bolts and glass was rigid. The bolted connection device consisted of bolt M20, steel pin and steel cylinder. Between the steel cylinder and the glass a POM was placed. The specimens were tested under tensile F_t and compressive F_c forces (Figure 4.2).
- **Eccentric rigid test, ER:** the force F was introduced eccentrically (60mm) from the glass plate centre line. The connection between glass and bolt was rigid. The bolted connection device was the same as the one described in axial rigid test. In addition to the bolted connection device utilising bolts M20, an investigation on bolted connection device utilising bolts M16 was performed. The specimens were tested under tensile F_t and compressive F_c forces (Figure 4.3).
- **Eccentric pinned test, EP:** the load F was introduced eccentrically (60mm) from the glass plate centre line. The connection between glass and bolts was articulated. The bolted connection devices were produced by SADEV and consisted of bolt M16, with articulation and connection head. The centre of the articulation was not in the glass plate centre line, but at the glass plate surface. The specimens were tested under tensile F_t and compressive F_c forces (Figure 4.3).

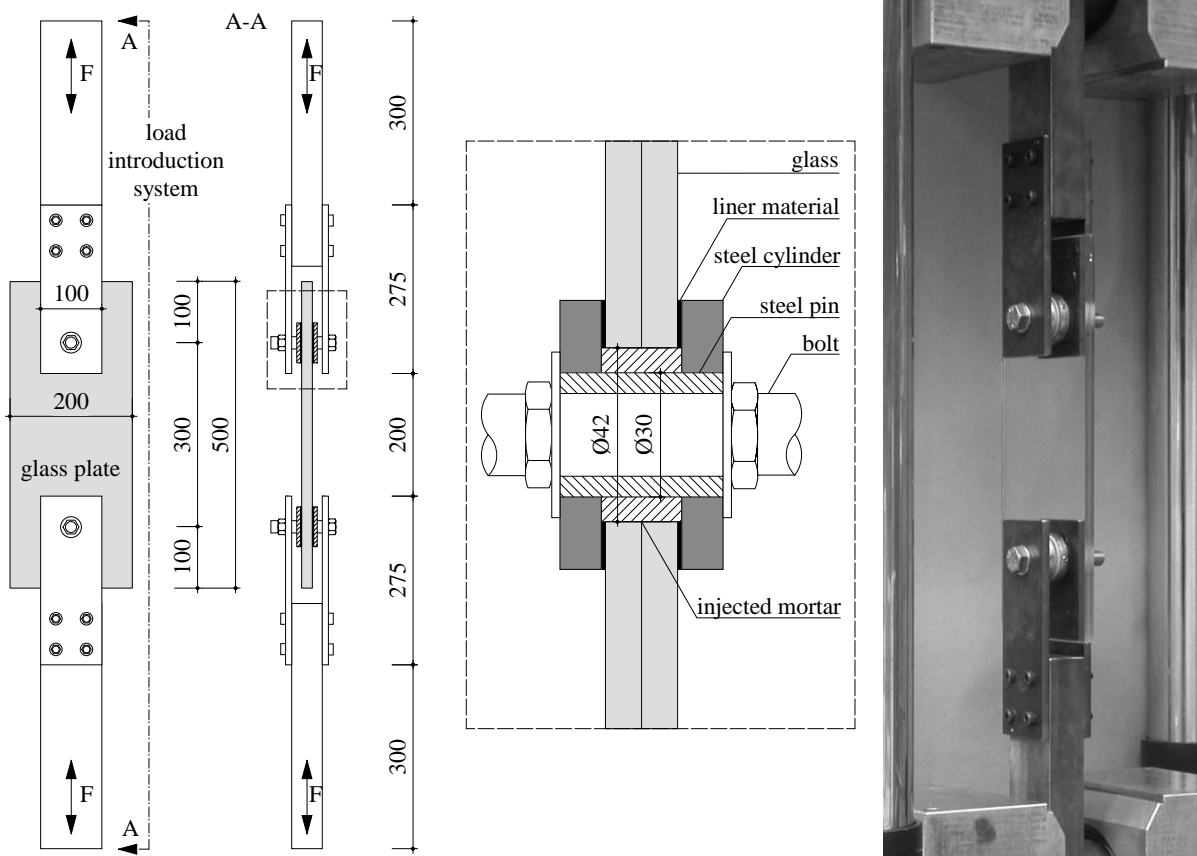


Figure 4.2 – Axial rigid connection: plan view, side view, connection devices and specimen photo

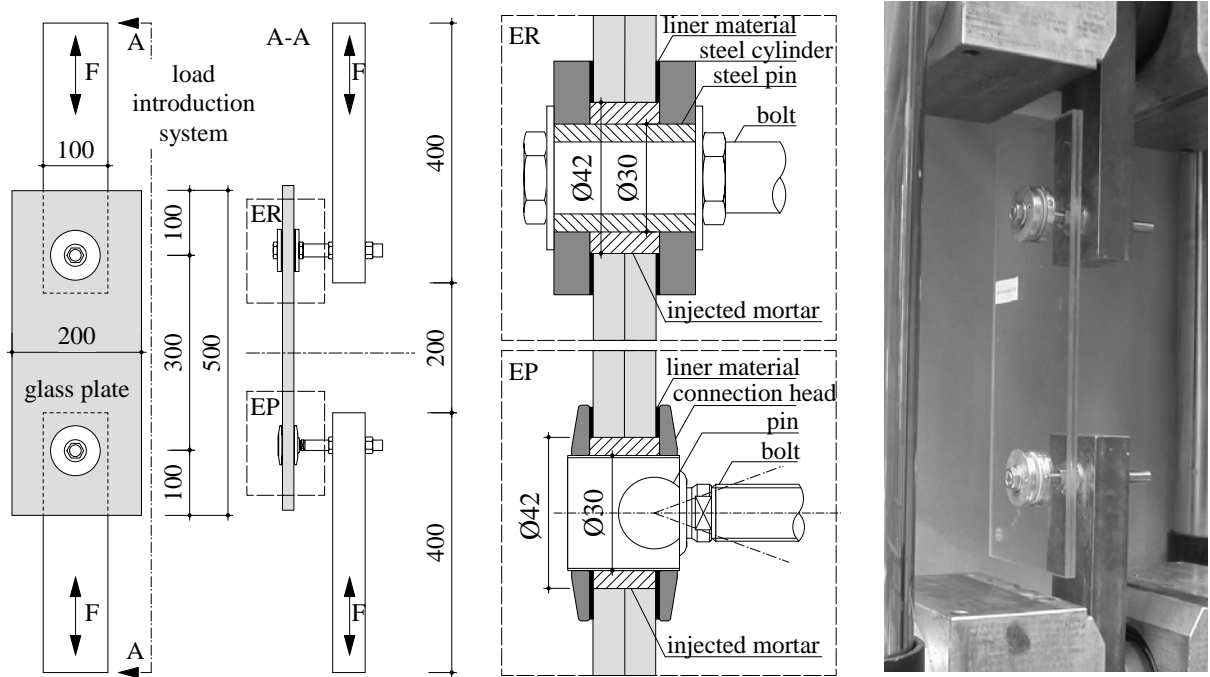


Figure 4.3 - Eccentric rigid and eccentric pinned connection: plan view, side view, connection devices and specimen photo

Table 4.4 shows the deformation and internal force distributions in the specimens (N and M diagram) for different test types subjected to tension and compression. The force F in axial rigid test AR introduces the normal force in the glass plate and displaces the specimen longitudinally in-plane δ_l . In the eccentric rigid test ER , due to eccentricity, the force F introduces, in addition to the normal force, a moment in the glass plate. The specimen displaces longitudinally in-plane δ_l and horizontally out-of-plane δ_h . In the eccentric pinned test EP the force F introduces a normal force in the glass plate, but also a small moment due to articulation position on the surface line and not on the centre line of the glass plate; the specimen displaces longitudinally in-plane δ_v and horizontally out-of-plane δ_h .

Table 4.4 – Point support connection tests: specimen deformation and internal forces distribution

	Axial rigid test		Eccentric rigid test			Eccentric pinned test		
	deformation	N diagram	deformation	N diagram	M diagram	deformation	N diagram	M diagram
tensile force								
compressive force								

Three different glass plate thicknesses were tested: 6 mm monolithic glass plates m (1x6), 2x6 mm laminated glass plate with 1.52 mm of PVB interlayer and 2x8 mm laminated glass plate with 1.52 mm of PVB interlayer. Three different glass companies supplied the glass plates: Pilkington, VIM (Verre Industriels Moutier) and GlasTrösch. The residual stresses σ_{res} on the glass surface (measured using Stress Measuring Devices “Gartner Scientific” [Gartner 2002]), glass thicknesses t_g , the glass plate widths b and glass hole diameters d were measured. Table 4.5 shows the nominal values, the average measured values, the extreme values (min. and max.) and the standard deviation for the 6 mm monolithic glass plate.

Table 4.5 – Measurements on 6 mm monolithic glass plate

	Pilkington				VIM				Glas Trösch			
	σ_{res} [N/mm ²]	t [mm]	b [mm]	d [mm]	σ_{res} [N/mm ²]	t [mm]	b [mm]	d [mm]	σ_{res} [N/mm ²]	t [mm]	b [mm]	d [mm]
nominal	35-55	6.00	200.0	42.00	35-55	6.00	200.0	42.00	35-55	6.00	200.0	42.00
average	52.35	5.89	199.7	42.62	50.40	5.84	202.5	42.13	55.62	5.92	200.3	42.03
min	49.08	5.91	200.0	42.9	49.08	5.85	202.8	42.18	52.35	6.01	200.7	42.06
max	55.62	5.85	199.0	42.34	52.35	5.82	202.3	42.01	58.9	5.85	199.8	42.01
st. dev.	2.31	0.025	0.373	0.207	2.92	0.009	0.173	0.042	2.32	0.070	0.371	0.017

Summary

The specimens differ by test types (axial rigid test, eccentric rigid test and eccentric pinned test), the force direction (tension and compression), the glass plate thickness (1x6, 2x6, 2x8) and the bolts diameter (M16, M20). For each parameter set, three specimens were built, resulting in totally 72 specimens. The specimen name is the abbreviation of the mentioned parameters, e.g. specimen ER-C-16-2x6-1 means eccentric rigid test (ER) under compression force (C) with M16 bolts (16), 2x6 laminated glass panel and first of the three series (1). Table 4.6 shows the summary of the tested specimens and their parameters.

Table 4.6 - Specimens summary for point supported connection tests

Test under tension force F_t				Test under compressive force F_c			
Specimens name	Bolt diameter [mm]	Glass thickness [mm]	Number of specimens	Specimens name	Bolt diameter [mm]	Glass thickness [mm]	Number of specimens
Axial rigid test				Axial rigid test			
AR-T-20-1x6	M20	6	3	AR-C-20-1x6	M20	6	3
AR-T-20-2x6		6/1.52/6	3	AR-C-20-2x6		6/1.52/6	3
AR-T-20-2x8		8/1.52/8	3	AR-C-20-2x8		8/1.52/8	3
Eccentric rigid test				Eccentric rigid test			
ER-T-20-1x6	M20	6	3	ER-C-20-1x6	M20	6	3
ER-T-20-2x6		6/1.52/6	3	ER-C-20-2x6		6/1.52/6	3
ER-T-20-2x8		8/1.52/8	3	ER-C-20-2x8		8/1.52/8	3
ER-T-16-1x6	M16	6	3	ER-C-16-1x6	M16	6	3
ER-T-16-2x6		6/1.52/6	3	ER-C-16-2x6		6/1.52/6	3
ER-T-16-2x8		8/1.52/8	3	ER-C-16-2x8		8/1.52/8	3
Eccentric pinned test				Eccentric pinned test			
EP-T-16-1x6	M16	6	3	EP-C-16-1x6	M16	6	3
EP-T-16-2x6		6/1.52/6	3	EP-C-16-2x6		6/1.52/6	3
EP-T-16-2x8		8/1.52/8	3	EP-C-16-2x8		8/1.52/8	3

4.2.2 Test set-up and test instrumentation

The specimens were prepared (assembling of connection devices and injection of the mortar) and tested (using testing machine SCHENCK) at the Structural Engineering Laboratory of EPFL, Lausanne (Switzerland) between September 2005 and March 2006. Tests were done 24 hours after the injection of the mortar, under constant environmental conditions (humidity 60% and temperature 23°C). The specimens were tested under displacement control with constant increments of 2.4 mm/min. For the measurements during the test and data acquisition, the software Catman was used.

The applied force F and the longitudinal displacement δ_l were measured directly by the testing machine. Additionally, the specimens were instrumented by six inductive transducers: V_1 and V_3 measured the longitudinal displacements of the glass between two connection devices; V_2 measured the longitudinal displacement between two connection devices (which account the longitudinal glass displacement as well as mortar deformation), while H_1 , H_2 and H_3 measured the horizontal out-of-plane displacement of the glass panel at the position of connection devices (H_1 and H_3) and in the middle of the glass plate span (H_2). The location and arrangements of the inductive transducers is shown in Figure 4.7

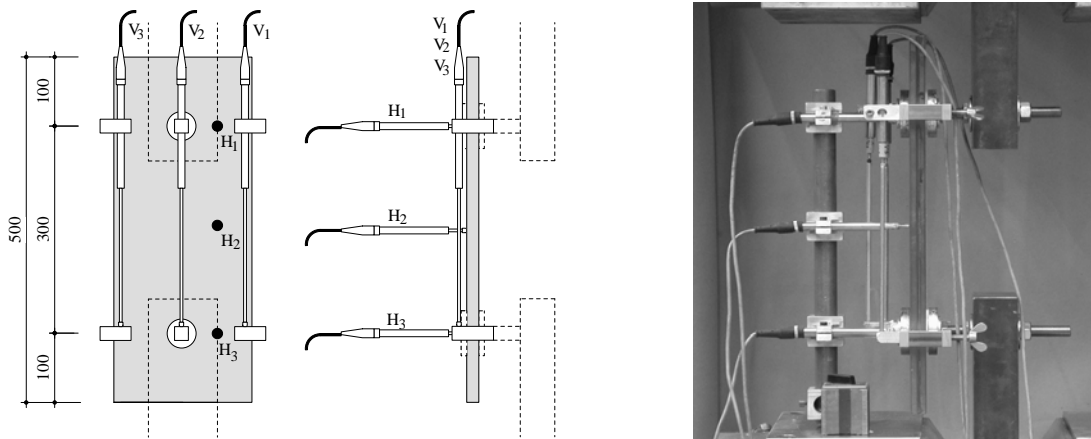


Figure 4.7 – Location and arrangements of inductive transducers

To measure the strain during the tests, two specimens were instrumented with strain gauges. At the front-side and back-side of the glass plate, around the upper hole, five rosette gauges (j11-j15, j21-j25) were glued at 0°, 45°, 90°, 135° and 180°, 40 mm from the glass hole centre (Figure 4.8). The rosette gauges measured the strain in local coordinate system. Additionally, on both sides of the plate, in the middle of the span, uni-directional strain gauges were glued (j10, j20). Specimens instrumented with strain gauges were tested in the elastic domain up to 50% of the estimated failure load. Strains were measured during axial rigid, eccentric rigid and eccentric pinned test, under tension and compression.

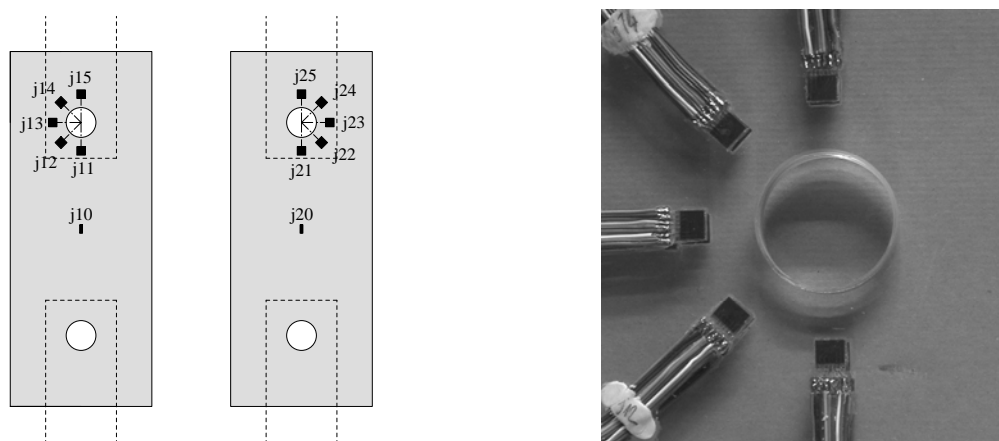


Figure 4.8 – Location and arrangements of strain gauges

4.2.3 Test results

4.2.3.1 Force F vs. longitudinal specimen displacement δ_L

Testing machine measured the applied force F and longitudinal specimen displacement δ_L (consisting of glass plate elongation and deformation of the connection devices). Tables 4.9 and 4.10 show the value of the force at the failure $F_{failure}$, longitudinal specimen displacement at failure $\delta_{L,failure}$ and failure modes for each specimen. The following failure modes occur: mortar failure (Mor), glass failure due to tension in net section (TNS), glass failure due to splitting tension (ST) and glass failure combination of tension in net section + bending (TNS+B) and splitting tension and bending (ST+B). More details about the failure modes are given in §4.2.3.4.

Table 4.9 – Test under compressive force, F_c

	Specimen name	$F_{failure}$ [kN]	$\delta_{L,failure}$ [mm]	Failure mode
Axial rigid test	AR-C-20-1x6-1	19.12	6.97	Mor
	AR-C-20-1x6-2	18.92	5.70	Mor
	AR-C-20-1x6-3	19.48	7.55	Mor
	AR-C-20-2x6-1	33.68	2.54	ST
	AR-C-20-2x6-2	30.44	2.25	ST
	AR-C-20-2x6-3	23.52	2.33	ST
	AR-C-20-2x8-1	48.88	2.34	ST
	AR-C-20-2x8-2	46.04	2.64	ST
	AR-C-20-2x8-3	51.12	2.51	ST
Eccentric rigid test	ER-C-20-1x6-1	11.60	7.26	ST + B
	ER-C-20-1x6-2	15.44	11.53	ST + B
	ER-C-20-1x6-3	11.96	7.34	ST + B
	ER-C-20-2x6-1	16.76	8.39	ST + B
	ER-C-20-2x6-2	17.44	10.26	ST + B
	ER-C-20-2x6-3	18.28	10.23	ST + B
	ER-C-20-2x8-1	22.80	10.80	ST + B
	ER-C-20-2x8-2	21.08	9.67	ST + B
	ER-C-20-2x8-3	19.00	10.32	ST + B
	ER-C-16-1x6-1	8.00	8.22	ST + B
	ER-C-16-1x6-2	7.64	12.63	ST + B
	ER-C-16-1x6-3	9.60	9.40	ST + B
	ER-C-16-2x6-1	11.24	9.68	ST + B
	ER-C-16-2x6-2	12.04	11.33	ST + B
	ER-C-16-2x6-3	12.04	12.19	ST + B
	ER-C-16-2x8-1	8.00	12.49	ST + B
	ER-C-16-2x8-2	7.64	8.61	ST + B
	ER-C-16-2x8-3	9.60	8.77	ST + B
Eccentric pinned test	EP-C-16-1x6-1	7.00	6.25	ST + B
	EP-C-16-1x6-2	9.96	9.86	ST + B
	EP-C-16-1x6-3	8.32	8.08	ST + B
	EP-C-16-2x6-1	12.96	12.36	ST + B
	EP-C-16-2x6-2	12.84	11.72	ST + B
	EP-C-16-2x6-3	11.76	8.87	ST + B
	EP-C-16-2x8-1	15.2	12.22	ST + B
	EP-C-16-2x8-2	17.04	18.87	instable
	EP-C-16-2x8-3	15.32	20.12	instable

Table 4.10 – Test under tensile force, F_t

	Specimen name	$F_{failure}$ [kN]	$\delta_{L,failure}$ [mm]	Failure mode
Axial rigid test	AR-T-20-1x6-1	14.34	3.96	Mor
	AR-T-20-1x6-2	15.08	7.78	Mor
	AR-T-20-1x6-3	12.05	1.75	TNS
	AR-T-20-2x6-1	24.56	3.58	Mor
	AR-T-20-2x6-2	20.04	2.92	TNS
	AR-T-20-2x6-3	32.80	2.33	TNS
	AR-T-20-2x8-1	38.92	1.58	TNS
	AR-T-20-2x8-2	39.48	2.23	TNS
	AR-T-20-2x8-3	49.80	2.78	TNS
Eccentric rigid test	ER-T-20-1x6-1	8.60	3.21	TNS + B
	ER-T-20-1x6-2	10.65	4.68	TNS + B
	ER-T-20-1x6-3	9.80	5.37	TNS + B
	ER-T-20-2x6-1	10.48	4.88	TNS + B
	ER-T-20-2x6-2	16.16	7.92	TNS + B
	ER-T-20-2x6-3	11.20	3.74	TNS + B
	ER-T-20-2x8-1	14.44	4.87	TNS + B
	ER-T-20-2x8-2	16.84	6.06	TNS + B
	ER-T-20-2x8-3	10.80	3.47	TNS + B
	ER-T-16-1x6-1	5.68	5.01	TNS + B
	ER-T-16-1x6-2	6.76	6.62	TNS + B
	ER-T-16-1x6-3	7.44	6.41	TNS + B
	ER-T-16-2x6-1	8.84	7.75	TNS + B
	ER-T-16-2x6-2	9.24	7.89	TNS + B
	ER-T-16-2x6-3	8.56	6.35	TNS + B
	ER-T-16-2x8-1	11.68	7.83	TNS + B
	ER-T-16-2x8-2	9.84	5.62	TNS + B
	ER-T-16-2x8-3	9.76	5.52	TNS + B
Eccentric pinned test	EP-T-16-1x6-1	9.08	7.45	TNS + B
	EP-T-16-1x6-2	9.28	8.57	TNS + B
	EP-T-16-2x6-1	12.56	8.61	TNS + B
	EP-T-16-2x6-2	13.64	15.32	TNS + B
	EP-T-16-2x6-3	14.52	10.95	TNS + B
	EP-T-16-2x8-1	17.28	18.72	TNS + B
	EP-T-16-2x8-2	15.92	14.74	TNS + B
	EP-T-16-2x8-3	12.64	11.23	TNS + B

Figure 4.11(a) shows compressive force F_c (left hand side of the graph) and tensile force F_t (right hand side of the graph) vs. longitudinal specimen displacement δ_L for axial rigid test AR, for each of the

glass thickness (only one test curve for each specimen type is plotted). Thicker glass plates gave higher stiffness and higher resistance to the specimen. The failure mode of the specimens can be identified from the graphs: the simultaneous failure of sheets in laminated glass (A-T-20-2x8), the successive failure of sheets in laminated glass (A-C-20-2x6) and failure of glass plate preceded by smashing of the mortar due to high compression stresses in the mortar (A-T-20-1x6). The curves for compressive and tensile cases, demonstrate similar behaviour.

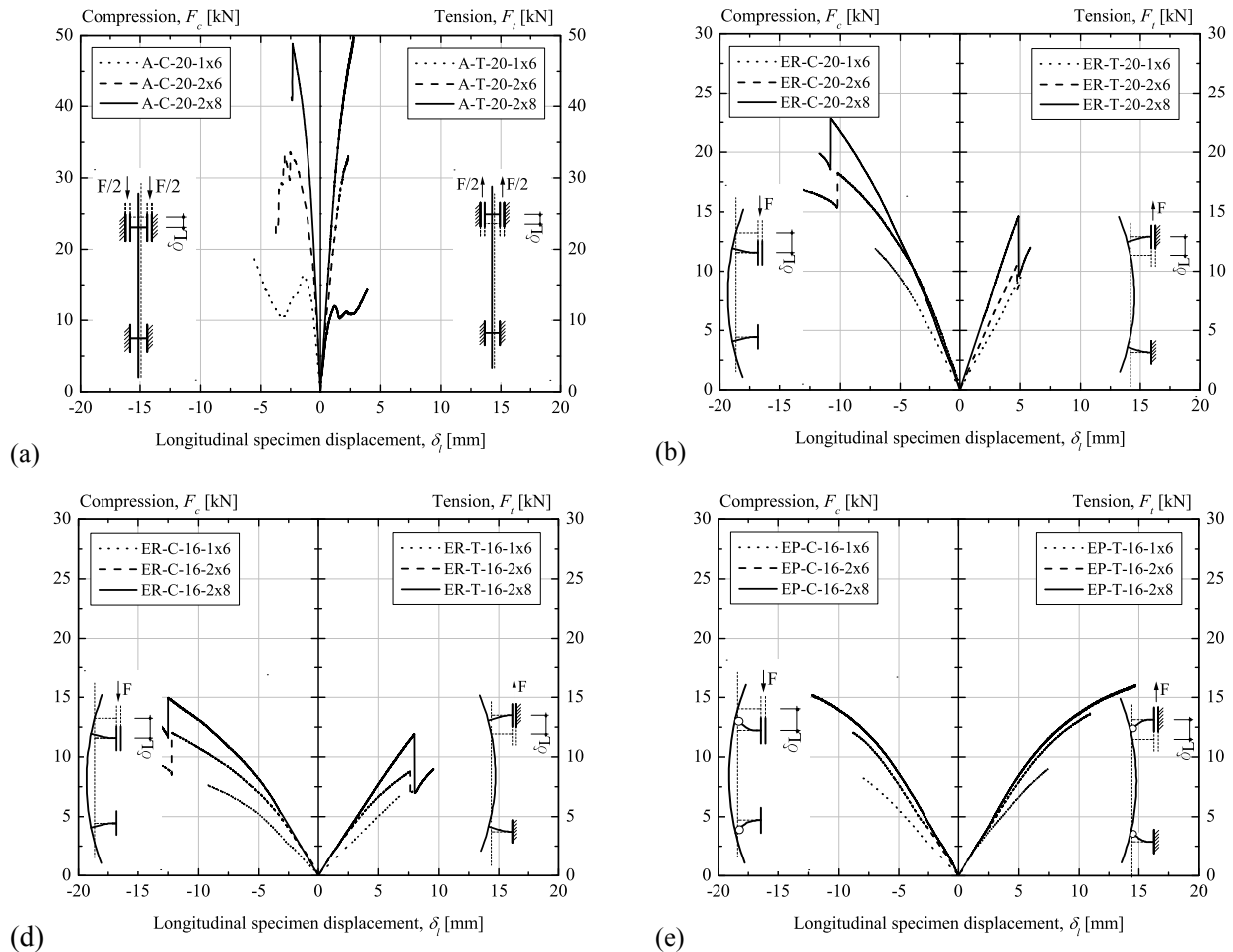


Figure 4.11 - Force F vs. longitudinal specimen displacement δ_l (a) axial rigid test AR (b) eccentric rigid test, ER, with M20 (c) eccentric rigid test, ER, with M16 (d) eccentric pinned test EP

Figures 4.11(b) and 4.11(c) show the compressive F_c and tensile forces F_t vs. longitudinal specimen displacement δ_l for eccentric rigid test ER with bolts M20 and M16. Due to additional moment in the glass plate introduced from force eccentricity, the specimen showed a drastically smaller resistance with higher displacement than in the axial rigid test. The strongest bolts M20 give higher rigidity and higher resistance to the specimen than the weaker bolts M16. Moreover, the specimens subjected to compression force demonstrate a slightly higher resistance than those under tension force. In all the ER tests with laminated glass (2x6 and 2x8), failure of glass sheets occurred successively.

Figure 4.11(d) shows the compressive F_c and tensile forces F_t vs. the longitudinal specimen displacement δ_l for the eccentric pinned EP case. Again, thicker glass plates gave higher stiffness and higher resistance to the specimen. The specimens demonstrated quite a high displacement. When subjected to compression and tension the specimens demonstrated similar resistance and displacements. In all laminated glass cases, the failure of both glass layers occurred simultaneously. The specimens showed an important ductility due to bolt yielding caused by high moment introduced by force eccentricity.

4.2.3.2 Force F vs. horizontal glass displacement δ_h

Horizontal glass displacement δ_h corresponds to the difference between the horizontal specimen displacement measured with inductive transducers H_2 (δ_{h2}) and average horizontal specimen displacement measured with inductive transducer H_1 (δ_{h1}) and H_3 (δ_{h3}), see Figure 4.7

$$\delta_h = \delta_{h2} - \left(\frac{\delta_{h1} + \delta_{h3}}{2} \right) \quad (4.1)$$

In the axial rigid tests AR , no significant horizontal displacement occurred. In the eccentric rigid ER and eccentric pinned tests EP significant horizontal displacements were recognized for both force directions - compression and tension (Fig. 4.12).

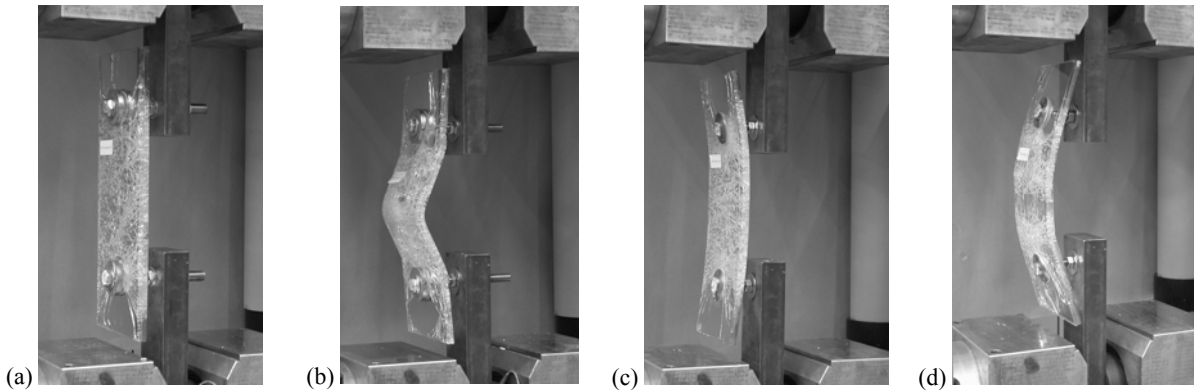


Figure 4.12 – Horizontal displacement δ_h (a) ER under tension (b) ER under compression (c) EP under tension (d) EP connection under compression

Figure 4.13(a) shows compressive F_c and tensile force F_t vs. horizontal glass displacements δ_h in eccentric rigid test ER with bolt M20. Thicker glass panels demonstrate smaller horizontal displacements. The horizontal glass displacement under tensile forces was increasing linearly, while the horizontal glass displacement under compressive force increased linearly only initially, while reaching a certain limit start to deviate from linearity. This happened due to stability phenomena when reaching the critical compressive load (normal force combined with the high moment due to force eccentricity)

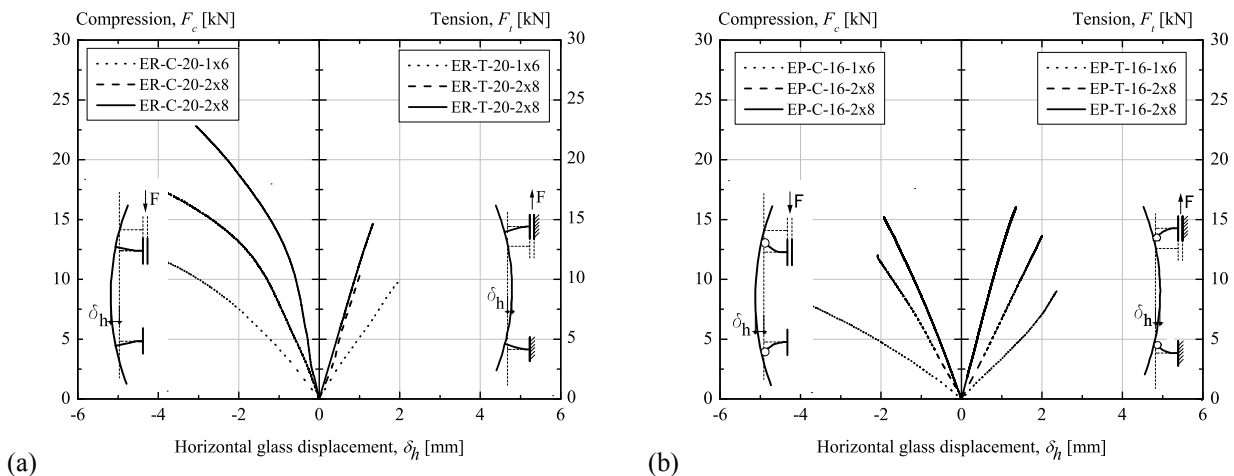


Figure 4.13 Force F vs. horizontal glass displacement δ_h (a) eccentric rigid test (b) eccentric pinned test

Figure 4.13(b) shows compressive F_c and tensile force F_t vs. horizontal glass displacement δ_h in eccentric pinned test EP . As in eccentric rigid test before, thicker glass panels demonstrate a smaller horizontal displacement. Horizontal glass displacements under compressive and tensile forces were increasing linearly. No stability problem was observed in specimens under compressive forces (normal force combined with very small moment caused by eccentricity of the pin).

4.2.3.3 Principal tension stress distribution σ_I

Distribution of principal tensile stresses σ_I on glass surface, on front and back-sides, 40 mm from centre of upper hole, are presented in this section (strain gauges location and arrangement are shown in Fig. 4.8). Figure 4.14 shows the distribution of principal tensile stresses σ_I for different values of applied force F for axial rigid test AR and eccentric rigid test ER in specimens with glass thickness $2X8$. The left hand side of each graph presents the stress distribution at front-side (empty dots, strain gauges j11-j15) while the right hand side of the graph presents stress distribution on back-side (full dots, stain gauges j21-j25) of the glass plate. In ideal case of axial rigid test, the two sides should show the same stress values, due to axial force introduction, but in reality it is not the case, because small force eccentricity exists, which causes different stresses on front and back sides of the glass plate.

Figure 4.14(a) shows the principal tensile stress distribution σ_I for different values of tensile force F_t (5, 10, 15 and 20 kN) in axial rigid test AR . It is observed that maximal principal tensile stresses were measured at $225^\circ/315^\circ$ at front side and $45^\circ/135^\circ$ at back side of the glass plate. The minimal principal tensile stress was measured at 180° . Figure 4.14(b) shows the principal stress distribution σ_I for different values of the compressive force F_c of 5, 10, 15 and 20 kN in axial rigid test AR . The maximal value of the stress was measured at 180° and the minimal at 0° .

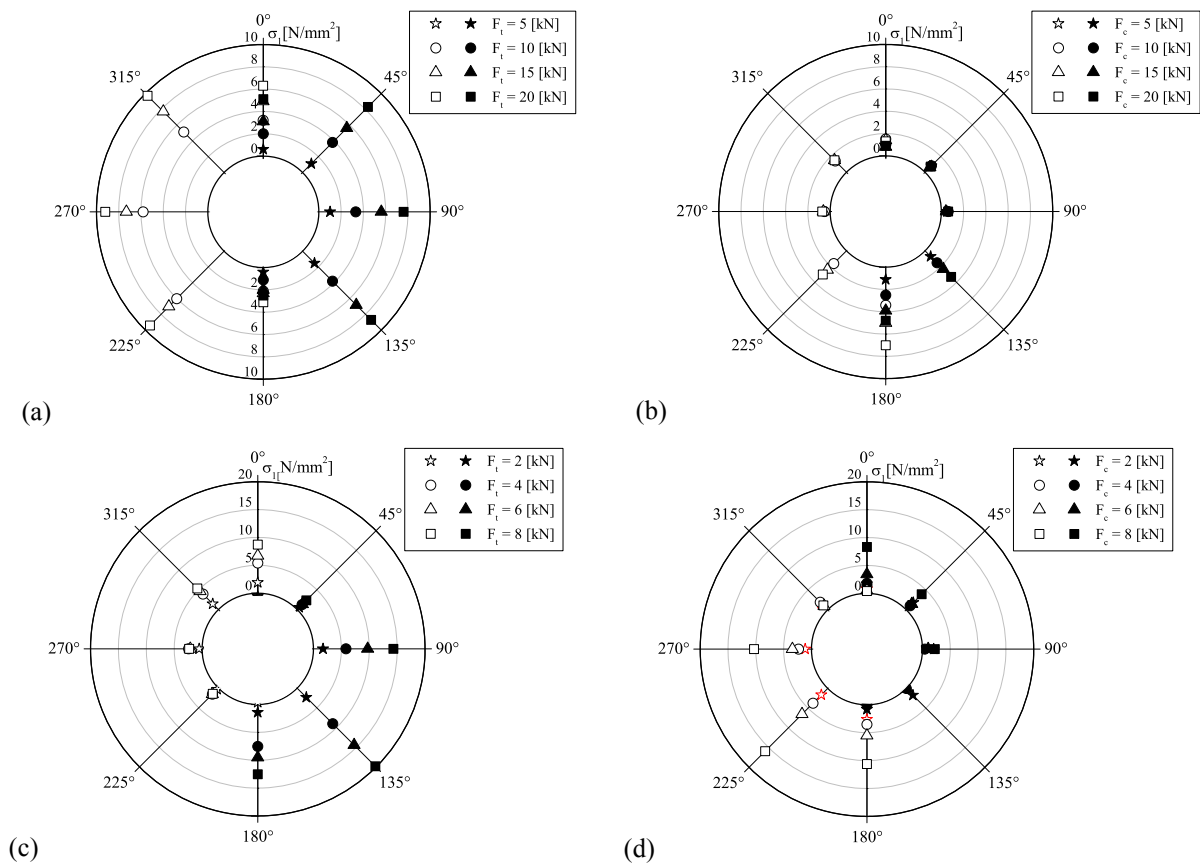


Figure 4.14 - Principal tensile stress σ_I distribution on glass surface at 40mm from the hole centre for different values of applied force (a) axial rigid test under tensile force (b) axial rigid test under compressive force (c) eccentric rigid test with M20 under tensile force; (d) eccentric rigid test with M20 under compressive force

Figure 4.14(c) shows the principal stress distribution σ_I for different values of the tensile force F_t (2, 4, 6 and 8 kN) in eccentric rigid test ER with bolts $M20$. The front and back sides show different stress distributions due to moment introduced by the eccentricity of the force. The maximal principal tensile stress was measured at the back side of the glass plate at 135° , while the minimum at the front side was at 180° . Opposite behaviour was observed in eccentric rigid test ER under compressive force F_c , where maximal stress was measured at the front side at 225° and the minimum at the back side at 180° .

4.2.3.4 Failure mode

Specimens under tensile force F_t failed due to *tension in the net section (TSN)*. The initial failure occurred due to stress concentration on the glass hole, perpendicular to the force direction, at the place of maximal tensile stresses. Specimens in axial rigid test failed only because of tension in net section (Fig. 4.15(a)) while specimens in eccentric rigid and eccentric pinned tests failed due to combination of tension in net section and bending caused by the force eccentricity (*TSN+B*) (Fig. 4.15(b)).

Specimens under compressive force F_c failed due to *splitting tension (ST)*. This failure mode occurred when high compressive forces were introduced into the glass plate between two bolts. Perpendicular to this compression field, due to Poisson's ratio, a tensile stresses existed which led to failure and crack propagation in the longitudinal direction of the specimen. The crack initiation was due to stress concentration at the glass hole, in the compressive force direction, at the place of maximal tensile stresses. After the first occurrence of a longitudinal crack in the middle of the glass plate, the specimen was still able to resist additional forces. As the force increased, more longitudinal cracks occurred. Specimens in the axial rigid test failed only because of splitting tension (Fig. 4.15(c)) while specimens in eccentric rigid and eccentric pinned test failed because of a combination of splitting tension and bending (*ST+B*) (Fig. 4.15(d))

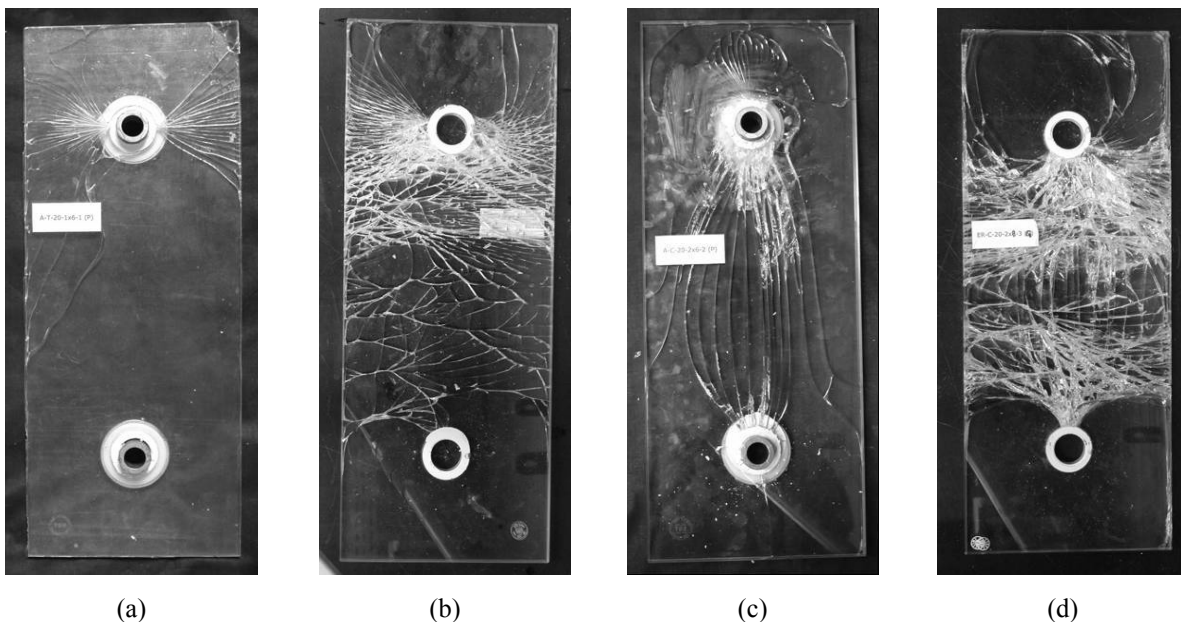


Figure 4.15 – Specimen failure modes (a) axial rigid test under tension (b) eccentric rigid test under tension (c) axial rigid test under compression (d) eccentric rigid test under compression

Laminated glass specimens (2x6 and 2x8), with eccentric rigid connection demonstrate residual resistance - the laminated glass sheets failed successively – firstly the inner glass sheet failed, but the system had a sufficient resistance to withstand further force until failure of the second sheet took place, which corresponded to system failure. The same failure scenario was recognised for specimens subjected to compression and tension.

In the specimens with monolithic glass (1x6) and axial rigid connection subjected to compression or tension, smashing of the mortar occurred due to high compressive stresses introduced by the bolts on small mortar area (*Mor*). Such specimens were still able to sustain the applied force until the failure of the glass plate due to tension in net section (specimens under tension) or splitting tension (specimens under compression) occurred.

4.3 POINT SUPPORTED PANEL TEST

Experimental investigation of Point support connection test lead to the conclusion that axially rigid connection is the most suitable of the investigated connection devices for load introduction and load transfer between the substructure and the glass plate. This kind of connection gave the specimen a small deformation, high resistance and consequently higher stiffness which offer the maximum potential for the use of glass as load-bearing element for stabilization of fully transparent pavilions.

The objective of the test presented in this section is to study the global behaviour of point supported full-size glass panel (with axially rigid connection) under different load cases focusing on following:

- global deformation of the glass panel for different load cases,
- stress distribution in the glass panel for different load cases,
- failure mode of the glass panel.

4.3.1 Specimen description

The specimen consisted of a glass panel, four connection devices and four substructures (Figure 4.16) [Mocibob et al.2007.1]. The glass panel was made of two layered laminated heat strengthened glass. The thickness of each glass sheet was 8 mm and the thickness of PVB interlayer was 1.52mm. Glass panel dimension was chosen to be 1200x3500mm which corresponds to real-size façade elements commonly used for building envelopes. Before heat strengthening and lamination of glass panels, four holes ($d=42\text{mm}$) were drilled in the corners of each glass sheet. For the point support connection devices, axially rigid connections were used (described in §4.2.1) with the only difference that stronger mortar Hilti HIT HY 70 [Hilti 2007] was utilised instead of Hilti HIT HY 50 [Hilti 2003] to avoid the mortar smash. The substructure consisted of two 100mm wide LNP 100x200x12 profiles made of steel S355. Three identical specimens were built and subjected to different load cases:

- **P1 (V)** the specimen was subjected to increasing in-plane shear force V (load case V).
- **P2 ($q+V$)** the specimen was subjected simultaneously to constant out-of-plane distributed load q ($q=0.4\text{ kN/m}^2$ – representing the wind load) and increasing in-plane shear force V .
- **P3 ($N+V$)** the specimen was subjected simultaneously to constant in-plane normal force N ($N=20\text{ kN}$ – representing the weigh of the roof) and increasing in-plane shear force V

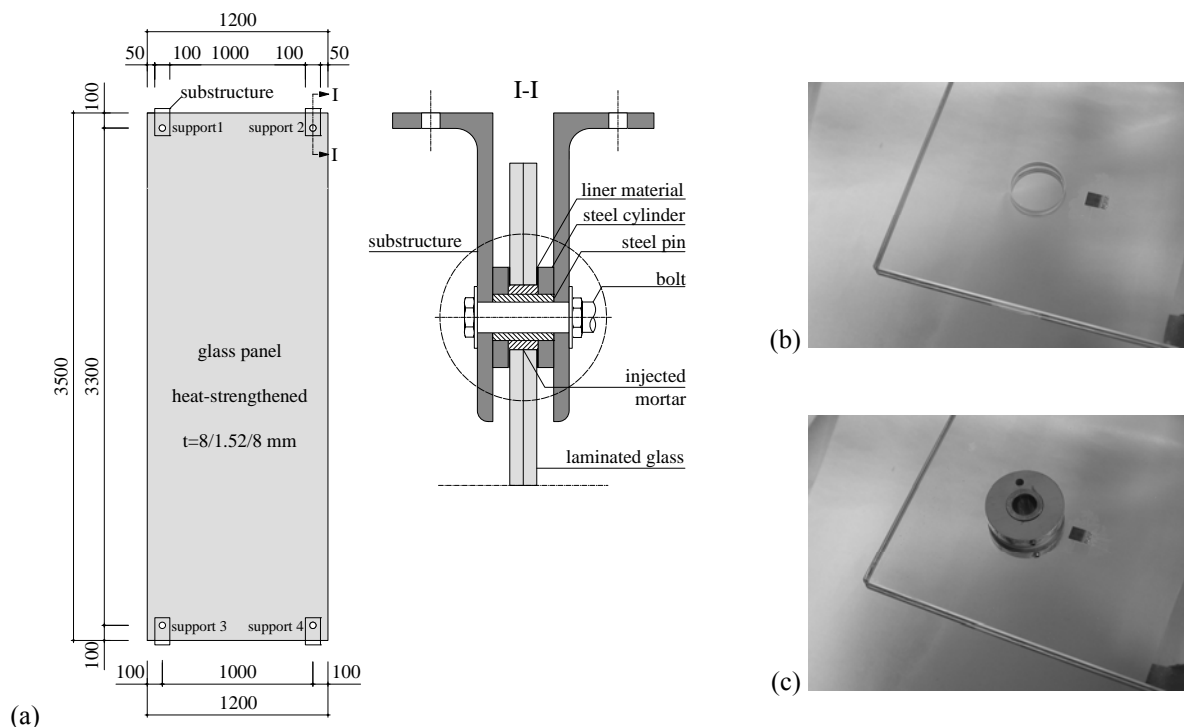


Figure 4.16 – Point supported panel test (a) specimen (b) substructures and connection devices (c) photos of glass panel without and with connection device

4.3.2 Testing frame and load introduction devices

For the experimental investigation purpose, a special testing frame was designed and built (Fig. 4.17). The testing frame was placed in a horizontal position instead of a vertical position as in the real building façade due to several reasons: easier positioning of the specimen in the testing frame, easier control of the specimen and measuring devices during the test, easier simulation of out-of-plane distributed load and, for safety reasons, to avoid pieces of broken glass falling from a significant height after the specimen failure.

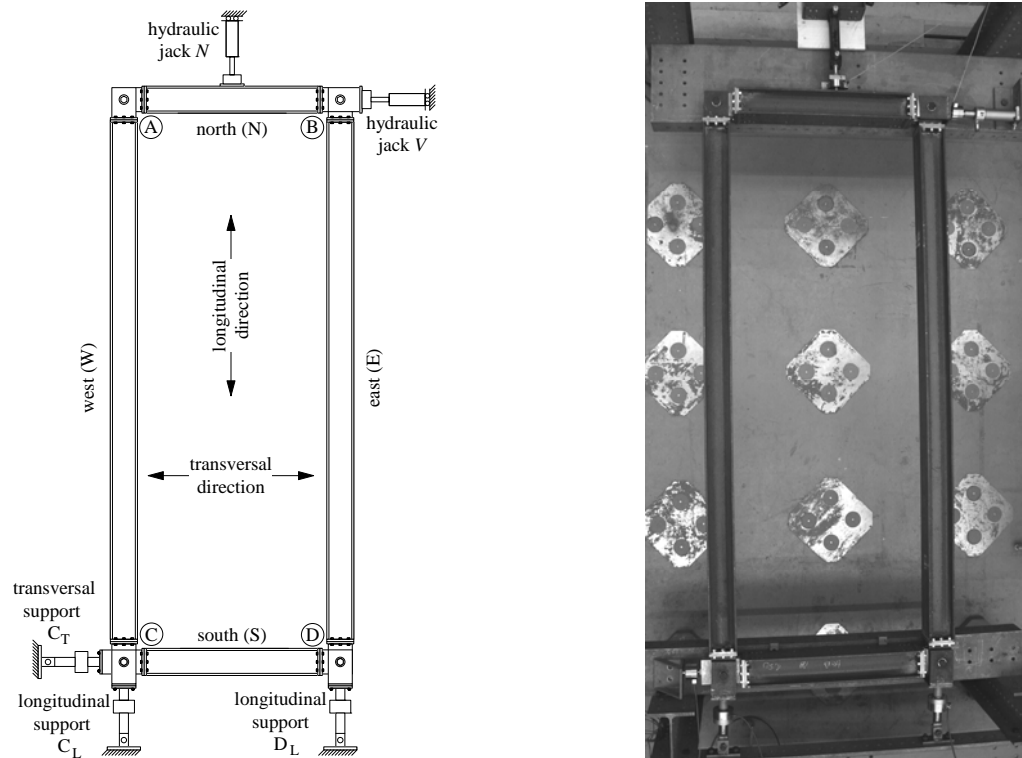


Figure 4.17 – Testing frame

The testing frame consisted of four steel profiles HEB 180 (N, E, S, and W), four pinned connection devices (A, B, C, D) and three frame supports (D_L , C_L , C_T). At the ends of steel profiles, steel plates were welded, on which pinned connection devices were bolted (Fig. 4.18(a)). The pinned connection devices allowed the axial force to be transferred between the steel profiles, but not the moments. Between the frame supports and the pinned connection devices, load cells measuring the support reactions were installed (Fig. 4.18.b). The supports constrained the displacement and allowed the rotation (simple supports). With three simple supports and four pins, the load frame is cinematically unstable (in in-plane direction). Once the glass panel was placed in the testing frame, it was employed as a stabilization element resisting the applied in-plane shear force V .

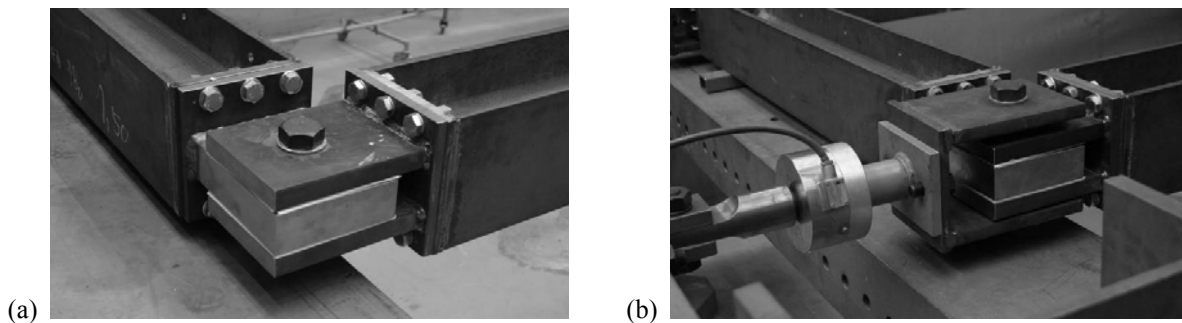


Figure 4.18 – Testing frame details (a) pinned connection A (b) frame support D_L with load cell

In-plane shear force was introduced by a hydraulic jack V (capacity of 100kN in compression and 50kN in tension) bolted to the pinned connection devices B (Fig. 4.19.a). The in-plane normal compressive force was introduced by a hydraulic jack N (200kN in compression) placed in the middle of the steel profile N (Fig. 4.20.b). Load cells measuring the force during the tests were included in the hydraulic jack. As the testing frame and glass panel were placed horizontally, the self-weight of the glass panel simulated the out-of-plane distributed load q as constant pressure perpendicular to the surface (0.4 kN/m^2). During the testing of specimen P1 and P3 temporary vertical support was placed in the middle of the glass panel to keep the glass panel horizontal and to compensate the effect of the glass panel self-weight. Teflon plates were placed between the glass and the temporary support to avoid the constraint of the in-plane movements.

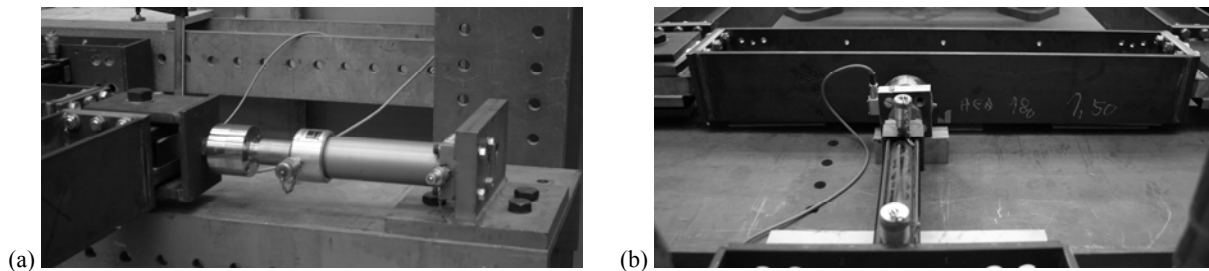


Figure 4.19 – Load introduction devices (a) hydraulic jack V (b) hydraulic jack N

4.3.3 Test set-up

The specimens were prepared (assemblage of connection devices and injection of the mortar) and tested in the Structural Engineering Laboratory at EPFL, Lausanne (Switzerland) during the period of March to July 2006. Every specimen was bolted to the testing frame steel profile N and S by four substructures (Fig. 4.20(a)). Glass supports 1, 2, 3 and 4 were fixed in longitudinal direction to enable the introduction of in-plane normal force in the glass panel. Due to different temperature expansion between glass panel and foundation/roof (in the fully-transparent pavilion application), a pair of sliding connections was constructed to avoid the introduction of additional stresses in the glass. Consequently, supports 1 was fixed in transversal direction (hole in the substructures was cylindrical) while supports 2 and 4 were free in transversal direction (holes in substructure were elongated) (Fig. 4.20(b)). Support 3 was also fixed in transversal direction to enable the introduction of in-plane shear force V from the hydraulic jack, through the testing frame, to the glass panel. Testing of the specimens took place minimum 24 hours after the injection of the mortar under constant environmental conditions (relative humidity of 60% and air temperature of 23°C).

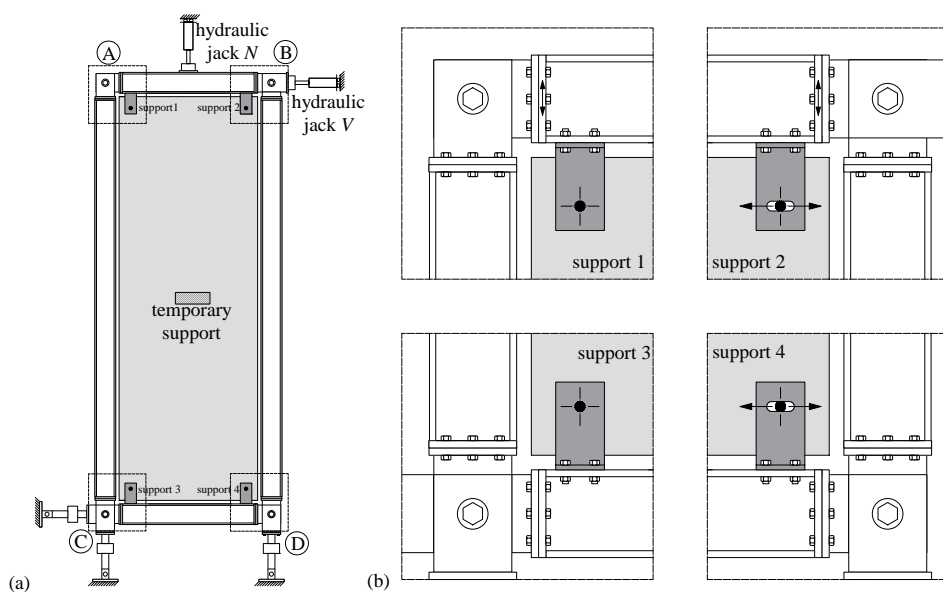


Figure 4.20 – Specimen and testing frame (a) specimen positioning (b) glass supports

4.3.4 Test instrumentation

The specimen and testing frame were instrumented with load cells, inductive transducers and strain gauges to measure the force introduced by hydraulic jacks, support reactions, specimen and testing frame deformation as well as stress distribution in glass panel.

Bi-directional load cell ($\pm 50\text{kN}$) was installed between the hydraulic jack V and pinned connection devices B to measure the in-plane shear force V . Uni-directional load cell (200kN) was installed between the hydraulic jack N and the steel profile N to measure the in-plane normal compressive force N . Three bi-directional load cells ($\pm 100\text{kN}$) were installed between the frame supports and corresponding pinned connection devices to measure the support reactions.

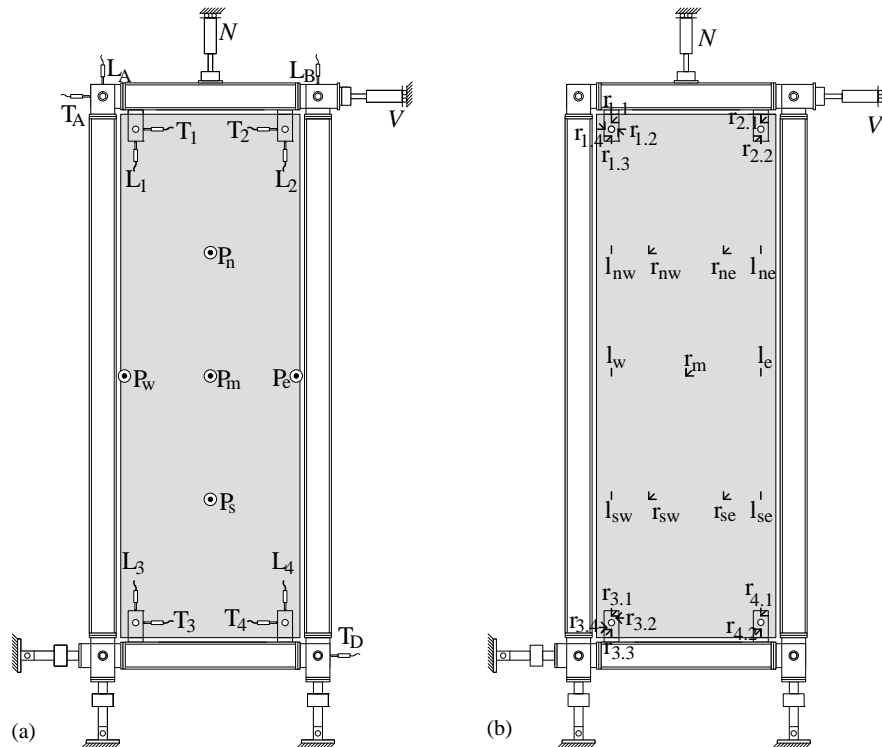


Figure 4.21 – Test instrumentation (a) inductive transducers (b) strain gauges

To monitor the deformation of the specimen and testing frame, several inductive transducers were installed measuring the relative displacement between the two movable points and absolute displacement between the movable and the referent fixed points (Fig. 4.21(a)). Relative displacements between the glass panel and substructures were measured by inductive transducers L_1 , L_2 , L_3 and L_4 in longitudinal and T_1 , T_2 , T_3 and T_4 in transversal direction. Inductive transducers T_A , L_A , L_B and L_D measured the absolute displacement of the testing frame. Absolute displacements of glass panel in perpendicular direction (the out-of-plane deflections) were measured by inductive transducers P_n , P_w , P_m , P_e and P_s .

To measure the strains at the glass panel surface, strain gauges (rosette gauges “r” and uni-directional gauges “l”) were glued around the glass supports, along the panel diagonals and along the panel longest edges (Fig. 4.21(b)). Only one specimen (P1) was instrumented with all strain gauges. It was firstly subjected to load cases $q+V$ and load case $N+V$ in the elastic range up to 50% of the estimated failure load and later, subjected to load cases V , up to failure. Other two specimens (P2 and P3) were instrumented by a few gauges ($r_{1.3}$, $r_{2.2}$, $r_{3.1}$, $r_{4.1}$, r_m) to compare and validate the results of the first specimen. Measurements were done utilising two HBM UPM 60 amplifiers. The measured data were collected using LABview, specialised PC software for testing.

4.3.5 Test results

4.3.5.1 In-plane shear force V vs. in-plane displacement u

During the tests, the load cell at hydraulic jack V measured the in-plane shear force V introduced through the testing frame to the specimen. Inductive transducers T_A , L_A and T_D which measured the absolute displacement of testing frame and inductive transducers L_1 , T_1 , L_2 , T_2 , L_3 , T_3 , L_4 and T_4 which measured the relative displacement between the glass panel and the substructure, allowed deduction of the in-plane panel displacement u .

Figure 4.22(b) shows the in-plane shear force V vs. in-plane displacement u in three tests. Table 4.23 summarizes the value of in-plane shear force at failure $V_{failure}$ and the value of in-plane panel displacement at failure $u_{failure}$. The stiffness of the specimen in in-plane direction is slightly influenced by the different load cases. The specimen in P1 and P2 failed at close values of in-plane shear force V , which can lead to the conclusion that out-of-plane distributed load has no influence on specimen shear resistance. This happens because the peak stresses for these two loads occur at different points of the glass panel: the peak stresses under in-plane shear force V occur on the internal edge of glass holes, in direction of the compression and tension diagonals, whereas the peak stresses under out-of plane distributed load q take place in the middle of the glass panel or on the glass surface near the hole.

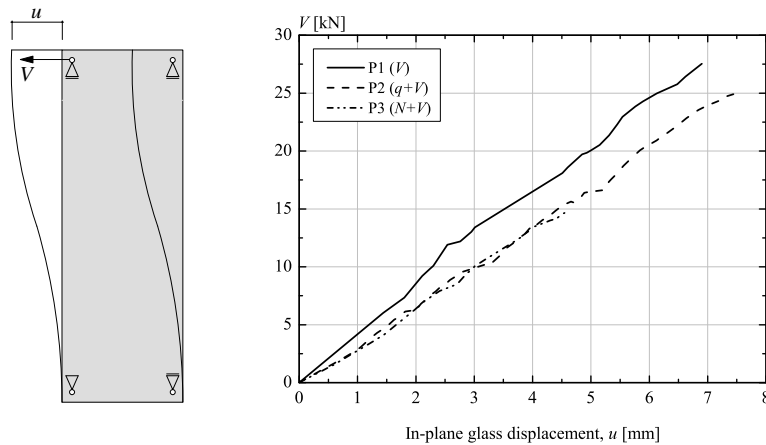


Figure 4.22 – In-plane shear loading V vs. in-plane displacement u

Specimen name	$V_{failure}$ [kN]	$u_{failure}$ [mm]
P1 (V)	27.54	6.90
P2 ($q+V$)	25.08	7.55
P3 ($N+V$)	14.67	4.55

Table 4.23 – Test summary

On the other hand, the in-plane normal compression force N significantly decreases the specimen resistance. This happens because in-plane normal compression force introduces additional stresses on the glass holes, at the same place where stress concentration due to in-plane shear force takes place.

4.3.5.2 In-plane shear force V vs. out-of-plane deflection w

During the tests, the inductive transducers P_n , P_w , P_m , P_e and P_s measured the out-of-plane deflection w of the glass panel. In this section, only the results of the inductive transducers positioned in the middle of glass span (P_w , P_m , P_e) in relation to in-plane shear force V are presented.

Figure 4.24(a) shows in-plane shear force V vs. out-of-plane deflection w in test P1 (load case V). In the middle of the panel a temporary support was placed which does not allow the out-of plane deflection of the middle point P_m (§4.3.3). Inductive transducer P_w measured a negative out-of-plane deflection, while P_e measured a positive one. This happened due to shear buckling of the glass panel which created out-of-plane buckles. The in-plane shear force V vs. out-of-plane deflection w in for test P2 (load case $q+V$) is presented in Figure 4.24(b). The specimen was firstly subjected to constant out-of-plane distributed load q which caused an initial deflection of the glass panel of 24.5 mm. Introducing the in-plane shear force V in the specimen, the deflection of glass panel firstly decreased, and only after a certain value of force the deflection started to increase again. As for test P1, the shear buckling caused a different deflection at the extreme points P_w and P_e .

For test P3 (load case $V+N$), the relationship between in-plane shear force V and out-of-plane deflection w is illustrated in Figure 4.24(c). The behaviour is similar to test P1, because temporary support was placed and because inductive transducers P_w measured the negative and P_e the positive deflection due to out-of-plane buckles caused by the shear buckling.

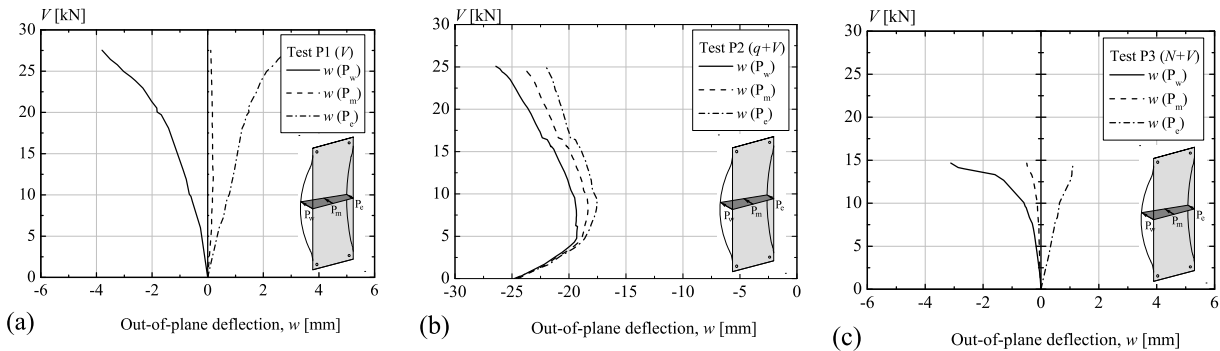


Figure 4.24 - In-plane shear force V vs. out-of-plane deflection w (a) test P1 (b) test P2 (c) test P3

4.3.5.3 In-plane shear force V vs. principal tensile stresses σ_I

The strain gauges measured the strain variation during the tests. Later, the strains were converted into principal stresses. The relation between in-plane shear load V and principal tensile stresses σ_I is presented in Figure 4.25. Only the results of principal tensile stresses measured by rosette gauges $r_{1,1}$ (at support 1), $r_{2,1}$ (at support 2), $r_{3,1}$ (at support 3) and $r_{4,1}$ (at support 4) are shown. The location and arrangements of rosette gauges is presented in Figure 4.21(b).

Figure 4.25(a) presents in-plane shear force V vs. principal tensile stresses σ_I for test P1 (load case V). The behaviour is linear-elastic. The maximal principal tensile stresses took place near the support 3, the support where failure of the glass panel initiated (more about the glass failure is given in §4.3.5.4.)

In-plane shear force V vs. principal tensile stresses σ_I for test P2 (load cases $q+V$) is presented in Figure 4.25(b). The initial stresses were caused by a constant out-of-plane distributed load q to which the specimen was initially subjected. Subsequently, the specimen was subjected to monotonic in-plane shear force V , and the stresses increased linearly. Again, the maximal principal tensile stress occurred near the support 3 where the failure started.

For test P3 (load cases $N+V$) the relation between in-plane shear force V and principal tensile stresses σ_I is shown in Figure 4.25(c). The initial stresses were caused by the constant in-plane normal compressive force N acting initially on the specimen, while increasing of the stresses occurred due to applied monotonic in-plane shear force V . In this test, only principal tensile stresses at support 1 and 3 were measured. The support 3 showed higher principal tensile stresses than the support 1. Failure started at support 3.

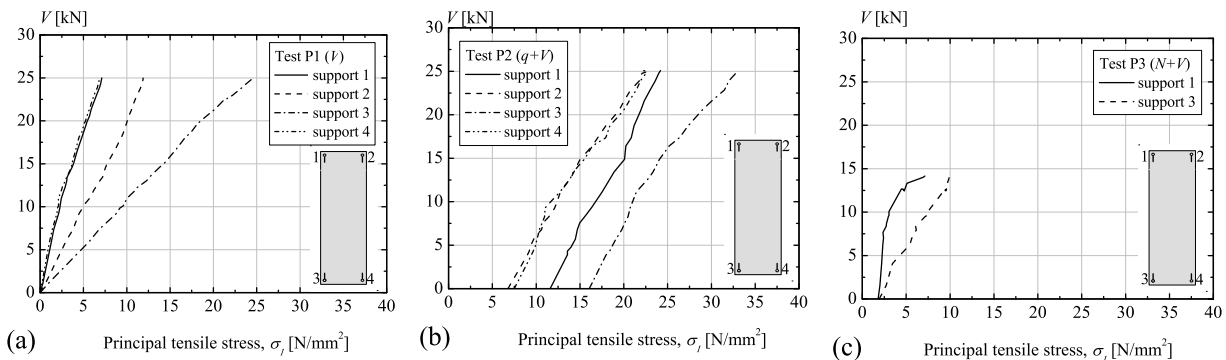


Figure 4.25 - In-plane-shear force V vs. principal tensile stresses σ_I (a) test P1 (b) test P2 (c) test P3

4.3.5.4 Failure mode

When a point supported glass panel is subjected to in-plane shear force V , compression diagonal between support 2 and 3 as well as a tensile diagonal between supports 1 and 4 occurs, crossing each other and creating a membrane effect. Two failure modes can be expected:

- failure due to shear buckling, caused due to out-of-plane deflection, buckles and bending of the glass panel. The panel fails at the place of maximal tensile stresses in the span,
- failure at the supports caused by stress concentration from load introduction or support reactions. The panel will fail at the place of maximum tensile stresses at the supports.

The three specimens demonstrate a single glass panel failure mode - **splitting tension**: perpendicular to the high compressive stress field (compression diagonal) between supports 2 and 3. Poisson's ratio caused tensile stresses which lead to failure. The failure initiation happens at the place of highest tensile stress (stress concentration) at the glass hole.

Glass panel P1 (load case V) failed uniquely due to splitting tension along compressive diagonal simultaneously, in both glass sheets (Fig. 4.26(a)). The failure initiated at support 3 and propagated towards support 2.

Figure 4.26(b) shows the glass panel failure mode for Test P2 (load case $q+V$). In addition to the splitting tension failure which occurred in the front sheet, the back sheet failed subsequently due to bending caused by distributed load q . In the middle of the glass panel span, negative bending moment occurred, while around a supports the positive bending moment took place.

Glass panel P3 (load case $N+V$) failed due to splitting tension along the compressive diagonal in the front and back glass sheets (Fig. 4.26(c)). The crack initiated at support 3 and propagated towards support 2.

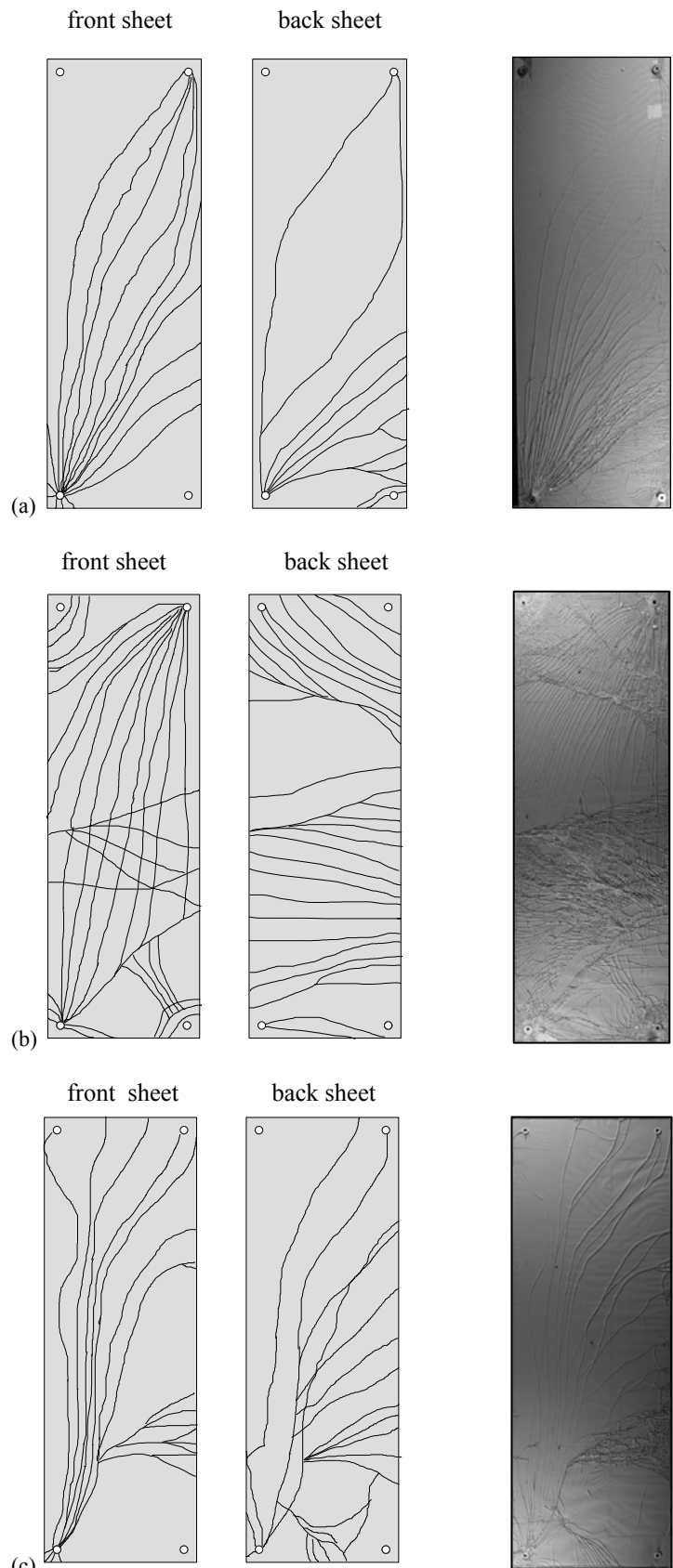


Figure 4.26 – Failure modes of point supported glass panel
(a) test P1 (b) test P2 (c) test P3

4.4 LINEAR SUPPORTED CONNECTION TEST

The objective of this experimental investigation was to study the shear behaviour of the adhesive used in glass/substructure connection and employment of mortar as a setting block. The investigation focused on the following points:

- adhesive deformation and resistance,
- mortar deformation and resistance,
- specimen failure mode

4.4.1 Specimen description

The specimen consisted of glass plate, connection devices and substructure. Laminated heat strengthened glass plates 200x490mm was chosen with glass thickness of 2x8mm and PVB thickness of 1.52mm. Connection devices consist of structural silicon Dow Corning DC993 [Dow Corning 2003], spacers and mortar Hilti HIT HY70 [Hilti 2007]. The substructures were made of two stainless steel profiles LNP of 80x80x8 and plate of 150x200x10mm bolted together. Three types of tests were developed [Mocibob et al. 2008])

- **Transversal shear test, TS:** the glass plate was glued to the substructure by adhesive. The adhesive was subjected to shear force in transversal direction. Two connection alternatives were distinguished: two side connection 2S, where the glass plate was glued to the substructure on two sides and three side connection 3S where the glass plate was glued to the substructure on three sides. The force in the adhesive was introduced by a special load introduction system (Fig. 4.27).

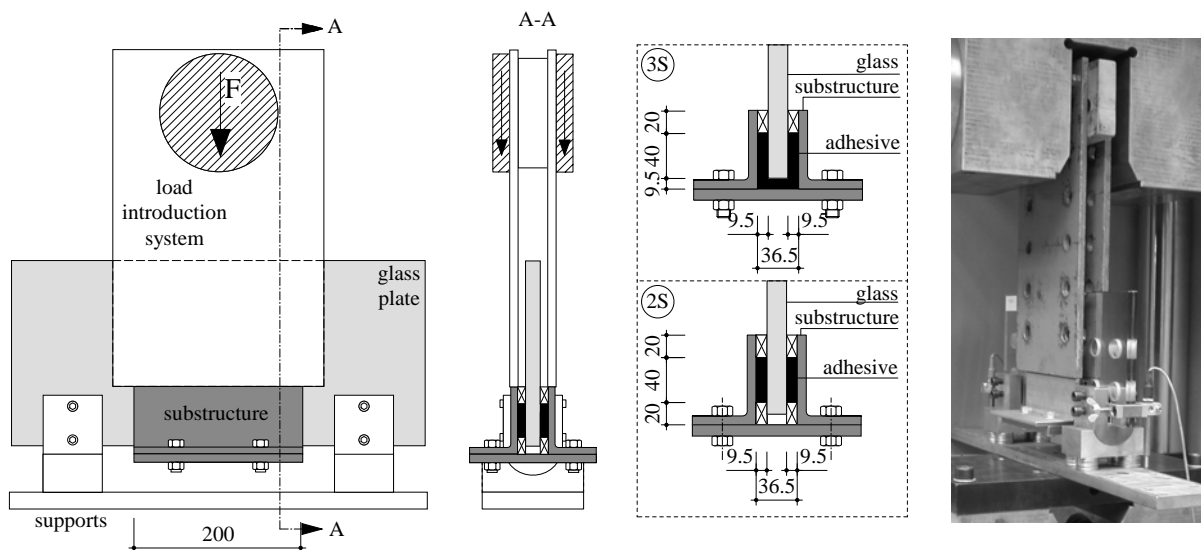


Figure 4.27 - Transversal shear test (TS)

- **Longitudinal shear test, LS:** the glass plate was glued to two substructures by adhesive. The adhesive was subjected to shear force in longitudinal direction. As for transversal shear test, three side connection 3S and two side connection 2S was distinguished. The force was introduced into the adhesive by load introduction system through two substructures in longitudinal direction. Two substructures were chosen to have symmetrical load introduction avoiding moments in the adhesive due eccentricity (Fig. 4.28).
- **Compression test, C:** the glass plate was glued to two substructures by adhesive on two sides and the gap between glass edge and substructure was filled by mortar. The mortar functioned as a setting block function to transfer the in-plane compression force from the substructure to the glass plate uniformly in both sheets of laminated glass. The load on the specimen was introduced by the load introduction system (Fig. 4.29).

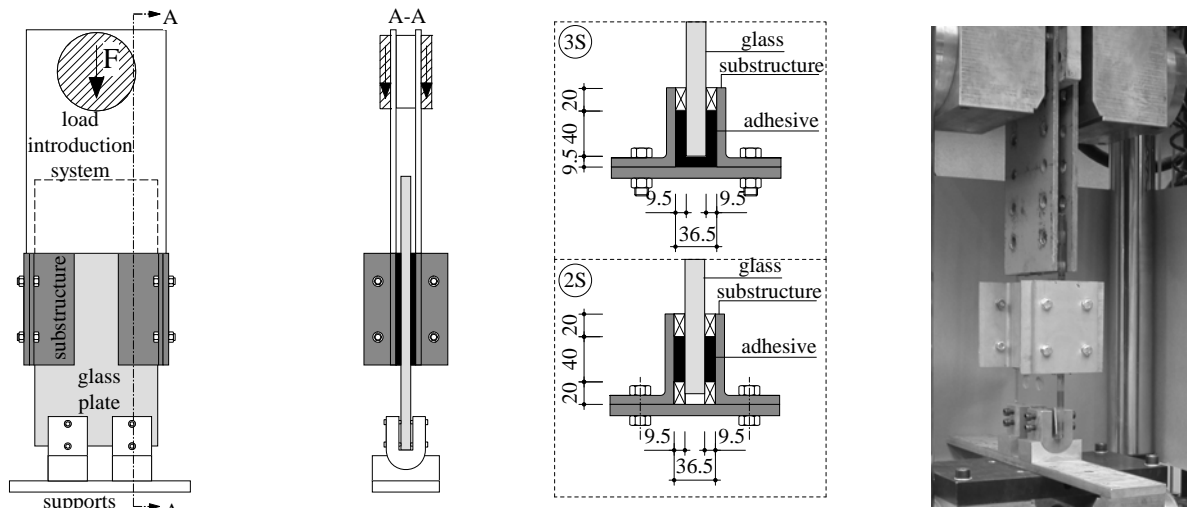


Figure 4.28 - Longitudinal shear test (LS)

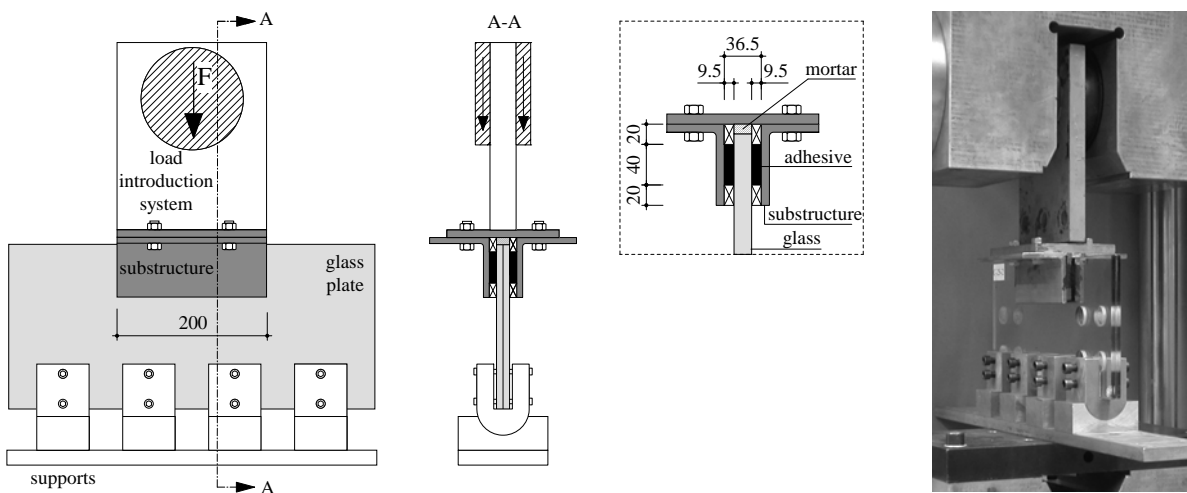


Figure 4.29 - Compression test (C)

Summary

The specimens differed by the test type (transversal shear test *TS*, longitudinal shear test *LS*, compression test *C*) and the number of glued sides (two sides connection *2S*, and three sides connection *3S*). For each selected parameter set two specimens were built, making a total of 10 specimens. The specimen name is the abbreviation of the mentioned parameter. For example, specimen *LS-3S-2* means longitudinal shear test (*LS*), with three side connection (*3S*), second specimen (*2*). Table 4.30 shows the summary of the tested specimens with the parameters for linear support connection tests.

Table 4.30 – Specimen summary for linear support – local behaviour test

Specimen name	Glued sides	Number of specimens	Specimen name	Glued Side	Number of specimens	Specimen name	Glued Side	Number of specimens
Transversal shear test			Longitudinal shear test			Compressive test		
TS-2S	2	2	LS-2S	2	2	C-2S	2	2
TS-3S	3	2	LS-3S	3	2			

4.4.2 Test set-up and test instrumentation

The glass plate and substructures were firstly cleaned and then glued in the workshop at Félix Constructions SA. The mortar injection and testing (using machine SCHENCK with capacity of 1000kN) was done in the Structural Engineering Laboratory at EPFL, Lausanne (Switzerland) in September 2007. Tests were made approximately 48 hours after gluing and 24 hours after mortar injection. The environmental conditions (humidity of 60% and temperature of 23°C) were kept constant during the testing. The specimens were tested under displacement control with constant increment of 0.1 mm/s in transversal and longitudinal shear tests and 0.05 mm/s in compression tests.

Specimen displacement δ and the applied force F were measured by the testing machine. Each specimen was additionally instrumented with two inductive transducers L_1 and L_2 to measure the relative displacement between the glass and the supports δ_g (Fig. 4.31).

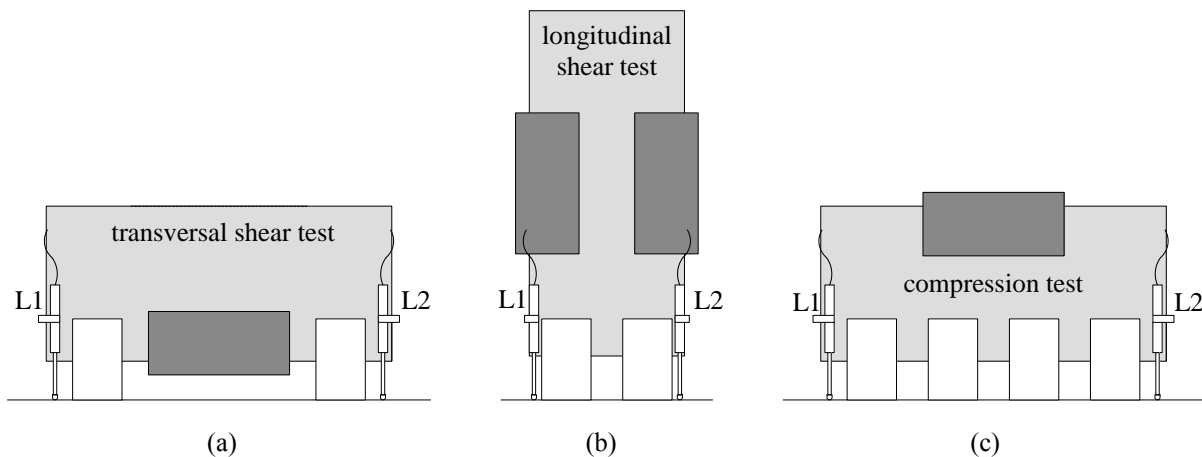


Figure 4.31 – Location and arrangements of inductive transducers
(a) tensile test (b) shear test (c) compression test

4.4.3 Test results

4.4.3.1 Force F vs. adhesive displacement δ_A in transversal and longitudinal shear test

In transversal and longitudinal shear tests, the difference between the specimen displacement δ , measured with the testing machine, and the relative displacement between the glass and the supports δ_g measured with the inductive transducers, correspond to the adhesive displacement δ_A .

$$\delta_A = \delta - \delta_g \quad (4.2)$$

Figure 4.32 shows the relation between the applied force F and the adhesive displacement δ_A in transversal shear test TS . The graph shows the results of one tested specimen with two sides $2S$ and one with three sides connection $3S$. The adhesive behaviour can be divided in three zones: the elastic zone where linear material behaviour was recognized, the plastic zone which took place after the yielding of adhesive and the softening zone where adhesive lost their resistance. The ductility of $2S$ specimens was much higher than the ductility of $3S$ specimens, while the maximum force of $3S$ specimens was slightly higher than the $2S$ specimens. Additionally, $3S$ specimens showed higher stiffness in elastic domain than the $2S$ specimens. This can be explained because in $2S$ specimens the entire adhesive was under shear force, while in $3S$ specimen two sides of the adhesive were under shear force and one side under tensile force. This additional side subjected to tensile force gives the adhesive higher stiffness. In the elastic domain of $3S$ specimens, two yielding point can be observed: the first yielding point (y_1) corresponds to start of plastification of the adhesive under tension, while the second yielding point (y_2) corresponds to the plastification of the adhesive under shear.

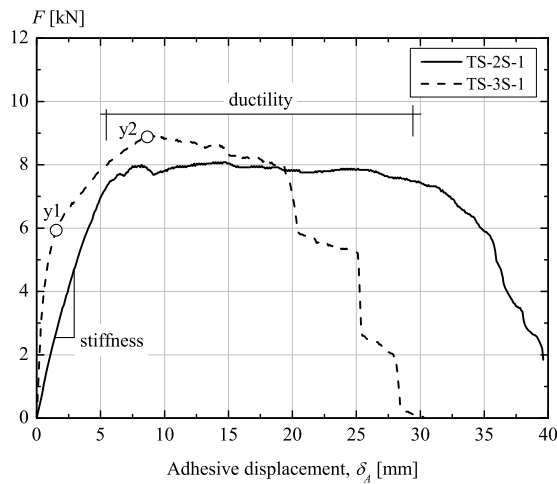


Figure 4.32 - Force F vs. adhesive displacement δ_A in transversal shear tests

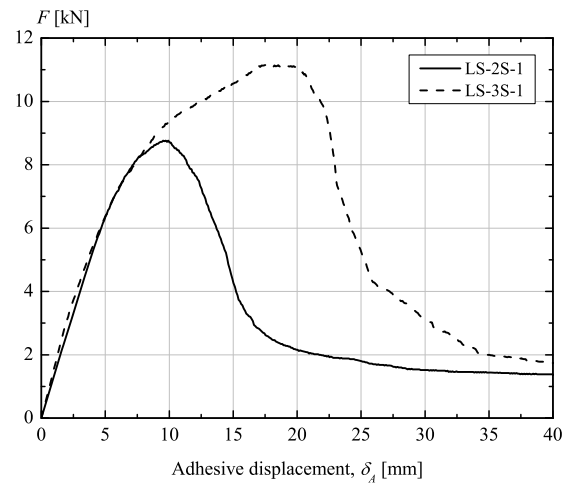


Figure 4.33 - Force F vs. adhesive displacement δ_A in longitudinal shear tests

Figure 4.33 shows the relation between the applied force F and adhesive displacement δ_A in longitudinal shear tests LS . Having two substructures and a double adhesive area, the values of the applied force F were divided by 2 to be comparable with the adhesive behaviour in transversal shear test. For the longitudinal shear test, adhesive behaviour can also be divided in the zones: the elastic, the plastic and the softening zone. Very small ductility was observed (short plastic zone). The 2S and 3S specimens show very similar behaviour (same stiffness in elastic domain) due to the fact that in both cases, the entire adhesive area was subjected to shear loading. As expected, 3S specimens demonstrate higher maximal force than 2S.

4.4.3.2 Force F vs. mortar displacement δ_M in compression test

In compression tests, the difference of the specimen displacement δ measured by the testing machine and the relative displacement between the glass and the supports δ_g measured by the inductive transducers correspond to the mortar displacement δ_M :

$$\delta_M = \delta - \delta_g \quad (4.3)$$

Figure 4.34 shows the relation between the applied force F and mortar displacement δ_M in compression tests. The mortar shows linear-elastic behaviour. In specimen C-2S-1, mortar and glass plate failure occurred simultaneously while in specimen C-2S-2 the specimen shows additional resistance after mortar failure.

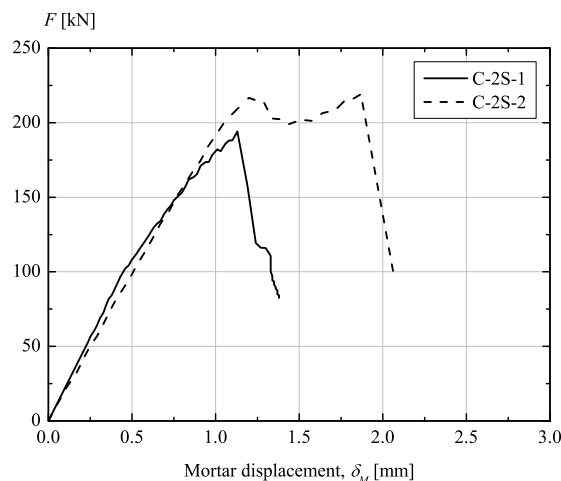


Figure 4.34 - Force F vs. mortar displacement δ_A in compression test

4.4.3.3 Test summary

Table 4.35 summarises the transversal shear, longitudinal shear and compressive test results. It shows the maximum elastic force $F_e = 0.9F_{max}$, adhesive displacement at the point of the maximum elastic force $\delta_{A,e}$ for transversal and longitudinal shear test, as well as the maximum forces F_{max} and mortar displacement at the point of maximal force $\delta_{M,F}$. Additionally, the failure mode of the specimens is mentioned. The failure mode abbreviations have the following meaning: cohesive failure (CF), adhesive failure (AF) and mortar failure (MF). Detailed explanations of failure modes are given in §4.4.3.3.

Table 4.35 – Result recapitulation for linear support – local behaviour tests

Specimen name	F_e [kN]	$\delta_{A,e}$ [mm]	Failure mode	Specimen name	F_e [kN]	$\delta_{A,e}$ [mm]	Failure mode	Specimen name	F_{max} [kN]	$\delta_{M,F}$ [mm]	Failure mode
TS-2S-1	7.24	5.43	CF	LS-2S-1	7.20	6.68	CF	C-2S-1	194.1	1.13	MF
TS-2S-2	9.14	14.85	CF	LS-2S-2	7.88	6.95	CF	C-2S-2	219.1	1.87	MF
TS-3S-1	8.03	5.61	CF	LS-3S-1	10.01	12.61	CF				
TS-3S-2	9.65	9.59	CF	LS-3S-2	8.73	8.27	CF				

4.4.3.4 Failure modes

All the specimens in transversal and longitudinal shear tests failed in the adhesive with cohesive failure (CF) - the rupture happens inside the adhesive. A second possible mode of failure, called *the adhesive failure*, which means the separation of adhesive from the glass or substructure at the contact areas, did not occur. Figure 3.3(a) shows the cohesive failure of the adhesive in transversal shear test. Figure 4.36(b) shows cohesive failure of the adhesive in longitudinal shear test.

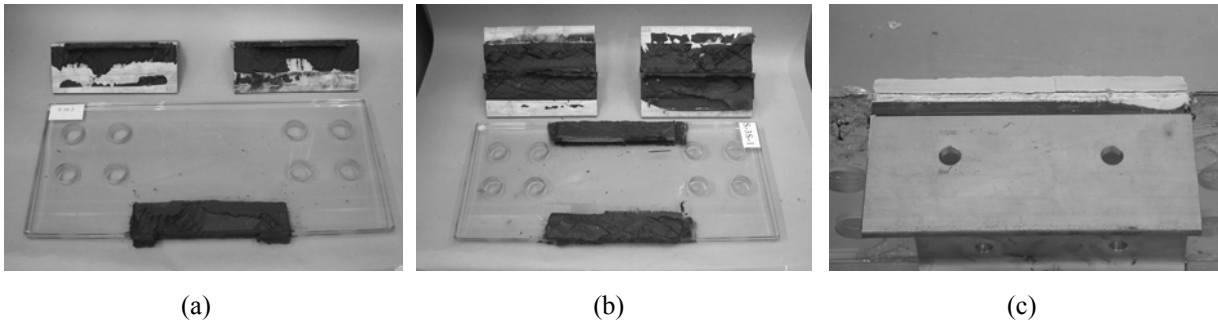


Figure 4.36 – Specimen failure modes (a) transversal shear test (b) longitudinal shear test (c) compressive test

In the compression tests, crushing of the mortar due to high compressive stresses occurred. Tests show that mortar failure was followed by failure of the glass plate. In some cases, the failure of the mortar and of the glass occurred simultaneously, while in the other cases the specimen was still able to carry the additional force up to failure of the glass plate. Figure 4.35(c) shows the failure of the mortar in compression test.

4.5 LINEAR SUPPORTED PANEL TEST

The findings from linear supported connection test (Section 4.4) were used to develop a full-size glass panel specimen and study its utilisation as load-bearing element for the stabilization of fully transparent pavilions. Although showing smaller resistance than the three sides connection 3S, two sides connection 2S was adopted due to its easier gluing process, easier mortar injection and a better stress distribution (avoiding the adhesive under tension).

The objective of this test was to study the shear buckling behaviour of full-size glass panel supported linearly by two shortest edges under different load cases. The research focused on the following:

- global deformation of the glass panel for different load cases,
- stress distribution in the glass panel for different load cases,
- failure mode of the glass panel for different load cases.

4.5.1 Specimen description

The specimens consisted of a glass panel, connection devices and two substructures (Fig. 4.37) [Mocibob et al. 2008]. The laminated glass panel was made of two sheets of heat strengthened glass. The thickness of each glass sheet was 8 mm and the thickness of PVB interlayer was 1.52mm. The dimension of the glass panel was 1200x3500mm, corresponding to the real-size façade elements. Connection device was two side connection 2S, described in §4.4.1, consisting of adhesive (structural silicon Dow Corning DC993 [Dow Corning 2003]), spacers and mortar (Hilti HIT HY 70 [Hilti 2007]). The thickness of the adhesive was 9.5mm, and the width 40mm. Setting blocks with length of 100mm were placed at $b/5$ from the corner. Substructure, made of stainless steel, consisted of two LNP 80x80x8 profiles and a plate of 200x15mm bolted together. Three identical specimens were built and tested under different load cases:

- **L1** the specimen was subjected to monotonic in-plane shear force V .
- **L2** specimen was subjected simultaneously to constant out-of-plane distributed load q ($q=0.4 \text{ N/mm}^2$ – representing the wind load) and monotonic in-plane shear force V .
- **L3** specimen was subjected simultaneously to constant in-plane normal force N ($N=20 \text{ kN}$ – representing the weight of the roof) and monotonic in-plane shear force V

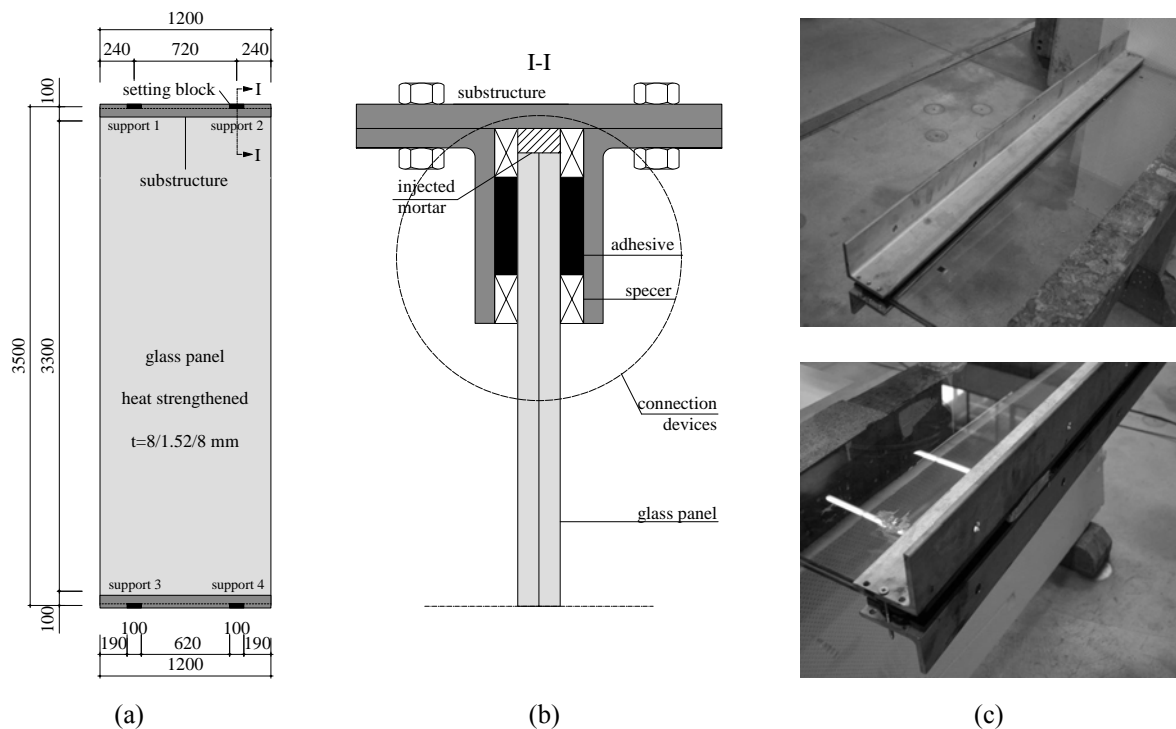


Figure 4.37 - Linear support panel test (a) specimen
(b) substructures and connection devices (c) photos of glass panel and substructure

4.5.2 Testing frame and load introduction devices

The testing frame and the load introduction devices used for *point supported panel test* were also adopted for *linear supported panel tests*. The description of the testing frame and load introduction devices are given in §4.3.2.

4.5.3 Test set-up

The glass panel and substructures were cleaned and glued by professionals in the workshop at Félix Constructions SA. First, the LNP profiles were glued to the glass panel by adhesives along the two shortest glass edges. 48 hours after the gluing process, the mortar for setting block was injected. Plate, as a part of the substructure, was bolted to LNP profiles. The injection of the mortar and testing were done in the Structural Engineering Laboratory of EPFL, Lausanne (Switzerland) between July and October 2007. The specimens were left for 7 days, to guarantee adhesive and mortar hardening, before being placed in the testing frame. The specimens were connected to the testing frame by bolts, connecting substructures with steel profiles N and S (Fig. 4.38(b)). The testing of the specimens was made under constant environmental conditions (humidity of 60% and temperature of 23°C).

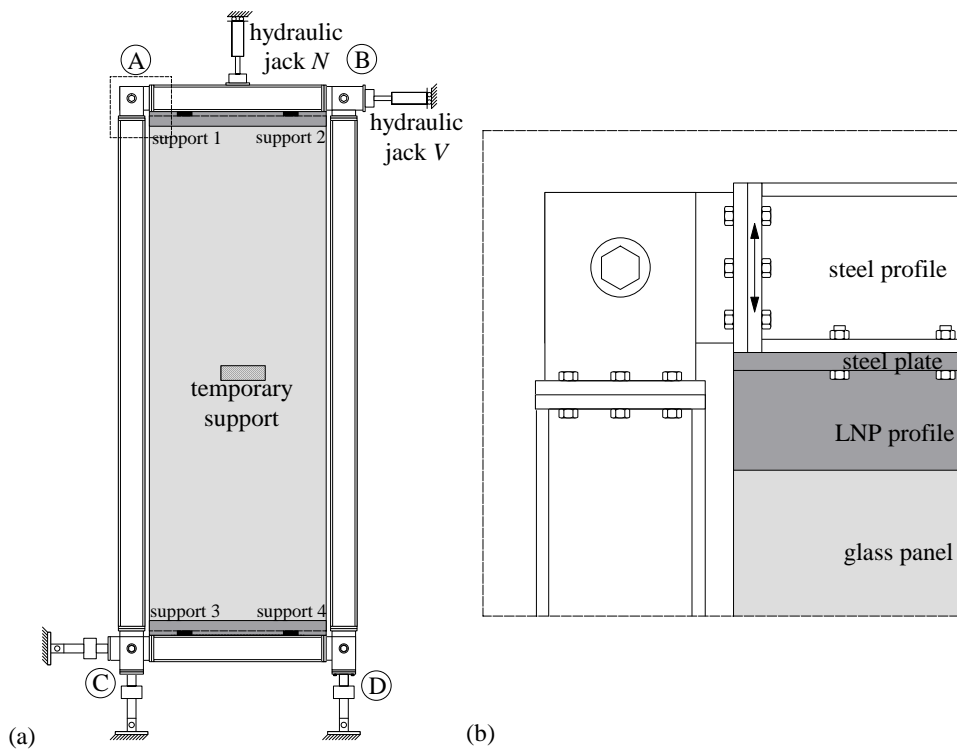


Figure 4.38 – Specimen and testing frame (a) specimen positioning (b) specimen/test frame connection

4.5.4 Test instrumentation

To measure the force introduction, support reactions, panel and testing frame deformation as well as stress distribution in the glass panel, the specimens and testing frame were instrumented with load cells, inductive transducers and strain gauges. The arrangement of load cells and inductive transducers measuring absolute displacements of the testing frame (T_A , T_D , L_A and L_B) was the same as in point supported panel test (§4.3.4).

The specimens were additionally instrumented with sets of inductive transducers measuring the relative displacement between the glass panel and substructures in longitudinal direction (inductive transducers L_1 , L_2 , L_3 and L_4) and in transversal direction (T_n and T_s). The out-of plane deflections of the glass panel were measured with inductive transducers P_n , P_w , P_m , P_e and P_s (Fig. 4.39(a)).

To measure the strain on the glass panel, strain gauges (rosette gauges “r” and un-axial gauges “l”) were glued onto the glass surface. The specimen (L1) was instrumented with strain gauges as shown in Figure 4.39(b). This specimen was subjected to load cases $q+V$ and $N+V$ in the elastic domain up to 50% of the estimated failure force. Later, the specimen was subjected to load case V up to failure. The other two specimens (L2 and L3) were equipped with 5 strain gauges (r_1, r_2, r_3, r_4 and r_m) to compare and validate the results from the first specimen. Measurements were done utilising two HBM UPM 60 amplifiers. The measured data were collected using LABview.

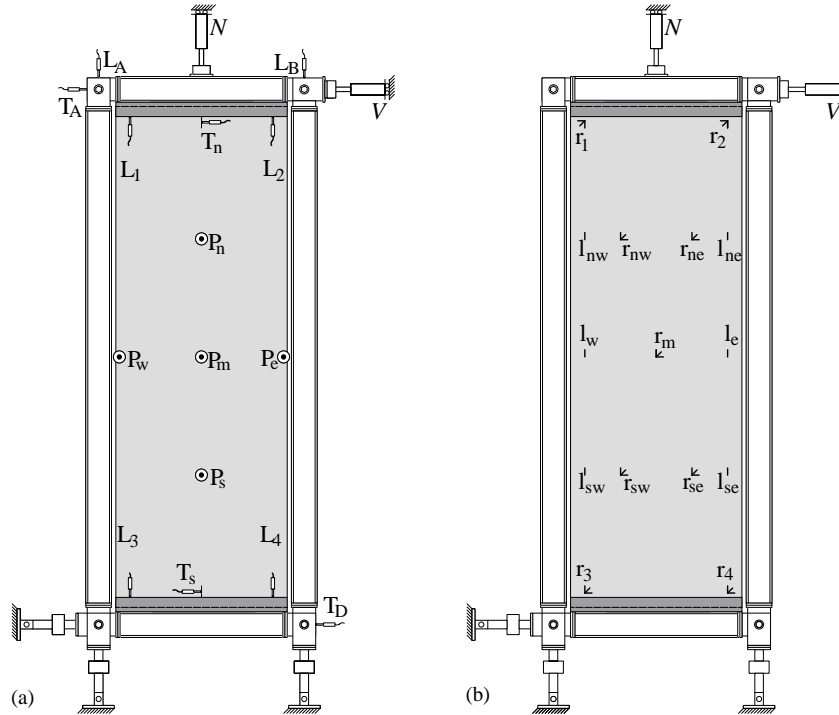


Figure 4.39 – Test instrumentation (a) inductive transducers (b) strain gauges

4.5.5 Test results

4.5.5.1 In-plane shear force V vs. in-plane panel displacement u

The load cell at the hydraulic jack V measured the in-plane shear force introduced through the testing frame to the specimen. Inductive transducers $T_A, T_D, L_A,$ and L_B measured the absolute displacements of testing frame while the inductive transducers L_1, L_2, L_3, L_4, T_n and T_s measured the relative displacements between glass panel and substructure. From these measurements, the relative in-plane displacements of the panel u were deducted.

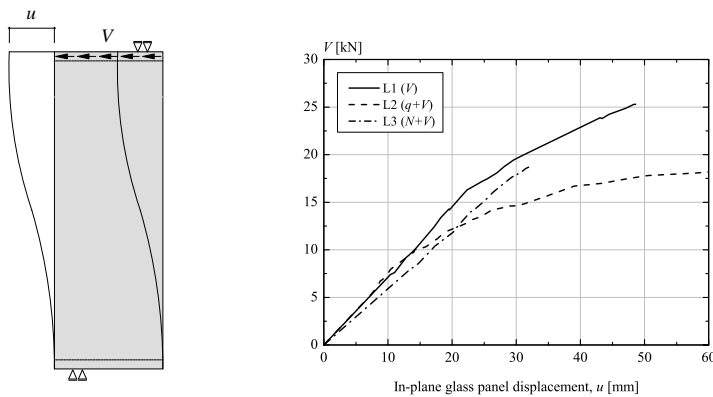


Figure 4.40– In-plane shear force V vs. in-plane panel displacement u

Specimen name	$V_{failure}$ [kN]	$u_{failure}$ [mm]
L1 (V)	25.29	48.62
L2 (q+V)	18.22	60.93
L3 (N+V)	18.77	32.22

Table 4.41– Tests summary

Figure 4.40 shows the in-plane panel displacement u in relation to applied in-plane shear force V for the three tests. Up to certain level, the linear-elastic behaviour of the specimens is recognised. Once the adhesive reached the yielding point, the specimens demonstrated a nonlinear behaviour. The elastic in-plane stiffness was similar in three tests. In test L2 (load cases $q+V$), the adhesive reached faster its yielding point (the adhesive was subjected to additional shear in transversal direction due to large out-of-plane deflection).

Table 4.41 shows the value of in-plane shear force at failure $V_{failure}$ and value of in-plane specimen displacement at failure $u_{failure}$. The failure of the specimens occurred at the compression setting block, due to high stress concentration. In-plane normal compressive force N introduced additional stresses at this place and therefore the failure force $V_{failure}$ of specimen L3 (load cases $N+V$) is smaller than the failure force of specimen L1 (load cases V).

4.5.5.2 In-plane shear force V vs. out-of-plane deflection w

The glass panel out-of-plane deflection w was measured by inductive transducers P_w , P_m , P_e and P_s (location and arrangement of inductive transducers is shown in Figure 4.39(a)). In this section, only the results of the inductive transducers positioned in the middle of the glass span (P_w , P_m , P_e) in relation to in-plane shear force V are presented.

Figure 4.42(a) shows in-plane shear force V vs. out-of-plane deflection w in test L1 (load cases V). In the middle of the glass plane a temporary support (§4.3.3) was placed which prevented the out-of-plane deflection of the middle point P_m . Inductive transducers P_w and P_e measured very small deflections which were almost negligible.

The relation between out-of-plane deflection w and in-plane shear force V for test L2 (load case $q+V$) is illustrated in Figure 4.42(b). The specimen was first subjected to constant out-of-plane distributed load q which caused an initial deflection of the glass panel of 21.7 mm. Introducing the monotonic in-plane shear force V in the specimen, the deflection and displacement of the glass panel increases drastically, reaching 111.34 mm at failure.

For test L3 (load case $V+N$) in-plane shear force V vs. out-of-plane deflection w is presented in Figure 4.42(c). The temporary support does not allow the out-of-plane deflection of the middle point P_m . Inductive transducer P_w measured the negative out-of-plane deflection, while P_e measured the positive out-of-plane deflection due to shear buckling of the glass pane. The deflection was linear until the adhesive started to yield.

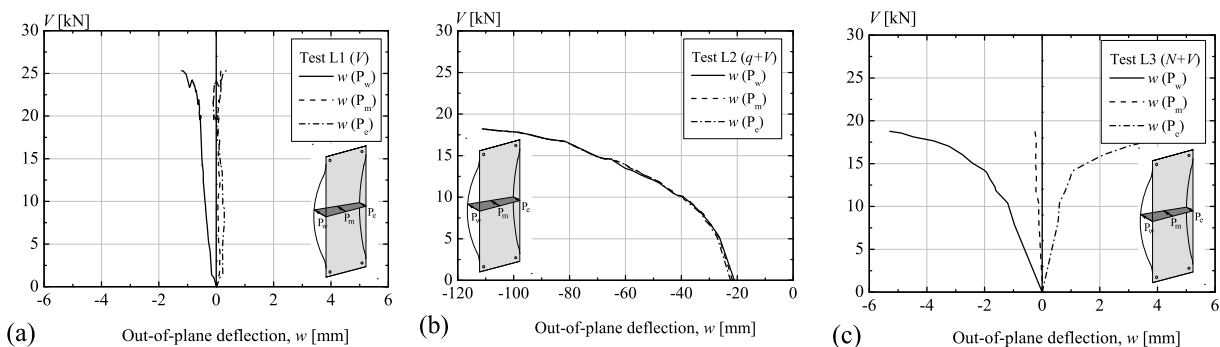


Figure 4.42 - In-plane shear force V vs. out-of-plane deflection w (a) test L1 (b) test L2 (c) test L3

4.5.5.3 In-plane shear force V vs. principal tensile stresses σ_1

The relations between principal tensile stresses σ_1 , measured during the tests with rosettes gauges r_1 (support 1), r_2 (support 2), r_3 (support 3) and r_4 (support 4), and in-plane shear force V are presented in Figure 4.43. The location and arrangements of the strain gauges are presented in Figure 4.39(b). The rosettes were placed 100mm from the glass edges (longitudinal and transversal edges).

Figure 4.43(a) shows in-plane shear force V vs. principal tensile stresses σ_1 for test L1 (load case V). Initially, linear-elastic behaviour of the principal tensile stresses was observed. After the adhesive reached the yielding point, the principal tensile stress distribution became nonlinear. At supports 2 and 3 (at the ends of compressive diagonal) the stresses increased because of compressive reactions of setting blocks. On the other hand, at supports 1 and 4 (tensile diagonal), the stresses decreased because of the tensile reactions of the yielded adhesive (the setting block was not able to support the tensile reaction). Failure of the glass panel occurred at the setting block near the support 3, the place of highest tensile stresses (more detail about the failure modes are given in § 4.5.5.4).

The relation between principal tensile stresses σ_1 and in-plane shear force V for test L2 (load case $q+V$) is presented in Figure 4.43(b). The initial tensile stresses were caused by the constant out-of-plane distributed load q . As before, linear-elastic stress distribution is observed until the start of adhesive yielding. Subsequently, nonlinear stress distribution is observed. At support 2 and 3, the stresses increase (reaction of compression setting blocks), while they decrease at support 1 and 4 (tensile reaction of the yielding adhesive).

For test 3 (load case $V+N$) the in-plane shear force V vs. principal tensile stresses σ_1 is shown in Figure 4.43(c). Small initial stresses were caused by the constant in-plane normal compressive force N . As was the case in the previous tests, linear part and non linear part of the stress distribution are observed.

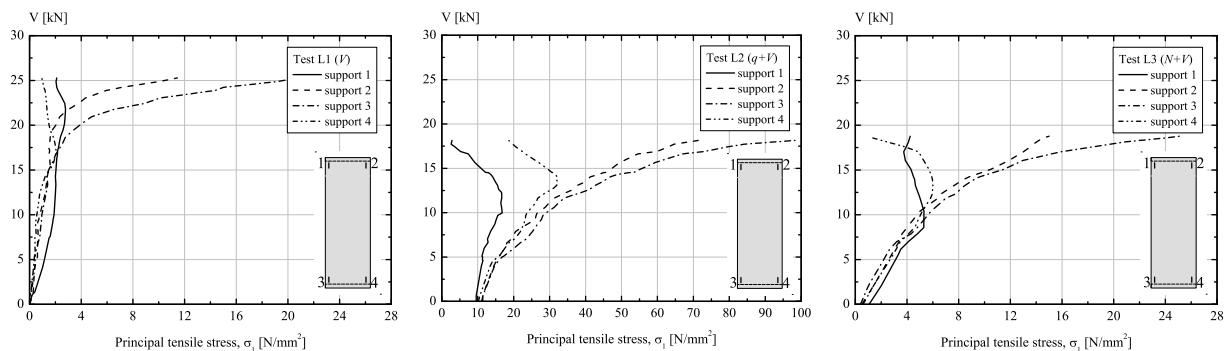


Figure 4.43 - In-plane shear force (V) vs. principal tensile stresses σ_1 (a) Test L1 (b) Test L2 (c) Test L3

4.5.5.4 Failure mode

When the specimen is subjected to in-plane shear force, a compressive diagonal occurs due to compressive reaction of two opposite setting blocks (supports 2 and 3), whereas the tensile diagonal occurs due to shear strength of the adhesive (supports 1 and 4). Two failure modes can be expected:

- failure due to shear buckling, causing out-of-plane deflection, buckles and bending of the glass. The panel fails at the place of maximal tensile stresses in the span,
- failure due to stress concentration at load introduction point. The panel fails at place of maximum tensile stresses at compression setting blocks.

In test L1 (load case V), high compressive stress field (compressive diagonal) occurred between the opposite setting blocks 2 and 3 with the stress peak at the contact point of glass edge and setting blocks. Perpendicular to the compression field, Poisson's ratio caused tensile stresses which led to failure (splitting tension). The highest tensile stresses were measured near the support 3 where the crack initiated. The crack path in the glass panel is illustrated in Figure 4.44(a). The front glass layer failed first in splitting tension. Immediately after, failure of the back glass failure occurred due to bending in the middle of the span and near the south supports.

Figure 4.44(b) shows the failure of the glass panel in test L2 (load case $q+V$). The front glass failed due to splitting tension in the compressive diagonal, with crack initiation at setting block 3. The back glass failed due to bending stresses in the middle of the glass span.

The front glass in test L3 (load case $N+V$) failed due to splitting tension at setting block 3 (Fig. 4.44(c)). The back-side layer failed as a combination of splitting tension and bending near the south support.

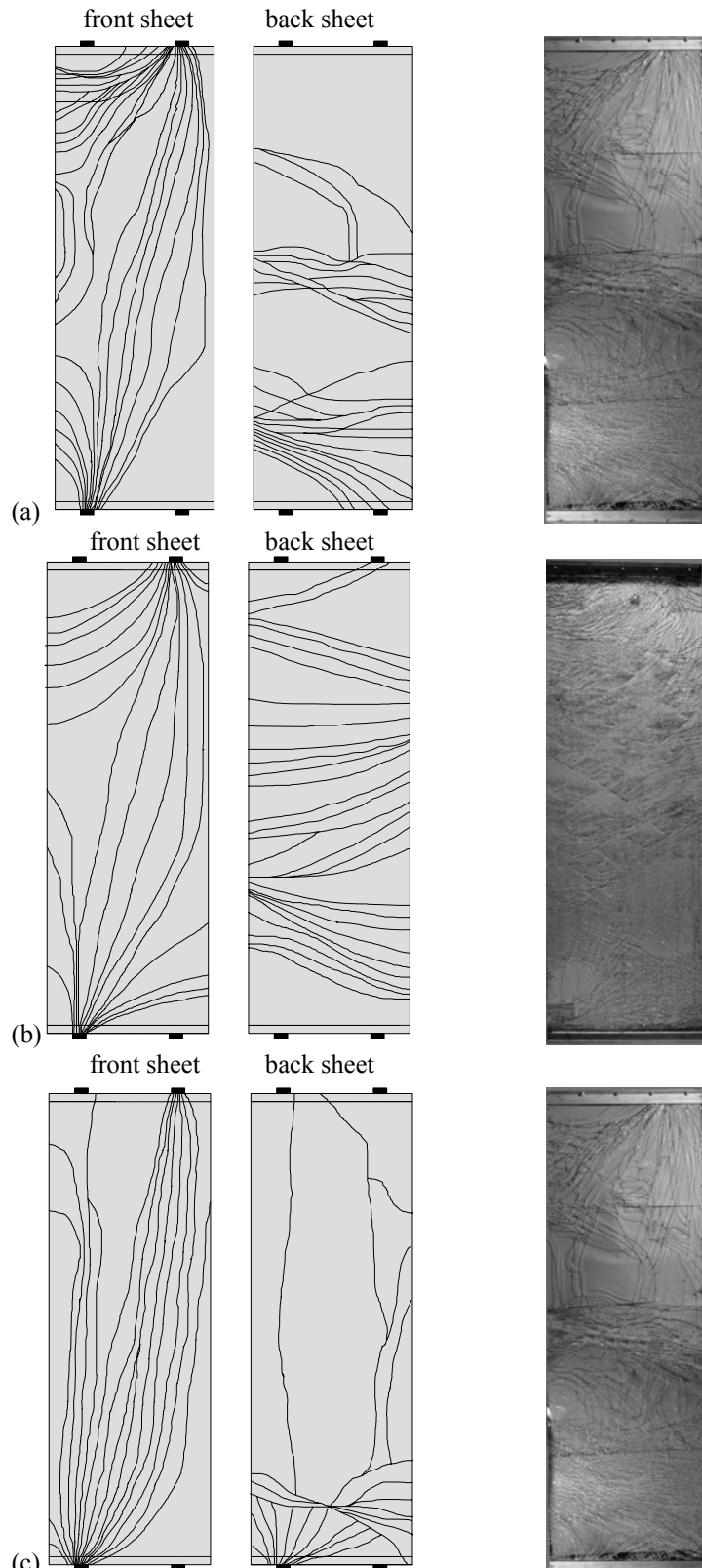


Figure 4.44 – Failure modes of linear supported glass panel
(a) test L1 (b) test L2 (c) test L3

4.6 SUMMARY AND CONCLUSIONS

The specimens, the testing frame and load introduction devices, the test set-up, test instrumentation and the main results of four groups of experimental investigation have been described in this Chapter:

The objective of **Point supported connection test** was to understand the behaviour of different types of glass/substructure bolted connection by means of load introduction paths (axial and eccentric), connection systems (rigid and pinned), load directions (compression and tension), glass thicknesses (monolithic and laminated) and bolt diameters (M16 and M20). Longitudinal displacements, horizontal displacements, stress distribution around the hole and failure modes of the specimens have been studied. From the test analyses, the following conclusion can be drawn:

- a force eccentricity has a significant influence on specimen resistance and deformation. The smallest is the eccentricity, the higher are the stiffness and resistance of the specimen,
- specimens with rigid connections show a higher stiffness, with significantly smaller displacements than the specimens with a pinned connection,
- bolt diameters have influence during the eccentric test: thinner bolts give smaller stiffness and smaller resistance to the specimens than thicker bolts,
- an axial rigid connection is the most suitable connection type giving the highest resistance with the smallest specimen displacement. It can be used to study the global behaviour of a glass panel.

The **Point supported panel test** was done to investigate the shear buckling behaviour of full-size glass panel with axial rigid connection subjected to different load case. The global specimen deformation, stress distribution and failure mode of the specimens have been studied. From the investigation the following conclusion have been drawn:

- in-plane specimen stiffness is slightly influenced on the load case
- a constant in-plane normal compressive force N significantly decreases the specimen resistance when subjected to increasing in-plane shear force V
- a constant out-of-plane distributed load q do not influence on the specimen resistance when subjected to increasing in-plane shear force V
- the glass panel is deformed out-of-plane due to initial geometrical imperfection which led to buckling of the panel causing out-of-plane buckles
- the glass panel fails due to splitting tension in the compression diagonal. The crack initiated at place of maximal stress concentration at the glass hole 3.

The **Linear supported connection test** was developed to study the adhesive behaviour in the glass/substructure connection and use of mortar as setting block. Two adhesive geometries were tested under different shear force directions (longitudinal and transversal). The setting block was subjected to compressive force. The adhesive deformation and resistance, the mortar deformation and resistance as well as the specimen failure modes have been studied with the following conclusion:

- the adhesive demonstrates elasto-plastic behaviour, with three zones: the linear, the plastic and the softening zone. The zone ranges depend on the shear force direction,
- a three side connection has bigger stiffness and higher resistance than two side connection when subjected to a transversal shear force
- a three side connection has the same stiffness but higher resistance than two side connection when subjected to a longitudinal shear force
- a cohesive failure of the adhesive took place
- two side connection was chosen for further investigation due to easier gluing process, mortar injection process and more comprehensive stress distribution
- the mortar demonstrated high resistance and is therefore adequate as a setting block.

The **Linear supported panel test** investigated the shear buckling behaviour of full-size glass panel linearly glued to the substructure on two shortest edges with mortar as a setting block. The global deformation, stress distribution and specimen failure mode for different load cases have been studied. The results lead to the following conclusions:

- the in-plane specimen stiffness does not depend on the load case when the adhesive is in the linear zone,
- the adhesive yielding has a significant influence on the global deformation of the specimen, introducing the ductility in the specimen,
- the specimens demonstrate high in-plane displacement and out-of-plane deflection
- in-plane normal compression force N and out-of-plane distributed load q decrease the specimen resistance interacted in-plane shear force V ,
- the glass panel is deformed out-of-plane due to initial geometrical imperfection which led to buckling of the panel, causing out-of-plane buckles,
- redistribution of the stresses occurs after yielding of the adhesive: the principal tensile stresses near the compressive setting block increase, while the principal tensile stresses near the setting block under tension decrease,
- glass panel fails due to splitting tension in the compression diagonal with the crack initiation at the place of stress concentration at contact of glass edge and compressive setting blocks.

The experimental investigations helped to understand the behaviour of bolted and glued glass/substructure connections and their local influence on surrounding glass area as well as the global behaviour of glass panels subjected to in-plane shear force. The test results will be utilised to verify the connections and panel models developed in Chapter 5.

5 MODELLING

5.1 INTRODUCTION

From the experimental investigation (Chapter 4) it has been concluded that the axial rigid connection in case of point supported glass panels and two side connections in case of linear supported glass panels show the most suitable solution for a potential use of glass envelope in building stabilization. The objectives of this chapter are to model the connections devices numerically, to study their local behaviour on the surrounding glass and to develop a numerical model of full-size glass panel to study its global behaviour under in-plane shear force. Figure 5.1 shows the organization of Chapter 5.

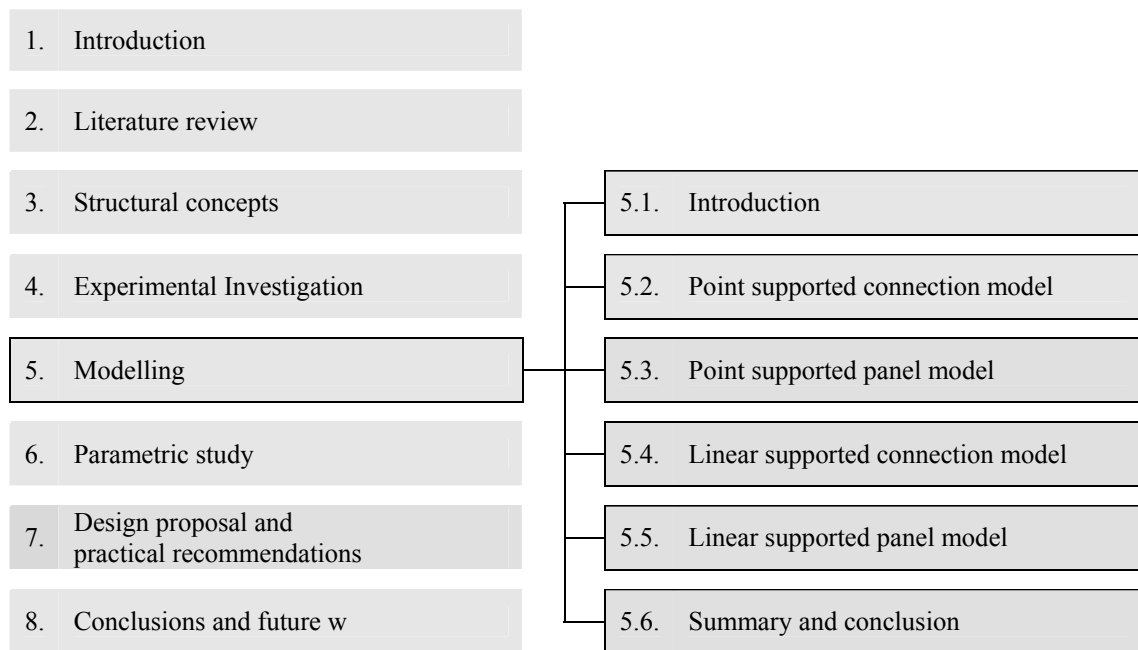


Figure 5.1 - Organization chart of Chapter 5

Point supported connection model. This section describes the developed numerical model of a small size glass plate with axial rigid connection under compressive and tensile forces. The simulated deformation and stress distributions are analysed and compared with the experimental results.

Point supported panel model. In this section the full-size glass panel supported by four points at the corners and subjected to in-plane shear force V is numerically modelled. Global behaviour of a glass panel and shear buckling phenomena are studied. Shear buckling coefficients are determined and deformation, stress distribution and support reactions are analysed. Influences of different load cases (interacting with in-plane shear force) are examined. The model is validated with experimental results.

Linear supported connection model. To study the adhesive behaviour in the glass/substructure connection under transversal shear force, a small size numerical model is developed in this section. The model deformation and stress distribution are used to determine the adhesive material law.

Linear supported panel model. In this section a full-size glass panel linearly supported on two shortest edges subjected to in-plane shear force V is numerically modelled. Global behaviour of a glass panel (deformation, stress distribution and support reactions) and shear buckling phenomena (shear buckling coefficients) are studied for different load cases (interacting with in-plane shear force). The model is validated with experimental results.

Summary and conclusions. At the end of the Chapter the summary and main conclusions are given.

5.2 POINT SUPPORTED CONNECTION MODEL

First, the analytical bases of plates with a hole subjected to uniaxial in-plane tensile load as well as to concentrated force introduced through bolt in the hole are first presented and the existing solutions are described. Then, the numerical model of glass plate with axial rigid connection subjected to compressive and tensile forces (concentrated force introduced by bolt) is developed. The results of a numerical simulation are compared with experimental results and existing solutions.

5.2.1 Analytical bases and existing solutions

The investigation contains the stress distribution and stress concentration factor around the circular hole in infinite and finite panels with a plate subjected to uniaxial in-plane tensile load and in-plane concentrated tensile force introduced by bolt in the hole.

5.2.1.1 Infinite plate with circular hole under uniaxial in-plane tensile load

The infinite plate with circular hole subjected to uniaxial in-plane tensile stress field σ is presented in Figure 5.2. The radius of the hole is a , while r and Φ are the polar coordinates of a point on the plate. Each point of the plate is subjected to the radial stress σ_r , the tangential stress σ_ϕ and the shear stress $\tau_{r\phi}$.

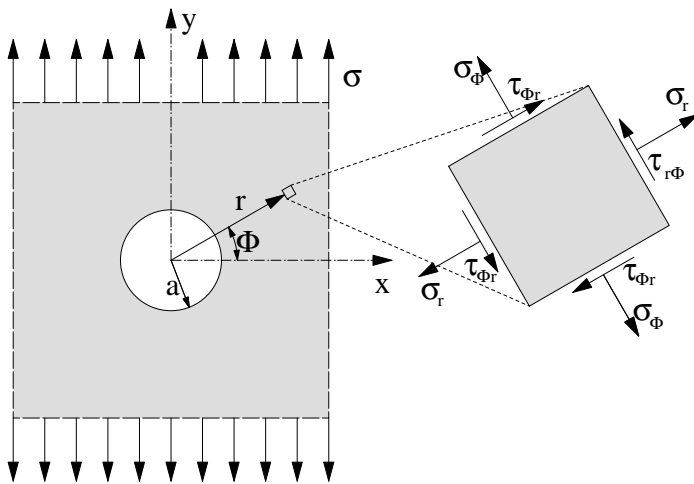


Figure 5.2 – Infinite panel with circular hole under uniaxial in-plane tensile and stresses in the plate

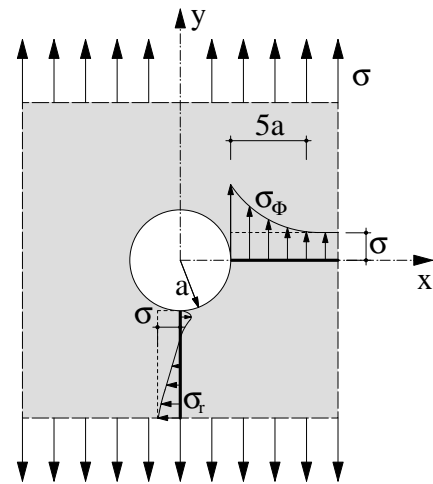


Figure 5.3 – Stress distribution in the plate

[Timoshenko et al. 1970] developed the stresses equations for an infinite plate with circular hole subjected to uniaxial in-plane tensile stress field σ in a polar coordinate system (r and Φ) as a function of applied stress σ :

$$\left. \begin{aligned} \sigma_r &= \frac{\sigma}{2} \left(1 - \frac{a^2}{r^2} \right) + \frac{\sigma}{2} \left(1 + \frac{3a^4}{r^4} - \frac{4a^2}{r^2} \right) \cos 2\phi \\ \sigma_\phi &= \frac{\sigma}{2} \left(1 + \frac{a^2}{r^2} \right) - \frac{\sigma}{2} \left(1 + \frac{3a^4}{r^4} \right) \cos 2\phi \\ \tau_{r\phi} &= -\frac{\sigma}{2} \left(1 + \frac{3a^4}{r^4} + \frac{2a^2}{r^2} \right) \sin 2\phi \end{aligned} \right\} \quad (5.1)$$

At the hole ($r = a$) only tangential stresses take place, while radial and shear stresses are zero. The Equation (5.1) obtains the following values:

$$\left. \begin{aligned} \sigma_r &= 0 \\ \sigma_\phi &= \sigma(1 - 2\cos 2\phi) \\ \tau_{r\phi} &= 0 \end{aligned} \right\} \quad (5.2)$$

At the hole, perpendicular to the direction of the applied stress σ ($\Phi = 0$ and π), the tangential stress σ_ϕ obtains the value of 3σ . By increasing the distance from the hole, the tangential stress σ_ϕ decreases. When r is larger than $5a$ the stress distribution recovers a uniform state $\sigma_\phi = \sigma$ (Fig. 5.3)

From Equation 5.1 the stress distribution at symmetric line of the panel, in the direction of applied stress σ ($\Phi = \pi/2; 3\pi/2$) are:

$$\left. \begin{aligned} \sigma_r &= \frac{3\sigma}{2} \left(\frac{a^2}{r^2} - \frac{a^4}{r^4} \right) \\ \sigma_\phi &= \frac{\sigma}{2} \left(2 + \frac{a^2}{r^2} + \frac{3a^4}{r^4} \right) \\ \tau_{r\phi} &= 0 \end{aligned} \right\} \quad (5.3)$$

The radial stresses σ_r along the plate symmetric line in the direction of applied stresses are zero at the hole ($r=a$), but moving away from the hole, they firstly decrease and later increase, reaching the value of $\sigma_r = \sigma$ (Fig. 5.3.)

5.2.1.2 Finite width plate with circular hole under uniaxial tensile load

The distribution of tensile stresses along the line perpendicular to the load direction in finite width plate with circular hole subjected to uniaxial in-plane tensile stress field σ is presented in Figure 5.4. The presence of a hole in the plate leads to in the modification of the simple stresses distribution and localized high stresses occur. The maximum tensile stress σ_{max} occurs at point A. This localization of high stresses is called stress concentration, measured by the *stress concentration factor* K_t .

The stress concentration factor K_t can be defined as the ratio of the peak stress in the plate (or stress in the perturbed region) to the reference nominal stress:

$$K_t = \frac{\sigma_{max}}{\sigma_{nom}} \quad (5.4)$$

σ_{max} maximum stress to be expected in the panel [N/mm²]
 σ_{nom} nominal stress reference [N/mm²]

The nominal stress reference is the net stress based on the cross section at the hole which is formed by removing the hole diameter from the gross section:

$$\sigma_{nom} = \frac{F}{(H - d)t} \quad (5.5)$$

F force applied through the bolts [N]
 H width of the plate [mm]
 d diameter of the hole [mm]
 t thickness of the plate [mm]

From here, the stress concentration factor becomes:

$$K_t = \frac{\sigma_{max}(H-d)t}{F} \quad (5.6)$$

Stress concentration factors can be obtained analytically from the theory of elasticity, computationally from the finite element method and experimentally using strain gauges or photo-elasticity.

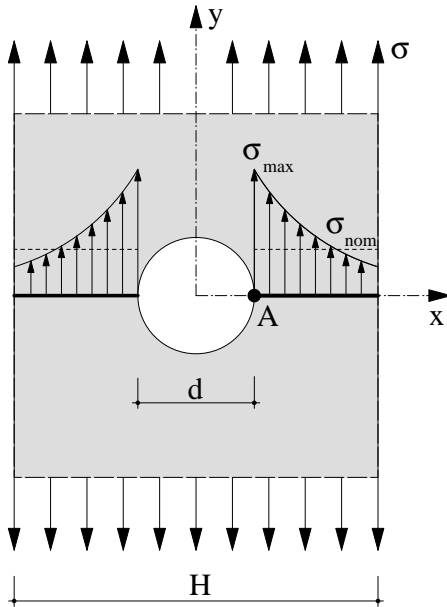


Figure 5.4 – Stress distribution in finite width plate with circular hole under uniaxial in-plane tensile load

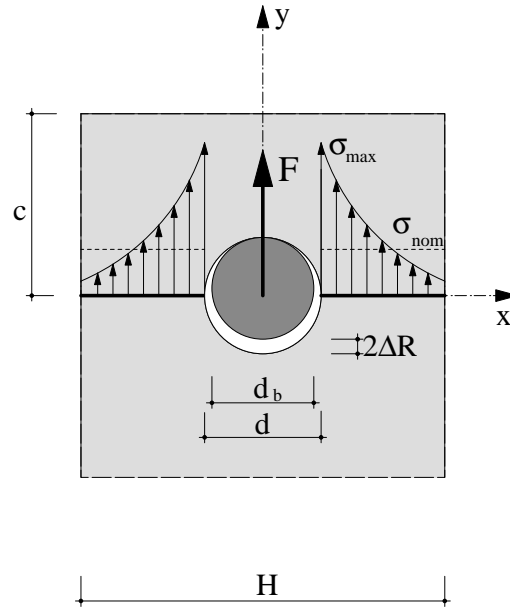


Figure 5.5 – Stress distribution in finite width plate with circular hole loaded through bolt in the hole

Based on several experimental investigations, for the case of a finite width thin plate with a circular hole subjected to uniaxial in-plane tensile, stress concentration factor according to [Pilkey 1997] for ratio $d/H < 0.5$ has the following value:

$$K_t = 2.00 + 0.284\left(1 - \frac{d}{H}\right) - 0.6\left(1 - \frac{d}{H}\right)^2 + 1.32\left(1 - \frac{d}{H}\right)^3 \quad (5.7)$$

[Peterson 1953] gave the following formula for stress concentration factor K_t :

$$K_t = 3.00 - 3.13\left(\frac{d}{H}\right) + 3.66\left(\frac{d}{H}\right)^2 - 1.53\left(\frac{d}{H}\right)^3 \quad (5.8)$$

[Heywood 1952] proposed an empirical formula covering the entire d/H range:

$$K_t = 2.0 + \left(1 - \frac{d}{H}\right)^3 \quad (5.9)$$

5.2.1.3 Finite width panel with circular hole loaded through bolt in the hole

Comparing the stress distribution in infinite plate under uniaxial in-plane tensile and finite width plate with circular hole loaded through bolt in a hole (Fig. 5.5) the problem gets more complex and a closed form solution is unfeasible to derive. Therefore, the experimental investigation or the approximate approach with finite element method is usually adopted to determine the stress concentration factor. Research and design guides provide useful practical solutions, but must be regarded as approximate. The level of accuracy is suitable for design using an appropriate resistance factor or a design factor.

[Frocht et al. 1940] did experimental investigation on aluminium panels of different width with aluminium and steel pins, measuring the stresses with strain gauges and the photo-elastic method. They concluded that the ratio d/H has the main influence on the stress concentration factor. By decreasing the ratio the stress concentration factors is increasing. Additionally, introducing a clearance (ΔR) between the bolt and the hole, the stress concentration factors increased, and tangential stresses are not longer at 90° but move and depend on the magnitude of the clearance. They moved towards the direction of the load. In case of no clearness of ($\Delta R = 0$) and the ratio $c/H > 1$ according to [Frocht et al. 1949] the stress concentration factor K_t can be determined with the following formula:

$$K_t = 12.882 - 52.714\left(\frac{d}{H}\right) + 89.762\left(\frac{d}{H}\right)^2 - 51.667\left(\frac{d}{H}\right)^3 \quad (5.10)$$

In structural glass design, the most used method is the one adopting the Peterson's Stress Concentration factors [Pilkey 1997]. The stress concentration is influenced by plate geometry (distance of the hole form the edge c , plate width H and plate thickness t) as well as the clearance of the pin in the hole (ΔR). For a perfectly fitting bolt, σ_{max} occurs at the point perpendicular to the load direction. If there is clearance between the bolt and the hole, σ_{max} increases in values and occurs at point between 55° - 90° . The stress concentration factor is not significantly affected if the bolt and the panel are made of a different material only if the ratio of their modulus of elasticity (E_{bolt}/E_{plate}) is between 1 and 3. Series of curves was derived to determine the stress concentration factor K_t for different clearance ΔR and different c/H ratio, as a function of d/H ratio for the case when $t/d < 0.5$.

[Duerr 2006] presents a review of theoretical and experimental studies of finite width panels with a circular hole loaded through a bolt in a hole and connects the foundation to develop a set of equations that define bolted connection strength and behaviour. From the collected experimental results from [Frocht et al. 1940] and [Scott et al.1982] as well as numerical results from [Ekvall 1986] stress concentration factor K_t for clearance $\Delta R = 0$ were defined by the following equation:

$$K_t = 1.5 + 1.25\left(\frac{H}{d} - 1\right) - 0.3175\left(\frac{H}{d} - 1\right)^2 \quad (5.11)$$

5.2.2 Numerical model

The numerical model of glass plate loaded through a bolt in a hole, representing the axial rigid connection tested in Section 4.2 and chosen as the most suitable for further research, has been developed with the finite element programme ANSYS 10 [Ansys 2005]. This is general-purpose computer-aided software for engineering technology and design analysis produced by Ansys, INC, Pennsylvania, USA. The numerical modelling consists of the following procedure:

- Construction of the model: element types, material properties, meshing of the model, boundary conditions, load introductions and solution procedure.
- Results: model deformation and stress distribution.
- Validation of the model: comparison of the results with experimental results and existing solutions.

5.2.2.1 Construction of the model

Due to symmetry of the specimen, only half of the glass plate with axial rigid connection (panel with circular hole loaded through bolt in the hole) is modelled to save the computational time and memory (Fig. 5.6). The geometrical and material properties of the numerical model are taken in the same way as in experimentally investigated specimen (Section 4.2): laminated glass plate 200x250 mm (half due to symmetry) with thickness of 8/1.52/8 mm (cyan colour in the Figure 5.7). The hole is constructed 100 mm from the edges and has 42 mm in diameter. The inner diameter of mortar is 30mm (red colour), the pin is 20 mm (green colour) and the bolt has M20 (yellow colour).

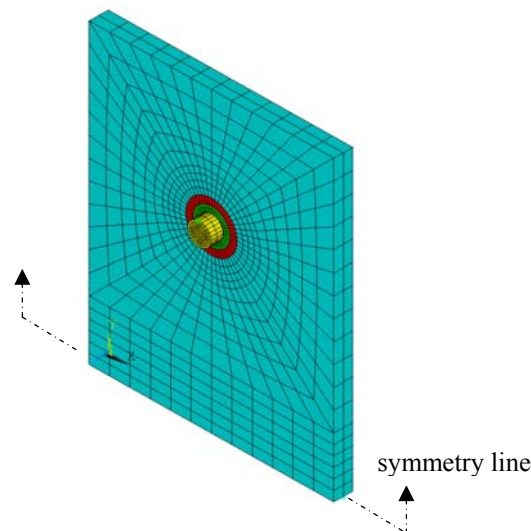


Figure 5.6 – Point support connection model

Element types

SOLID95 element is used to model the glass plate, PVB interlayer, the pin and the bolt. It is a 3D volume element defined by 20 nodes having three degrees of freedom per node: translations in the x, y and z directions. It has large deflection capabilities and can tolerate irregular shapes (Fig. 5.7(a)).

INTER194 element is used to model the mortar. It is a 3D gasket element defined by 16 nodes able to transfer only compressive force between the mating components. The deformation of a gasket is restricted to one direction, that is, through thickness. The element is composed of bottom and top surfaces while the mid-plane is created by averaging the coordinates of node pairs from the bottom and the top (Fig. 5.7.b).

CONTA174 and TARGE170 elements are used to simulate the contact between the bolts and the pin. The surface of bolt is taken as a contact surface and the surface of the pin as a target surface. The contact and target surfaces constitute a contact pair. The contact occurs when the element surface penetrates the specified target surface. CONTA174 is a 3D surface-to-surface 8-node contact element, TARGE170 is 3D target surfaces element paired with an associated contact element (Fig. 5.7(c)).

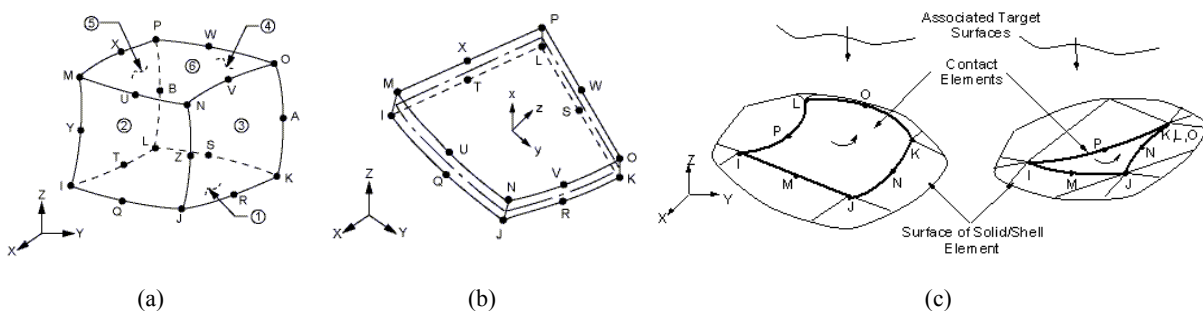


Figure 5.7 – Element types (a) Solid 95 (b) Inter194 (c) Conta174 and Targe170

Material properties

Table 5.8 shows the properties of the utilised material to construct the model (material low, modulus of elasticity E , Poisson's ratio ν material yielding point f_y)

Table 5.8 – Material properties of point supported connection model

Material	Material low	E [N/mm ²]	ν [-]	f_y [N/mm ²]
Glass panel	linear	70'000	0.23	-
Mortar	linear	2'780	0.30	-
PVB interlayer	linear	1.5	0.49	-
Pin (steel)	bilinear	210'000	0.30	235
Bolt 10.9 (stainless steel)	bilinear	197'000	0.30	900

Meshing of the model

The manual meshing is utilised. The mesh is denser near the glass hole to get more accurate results. Several mesh densities are tested to achieve the convergence. Modelled mesh is shown in Figure 5.9.

Boundary condition

Since the numerical model presents half of the specimen, boundary conditions at the bottom of the model ($y = 0$) symbolise the line of symmetry, which prevents a vertical displacement in y direction and two horizontal displacements in x and z direction (Fig. 5.8a)). Nodes at the ending areas of the bolt are coupled with supports allowing the vertical displacement in y direction and preventing horizontal displacement in x and z direction (Figure 5.9.c).

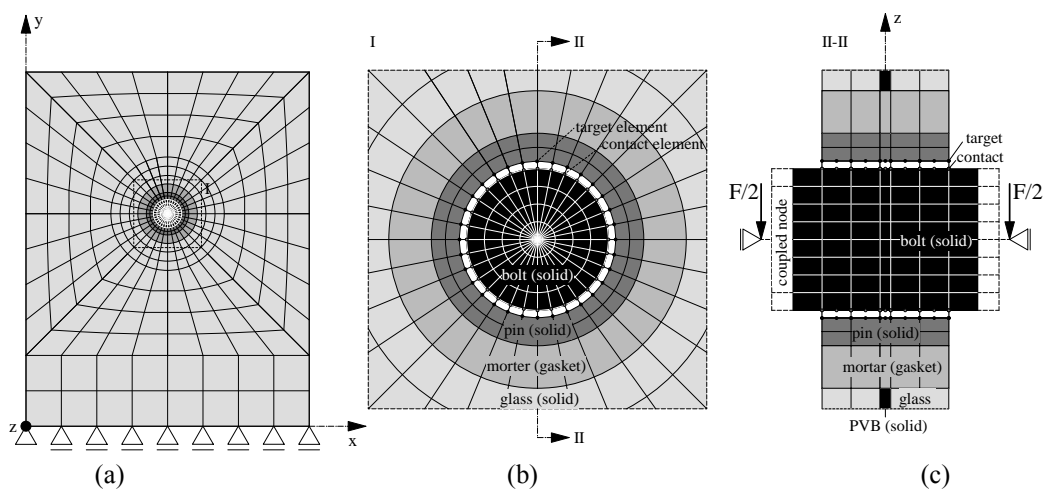


Figure 5.9 – Point support connection model (a) front view (b) connection devices (c) cross section

Load introduction

Half of the force $F/2$ is introduced at the extremities of the bolt, at the support of coupled nodes. When simulating the specimens under tensile, the direction of the force was in the positive y direction, while on the other hand when simulating the specimens under compressive, the force direction was in the negative $-y$ direction (Fig. 5.9(c))

Solution procedure

Due to the nonlinear geometrical behaviour of the contact and target element, as well as the nonlinear material behaviour of the pin and the bolt, a nonlinear analysis was carried out. Newton-Raphson approach to solve non linear problems was adopted. The load was subdivided into increments applied over steps.

5.2.2.2 Results

Stress distribution in glass plate with axial rigid connection subjected to tensile force F_t

Figure 5.10.a shows the distribution of principal tensile stresses σ_t in the glass plate when it is subjected to tensile force F_t . When the clearance ΔR between the bolt and the pin is zero, the maximum tensile stress occurs perpendicular to the load direction (in red on the figure) while the minimum principal tensile stresses occurs also at the glass hole on the line of force direction on the side not subjected to the force (in blue on the figure) (Fig. 5.10(b)). Vector presentation shows the direction of the principal stresses. At the place of maximum principal tensile stress (black arrow) no principal compressive stress (blue arrow) occurs. At the place of maximum compressive stress, at the contact point between the connection device and the glass panel, small principal tensile stress occurs (Fig. 5.11(c)).

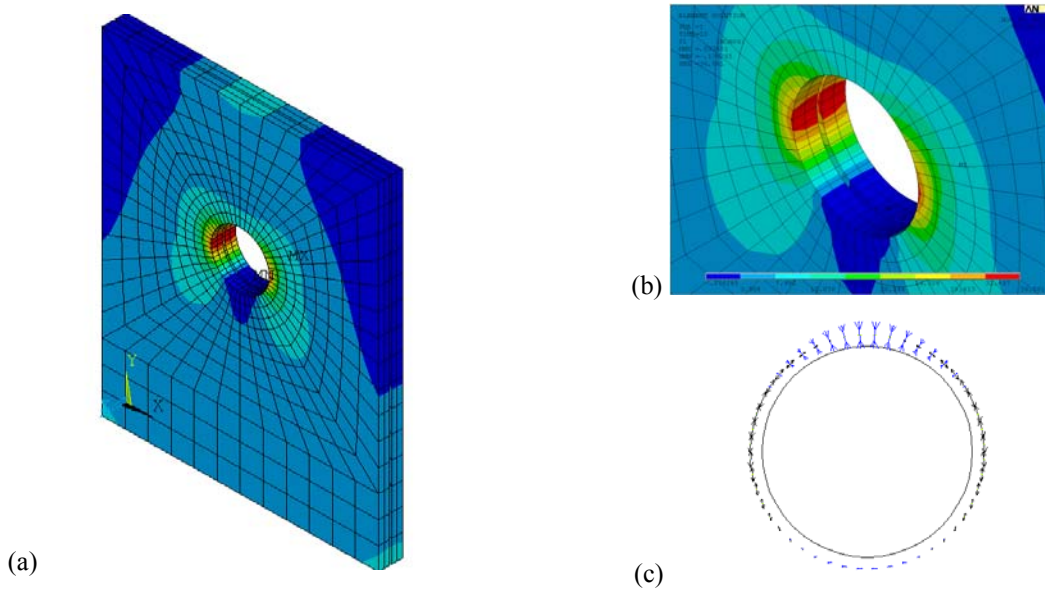


Figure 5.10 – Principal tensile stresses σ_t in glass panel subjected to tensile force F_t
 (a) entire glass plate (b) stresses around the hole (c) vector presentation of principal stresses

Distribution of principal tensile stresses σ_t and nominal tensile stresses σ_{nom} at the line perpendicular to force direction is illustrated in the Figure 5.11(a). The maximum principal tensile stresses occur at the glass hole and decrease when moving to the edge. After a certain distance, the principal tensile stresses get smaller than the nominal tensile stresses. Figure 5.11(b) shows the distribution of principal tensile stresses at the glass hole, with maximum stress at $270^\circ/90^\circ$ and minimum at 180° .

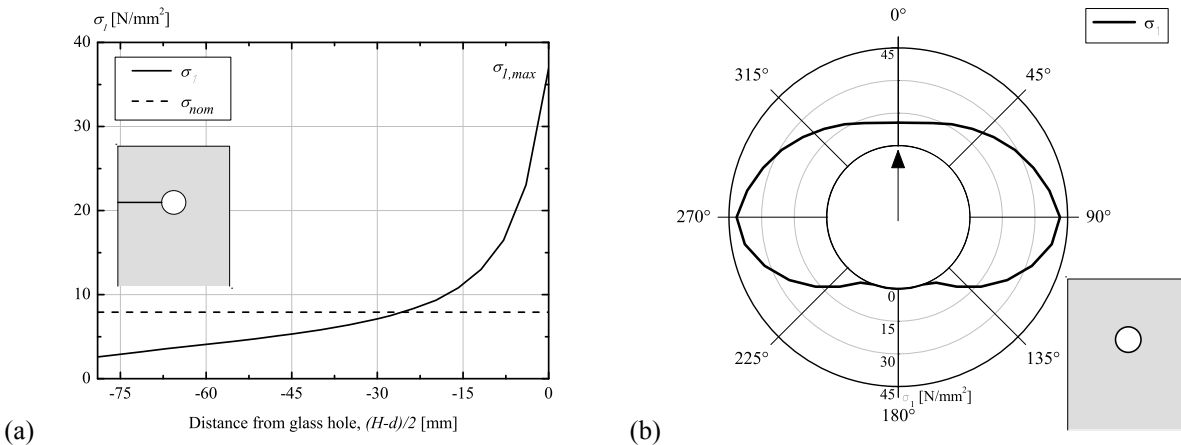


Figure 5.11 – Distribution of principal tensile stresses σ_t
 (a) along the line perpendicular to the force direction (b) at the glass hole

For glass plate under tensile force F_t , the value of maximal tensile stress $\sigma_{l,max}$ at the glass hole is examined (at 90°), keeping constant the diameter of glass hole d and increasing the glass plate width H . Figure 5.12 shows the stress concentration factor K_t in relation to d/H ratio. When decreasing the d/H ratio the stress concentration value increases.

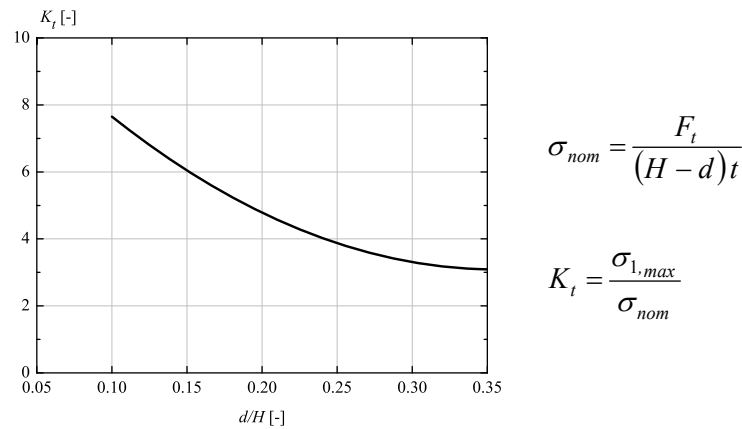


Figure 5.12 – Stress concentration factor K_t (glass panel under tensile force F_t)

By keeping the distance from glass hole to one lateral edge constant and by increasing the distance between glass hole and opposite lateral edge, the stress concentration factor K_t for glass plate under tensile force F_t remains constant.

Stress distribution in glass plate with axial rigid connection subjected to compressive force F_c

The distribution of principal tensile stresses σ_t in glass panel subjected to compressive force F_c is shown in Figure 5.13(a). The clearness ΔR is assumed to be extremely small: 0.05 mm. The maximum tensile stress occurs at the glass hole (in red on the figure) in the direction of the applied force at the contact area between connection devices and the glass plate (Fig. 5.13(b)). From the vector presentation on principal stresses at the glass hole (Fig. 5.13(c)) can be observed that the maximum tensile and maximum compressive stresses take place at the same point.

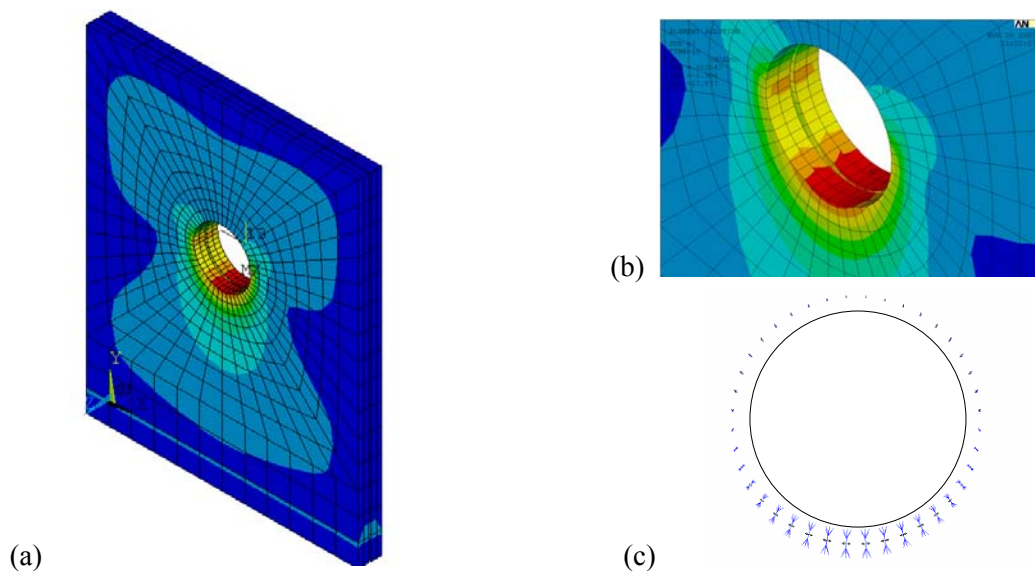


Figure 5.13 – Principal tensile stresses σ_t in glass panel subjected to compressive force F_c
 (a) entire glass plate (b) stresses around the hole (c) vector presentation of principal stresses

When analysing the principal tensile stresses in the direction of compressive force, it can be seen that the maximal principal tensile stresses take place at the glass hole, at the contact area of connection

devices and glass panel, and decrease by moving away from the hole. They disappear after a certain distance (Fig. 5.14(a)). It can be concluded that the connection devices have only a local influence on stress distribution in the surrounding glass plate. The principal tensile stress distribution at the glass hole is shown in Figure 5.14(b). The maximum is at 180° , and with local extremes at 90° and 270° and the minimum at 0° .

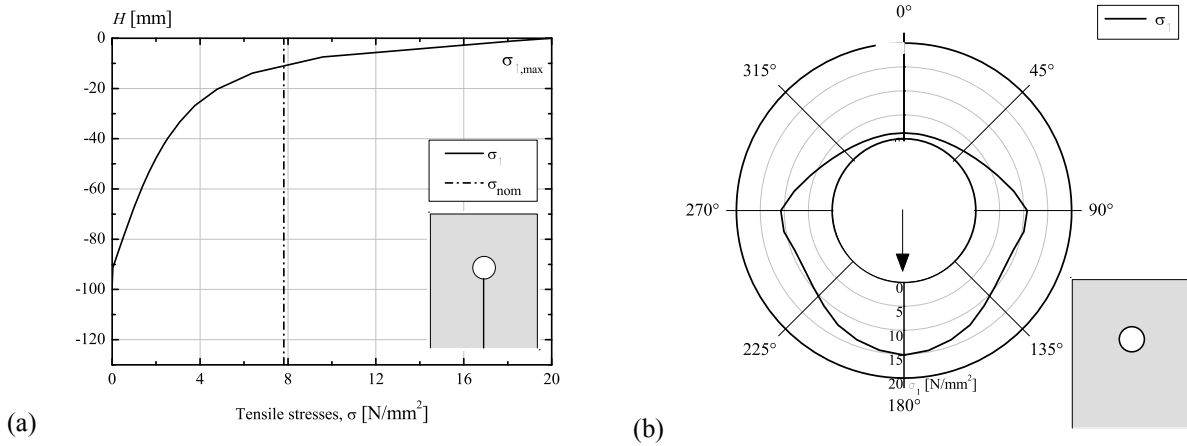


Figure 5.14 – Principal tensile stress σ_l distribution
(a) along the line in the direction of applied force (b) at the edge of glass hole

For glass plate under tensile force F_c , the value of maximal tensile stress $\sigma_{l,max}$ at the glass hole is examined (at 180°), increasing the diameter of glass hole d . Figure 5.15 shows the stress concentration factor K_c in relation to d . By increasing the diameter, the stress concentration value decreases.

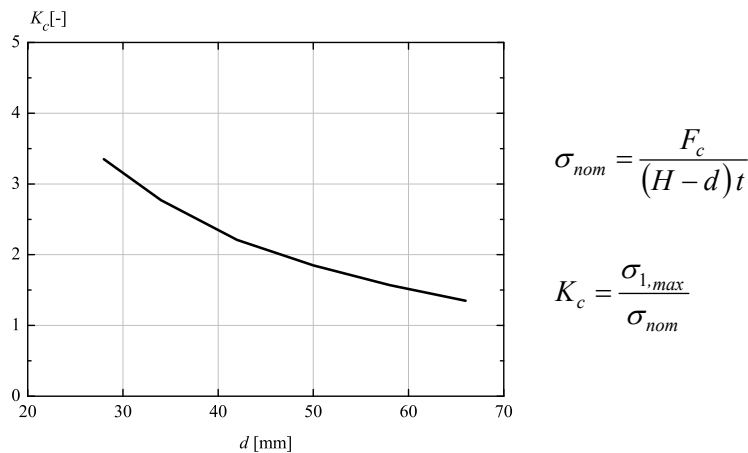


Figure 5.15 – Stress concentration factor K_c (glass panel under tensile force F_c)

By keeping the diameter of the glass hole d constant and increasing the glass panel width H , the stress concentration factor K_c for glass plate under tensile force F_c remains constant.

5.2.3 Validation of the Point Supported Connection Model

5.2.3.1 Comparison of numerical model results and existing solutions

Figure 5.16 compares the stress concentration factor K_t of the numerical model results and the existing solutions proposed by [Frocht et al. 1940], [Pilkey 1997] and [Duerr 2006] presented in §5.2.1. To make a valuable comparison, identical conditions are chosen: clearness $\Delta R = 0$, ratio $t/d > 0.5$ and $c =$

$H/2$. The numerical model result is closest to the solution proposed by [Pilkey 1997] and is parallel (offset approximately 0.7) with the solution proposed by [Frocht et al. 1940].

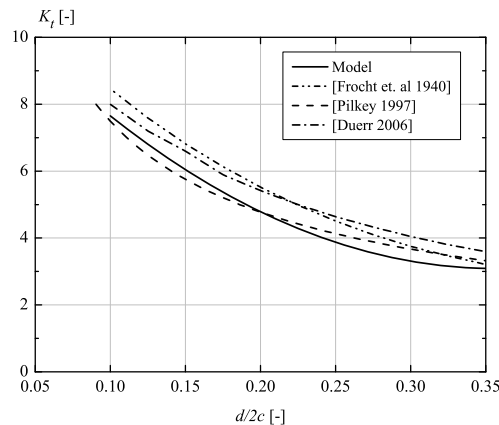


Figure 5.16 – Stress concentration factor K_t as function of ratio d/H

5.2.3.2 Comparison of numerical model results and experimental investigation results

During the experimental investigation, two specimens were equipped with a set of strain gauges located 40mm from the hole centre (detailed explanations in §4.2.2). The principal tensile stresses obtained from the tests are compared with the principal tensile stresses obtained from the numerical simulation at the glass panel surface at 40mm from the glass hole centre. The results of experimental test and numerical simulation are shown in Figure 5.17

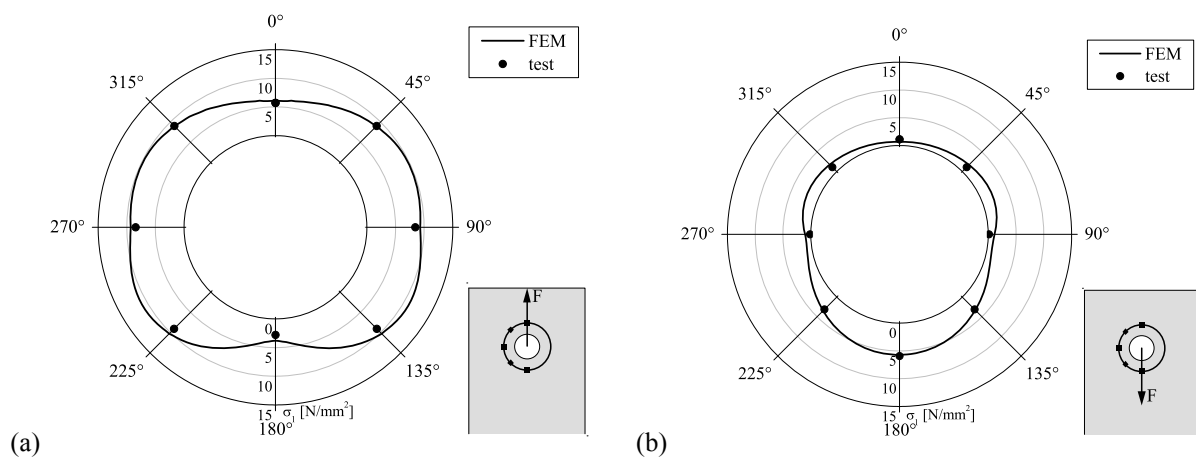


Figure 5.17 – Comparison of principal tensile stresses σ_1 40 mm far from the hole centre in test and numerical model (a) specimen/model under tensile force (b) specimen/model under compressive force

Figure 5.17(a) shows the principal tensile stresses when specimen/model is subjected to tensile force F_t . The numerical simulation results fit very well with the stresses measured during the test. At $0^\circ/45^\circ/315^\circ$, the compared stresses are identical and fit perfectly, while at $90^\circ/135^\circ/180^\circ/225^\circ/270^\circ$, the numerical simulation shows slightly higher stresses than the measured ones. For a specimen/model subjected to compressive force, the principal tensile stresses are compared in Figure 5.17(b). The results fit well. At $135^\circ/180^\circ/225^\circ$, at $45^\circ/90^\circ/270^\circ/315^\circ$ the numerical simulation shows slightly higher stresses than measured, while at 0° the numerical simulation shows smaller stresses than the measured ones.

As a conclusion, numerical results have very good correlation with the experimental results.

5.3 POINT SUPPORTED PANEL MODEL

In this section, the structural model of point supported glass panel under in-plane shear force V is firstly explained. Then, the existing shear buckling theories are described and the determination of critical shear buckling force for simpler cases based on plate and sandwich theory are given. Finally, the numerical model of point supported glass panel under in-plane shear force V is developed to study its shear buckling behaviour. Based on a validated numerical model (comparing the numerical model and experimental investigation results) shear buckling coefficients and critical shear buckling loads are determined, the global panel deformation and stress distribution are analysed, the shear buckling and post-buckling behaviours are studied.

5.3.1 Point support structural model

Structural model of glass panel supported by points on four corners is shown in the Figure 5.18(a) with its boundary conditions and support reactions when subjected to in-plane shear force V (for more detail see §3.3). Support 3 is fixed for the whole translation (x , y and z direction) and rotation around x and y axes. Supports 1, 2 and 3 are fixed for translation in y and z direction and for rotation around x and y axis. The in-plane shear force V is applied at support 1 in $-x$ direction.

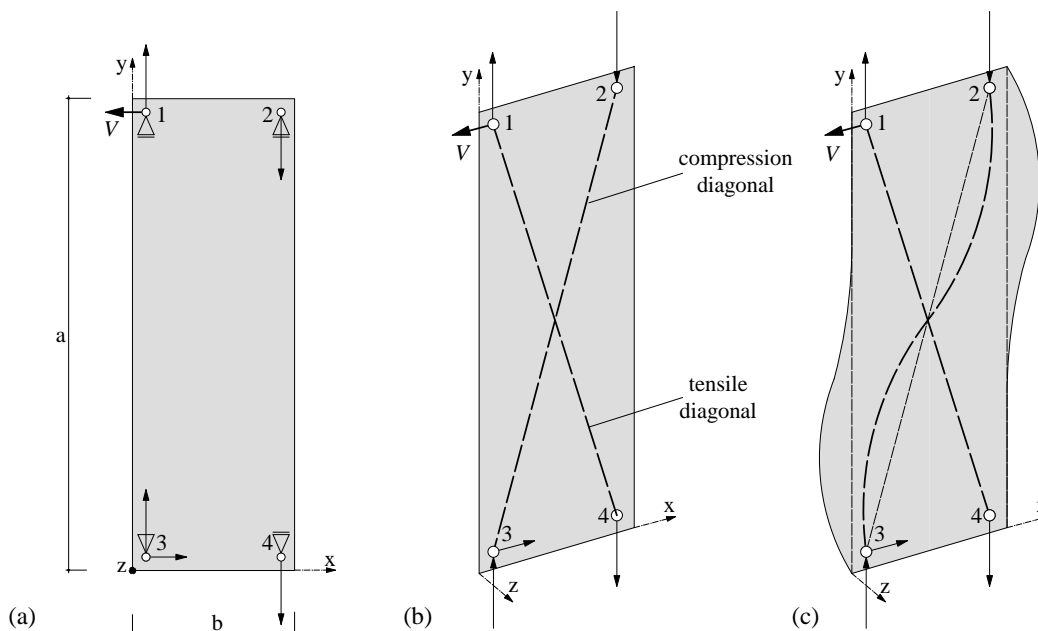


Figure 5.18 – Structural model of point supported glass panel (a) glass panel, boundary conditions and support reactions (b) membrane effect due to compressive and tensile diagonals (c) out-of plane deflection

In-plane shear force V will cause compressive reaction of support 2 and support 3 which lead to the formation of compressive diagonal between these two supports. Compressive diagonal is willing to buckle the panel out-of plane. Contemporarily, tensile reaction forces in support 1 and support 4 create a tensile diagonal which tries to keep the buckled compressive diagonal (Fig. 5.18(b)) straight. These two crossing diagonals cause the membrane effect, which gives the glass panel the favourable stiffening effect. Due to this membrane effect, critical shear force is not the upper limit of the plate resistance, but higher loads than the critical ones can then be applied to the panel (a so called post-buckling reserve).

When the panel with initial geometrical imperfection is subjected to in-plane shear force V , it will deflect out-of-plane. The plate will return to its initial position when the force acts no more. It is valid only when the applied force is smaller than the critical shear buckling forces V_{cr} . If the applied force is higher than the critical shear buckling force, the panel will remain in the deformed position forming buckles (Fig. 5.18(c)).

5.3.2 Analytical bases and existing solutions

Shear buckling is a phenomena occurring in thin plates when subjected to in-plane shear force. Failure mode is characterized by a sudden failure of a structural member subjected to shear stresses, where the actual shear stresses at failure are smaller than the ultimate shear stresses the material is capable of withstanding. The buckling theories describe the forms and the constraints thin plates are subjected to under given external conditions.

The first research on buckling phenomena was done by Euler in 1744 developing the bifurcation theory. This theory was used as a basis for elastic buckling theory proposed by [Timoshenko et al. 1961] where following hypotheses were assumed:

- the panel is perfectly straight (without the initial geometrical imperfection),
- the in-plane shear force acts in plate axis
- the plate is made of infinite linear elastic material (Hook law)
- the small displacement theory is applied.

At bifurcation point the buckling occurs suddenly, the out-of-plane deflection w goes in unknown direction and with infinite amplitude (Fig. 5.19(a)). The stress at bifurcation point is called critical shear buckling stress τ_{cr} and the corresponding load critical shear buckling load V_{cr} .

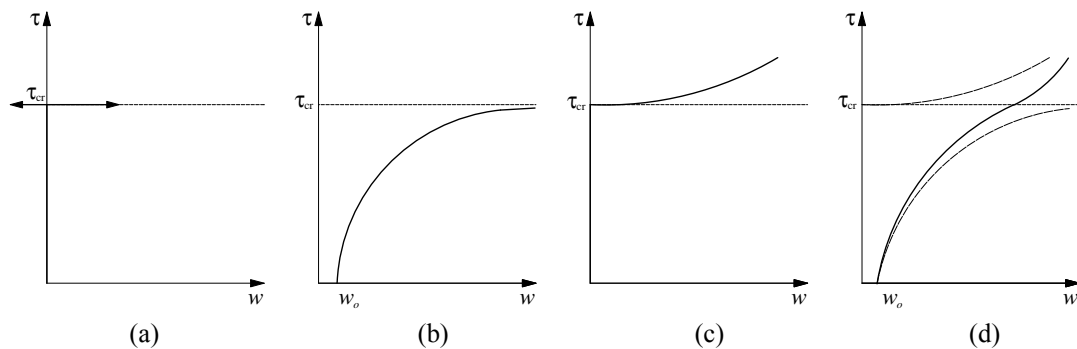


Figure 5.19 – Shear buckling theories (a) elastic buckling theory (b) elastic buckling theory with initial imperfection (c) nonlinear buckling theory (d) nonlinear buckling theory with initial imperfection

The elastic buckling theory is not feasible in the reality. Due to fabrication process, it is impossible to produce an ideally straight panel. The small displacement theory is not valuable for big out-of-plane deflection. The load application exactly in the panel axis is impossible in the reality.

By utilising the elastic buckling theory and assuming the panel has an initial geometrical imperfection w_0 the plate under in-plane shear force V will deflect out-of-plane as shown in Fig 5.19(b). The critical shear buckling stress τ_{cr} represents the stress limit that the deflection asymptotically tries to reach.

However, the elastic buckling theory gives accurate results only for small out-of-plane deflection – when the maximum deflection is less than half of the panel thickness. By increasing the deflection, the membrane stresses induced by the panel geometry will have significant influence on its behaviour – nonlinear analyses for large displacement which take into account the change of geometry should be also used. When large displacement theory is applied on a perfectly straight panel under in-plane shear force V , the panel will stay undeformed until its critical point. At bifurcation point, it will deform suddenly, but it will still be able to carry the additional load before the failure (Fig 5.19(c)). The post buckling reserve is the panel ability to acquire more force after reaching its critical point, which occurs due to membrane effect in the panel.

The plate with initial imperfection w_0 , subjected to in-plane shear force, when applying large displacement theory, will deform out-of-plane w as shown in Figure 5.18(d). The behaviour of such plate resembles the behaviour of a plate with initial imperfection adopting small displacement theory for the value smaller than the critical one, and a case of the ideal plate adopting large displacement theory for the post-critical domain. Such plate behaviour is close to reality and, therefore, the nonlinear buckling theory with initial imperfection will be adopted for further research.

5.3.2.1 Plate theory

Plate theory can be used to determine the critical shear buckling force V_{cr} and shear buckling coefficient k_τ for monolithic glass panel under in-plane shear force V . The earliest solution of a buckling analysis using plate theory was given by [Bryan 1891] but extensive analyses of this problem were given by [Timoshenko et al. 1961] describing the balance-of-force and stationary potential energy criteria for equilibrium on rectangular plate, as well as adjacent-equilibrium and minimum potential energy criteria for loss of stability [Brush et al. 1975]. The idea of plate theory is to reduce a 3D problem to an approximate 2D [Bruhns 2001] with following assumptions:

- the plate is initially flat,
- the material is elastic, homogeneous and isotropic,
- thickness is small compared to area dimension,
- slope of the deflection is small compared to unity,
- deformation is such that straight lines initially normal on the middle surface remain straight and normal on that surface (Bernoulli's hypothesis),
- strains in the middle surface, due to deflection, are negligible compared to strain due to bending,
- deflection of the plate occurs by virtue of displacements of points in the mid-surface

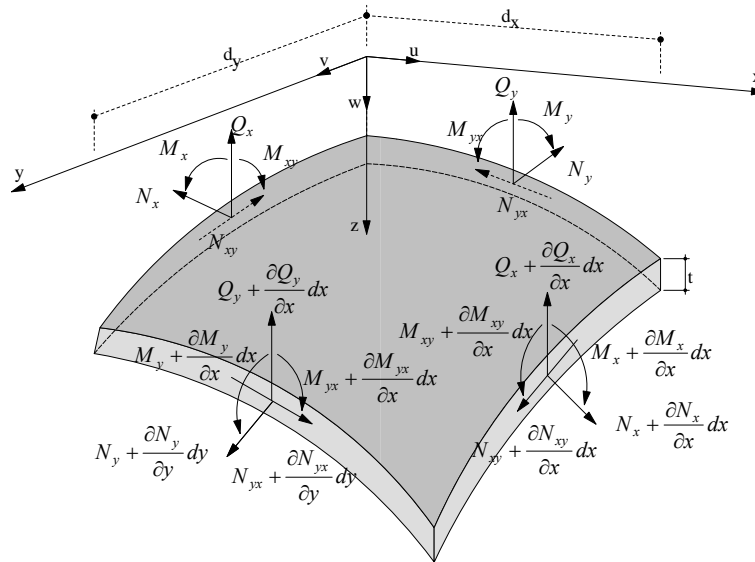


Figure 5.20 – Internal forces acting on plate element

Internal forces acting on the plate element as shown in Figure 5.20 are expressed in terms of forces and moments per unit length along the element edge. The force and moments are related to the internal stresses by the equation:

$$\left. \begin{aligned} N_x &= \sigma_x t & M_x &= \sigma_x z t & Q_x &= \tau_{xz} z t \\ N_y &= \sigma_y t & M_y &= \sigma_y z t & Q_y &= \tau_{yz} z t \\ N_{xy} &= N_{yx} = \tau_{xy} t & M_{xy} &= M_{yx} = \tau_{xy} z t & & \end{aligned} \right\} \quad (5.12)$$

Taking the nonlinear interaction between forces and rotations into account, the equilibrium equation of forces and moments for the plate element in a deformed configuration is:

$$D \cdot \Delta^2 w + N_x \frac{\partial^2 w}{\partial x^2} - 2 \cdot N_{xy} \frac{\partial^2 w}{\partial x \partial y} + N_y \frac{\partial^2 w}{\partial y^2} + Q_x \frac{\partial^2 w}{\partial x^2} - 2 \cdot Q_{xy} \frac{\partial^2 w}{\partial x \partial y} + Q_y \frac{\partial^2 w}{\partial y^2} + \dots = p \quad (5.13)$$

Equilibrium equation is also known as von Karman equation for large deflection of the plate. It can be also derived on the basis of the stationary potential energy criterion.

For the plate subjected only to the shear loading $N_{xy} = V$, assuming other components to be equal to zero, the non linear equilibrium equation (5.13) is reduced to the following form:

$$D \cdot \Delta^2 w = 2 \cdot V \frac{\partial^2 w}{\partial x \partial y} \quad (5.14)$$

D	flexural stiffness [N·mm]
	$D = \frac{E \cdot t_g^3}{12(1-\nu^2)}$
w	out-of-plane deflection function of the plate [mm]
E	module of elasticity of glass [N/mm ²]
t_g	glass panel thickness [mm]
ν	Poisson's ratio of glass [-]

The out-of-plane deflection function $w=w(x,y)$ of the plate is assumed to have the following form:

$$w(x, y) = f(y) e^{ikx/b} \quad (5.15)$$

By introducing the value w (5.15) in the differential equation (5.14), critical shear load can be expressed in the following form:

$$V_{cr} = \frac{\pi^2 D}{b^2} \cdot k_\tau = \frac{\pi^2 E \cdot b \cdot t_g}{12(1-\nu^2)} \cdot \left(\frac{t_g}{b}\right)^2 \cdot k_\tau \quad (5.16)$$

From where the critical shear buckling stress τ_{cr} becomes:

$$\tau_{cr} = \frac{V_{cr}}{t_g \cdot b} = \frac{\pi^2 E}{12(1-\nu^2)} \cdot \left(\frac{t_g}{b}\right)^2 \cdot k_\tau \quad (5.17)$$

b	glass panel width [mm]
k_τ	shear buckling coefficient [-]

Shear buckling coefficient depends on the boundary conditions and geometry ratio $\alpha = a/b$. [Southwell et al. 1924] carried out the analyses and derived the shear buckling coefficient formulas for simplest cases: four side simply supported and four side clamped rectangular panel (Fig. 5.21):

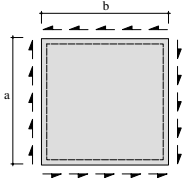
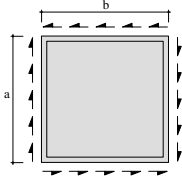
Simply supported panel		$\left. \begin{aligned} k_\tau &= 4.00 + \frac{5.34}{\alpha^2} & \alpha \leq 1 \\ k_\tau &= 5.34 + \frac{4}{\alpha^2} & \alpha \geq 1 \end{aligned} \right\} \quad (5.18)$
Clamped panel		$\left. \begin{aligned} k_\tau &= 5.60 + \frac{8.98}{\alpha^2} & \alpha \leq 1 \\ k_\tau &= 8.98 + \frac{5.60}{\alpha^2} & \alpha \geq 1 \end{aligned} \right\} \quad (5.19)$

Figure 5.21 – Shear buckling coefficient k_τ for four side simply supported and four side clamped monolithic panel

5.3.2.2 Sandwich theory

The sandwich theory is used to determine the critical shear buckling force V_{cr} and shear buckling coefficient $k_{\tau, lam}$ in sandwich panel under in-plane shear force V . Laminated glass can be understood as a sandwich structure as it is made of two glass layers and a thin PVB foil in between and, therefore, the sandwich theory in buckling analysis can be applied. The sandwich theory is used for thick faces and thin core, as in case of laminated glass.

[Kuenzi et al. 1975] solved the problem of rectangular isotropic sandwich plates, simply supported or clamped, subjected to in-plane shear load where different deflection assumptions were adopted for the various boundary conditions and shear load values. [Allen 1969] gave the main and fundamental equations for bending, buckling and vibration of sandwich panels. [Zenkert 1997] developed the theory for orthotropic plates with the constant properties through the panels with the following hypotheses:

- the material of the face layers and the core is elastic,
- the face layers are flat and have a constant thickness,
- the thickness and the rigidity of the faces can not be neglected,
- the transversal normal stiffness of the core is infinite, keeping the face parallel,
- the core is a soft elastic material,
- the properties are constant through the panel.

Figure 5.22 shows the composition of the laminated glass plate and its position in respect to the axis. Glass is a linear elastic material with modulus of elasticity E and Poisson's ratio ν . PVB interlayer is thin and soft regarding the glass layer and, therefore, the only shear stresses are considered without taking the normal stresses into account.

Although being a visco-elastic material whose shear modulus G_{PVB} depends on temperature and load duration, the PVB interlayer is assumed to be a linear-elastic material. When the interlayer has very small shear stiffness (long term load, high temperature) the glass panel behaves independently and the buckling force is the sum of two separate buckling forces – the bending stiffness is governed by the sum of the bending stiffness of the two individual glass panels. On the other hand when the interlayer has large shear stiffness (short term load, impact and low temperature) the glass panels are coupled and the bending stiffness of the composed cross-section governs the buckling force.

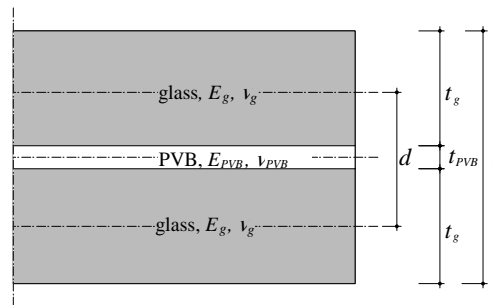


Figure 5.22 – Laminated glass sandwich

The equilibrium equation of forces and moments for a sandwich plate subjected to in-plane shear force V in a deformed configuration is:

$$\frac{D_i}{S} \Delta^3 w - \frac{D_{lam}}{D_o + D_c} \Delta^2 w = 2 \cdot V \frac{\partial^2 w}{\partial x \partial y} \left(\frac{\Delta w}{S} - \frac{1}{D_o + D_c} \right) \quad (5.20)$$

D_i flexural stiffness of the faces around their individual neutral axes (for laminated glass with two glass sheets with identical thickness t_g)

$$D_i = \frac{Et_g^3}{12(1-\nu^2)} + \frac{Et_g^3}{12(1-\nu^2)} = \frac{Et_g^3}{6(1-\nu^2)}$$

$$\begin{aligned}
D_o & \text{ flexural stiffness of the faces around the middle axis} \\
D_o & = \frac{Etd^2}{2(1-\nu^2)} \\
D_c & \text{ flexural bending stiffness of the core (negligible)} \\
D_c & = \frac{E_{PVB}t_{PVB}^3}{12(1-\nu_{PVB}^2)} \\
D_{lam} & \text{ flexural rigidity of a sandwich} \\
D_{lam} & = D_i + D_o + D_c = \frac{Et_g^3}{6(1-\nu^2)} + \frac{Et_g d^2}{2(1-\nu^2)} = \frac{Et_g(t_g^2 + 3d^2)}{6(1-\nu^2)} \\
S & \text{ shear stiffness} \\
S & = \frac{G_{PVB}d^2}{t_{PVB}} \\
t_g & \text{ thickness of individual glass sheet [mm]} \\
t_{PVB} & \text{ thickness of PVB interlayer [mm]} \\
t & \text{ total glass panel thickness [mm]} \\
t & = \sum t_g + t_{PVB}
\end{aligned} \tag{5.21}$$

The out-of-plane deflection function of the sandwich plate is assumed to have the following form:

$$w(x, y) = f(y) e^{ikx/b} \tag{5.22}$$

By introducing the deflection function w (5.21) in the differential equation (5.20), V_{cr} becomes:

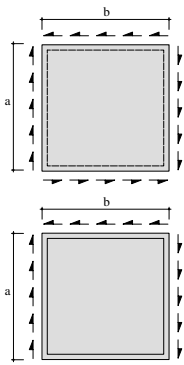
$$V_{cr} = \frac{\pi^2 D_{lam}}{b^2} k_{\tau, lam} = \frac{\pi^2 E \cdot b \cdot t_g}{12(1-\nu^2)} \left(\frac{2t_g^2 + 6d^2}{b^2} \right)^2 k_{\tau, lam} \tag{5.23}$$

from where the critical shear-buckling stress τ_{cr} for laminated glass becomes:

$$\tau_{cr} = \frac{V_{cr}}{2t_g \cdot b} = \frac{\pi^2 E}{24(1-\nu^2)} \left(\frac{2t_g^2 + 6d^2}{b^2} \right)^2 k_{\tau, lam} \tag{5.24}$$

$k_{\tau, lam}$ shear buckling coefficient of laminated glass panel [-]

[Kuenzi and al. 1862] suggested the approximate design formula for shear buckling coefficient $k_{\tau, lam}$ for rectangular sandwich panels, simply supported or clamped on four sides (Fig. 5.23):

$$\begin{aligned}
& \text{Simply supported plate} \\
& \text{Clamped plate}
\end{aligned}$$


$$\begin{aligned}
k_{\tau, lam} & = \frac{\frac{16}{3} + \frac{4}{\alpha^2}}{1 + \frac{\pi^2 D}{b^2 S} \left(\frac{13}{3} + \frac{3}{\alpha^2} \right)} \\
k_{\tau, lam} & = \frac{9 + \frac{17}{3\alpha^2}}{1 + \frac{\pi^2 D}{b^2 S} \left(\frac{23}{3} + \frac{13}{3\alpha^2} \right)}
\end{aligned} \tag{5.25}$$

$$\begin{aligned}
k_{\tau, lam} & = \frac{9 + \frac{17}{3\alpha^2}}{1 + \frac{\pi^2 D}{b^2 S} \left(\frac{23}{3} + \frac{13}{3\alpha^2} \right)}
\end{aligned} \tag{5.26}$$

Figure 5.23 – Shear buckling coefficient $k_{\tau, lam}$ for sandwich panels for four side simply supported and four side clamped monolithic panel

5.3.3 Numerical modelling

The numerical model of point supported glass panel is developed by using the Finite Element programme ANSYS 10.0 [Ansys 2005]. It enables the prediction of shear buckling (shear buckling coefficient) and global behaviour (deformation, stress distribution and support reactions) of a glass panel subjected to in-plane shear. The numerical model is divided into a finite number of elements satisfying the equilibrium and compatibility at each node and along the boundaries between the elements. The following topics are elaborated:

- Construction of the numerical model: element types, material properties, mesh, boundary conditions, load introductions and solution procedure
- Shear buckling coefficient
- Influence of initial imperfections
- Results
- Interaction
- Validation of the numerical model compared with experimental investigation results (Section 4.3)

5.3.3.1 Construction of the model

A full-size glass panel is numerically modelled with the material and geometrical properties defined in *standard point supported glass panel* (Section 3.2). The height of the glass panel is $a = 3500\text{mm}$, the width $b = 1200\text{mm}$ and the thickness $t = 8/15.2/8\text{ mm}$. The holes are constructed at the corners 100 mm from the edges with a diameter of 42 mm. The initial geometrical imperfection is chosen to be the first shear buckling mode shape with the amplitude of $w_o = a/1000$ (Figure 5.24)

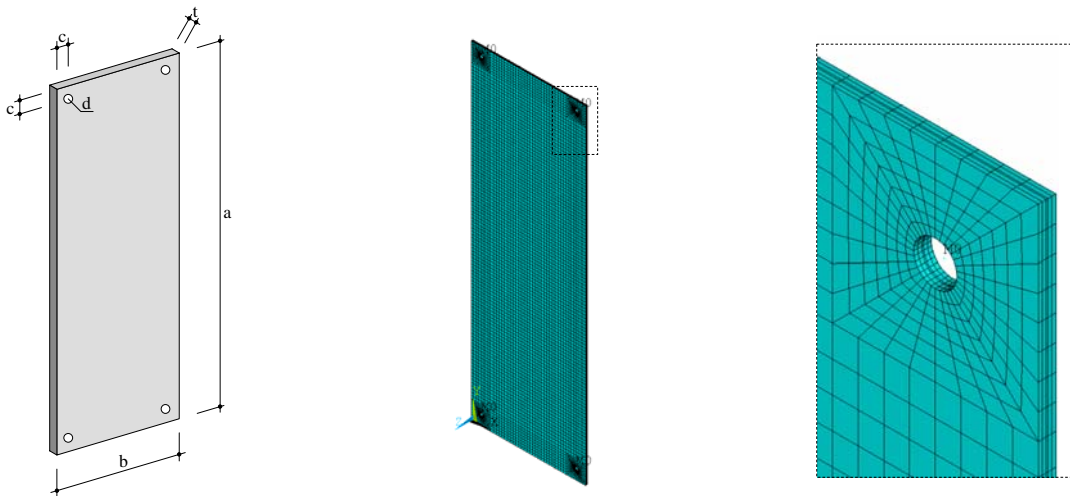


Figure 5.24 – Point supported panel model

Element type

SOLID95 element was used to model the PVB interlayer. Details are given in §5.2.2.1 and Figure 5.9(a).

SELL91 element was used to model the glass panel. It is a nonlinear layered structural shell element used for layered applications of a structural shell model as well as for modelling thick sandwich structures (Fig. 5.25). The element has six degrees of freedom at each node: translations in the nodal x , y and z directions and rotations around the nodal x , y and z -axes. The SHELL91 is suitable for large strain analyses as it allows a change in thickness during loading caused by Poisson's effect.

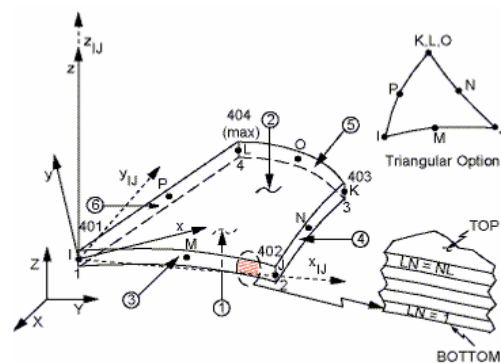


Figure 5.25 – Element types SHELL91

Material properties

Table 5.26 shows the material laws and material properties (modulus of elasticity E , Poisson's ratio ν).

Table 5.26 – Material properties

Material	Model	E [N/mm ²]	ν [-]	f_v [N/mm ²]
Glass panel	linear	70'000	0.23	-
PVB interlayer	linear	1.5	0.49	-

Meshing of the model

The model mesh is configured to lead the results to a convergence. The size of the mesh was determined by the solid element constraints that the length ratio of element edges can not be smaller than 1/20 and the angle between element edges can not be less than 70°. Consequently, the optimal combination of mesh accuracy and elements size was found. A meshed model is shown in Figure 5.27. The opposite nodes at the surface of PVB volume are coupled in z direction to avoid the delaminating.

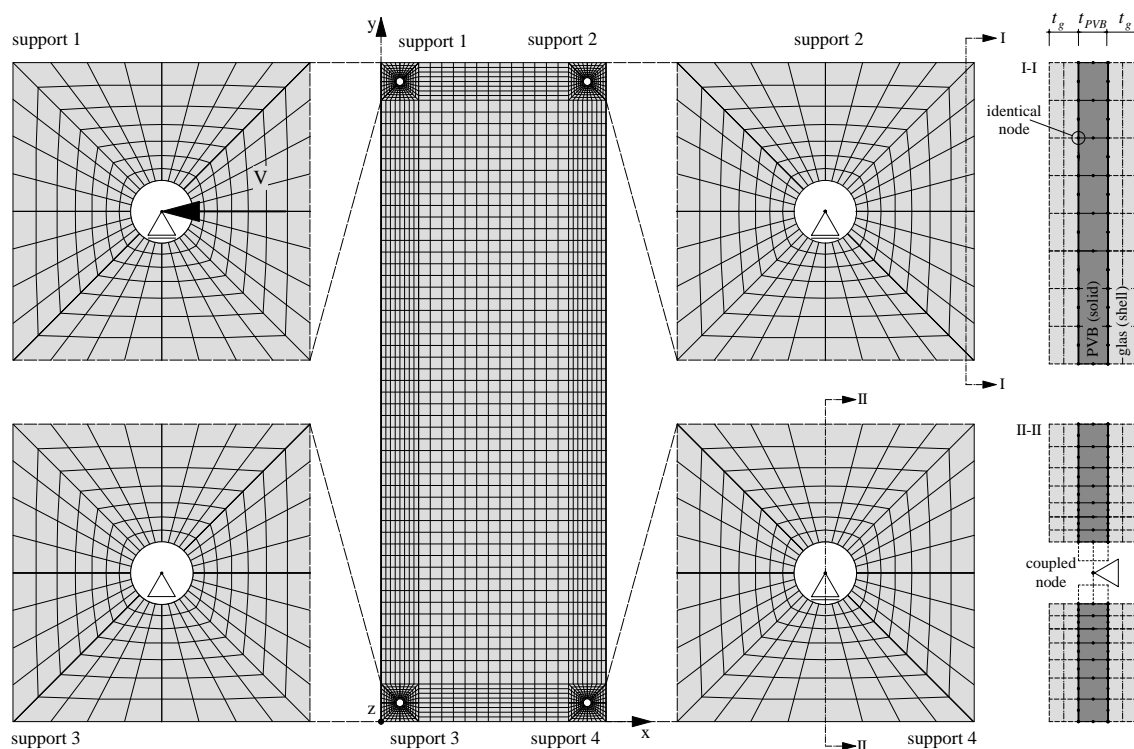


Figure 5.27 – Model mesh with support details and boundary conditions

Boundary conditions

Displacement degree of freedom (x , y and z) of the nodes at glass hole were coupled together. The movement of coupled nodes at support 1, 2 and 4 was not permitted in x and z direction, while the movement of coupled nodes at support 3 was fixed in all three directions.

Load introduction

In-plane shear force V is applied as a concentrated force at support 1, acting in $-x$ direction.

Solution procedure

The solution procedure is divided in two steps: elastic buckling analyses and nonlinear buckling analyses. The elastic buckling analysis is used to predict the critical shear force and the corresponding shear buckling shapes. The unity in-plane shear load $V=1\text{kN}$ is applied and the response is calculated ignoring the large displacement effect and time-varying loads. The eigenvalues calculated by the elastic buckling analysis represent the shear buckling load factor. Since the unit load is specified, the load factors represent critical shear load V_{cr} . Obtained shear buckling mode shape is selected to represent the initial imperfection: the out-of-plane deflections necessary to initiate a buckling response. The next step is nonlinear buckling analyses. The initial geometrical imperfection is introduced by adding the shear buckling mode shape from the elastic buckling analysis. For the nonlinear buckling analysis, the "Newton-Raphson" approach was employed. In this approach, the load is subdivided into a series of load increments which are applied over a number of load steps.

5.3.3.2 Shear buckling coefficients

From the elastic buckling analysis, critical force V_{cr} of point supported glass panel is determined. Knowing the critical shear force of monolithic glass panel, the shear buckling coefficient k_τ becomes (from Equation 5.16):

$$k_\tau = \frac{b^2}{\pi^2 D} V_{cr} = \frac{12(1-\nu^2)}{\pi^2 E t_g} \left(\frac{b}{t_g} \right)^2 V_{cr} \quad (5.27)$$

For laminated glass panel, shear buckling coefficient $k_{\tau,lam}$ becomes (from Equation 5.22):

$$k_{\tau,lam} = \frac{b^2}{\pi^2 D_{lam}} V_{cr} = \frac{12(1-\nu^2)}{\pi^2 E t_g} \left(\frac{b^2}{2t_g^2 + 12d^2} \right) V_{cr} \quad (5.28)$$

The Figure 5.28 shows the shear buckling coefficient in a monolithic glass panel k_τ and a laminated glass panel $k_{\tau,lam}$ in relation to the geometrical ratio $\alpha=a/b$ (for constant $c=100\text{m}$ and $d=42\text{mm}$). The shear buckling coefficient in laminated glass is additionally dependant of the stiffness of the PVB interlayer. Therefore, several curves are given for different PVB shear modulus.

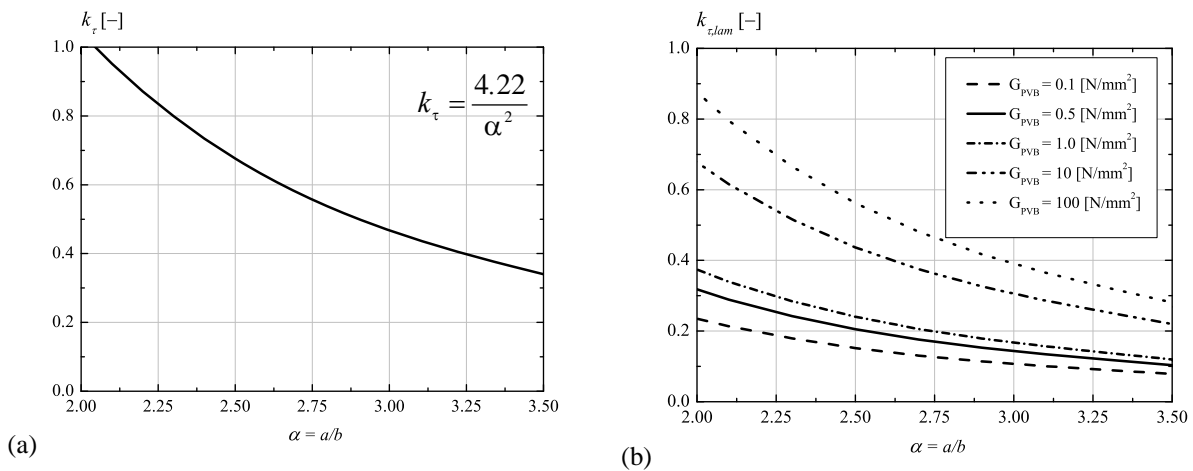


Figure 5.28 – Shear buckling coefficient for (a) monolithic glass panel k_τ (b) laminated glass panel $k_{\tau,lam}$

5.3.3.3 Results

In-plane shear force V vs. out-of-plane deflection w_{max}

Due to the initial geometrical imperfection and the large displacement theory, the nonlinear buckling analysis shows that the glass panel subjected to in-plane shear force V deflect out-of-plane w . Figure 5.29(a) shows out-of-plane deflection w of the glass panel. The compressive diagonal tries to buckle the glass plate, while the tensile diagonal tries to keep it straight. Consequently, two semi-buckles are created, one in z direction (positive semi-buckle, in red in the Figure) and the second in $-z$ direction (negative semi-buckle, in blue in the figure).

The in-plane shear force V vs. maximal out-of plane deflection w_{max} of the glass panel is presented in Figure 5.29(b). The maximum out-of plane deflection does not occur always at the same point, but moves along the free edge on the top of the semi-buckle. Due to the membrane effect, the glass panel can be subjected to the force higher than the critical shear force V_{cr} . At this point V - w_{max} curve inflects. This additional glass panel resistance is called the post-buckling reserve.

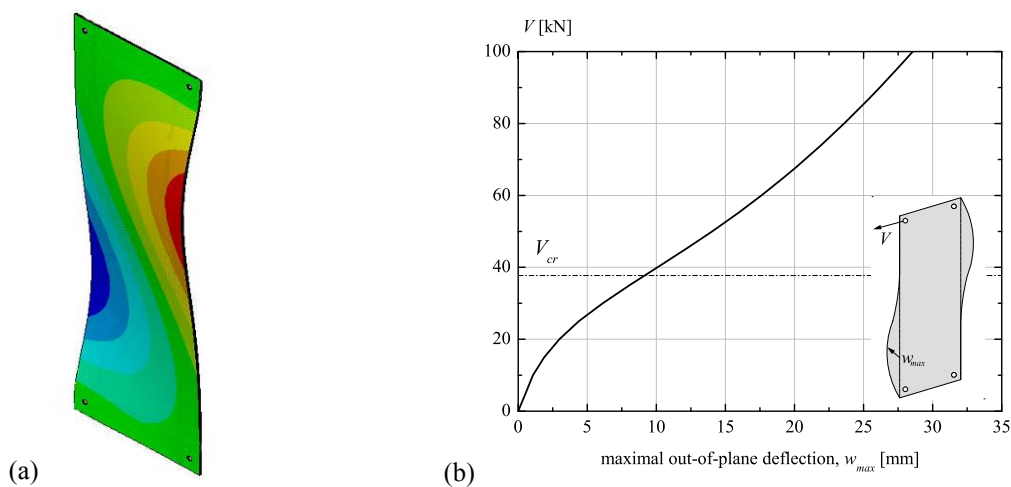


Figure 5.29 – (a) out-of-plane deflection (b) in-plane shear force V vs. maximal out-of-plane deflection w_{max}

In-plane shear force V vs. in-plane displacement u

Figure 5.30 shows the relation of in-plane shear force V vs. in-plane displacement u of glass panel at support 1. Until the critical shear force V_{cr} is achieved, the quasi-linear behaviour of in-plane displacement is observed. Due to shear buckling, the curve deviates at the critical value and a nonlinear behaviour can be observed. This non linear behaviour introduces ductility to the system.

In-plane shear force V vs. support reactions R

The tensile support reaction R_1 (the resultant of the vertical support reaction and the applied in-plane shear force V) and the tensile support reaction R_4 , leads to formation of a tensile diagonal between supports 1 and 4. Being a sum of two forces, the tensile force at support 1 is higher than the tensile force at support 4. The compressive support reaction R_2 and the compressive support reaction R_3 (the resultant of both vertical and horizontal support reactions) creates the compressive diagonal in the glass panel. The compressive support reaction R_3 (being the sum of two forces) is higher than the compressive support reaction R_2 .

Figure 5.31 shows the relation between the in-plane shear force V and support reactions R . The negative is the compressive support reaction (R_3), while the positive is the tensile support reaction (R_1). The support reactions increase linearly with the increase of in-plane shear force up to a value close to the critical shear force V_{cr} when it deviates, demonstrating a nonlinear behaviour. The compressive support reaction curves increase more rapidly, while the tensile support reaction increases more slowly.

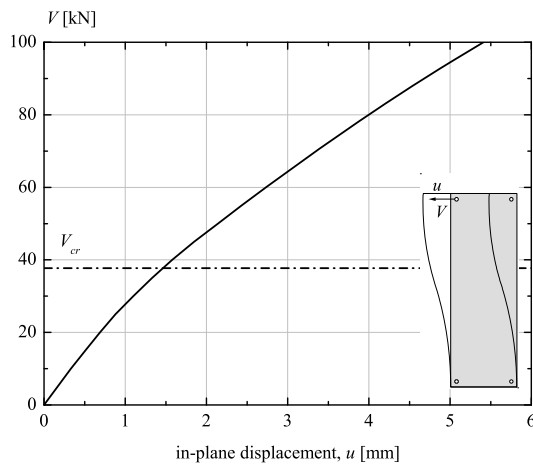


Figure 5.30 – In-plane shear force V vs. in-plane displacement u

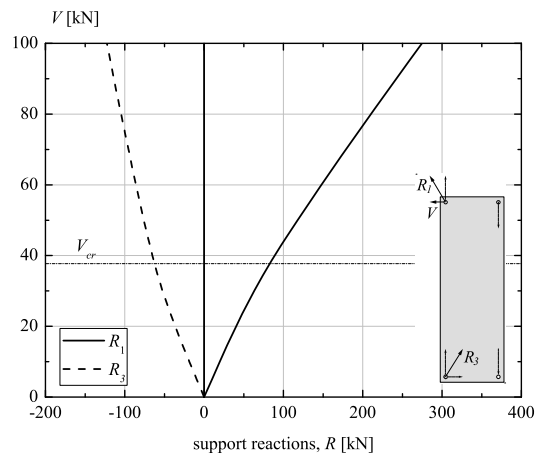


Figure 5.31 – In-plane shear force V vs. support reactions R

Tensile stress distribution in the glass panel

The distribution of principal tensile stresses σ_1 in the glass panel subjected to in-plane shear force V can be divided in:

- Principal tensile stresses σ_1 around the glass hole caused by the load introduction and support reactions. High stress concentration occurs localised near the glass hole. The local behaviour of point support connection and its influence on surrounding glass is studied in Section 5.2.
- Principal tensile stresses σ_1 caused by shear buckling of glass panel. They occur in the glass panel span, at the point of bending caused by semi-buckles.

Figure 5.32(a) presents the principal tensile stresses σ_1 on the front-side of the subjected glass panel surface. Red colour shows the place of maximal stresses occurring at the supports (maximal is at support 3). High principal tensile stresses occur also due to shear buckling around the support 3 (negative semi-buckles) and near support 2 (positive semi-buckles). The principal tensile stress distribution on the back-side of the glass panel surface is presented in figure 5.32(b). Maximal stresses are at supports, while high stresses due to shear buckling, take place around the supports 2 and 3.

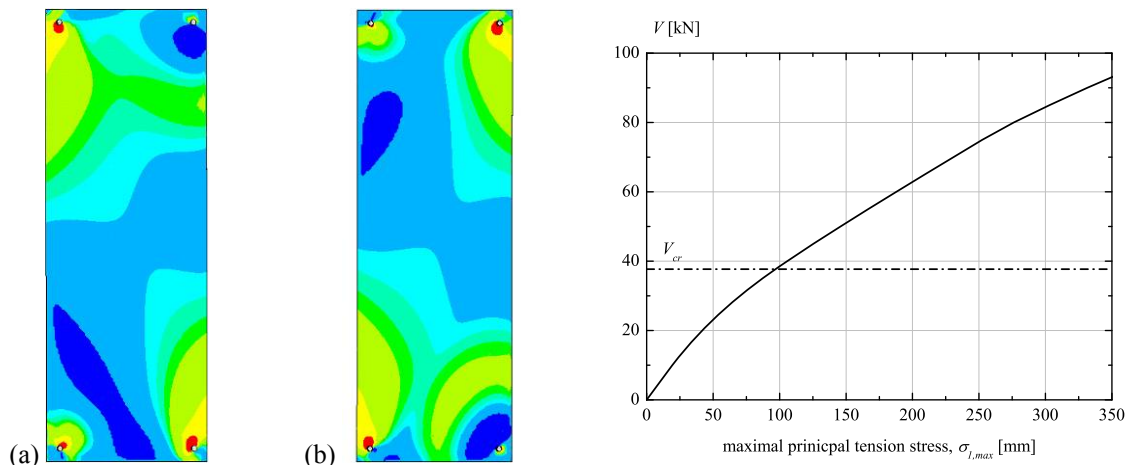


Figure 5.32 – Distribution of principal tensile stresses in glass panel (a) front side (b) back side (c) in-plane shear force V vs. maximal principal tension stresses $\sigma_{1,max}$

The Figure 5.32(c) shows the in-plane shear force V vs. principal tensile stresses σ_1 at the supports (maximal at support 3) and in the glass span due to buckling. The linear behaviour is observed up to critical shear buckling force V_{cr} when the curve deviates.

5.3.3.4 Influence of initial geometrical imperfection shape

Initial geometry imperfection is supposed to have a significant impact on the shear buckling behaviour. If the plate is absolutely flat and the loading on the structure is perfectly in-plane, the out-of-plane deflections necessary to initiate a nonlinear buckling will never occur – the instability due to bifurcation will take place. In reality, this is not the case and the initial imperfection due to fabrication should be taken into account. To analyse the influence of the different initial geometry imperfection, the following out-of-plane perturbation shapes were chosen:

- Imperfection 1: first buckling mode shape, $w_o = a/1000$ (Fig. 5.33(a))
- Imperfection 2: second buckling mode shape, $w_o = a/1000$ (Fig. 5.33(b))
- Imperfection 3: shape caused by out-of-plane distributed load q , $w_o = a/1000$ (Fig. 5.33(c))

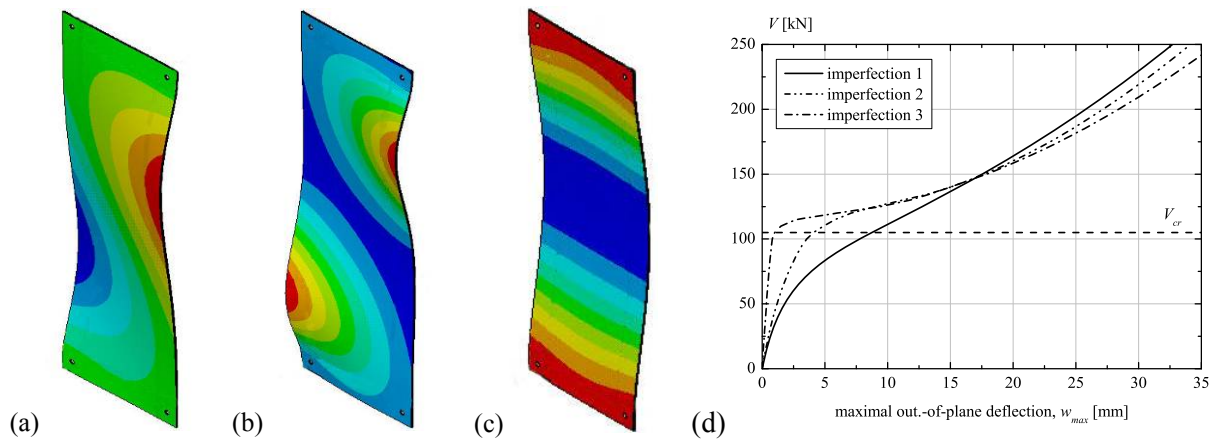


Figure 5.33 – Initial geometrical imperfection (a) imperfection 1 (b) imperfection 2 (c) imperfection 3 (d) in-plane shear force V vs. out-of-plane deflection w_{max} for different imperfections

Figure 5.33(d) shows the influence of different initial geometrical imperfection shapes on out-of-plane glass panel deflection w_{max} . For values smaller than approximately 1.5 of critical shear buckling force V_{cr} , the most unfavourable behaviour is demonstrated by the glass panel with the first buckling mode shape (imperfection 1), while the most favourable is the imperfection 3. Above this value the behaviour changes and the most favourable turns out to be the glass panel with first buckling mode shape as the initial imperfection (imperfection 1), while the most unfavourable is the imperfection 3. The sudden perturbation of the V - w_{max} curve is observed for imperfection 2 and imperfection 3 at a place near the critical shear buckling force V_{cr} . It occurs due to a snap-through of the glass panel, when semi-buckles change the directions (initial geometrical shape of imperfection 2 (Fig. 5.33(a)) and imperfection 3 (Fig. 5.33(b)) changes in a deformed shape (Fig. 5.29(a)).

5.3.3.5 Interaction

Modelled glass panel is subjected to different load cases to investigate the influence of the out-of-plane distributed load q and in-plane normal compressive force N on shear buckling behaviour of point supported glass panel. The following load cases are analysed:

Load case $q+V$

Modelled glass panel is subjected to a constant out-of-plane distributed load q . It is applied as a uniform pressure perpendicular to the glass panel surface in $-z$ direction (Fig. 5.34(a)) with the value of $q = 0.4 \text{ kN/m}^2$ (used in experimental investigation, which corresponds to the perpendicular wind load simulated by the self weight of glass panel, abbreviation $q_{0,z}$). The obtained glass panel out-of-plane deflection is settled to be the initial geometrical imperfection of the glass panel on which the increasing in-plane shear force V is applied as a concentrated force at the support 1 in the $-x$ direction (Fig. 5.34(c)). The nonlinear buckling analysis is made.

Load case $N+V$

The initial geometrical imperfection shape is settled to be Imperfection 3 (§5.3.3.4, Fig. 5.33.c) with an amplitude $w_o = a/1000$ because the glass panel under the in-plane normal compressive force N applied on such initial imperfection shows the highest out-of-plane deflection. A pair of in-plane normal compressive forces $N = 20 \text{ kN}$ (used in experimental investigation, which corresponds to the roof weight, abbreviation N_{20}) is applied as a concentrated force at the support 1 and support 2 in the $-y$ direction (Fig. 5.33(b)). On such a deformed glass panel the in-plane shear force V is applied as a concentrated force at support 1 in the $-x$ direction. The nonlinear buckling analysis is made.

Load case $q+N+V$

A glass panel deformed by out-of-plane distributed load q ($q=0.4 \text{ kN/m}^2$) is subjected to the in-plane normal compressive force N ($N = 20 \text{ kN}$). The obtained out-of-plane deflection is established to be the initial geometrical imperfection of the glass panel subjected to in-plane shear force V applied as a concentrated force at support 1 in the $-x$ direction. The nonlinear buckling analysis is made.

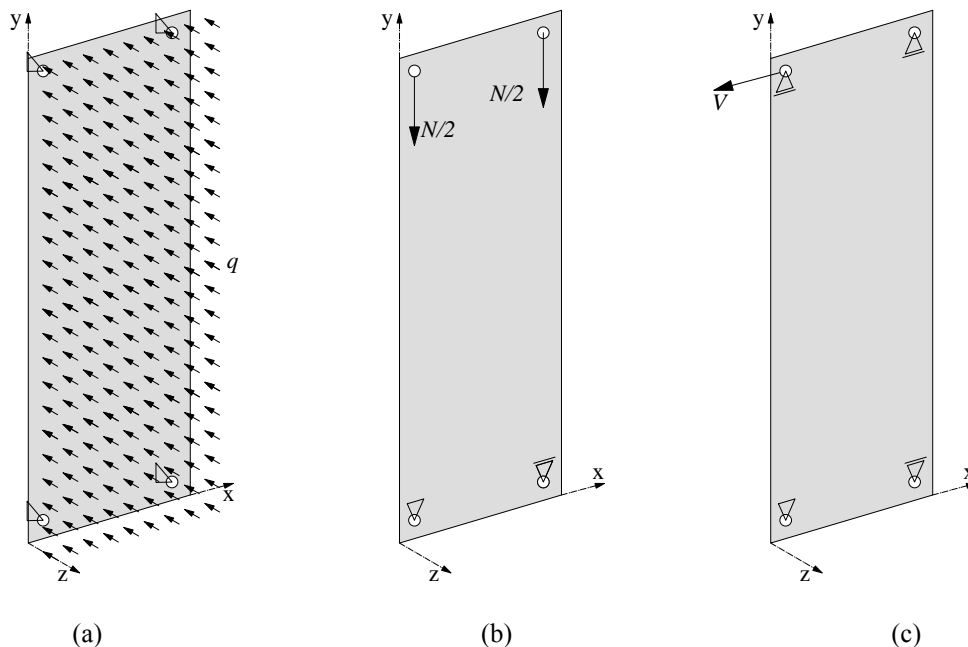


Figure 5.34 – Point supported glass panel subjected to (a) out-of-plane deflection q (b) in-plane normal compressive force N (c) in-plane shear force V

The deformation shape of the glass panel subjected to the in-plane shear force V consists of two semi-buckles as shown in Figure 5.29(a). However, the initial geometrical imperfection shape for load case $q_{0.4}+V$, load case $N_{20}+V$ and load case $q_{0.4}+N_{20}+V$ have the shape as in Figure 5.33(c). The in-plane shear force V will try to deform this initial geometrical imperfection shape in its natural shape with two semi-buckles. Consequently, a perturbation of the deflection can take place due to a snap-through point in which a sudden change of the deflection direction occurs. In the initial geometrical imperfection the entire glass is deflected in $-z$ direction, but when subjected to the in-plane shear force, one semi-buckle tries to deflect in $+z$ direction while the second semi-buckle deflects further in $-z$ direction.

Four values of out-of-plane distributed load q in load cases $q+V$ are analysed:

- $q_{0.2} = 0.2 \text{ kN/m}^2$
- $q_{0.4} = 0.4 \text{ kN/m}^2$
- $q_{0.6} = 0.6 \text{ kN/m}^2$
- $q_{0.8} = 0.8 \text{ kN/m}^2$

For a small value of out-of-plane distributed load q ($q_{0.2}$ and $q_{0.4}$), the amplitude of the initial geometrical imperfection is small (Fig. 5.35(a)). The applied in-plane shear force V deforms the glass plate producing two semi-buckles (one in z direction and other in $-z$ direction). There is a snap-through point in which the out-of-plane deflection shapes change suddenly (Fig. 5.34(b)(c)). For a higher value of out-of-plane distributed load q ($q_{0.6}$ and $q_{0.8}$) the amplitude of the initial geometrical imperfection is large. Subsequently applied in-plane shear force V is still capable of creating two semi-buckles, but it is not capable of changing the deflection direction of the glass panel. Both semi-buckles occur in the $-z$ direction avoiding the snap-through point and the sudden change in deflection direction (Fig. 5.35(c)(d)).

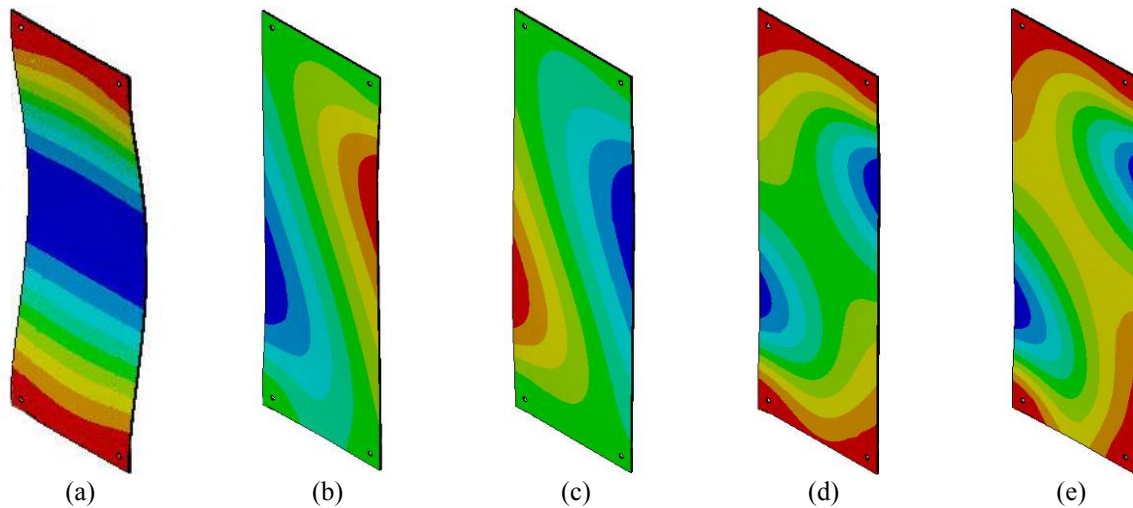


Figure 5.35 – Glass panel out-of-plane deflection shape when subjected to (a) q (b) $q_{0.2} + V$ (c) $q_{0.4} + V$ (d) $q_{0.6} + V$ (e) $q_{0.8} + V$

Figure 5.36 shows the in-plane shear force V vs. maximal glass panel out-of plane deflection w_{max} for different values of out-of-plane distributed load q . The curves do not start from zero, but from the deflection caused by a constant out-of-plane distributed load. The sudden perturbation of the out-of-plane deflection due to snap-through point is observed in the glass panel subjected to distributed force $q_{0.2}$ and $q_{0.4}$, while out-of plane deflection of the glass panel subjected to distributed load $q_{0.6}$ and $q_{0.8}$ is smooth. Figure 5.37 shows the in-plane shear force V vs. in-plane displacement u for different values of out-of-plane distributed load q . The in-plane displacement is linear and independent of the whole out-of-plane distributed load q for the values smaller than the critical shear buckling force V_{cr} when the sudden perturbation occurs due to a snap-through. In glass panels with perturbation ($q_{0.2}$ and $q_{0.4}$) the in-plane displacements suddenly increase, but after the stabilisation they get parallel with the in-plane displacement of the glass panel without the perturbation ($q_{0.6}$ and $q_{0.8}$)

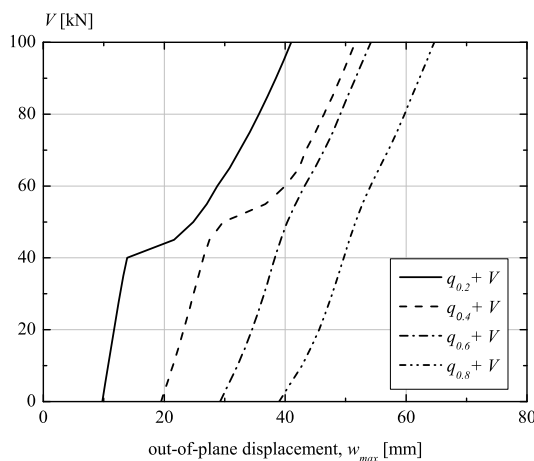


Figure 5.36 – In-plane shear force V vs. maximal out-of-plane deflection w_{max}

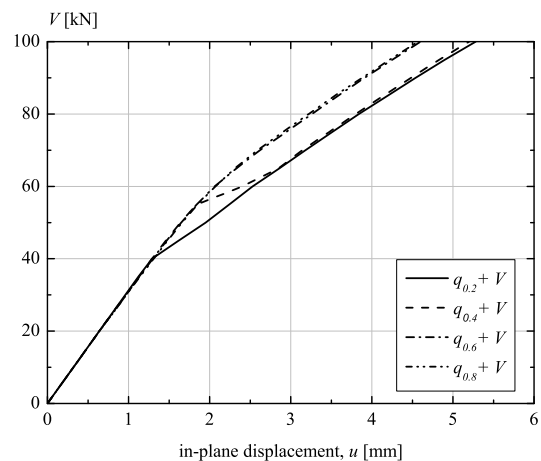


Figure 5.37 – In-plane shear force V vs. in-plane displacement u

The Figure 5.38 shows the in-plane shear force V vs. maximal out-of-plane deflection w_{max} for different load cases. Each load case has different initial geometrical imperfection amplitude. The load case V has the initial imperfection corresponding to the first buckling mode shape, and therefore a smooth out-of-plane deflection takes place. Other load cases have the initial imperfection illustrated in Figure 5.35(a). When the initial imperfection amplitude is big enough, no snap-trough point occurs (load cases $q_{0.4}+N_{20}+V$). The value of the initial imperfection influences the glass panel deflection path: the curve with a small imperfection increases with negative progression until the critical shear force, while the curve with large imperfection increases with positive progression.

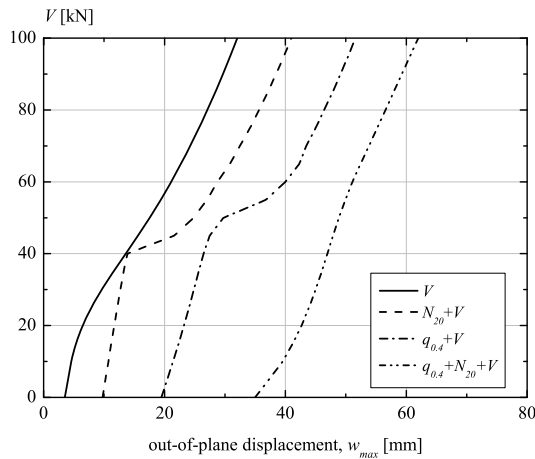


Figure 5.38 – In-plane shear force V vs. maximal out-of-plane deflection w_{max} for all load cases

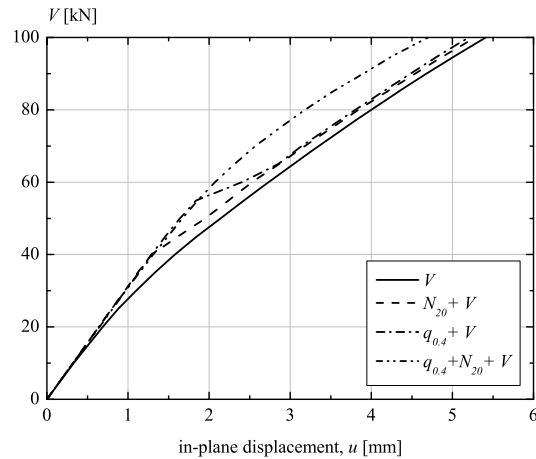


Figure 5.39 – In-plane shear force V vs. in-plane displacement u for all load cases

The influence of different load cases on in-plane shear force V vs. in-plane deflection u relation is shown in Figure 5.39. Until the critical shear force, the behaviour is linear while for higher values two asymptotes occur: the lower asymptote that corresponds to the glass panel under the load case V and the higher one for glass panel under load case $q_{0.4}+N_{20}+V$. The load cases with snap-through points (load case $N_{20}+V$ and $q_{0.4}+V$) are parallel to the higher asymptote for the value smaller than the critical, and to the lower asymptote for the value higher than the critical.

5.3.4 Validation of the point supported glass panel model

To verify the model, the results obtained from numerical simulation are compared with the results of experimental investigations. To make the comparison feasible, the numerical model and the tested specimens should have identical boundary conditions and be subjected to the same loads. The specimen P1 was placed in a horizontal position with a temporary support. Although temporary support was supposed to be in the middle of the glass span, during the installation in the testing frame, it moved 100mm on the north and 200mm on the east of the glass panel centre. The self weight of the glass panel acted as a distributed load perpendicular to the surface.

The numerical model is built with same input data (the temporary support and the additionally distributed load). Firstly the model is subjected to a constant out-of-plane distributed load of $0.4[\text{kN}/\text{m}^2]$ (self weight glass panel). This out-of-plane deflection is taken as the initial geometrical imperfection. On such a deformed glass panel, the in-plane shear force V is applied and a nonlinear buckling analysis is made.

Figure 5.40(a) shows the out-of-plane measurements of inductive transducers P_n and P_s during the test P1 and the results of the numerical model at the same places. The correlation between the test and the numerical model is good. Shear buckling of the glass panel creates two semi-buckles (Fig. 5.27(a)), one in the positive direction and the second in the negative direction. This is the reason why the transducers P_n and P_s measured the out-of-plane deflection in opposite directions. Although a symmetrical behaviour was expected, this is not the case due to the asymmetrical position of a temporary support.

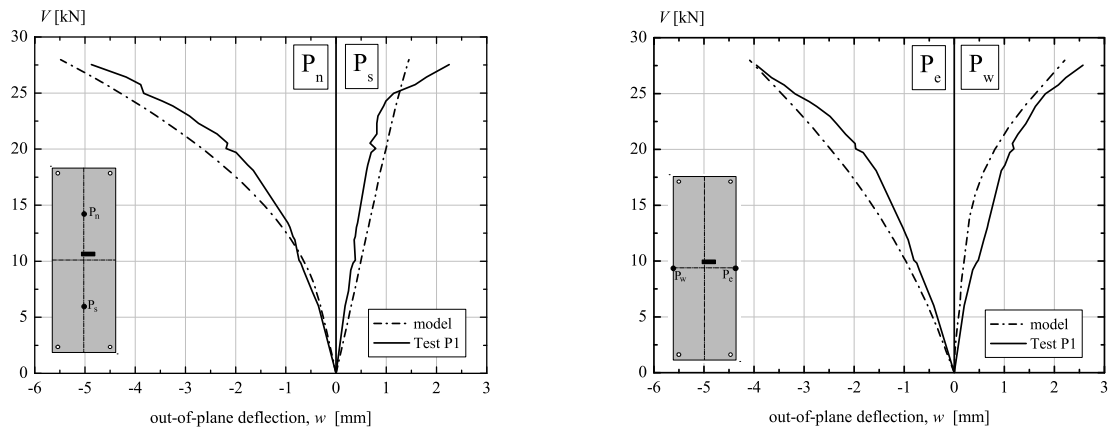


Figure 5.40 – Comparison of numerical model and experimental investigation results
(a) at place P_n and P_s (b) at place P_e and P_w

The comparison of out-of-plane deflection at point P_e and P_w measured during the test P1 and the deflection at equivalent points obtained by numerical simulation is shown in Figure 5.40(b). The numerical model result fits well with the experimental results. Due to shear buckling, one transducer measured a positive while the second measured a negative deflection. Again, the asymmetric deflection occurs due to a temporary support position.

5.4 LINEAR SUPPORTED CONNECTION MODEL

This section focuses on shear behaviour of the adhesive used in the glass/substructure connection. From the experimental investigation (§4.4) a two side connection is chosen as the most suitable one and furthermore studied here. The analytical bases of the adhesive shear behaviour are firstly explained. Later, the numerical model of the adhesive glass/substructure connection is developed and the adhesive material law is defined and verified by comparing it with experimental results.

5.4.1 Analytical bases

The adhesive in the glass/substructure connection is subjected to a complex stress state which can be simplified by superposing the hydrostatic and the deviatoric stresses [Adams et al. 1979]. The hydrostatic stress component is the mean of the three normal stresses and tends to change the material's volume, but not its shape, since all the faces of the element are subjected to the same stress. The deviatoric stress component is the normal stress reduced by the value of the hydrostatic stress component which tends to change the shape of the material element, but not its volume (Figure 5.41)

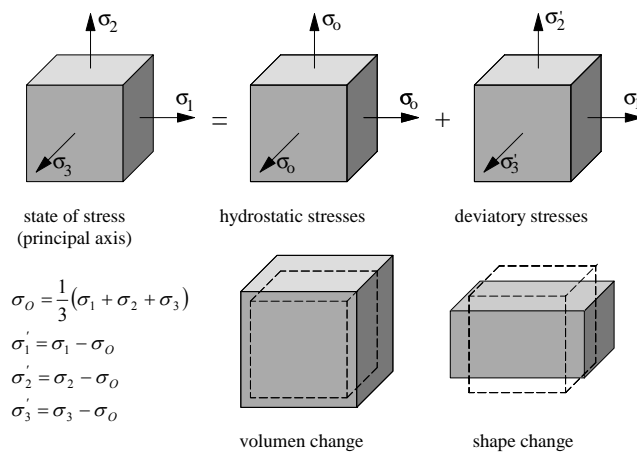


Figure 5.41 – Hydrostatic and deviatoric stress component in the adhesive

5.4.1.1 Linear shear stress distribution in the adhesive

The stress distribution is assumed to be constant across the width of the adhesive and stress concentration at the edge overlap is ignored (Fig. 5.42(b)). This analysis is usually applied to large width joints where plain-stress or plain-strain analyses are performed. The adherent (glass and substructure) is assumed to be rigid and the shear stress distribution remains constant in adhesive along the bond line.

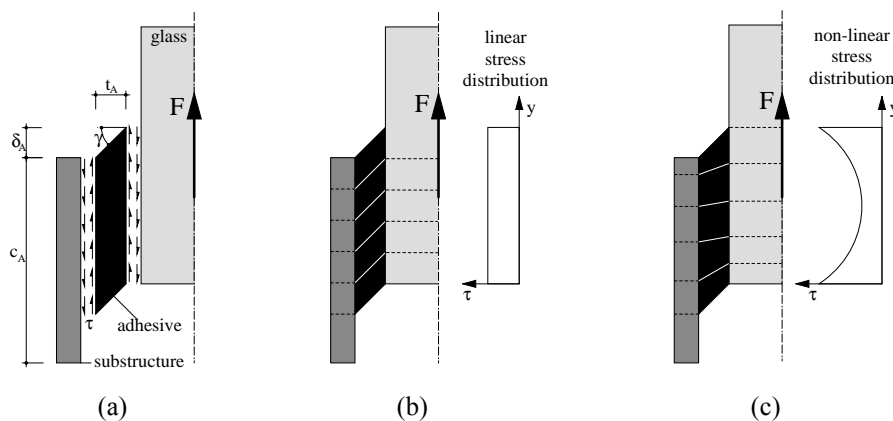


Figure 5.42 – Shear stress in adhesive (a) geometrical properties (b) linear distribution (c) nonlinear distribution

Constant shear stresses τ_{xy} in the adhesive is expressed as the quotient of force F and the area of the adhesive in which shear stresses act.

$$\tau_{xy} = \frac{F}{2 \cdot c_A l_A} \quad (5.29)$$

c_A width of the adhesive [mm]
 l_A length of the adhesive [mm]

The deformation of the adhesive δ_A is the quotient of shear stress and adhesive shear stiffness.

$$\delta_A = \frac{\tau_{xy} t_A}{G_A} \quad (5.30)$$

t_A is the thickness of the adhesive [mm]
 G_A is the adhesive shear modulus [N/mm²]
 $G_A = \frac{E_A}{2(1+\nu_A)}$
 E_A adhesive modulus of elasticity [N/mm²]
 ν_A Poisson's ratio [-]

Shear strain γ_A is a non-dimensional value expressed as the quotient of the adhesive deformation δ_A and the adhesive thickness t_A and/or shear stress τ_{xy} and adhesive shear modulus G_A .

$$\tan \gamma_A = \frac{\delta_A}{t_A} = \frac{\tau_{xy}}{G_A} \quad (5.31)$$

5.4.1.2 Non linear shear stress distribution in the adhesive

In the reality the shear stress distribution in the adhesive is not constant. The shear stresses are higher at the ends of the bond line and smaller in the middle of the bond line (Fig. 5.42(c)). This stress concentration depends on the adhesive adhering to the stiffness ratio [Renton et al. 1975]. Stiffer adhesives cause higher shear stress concentrations at the overlap ends than soft adhesives (Fig. 5.43).

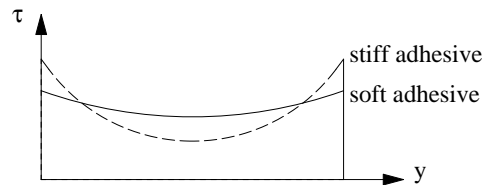


Figure 5.43 – Shear stress distribution along the bond line

When the adherent (glass and substructure) is assumed to be elastic, the adhesive deforms only in shear while the adherents deform only in tensile [Volkersen 1965]. The maximum shear stresses occur at the overlap's ends and depend on adhesive shear modulus to adherent elasticity modulus ratio.

Additionally, in a double-lap joint, although symmetric, the internal adherent (glass) is loaded in tensile while the external adherent (substructure) is also subjected to bending and therefore additional through-thickness compressive stresses are developed across the adhesive layer at the loaded overlap, and through-thickness tensile stresses in the unloaded end [Matthews et al. 1982].

So far, a lot of work and experimental investigation has been conducted to determine the stress distribution in the adhesive joint, but no analytical formula has been neither derived nor proposed. Due to a material non-linearity of the adhesives as well as to complex geometry and variable boundary conditions configuration, a finite element analysis is recommended.

5.4.1.3 Nonlinear adhesive behaviour

The nonlinear material behaviour of adhesive is approximated in the simplest way by bilinear elasto-plastic laws [Harris et al. 1984], [Dorn et al. 1993], by hyper-elastic material law or with a material curve fitting the test data [Crocombe 1989]. In the polymer mechanics field more complex material laws are defined taking into account the viscosity, plasticity and behaviour in a damaged state [Keck 1998].

[Hart-Smith 1973] performed a nonlinear analysis of double-lap joints showing that the only significant factor for the adhesive which affects the joint strength is the shear/strain energy. Thus, a ductile adhesive with a large area under the stress/strain curve will generate a higher joint strength than a stronger brittle adhesive with a small area under the stress-strain curve. Hart-Smith developed two material laws for shear stress/strain curve (Figure 5.44):

- idealized elasto-plastic material law

$$\tau_{xy} = \begin{cases} G_A \cdot \gamma & \gamma \leq \gamma_e \\ \tau_p & \gamma_e \leq \gamma \leq \gamma_p \end{cases} \tag{5.32}$$

G_A adhesive shear modulus [N/mm²]
 γ_e, γ_p elastic and plastic shear strain [-]
 τ_p plastic shear stress [N/mm²]

- bilinear material law

$$\tau_{xy} = \begin{cases} G_{A,e} \cdot \gamma & \gamma \leq \gamma_e \\ \tau_p + G_{A,p} \cdot (\gamma - \gamma_e) & \gamma_e \leq \gamma \leq \gamma_p \end{cases} \tag{5.33}$$

$G_{A,e}$ elastic adhesive shear modulus [N/mm²]
 $G_{A,p}$ plastic adhesive shear modulus [N/mm²]

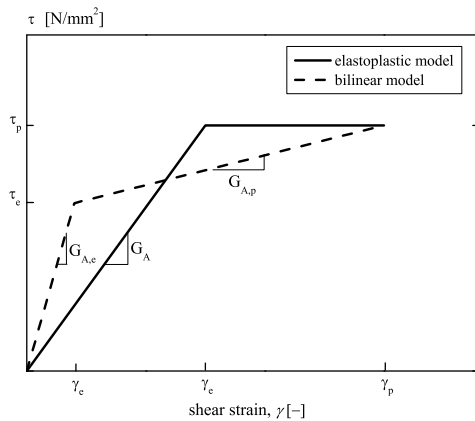


Figure 5.44. – Adhesive material law

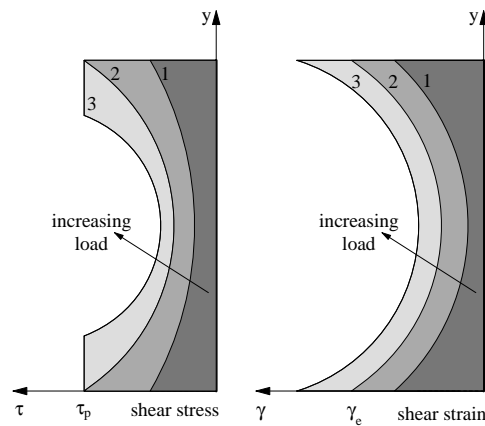


Figure 5.45. – Shear stress and shear strain distribution at the bond line

Figure 5.45 illustrates the shear stress and shear strain distribution in the adhesive bond line, assuming an idealized elasto-plastic adhesive material law, when the applied load is progressively increased. The shear stress distribution is proportional to the loading level as long as the maximum shear strains at the edges of the adhesive layer do not exceed the elastic strain. When the load level increases, the shear stress reaches the maximum value and the yielding of the adhesive. Increasing of the load leads to an enlargement of plastic areas from the edges to the middle of the adhesive layer. Thus, the elasto-plastic adhesive allows a higher load-carrying capacity and larger deformations than elastic adhesives.

5.4.2 Numerical modelling

The numerical model of glass plate connected to the substructure by the adhesive, representing the two sides connection in transversal shear test (Section 4.4) as the most suitable for further research, has been developed with the finite element programme ANSYS 10 [Ansys 2005]. The main objective is to study the shear behaviour of the adhesive and constitute the adhesive material law. The following procedures are undertaken:

- Construction of the model: element types, material properties, meshing of the model, boundary conditions, load introductions and solution procedure.
- Results: adhesive behaviour under transversal shear force
- Validation of the model: comparison of the results with experimental results

5.4.2.1 Construction of the model

Figure 5.46 shows the model of a glass plate (cyan colour) connected by the adhesive (red colour) to the substructure (green colour). Geometrical properties of the model are the same as the geometrical properties of the specimen (TS-2S) utilised in experimental investigations (Section 4.4). The exception is that monolithic instead of laminated glass plate is modelled, whose length corresponds to the adhesive length of 200mm instead of the entire glass plate length of 490 mm (glass dimension has no influence on adhesive behaviour). The adhesive thickness is 9.5mm and width 40mm.

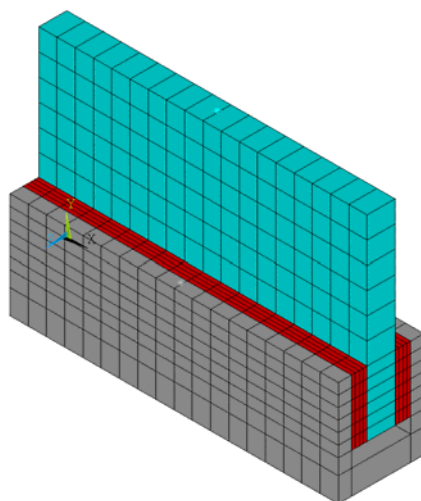


Figure 5.46 – Linear support connection model

Element type

SOLID95 element was used to model all the volumes: the glass, the adhesive and the substructure. The detailed explanation of the element type is given in §5.2.2.1 and Figure 5.9(a).

Material properties

Table 5.47 shows the properties of the material used to construct the linear supported connection model (material law, modulus of elasticity E , Poisson's ratio ν material yielding point f_y)

Table 5.47 – Material properties

Material	Model		E [N/mm ²]	ν [-]	f_y [N/mm ²]
Glass panel	linear	isotropic	70'000	0.23	-
Substructure (stainless steel)	linear	isotropic	210'000	0.30	-
Adhesive	elasto-plastic	isotropic	2.4	0.49	0.95

A substructure made of stainless steel is modelled as a linear material, although being nonlinear because it has no influence on the adhesive behaviour due to small applied forces (far from the steel yielding point). In such a way a numerical cost is decreased and the analysis is faster.

To model the adhesive the idealized elasto-plastic material law, based on [Hart-Smith 1973] is chosen, with modulus of elasticity $E_A = 2.4 \text{ [N/mm}^2\text{]}$ and plastic shear stress $\tau_{pl} = 0.95 \text{ [N/mm}^2\text{]}$ [Dow Corning 2003]. The adhesive Poisson's ratio is $\nu = 0.49$.

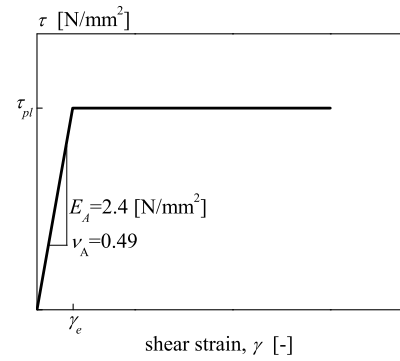


Figure 5.48 – adhesive material model

Meshing of the model

The manual meshing is utilised. Mesh density is chosen to provide convergence results (Figure 5.48).

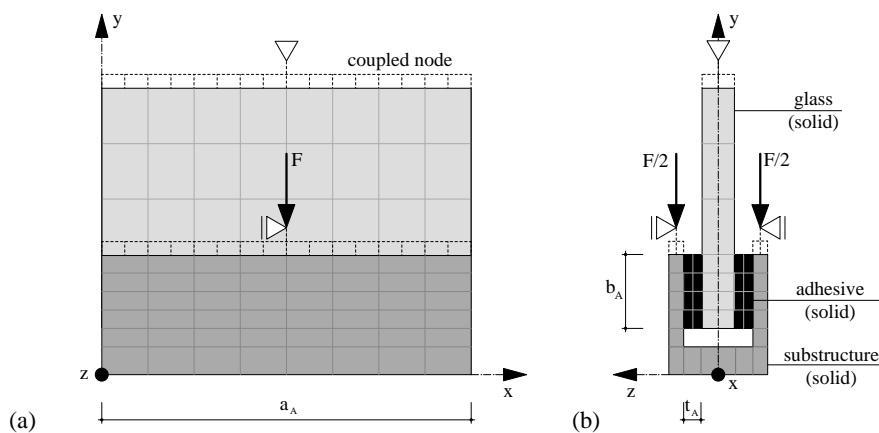


Figure 5.49 – Linear supported connection model (a) front view (b) side view

Boundary conditions

At the top of the glass plate the nodes are coupled and fixed in all three translator directions preventing the displacement in x , y and z directions. Additionally, the top nodes of the substructure are coupled in two groups supported by a simple support preventing the displacement in z and x directions, but allowing the displacement in y direction.

Load introduction

Half of the concentrated force $F/2$ is applied in $-y$ direction, at each group of two coupled nodes at the top of the substructures. This force introduced the transversal shear to the adhesive.

Solution procedure

Due to a nonlinear material behaviour of adhesive, to resolve the model, the nonlinear analysis was carried out. Newton-Raphson approach to solve nonlinear problems was adopted. The load was subdivided into 5 load increments and the load increments were applied over 10 load steps.

5.4.2.2 Results

Vertical displacement of the model is concentrated in the adhesive displacement due to its high deformability (small elastic modulus) in comparison with glass or substructure (high elastic modulus) (Figure 5.50.a).

Distribution of shear stresses in the adhesive is illustrated in the Figure 5.50.b. The stress is not distributed uniformly, the higher stresses occurred at the overlap end of the bonded area (blue colour) and the minimum in the middle of the bonding area (red colour).

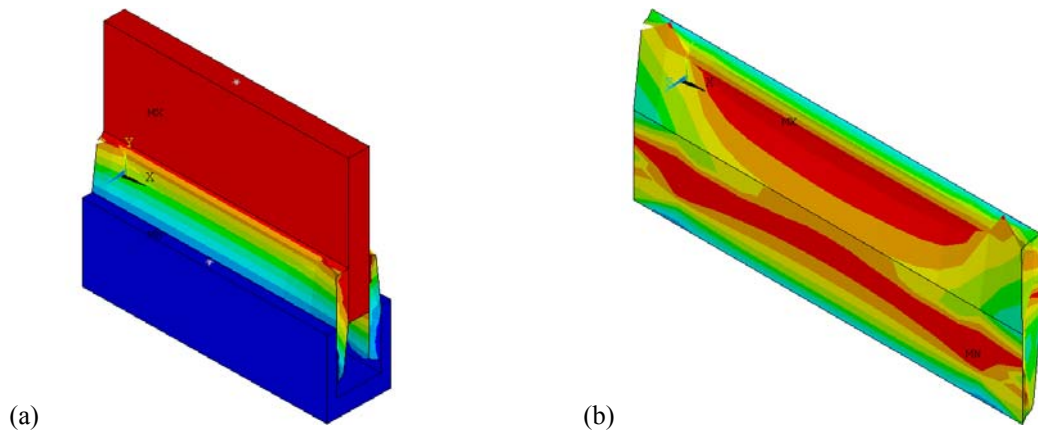


Figure 5.50 – Numerical model subjected to transversal shear force F
(a) model deformation (b) stress distribution in the adhesive

Figure 5.51 shows the relation between the adhesive shear strain γ_A and the shear stress τ . The dotted line shows the assumption of a nonlinear stress distribution on the overlap area, with peak stresses at the overlap edges (real stress distribution), while the full line shows the behaviour when constant shear stress distribution on the overlap area is assumed (the simplified stress distribution).

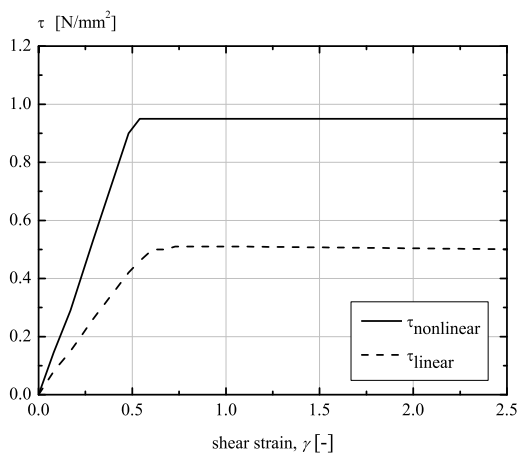


Figure 5.51 – Shear stress τ vs. shear strain γ_A for assumption of a linear and a nonlinear stress distribution

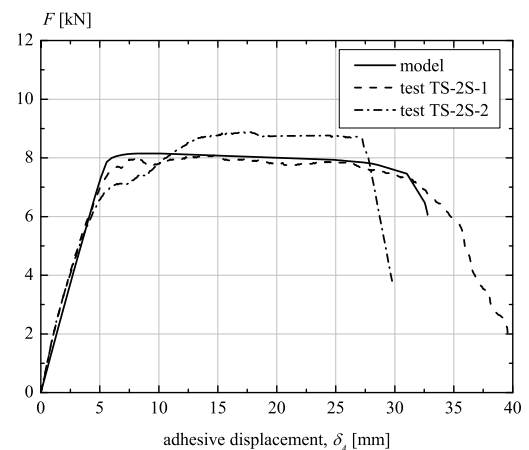


Figure 5.52 – Force F vs. adhesive displacement δ_A , for numerical simulation and experiment results

5.4.3 Validation of the linear support connection model

To validate here developed numerical model and the assumed adhesive material law (idealized elastoplastic), the numerical results and the transversal shear tests results are compared. Figure 5.52 shows the relation of the applied transversal shear force F vs. the numerically simulated and experimentally tested adhesive displacement δ_A . From the graph, a good agreement between those is recognised. The stiffness in elastic domain of a numerical model and a real specimen are identical, which leads to conclusion that the chosen modulus of elasticity agrees with the real one.

Due to a high adhesive deformation, the relative displacement between the glass and the substructure is large. This will significantly influence the global behaviour of a glass panel and therefore the adhesive can not be neglected in the numerical modelling of a full-size linear supported glass panel.

5.5 LINEAR SUPPORTED PANEL MODEL

The analytical bases of shear buckling theories are given in Section 5.3. The structural model of a linear supported glass panel under in-plane shear force V is described and a numerical model is developed. The shear buckling coefficient is determined, the global glass panel deformation is studied, the stress distribution is analysed and different load interactions are investigated. The model is validated by comparing it with experimental results.

5.5.1 Linear support structural model

The structural model of linear supported glass panel subjected to in-plane shear force V is shown in the Figure 5.53. The glass panel is glued by adhesive to the substructure on two short sides. The adhesive has a function to transfer the in-plane shear force V from the substructure to the glass panel. Two setting blocks at the bottom and two at the top of the glass panel have the function to carry the permanent load (glass panel self weight, roof, snow etc).

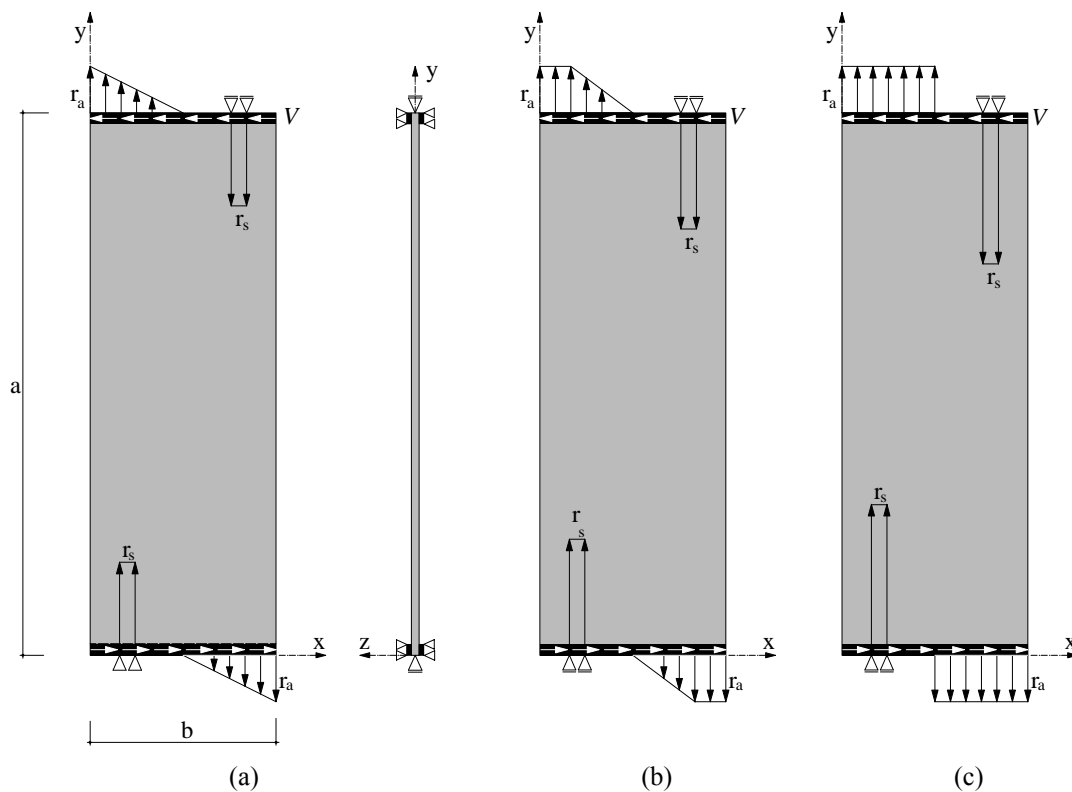


Figure 5.53 – Structural model of linear supported glass panel (a) adhesive in linear elastic zone (b) part of adhesive in plastic zone (c) entire adhesive in plastic zone

In-plane shear force V is applied at the upper substructure (connected to the roof), and via adhesive is transferred to the glass panel. The horizontal reaction is transferred through the lower adhesive to the substructure (connected to the foundation). This force and reactions try to rotate the glass panel. Consequently, a pair of force exists which rotates the glass panel in the opposite direction, carrying the glass panel in equilibrium.

The setting blocks are able to support only the compressive forces, but not the tensile. When the glass panel is subjected to the in-plane shear force, the setting block 2 and 3 are under compressive and react as supports (reaction r_s). The setting blocks 1 and 4 are under tensile and therefore unable to behave as a support. Consequently, the tensile reactions at support 1 and support 4 are taken by the adhesive (reaction r_a). It is assumed that only half of the adhesive length is subjected to a tensile reaction.

The highest stresses in the adhesive take place at extremes of the connection, at a point where the interaction of shear force V and maximal tensile reaction r_a occurs. Being an elasto-plastic material, the adhesive will start to plastify when reaching the yielding point. When the stresses are smaller than the adhesive yielding point, the stress distribution in the adhesive is triangular (Fig. 5.53(a)). Upon reaching the yielding point, the plastification of adhesive occurs at the extremes, and the stress distribution has the shape illustrated in Figure 5.53(b). Further increase of the in-plane shear force leads to full plastification of the adhesive (Fig. 5.52(c)).

Due to initial geometrical imperfection, the glass panel under in-plane shear force V deflects out-of its plane. Compressive reaction forces at setting blocks 2 and 3 create a compressive diagonal between them which tends to buckle out-of-plane. In the same moment, tensile reactions, caused by the adhesive, create the tensile diagonal which tries to keep the buckled compressive diagonal straight. The crossing of compressive and tensile diagonals causes the membrane effect (Fig 5.54(a)). The effectiveness of the membrane effect in the glass panel behaviour depends on the adhesive stiffness. Namely, being a material with a small module of elasticity, the adhesive demonstrates a very high deformation, influencing the tensile reactions and global glass panel behaviour.

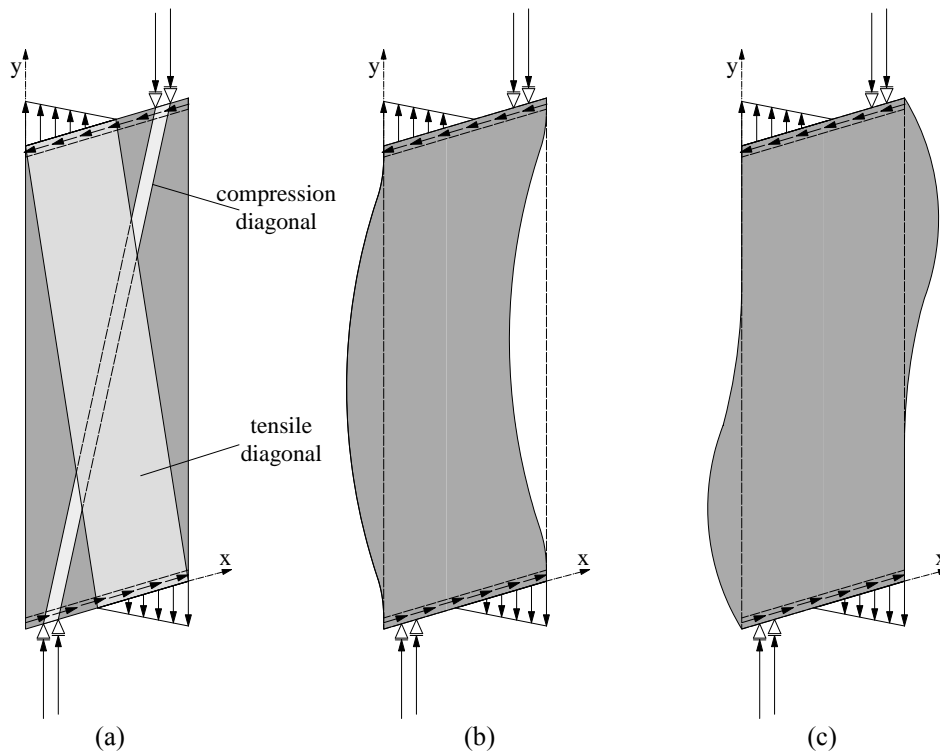


Figure 5.54 – membrane effect in the glass panel (a) compressive and tensile diagonal (b) out-of-plane deflection with soft adhesive (c) out-of-plane deflection with strong adhesive

When a soft adhesive is used (the adhesive with small modulus of elasticity) the weak tensile diagonal will not be able to keep the buckled compressive diagonal and the out-of-plane deflection, as shown in Figure 5.54(b), takes place. In extreme cases, the column buckling stability problem can occur, without the system post-buckling reserve. On the other hand, when stiff adhesive is used, the tensile diagonal will be strong enough to keep the compressive diagonal, and the out-of-plane deflection with two semi-buckles occurs (Fig. 5.54(c)).

5.5.2 Analytical bases and existing solutions

The analytical bases of shear buckling theories, plate and sandwich theories to determine the critical load, as well as the existing solution for simple cases of plate shear buckling is given in §5.3.1.

5.5.3 Numerical modelling

The numerical model of a linear supported glass panel is developed by using the Finite Element programme ANSYS 10.0 [Ansys 2005] with the following objectives:

- Construction of the model: element types, material properties, meshing of the model, boundary conditions, load introductions and solution procedure.
- Shear buckling coefficient
- Results
- Influence of the initial imperfection shape
- Load interaction
- Validation of the model: comparison of the numerical model results with the experimental results

5.5.3.1 Construction of the model

The full-size linear supported glass panel numerical model is shown in Figure 5.55. The dimensions correspond to the *standard linear support glass panel* defined in Section 3.3. The height of the glass panel is $a=3500\text{mm}$, the width $b=1200\text{mm}$ and the nominal thickness $t=8/15.2/8\text{ mm}$ (according to [Luible 2002] the real thickness is 97.6% of the nominal thickness given by the manufacturers). The adhesive width is $c_A=40\text{mm}$ and adhesive thickness is $t_A=9.5\text{mm}$. The setting blocks are $d_A=100\text{mm}$ wide and $b/5$ (240mm) from the corners. The initial geometrical imperfection is $w_o=a/1000 = 3.5\text{ mm}$.

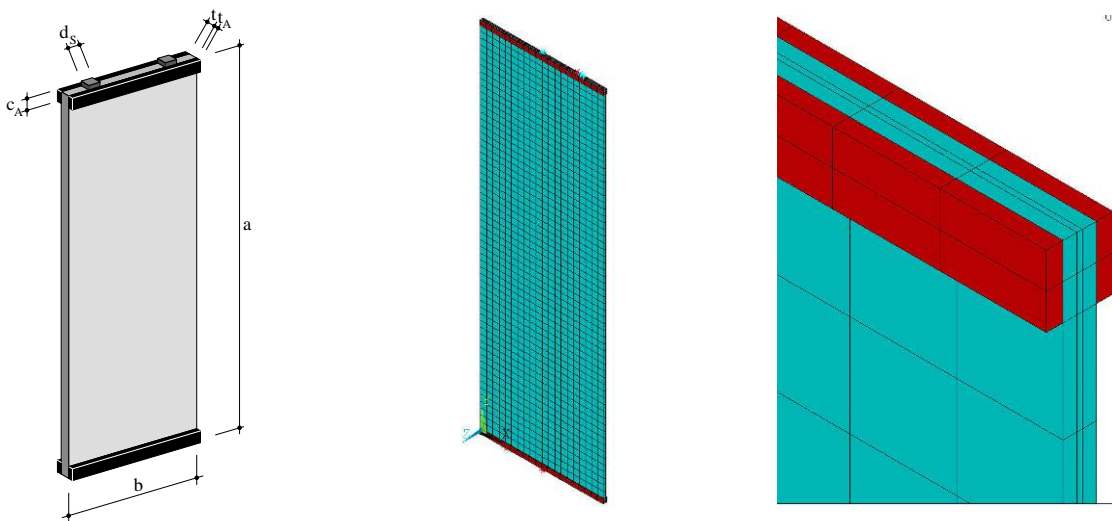


Figure 5.55 –Linear support glass panel model

Element type

SOLID95 element was used to model all the entities: the PVB interlayer, the glass panel and the adhesive. The detailed explanation of the SOLID95 element type is described in §5.2.2.1 and presented in Figure 5.9.a.

Material properties

Table 5.55 shows material laws and material properties. For the adhesive, the idealized elasto-plastic model is used, determined from linear support connection model results (Fig. 5.48).

Table 5.56 – Material properties

Material	Model	E [N/mm ²]	ν [-]	f_y [N/mm ²]
Glass panel	Linear	70'000	0.23	-
PVB interlayer	Linear	1.5	0.49	-
Adhesive	elasto-plastic	2.4	0.49	0.95

Meshing of the model

As in the case of a point supported glass panel model, the determinant criteria for linear support mesh density was the constraint that the length ratio of the element edges can not be less than 1/20. Due to small thickness of PVB interlayer (1.52mm), the maximum element length can be 30 mm. Model meshing is shown in the Figure 5.57. The opposite nodes at the surface of PVB volume are coupled in z direction to avoid the delaminating of the layer.

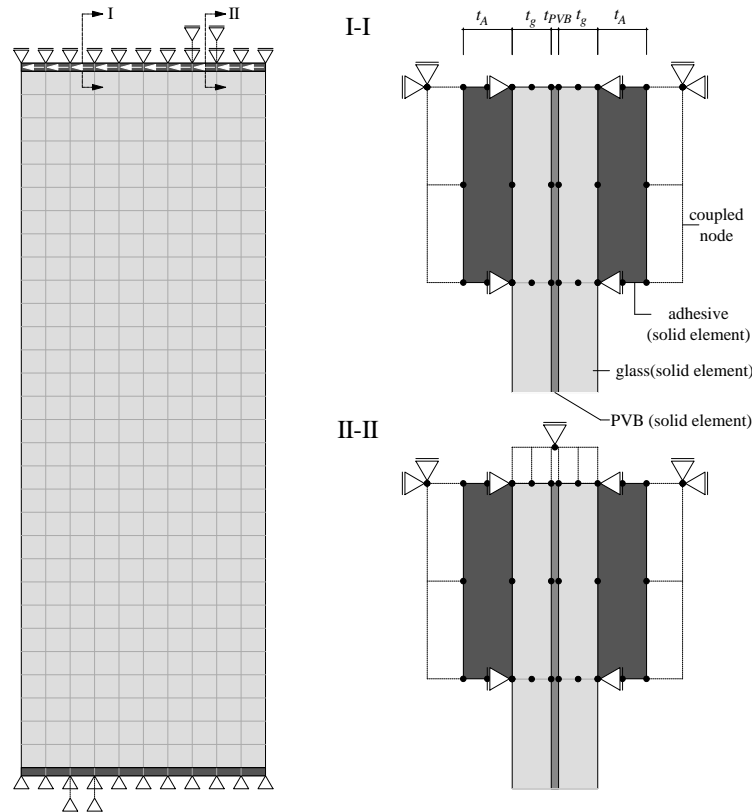


Figure 5.57 – Linear supported glass panel model mash with supports details and cross section I-I and II-II

Boundary conditions

At the lower edge of the bottom adhesive the supports prevent the displacement in x , y and z directions. At the upper edge of top adhesive the support prevents the displacement in x and z directions. Additionally, along the bond line of the adhesive and the glass panel there are supports preventing displacement in z direction, simulating the spacers. At the place of setting blocks the nodes are coupled and the displacement constrains in y direction (only for supports under compressive), but allows the movement in $-x$ direction which occurs due to the adhesive sliding (Fig. 5.56).

Load introduction

In plane shear force V was applied as a linear force along the top adhesive, acting in $-x$ direction.

Solution procedure

To solve the nonlinear buckling analysis of a linear supported glass panel, the same procedure which was utilised to resolve the nonlinear buckling analyses of point supported glass panels can be adopted. The procedure is described in §5.3.3.1.

5.5.3.2 Shear buckling coefficient

The elastic buckling analysis of linear support glass panel model is performed to determine the critical shear force V_{cr} . By introducing the critical force for a monolithic glass panel in Equation (5.27) the shear buckling coefficient k_τ for linear supported monolithic glass panel is determined. The Figure 5.58(a) shows the relation between the shear buckling coefficient k_τ and the glass panel ratio $\alpha = a/b$.

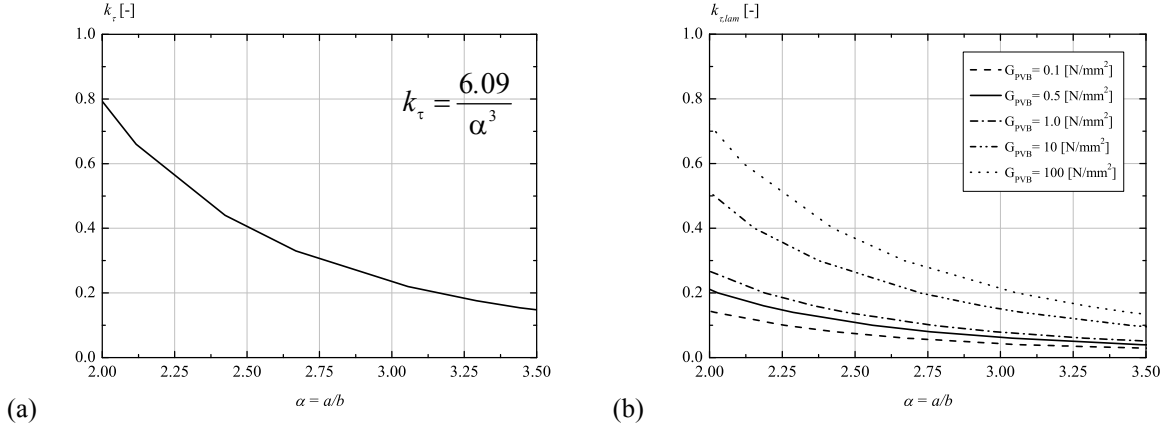


Figure 5.58 – shear buckling coefficient for linear supported glass panel a) monolithic k_τ b) laminated $k_{\tau,lam}$

By determining the critical shear force by elastic buckling analyses of linear supported laminated glass panels and introducing it in the equation (5.28), the shear buckling coefficient $k_{\tau,lam}$ for laminated glass panel is determined. Figure 5.58(b) shows the relation of the shear buckling coefficient $k_{\tau,lam}$ and the glass panel geometry ratio $\alpha = a/b$ for different values of PVB stiffness (PVB shear modulus G_{PVB}).

Figure 5.58 is valuable for the glass panel glued to the substructure by the adhesive with modulus of elasticity $E_A = 2.4 \text{ N/mm}^2$. Since the global behaviour of the glass panel depends highly of the adhesive stiffness, it also influences the shear buckling coefficient.

Figure 5.59 shows the adhesive coefficient $\beta_A = k_\tau/k'_\tau$ as a ratio between the shear buckling coefficient when “standard” adhesive with modulus of elasticity $E_A = 2.4 \text{ N/mm}^2$ is used (k_τ) and the “modified” shear buckling coefficient when adhesive with another modulus of elasticity is used (k'_τ). The adhesive coefficient β_A can be read from the graph or calculated from the empiric formula:

$$\beta_A = 0.0125E_A + 0.97 \tag{5.34}$$

The shear buckling modulus of such glass plate becomes (for monolithic and laminated glass panels):

$$k'_\tau = \beta_A \cdot k_\tau \quad (k'_{\tau,lam} = \beta_A \cdot k_{\tau,lam}) \tag{5.35}$$

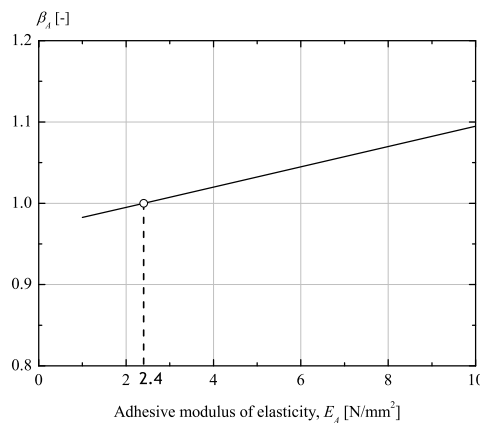


Figure 5.59 – Adhesive coefficient $\beta_A = k_\tau/k'_\tau$

5.5.3.3 Results

In-plane shear force V vs. out-of-plane deflection w_{max}

Glass panel deforms out-of-plane under in-plane shear force V due to the initial geometrical imperfection. The buckling mode shapes depend on the adhesive stiffness used to connect the glass panel to the substructure. When a soft adhesive is used, the first buckling mode shape, as well as the glass panel out-of-plane deformation under V , has the shape as illustrated in Figure 5.60(a). On the other hand, when a stiff adhesive is used, the first buckling mode shape, as well as the glass panel out-of-plane deflection under V , has the shape as presented in Figure 5.60(b). The adhesive utilised in this model has the modulus of elasticity of $E_A=2.4 \text{ N/mm}^2$ and is characterised as “soft”. Hence, the first case is assumed.

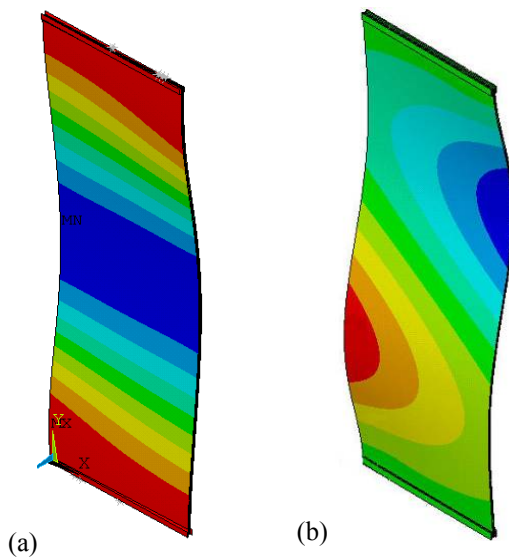


Figure 5.60 – Glass panel deformation under shear force V (a) soft adhesive (b) stiff adhesive

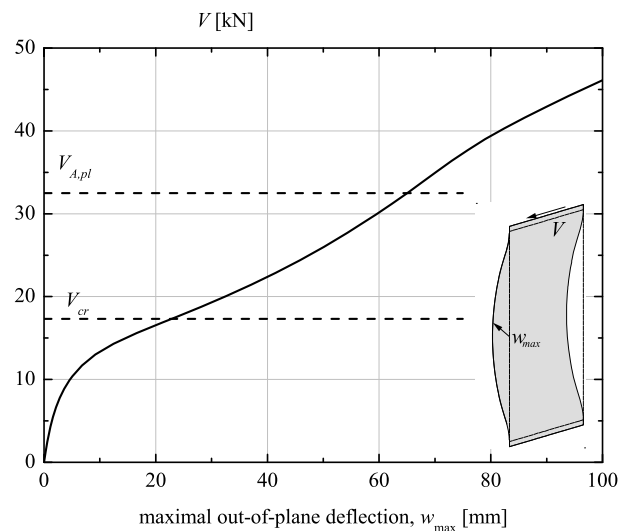


Figure 5.61 – In-plane shear force V vs. maximal out-of-plane deflection w_{max}

The Figure 5.61 shows the relation between the applied in-plane shear force V vs. maximum out-of-plane deflection w_{max} . The maximum out-of-plane deflection occurred in the middle of the glass span. Although the tensile diagonal formed by a soft adhesive is not capable of keeping the compressive buckle straight, it is strong enough to create the membrane effect in the glass panel and introduce the post-buckling reserve: the in-plane shear force higher than the critical value V_{cr} occurs.

At the critical point the curve inflects and starts to increase with a positive progression. At a certain value of in-plane shear force the yielding of the adhesive takes place. The value of the force at this point is called the adhesive yielding force $V_{A,pl}$. This occurrence influences the global behaviour of the glass panel and its out-of-plane deflection as shown in figure 5.61. At this point the curve inflects for the second time. It is still on the increase but with a negative progression. In case of a thicker glass panel, the adhesive yielding force can occur before the critical shear buckling force.

In-plane shear force V vs. in-plane displacement u

The glass panel in-plane displacement u in $-x$ direction in relation to the applied in-plane shear force V is illustrated in figure 5.62. The in-plane displacement takes into account the displacement of the glass and sliding of the adhesive. The system behaves linearly until reaching the critical shear force V_{cr} . Due to shear buckling, the curves deviate. The second deviation takes place at the adhesive yielding force $V_{A,pl}$. The system demonstrates a nonlinear and a ductile behaviour. After each deviation the in-plane displacement still increases but with a negative progression.

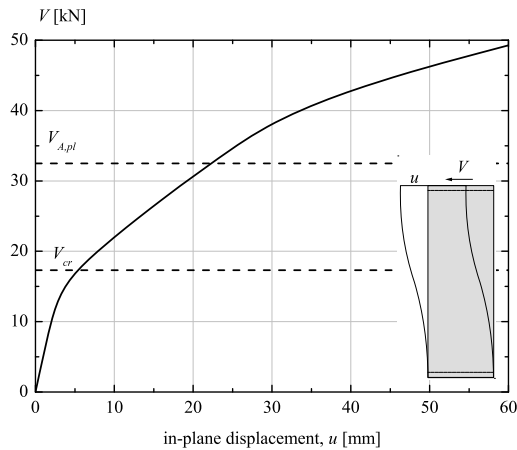


Figure 5.62 – In-plane shear force V vs. in-plane displacement u

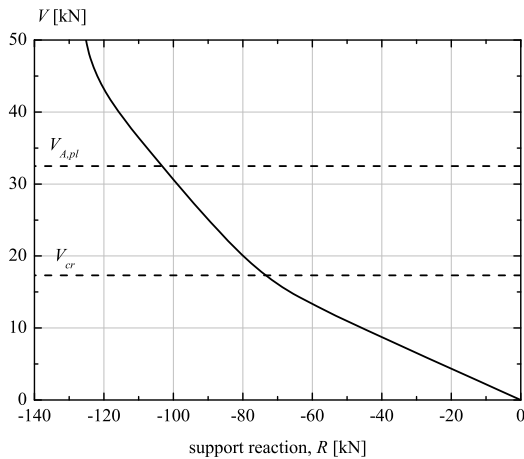


Figure 5.63 – In-plane shear force V vs. reaction support R_3

In-plane shear force V vs. support reaction R

The higher tensile stresses take place at the compressive setting blocks 2 and 3 at the place of load introduction. Therefore, the support reaction on the setting block 3 is analysed. The Figure 5.63 shows the applied in-plane shear force V vs. support reaction at setting block 3 R . The negative sign of the reaction means compressive. The linear behaviour is recognised until the critical shear buckling force V_{cr} when the curve deviates and continues to be linear until the second deviation at adhesive yielding force of the $V_{A,pl}$. After each deviation, the support reaction increases with a positive progression.

Stress distribution in the adhesive and the glass panel

Higher stresses in the adhesive took place at their extremes where the longitudinal shear (due to in-plane shear force) and the transversal shear (due to adhesive reaction, wishing to create a tensile diagonal in the glass panel) interact. This occurred on the right side of the bottom adhesive connection and on the left side of the top adhesive connection. On the point where the adhesive reaches its yielding point the adhesive plastification starts. Figure 5.64 presents the shear stresses in the top adhesive connection. The red colour shows the place of the highest stresses while blue colour shows the place without stresses (near the setting compressive setting block).



Figure 5.64 – Shear stress distribution in adhesive top connection

The principal tensile stresses σ_1 in the glass panel occur:

- On one side, the stress concentration occurs near the setting blocks 2 and 3 due to high compressive stresses introduced by the compressive support reaction. Perpendicular to this compressive stresses, due to the Poisson's ratio, the tensile stresses take place. On the other side, the tensile stresses introduced by the tensile reactions (due to adhesive shear) are relatively small.
- Tensile stresses due to out-of plane shear buckling occur in the middle of the glass panel span (due to negative bending) and parallel to the linear supports (due to positive bending) at the extremes of the tensile diagonal.

Figure 5.65(a) shows the distribution of principal tensile stresses on the front side of the glass panel. Red colour shows the maximum tensile stresses near the setting blocks 2 and 3. High stresses (yellow colour) are also visible in the middle of the glass span due to a negative bending caused by buckling.

On the back side of the glass panel (Fig. 5.65(b)), the maximum principal tensile stresses occurred again at supporting blocks 2 and 3, and, due to a positive bending caused by buckling, near the linear supports at the extremes of a tensile diagonal.

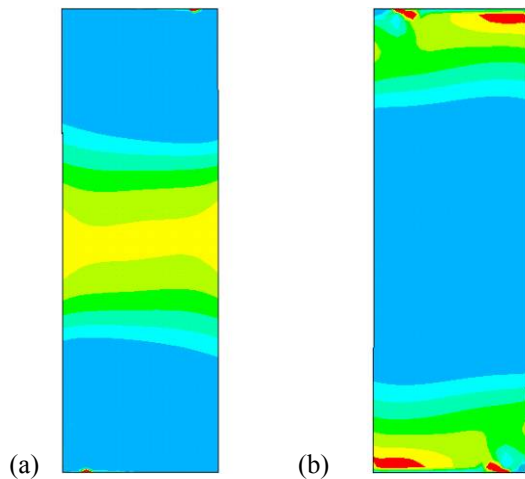


Figure 5.65 – Principal tensile stress in glass panel
(a) front side (b) back side

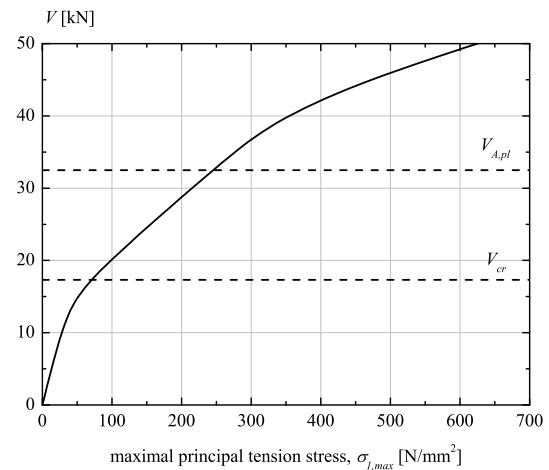


Figure 5.66 – In-plane shear force V
vs. principal tensile stresses σ_I

The Figure 5.66 shows the in-plane shear force V vs. principal tensile stresses σ_I at the supports (setting block 3) and in the glass span due to buckling. The linear behaviour is observed up to the critical V_{cr} when the curve deviated. The second deviation occurs at $V_{A,pl}$.

5.5.3.3 Initial imperfection

The initial geometrical imperfection shape has a significant influence on plate buckling behaviour [Luible 2002]. Therefore, three different initial geometry imperfection shapes are chosen to analyse their influence on shear buckling behaviour:

- Imperfection 1: First buckling mode shape, $w_o = a/1000$ (Figure 5.66.a)
- Imperfection 2: Second buckling mode shape, $w_o = a/1000$ (Figure 5.65.b)
- Imperfection 3: Third buckling mode shape, $w_o = a/1000$ (Figure 5.65.c)

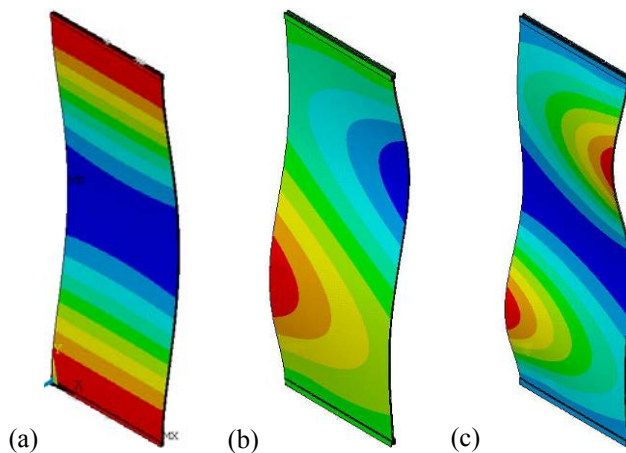


Figure 5.67 – Initial geometrical imperfection a) 1st buckling shape b) 2nd buckling shape c) 3rd buckling shape

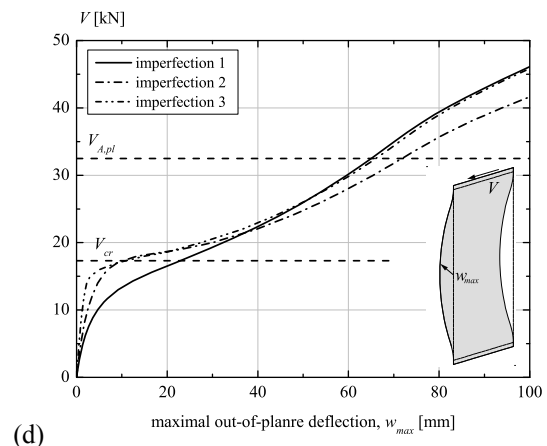


Figure 5.68 – Influence of different initial geometrical imperfection on out-of-plane deflection

Figure 5.67 shows similar behaviour to point supported glass panel results (§5.3.3.4). For the value smaller than $1.5V_{cr}$, the most unfavourable behaviour is observed for the glass panel with the initial geometrical imperfection corresponding to the first buckling mode shape. For values higher than $1.5V_{cr}$, the third buckling mode shape shows the most unfavourable behaviour. The sudden change of the out-of-plane deflection observed in the glass panel with the second and the third buckling mode shape correspond to the snap-through of the buckles when changing their deflection direction (from $+z$ to $-z$ deflection).

5.5.3.4 Load interaction

To study the influence of out-of-plane distributed load q and in-plane normal compressive force N on glass panel shear buckling, the developed numerical models are subjected to the following load interactions:

- **Load case $q+V$**

Constant out-of-plane distributed load q is applied to the model as a pressure perpendicular to the glass panel surface in $-z$ direction (Fig. 5.69(a)). The value $q = 0.4\text{kN/m}^2$ ($q_{0.4}$), as in experimental investigation, corresponds to the perpendicular wind load simulated by the self weight of the glass panel. Out-of-plane deflection of the glass panel subjected to distributed load $q_{0.4}$ is settled to be the initial geometrical imperfection shape on which an increasing in-plane shear force V is applied as a linear force along the adhesives on the top of glass panel edge in the $-x$ direction (Fig. 5.69(c)). The nonlinear shear buckling analysis is made.

- **Load case $N+V$**

The glass panel with the initial geometrical imperfection (third buckling mode shape with an amplitude of $w_o = a/1000$) is subjected to the constant in-plane compressive force $N = 20\text{kN}$ (abbreviation N_{20}), as was used in experimental investigation to simulate the roof. It is applied as a concentrated force at the setting block 1 and setting block 2 in the $-y$ direction (Fig 5.69(c)). On such a deformed glass panel, the increasing in-plane shear force V is applied as a linear force along the two adhesives on the top of glass panel edge in the $-x$ direction. The nonlinear shear buckling analysis is made.

- **Load case $q+N+V$**

Constant out-of-plane distributed load q acting with the value of $q = 0.4\text{N/m}^2$ ($q_{0.4}$) deflects the glass panel out-of-plane. The in-plane normal compressive force is $N = 20\text{ kN}$ (N_{20}). On such a deformed shape the increasing in-plane shear force V is introduced and a nonlinear buckling analysis is conducted.

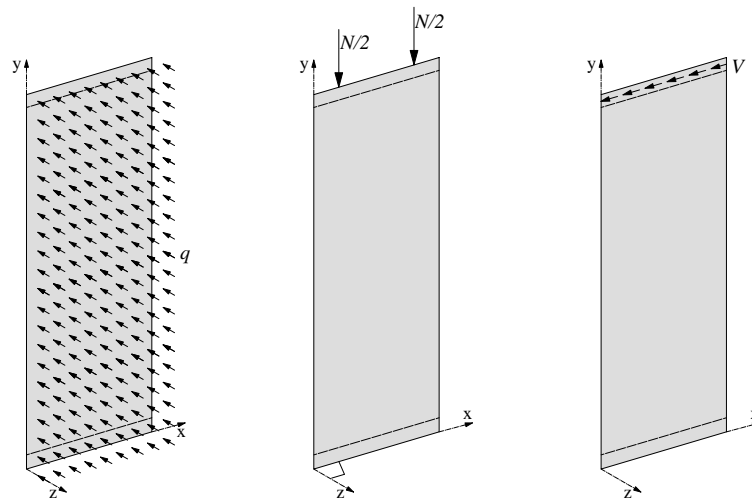


Figure 5.69 – Linear supported glass panel subjected to (a) out-of-plane deflection q (b) in-plane normal compressive force N (c) in-plane shear force V

Figure 5.70 shows the results of in-plane shear force V vs. maximal glass panel out-of plane deflection w_{max} for a glass panel subjected to in-plane shear force V only, and to three load interactions (load case $q_{0.4}+V$, load case $N_{20}+V$ and load case $q_{0.4}+N_{20}+V$). Each load case has the same initial imperfection shape but a different amplitude. The glass panel under load case V demonstrates higher stiffness. The glass panel under load case $N_{20}+V$ demonstrates less stiffness, the glass panel under load case $q_{0.4}+V$ even less while, understandably, the glass panel under all loads $q_{0.4}+N_{20}+V$ demonstrates the smallest stiffness. The stiffness of the system is closely related to the initial imperfection amplitude – the highest the initial imperfection amplitude, the smallest the stiffness of the system.

A similar behaviour can be noticed in in-plane stiffness (Fig. 5.71) where the influence of different load cases in in-plane shear force V vs. in-plane displacement u is illustrated. For all load cases the stiffness is equal for the values smaller than the critical shear force V_{cr} . For the higher values, the in-plane stiffness starts to decrease with the following sequences: load case V , load case $N_{20}+V$, load case $q_{0.4}+V$ and load case $q_{0.4}+N_{20}+V$.

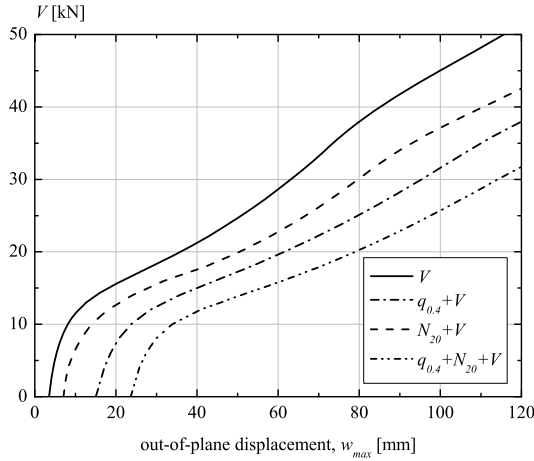


Figure 5.70 – In-plane shear force V vs. maximal out-of-plane deflection w_{max}

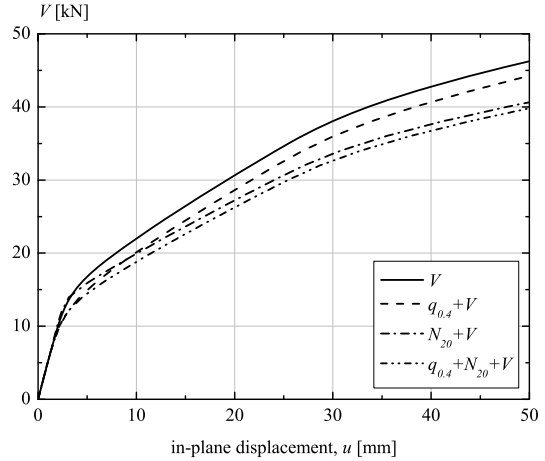


Figure 5.71 – In-plane shear force V vs. in-plane displacement u

5.5.4 Validation of the linear supported glass panel model

The numerical model is validated by comparing its results with the results obtained from experimental investigations in Linear supported panel test (Section 4.5). During the test L1 (load case V) the out-of-plane deflection was measured with inductive transducers P_n , P_s , P_w , and P_e . The glass panel was placed in a horizontal position with a temporary support exactly in the middle of the glass panel span. The self weight of the glass panel acted as a distributed load perpendicular to its surface. The developed numerical model was updated by introducing the additional boundary condition in the middle of glass panel preventing the displacement in $-z$ direction, as well as a distributed load perpendicular to the surface in $-z$ direction with value of $q=0.04$ kN/mm² to replicate the conditions of test L1. The out-of-plane deflection obtained from this additional distributed load is taken as the initial geometry imperfection of the glass panel. On such a deformed glass panel the in-plane shear force V is applied and a nonlinear buckling analysis is conducted.

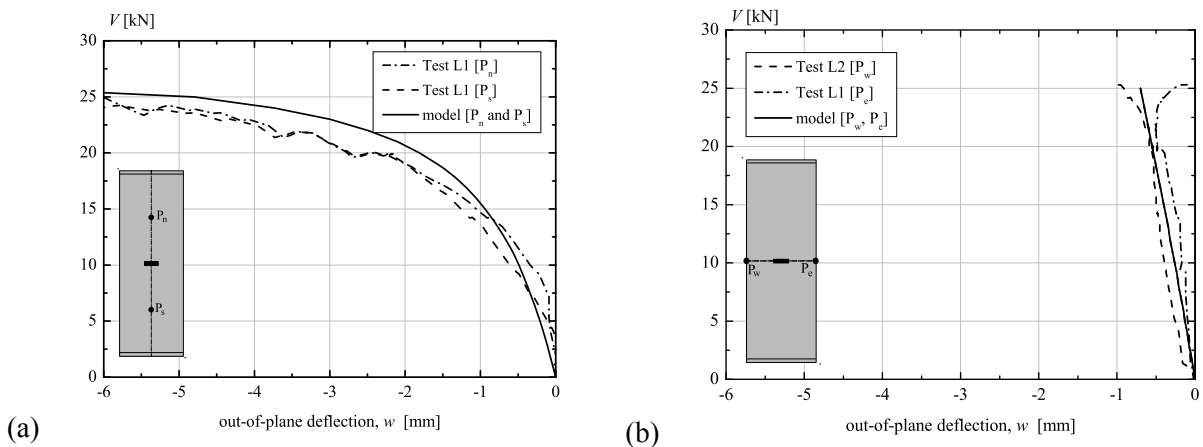


Figure 5.72 – Comparison of numerical model results and experimental results (a) at place P_n and P_s (b) at place P_e and P_w

The glass panel out-of-plane deflection measured during the Test L1 and numerical model results at these points are compared. Figure 5.71(a) shows the measurements of inductive transducers P_n and P_s during the test L1 and the numerical model results at the same points, in relation to the applied in-plane shear force V . As the temporary support was placed exactly in the middle of the glass span, the symmetrical out-of-plane deflection is recognised for test results as well as for numerical model results. The comparison of out-of-plane deflection at point P_e and P_w in test L1 and numerical model is shown in Figure 5.70(b). The numerical simulation results fit very well with the deflection measured during the experimental investigation.

5.6 SUMMARY AND CONCLUSIONS

The objectives of this Chapter were to develop the following numerical models:

- Point support connection model (Section 5.2)
- Point supported panel model (Section 5.3)
- Linear support connection model (Section 5.4)
- Linear supported panel model (Section 5.5)

The **Point supported connection model** is developed to study the local behaviour of the axial rigid connection at the glass hole and in the surrounding glass area. The numerical model is validated by comparing the results with experimental results and the existing solutions. From here, the following conclusions have been drawn:

- In a glass plate with a hole loaded with tensile force through the bolt in the hole, the maximal principal tensile stresses at the glass hole (clearance $\Delta R=0$) occur perpendicular to the force direction. No principal compressive stresses occur at this place.
- In a glass plate with a hole loaded with compressive force through the bolt in the hole, the maximal principal tensile stresses at the glass hole (clearance $\Delta R=0$) occur in the line of force direction, at the contact point between the connection device and the glass. At the same point, maximal principal tensile and compressive stresses occur.
- The stress concentration is mainly influenced by the distance between the glass hole and the edge (glass panel under tensile force) and glass hole diameter (glass panel under compressive force).
- The stress concentrations decrease when moving from the hole and reaching its nominal values at a certain distance. Consequently, the axial rigid connection subjected to tensile or compressive force has only a local influence on the small surrounding area of the glass panel.

The **Point supported panel model** is developed to study the shear buckling behaviour of a full-size point supported glass panel subjected to in-plane shear force V . By elastic buckling analysis the critical in-plane shear force V_{cr} , the shear buckling coefficient k_τ and the initial geometric imperfection shapes are determined. By nonlinear buckling analysis the global behaviour of the glass panel is studied by means of glass panel out-of-plane deflection w , in-plane displacement u , support reactions R and distribution of principal tensile stress σ_l . The influence of different shapes of the initial imperfection on glass panel response is investigated. Additionally, the interaction of in-plane shear force V with out-of-plane distributed load q (load cases $q+V$), in-plane normal compressive force (load case $N+V$) as well as the interaction with both q and N (load cases $q+N+V$) are studied. The numerical results are validated by comparing them with the experimental investigation results. The following conclusions can be drawn:

- Due to the membrane effect caused by compressive and tensile diagonal, a force higher than the critical one can be reached, demonstrating the post-buckling reserve of the system.
- Shear buckling coefficient k_τ depends on glass panel ratio $\alpha=a/b$ for monolithic glass, and the additional on PVB stiffness for laminated glass.
- The first buckling mode shape has the most unfavourable influence on glass panel behaviour and is therefore settled as default for further analyses.
- Maximum tensile stresses occur due to stress concentration at the compressive supports.

- The in-plane displacement is linear until the critical shear force when it deviates due to buckling, showing a nonlinear behaviour and introducing the ductility to the system. The principal tensile stress and support reactions showed a similar behaviour.
- Different load cases drastically influence the shear buckling behaviour of the glass panel. If the shape of the initial imperfection and the final deformation defer, the snap-trough point occurs which perturbed the glass panel behaviour.
- The in-plane stiffness is linear for all load cases up to the critical shear force. For higher values, the in-plane stiffness is between the two asymptotes, caused by a different initial imperfection shape.

The **Linear supported connection model** is developed to study the adhesive behaviour in the glass/substructure connection under shear force. The deformation and the stress distribution in the adhesive are used to determine the adhesive material law. The numerical model is validated by comparing the results with the experimental results. The main conclusions from this study are:

- The idealized elasto-plastic adhesive material model with the adhesive modulus $E_A=2.4 \text{ N/mm}^2$ and yielding stress of $\tau_p=0.95 \text{ N/mm}^2$ shows good agreement with experimental results.
- Parabolic stress distribution on bonding area between the adhesive and the glass/substructure is recognised, with peak stresses at the bond line.
- The adhesive will have high influence on global glass panel behaviour.

Linear supported panel model is developed to study the shear buckling behaviour of linear supported glass panel subjected to in-plane shear force V . The numerical model consists of *the* full-size glass panel and the adhesive connection. The critical in-plane shear force V_{cr} , shear buckling coefficient k_τ and the initial geometric imperfection shapes are determined by elastic buckling analysis, while the nonlinear buckling analysis is used to study the global glass panel behaviour by means of glass panel out-of-plane deflection w , in plane displacement u , support reactions R and tensile stress distribution. Influence of the initial geometrical imperfection on glass panel response is investigated. Different loads cases, interaction of the in-plane shear force V with the out-of-plane distributed load q (load case $q+V$), in-plane normal compressive forces N (load case $N+V$) as with q and N (load case $q+N+V$) are analysed. To validate the model, the results are compared with the experimental results. The investigation performed with the numerical model leads to the following conclusions:

- The adhesive shows high influence on the glass panel deformation. Soft adhesives produce a weak tensile diagonal that is not capable of keeping the compressive diagonal buckling straight, but is strong enough to introduce a membrane effect and to give the system the post-buckling reserve.
- If the glass panel critical shear force is smaller than the adhesive yielding force, two inflection points in out-of-plane deflection are visible: at the critical force and at the adhesive yielding force.
- If the adhesive yielding force occurs before the glass panel critical shear force, no inflection point occurs in glass panel out-of-plane deflection.
- The adhesive yielding introduces ductility to the specimen (in-plane displacement).
- The first buckling mode shape has the most unfavourable influence on glass panel behaviour and therefore *is* settled as default for further analyses.
- The maximum tensile stresses occur at the place of compressive load introduction at setting blocks. Higher stresses occur also due to buckling of the glass panel at the maximal bending point.
- The glass panel out-of plane stiffness decreases with different load cases with the following sequence: load case V , load case $V+N$, load case $q+V$ and load case $q+N+V$. The stiffness is related to the initial imperfection amplitude.
- The in-plane stiffness is linear and identical for all load cases up to the critical shear force. For higher values, the in-plane stiffness decreases with the same sequences as the out-of-plane deflection.

Connection models helped understand the stress distribution around the glass hole and the adhesive behaviour under shear load. The panel models explain the shear buckling behaviour of point supported and linear supported glass panels. Panel models will be further utilised for parametric study to identify the main parameters and investigate their influence on shear buckling behaviour.

6 PARAMETRIC STUDY

6.1 INTRODUCTION

The numerical models developed in Chapter 5 and verified by the experimental investigation results from Chapter 4 will be used as a base for the present parametric study. The objective is to identify the most important parameters evaluating their influence and relative importance on glass panel behaviour. Results of this study will be used to develop design method and recommendations for practical use of glass panels in building stabilization (Chapter 7). The organization chart of Chapter 6 is presented in Figure 6.1

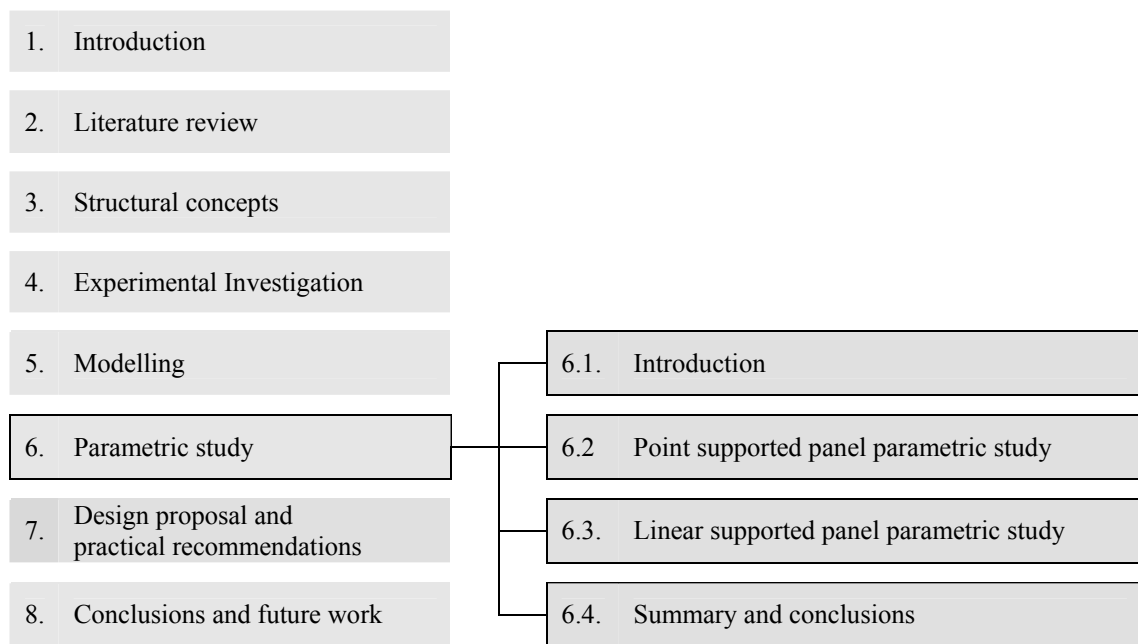


Figure 6.1 – Organization chart of Chapter 6

Point supported panel parametric study. This section deals with the investigation of the parameters regarding the geometrical/material glass panel properties in order to study the global behaviour of point supported glass panel subjected to in-plane shear force V . The influence of glass panel thickness, glass panel width, initial geometrical imperfection of glass panel and PVB shear modulus is analysed to evaluate their relative importance.

Linear supported panel parametric study. This section deals with two groups of parameters investigated in order to identify their influence on linear supported glass panel behaviour under in-plane shear force V : the geometrical/material glass panel properties (glass panel thickness, glass panel width and PVB shear modulus) and the geometrical/material adhesive properties (adhesive thickness, adhesive stiffness).

The influence of the parameters on following glass panel behaviour will be studied (for both point supported and linear supported glass panels):

- **V_{cr} values:** values of critical shear buckling force V_{cr} .
- **V - w_{max} behaviour:** in-plane shear force V vs. maximal out-of-plane deflection w_{max} .
- **V - u behaviour:** in-plane shear force V vs. in-plane displacement u .
- **V - $\sigma_{1,max}$ behaviour:** in-plane shear force V vs. maximal principal tensile stresses $\sigma_{1,max}$.
- **V - R behaviour:** in-plane shear force V vs. supports reactions R

Summary and conclusions. At the end, the summary and the main conclusions are given

6.2 POINT SUPPORTED PANEL PARAMETRIC STUDY

The chosen parameters defining the geometrical/material glass panel properties are shown in Figure 6.2. The base value of parameters are taken from *standard point supported glass panel* (Section 3.2) and also used for experimental investigation and numerical modelling.

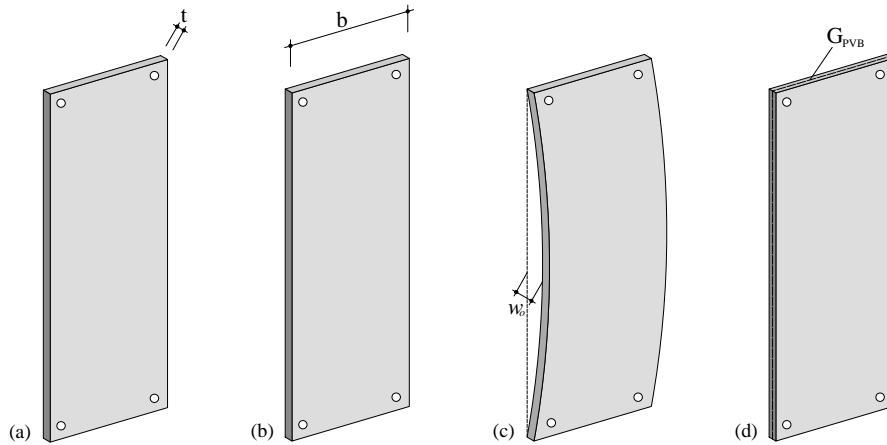


Figure 6.2 – Investigated parameters in point supported glass panel parametric study
(a) glass panel thickness t (b) glass panel width b (c) initial imperfection w_o (d) PVB shear modulus G_{PVB}

Glass panel thickness, t [mm]

Glass panel thickness t is a sum of glass sheet thicknesses Σt_g and PVB interlayer thickness t_{PVB} (eq. 5.24). Two layered laminated glass is chosen with 1.52 mm of PVB interlayer. Base value of the parameter is of 8/1.52/8 mm. Other investigated glass panel thicknesses are commonly used in the glazing system: 12/1.52/12, 15/1.52/15 and 19/1.52/19 mm (Fig 6.2(a))

Glass panel width, b [mm]

Keeping constant the height of the glass panel at 3500mm, which presents a typical height of a storey, the glass panel width b is varied. The base parameter value is 1200 mm, while varied values are 1000, 1400 and 1600 mm, representing the commonly used glazing width (Fig. 6.2(b))

Initial imperfection, w_o [mm]

The first buckling mode shape, being the most critical, is selected as the initial geometrical imperfection shape. In relation to the glass panel height, the base parameter value is chosen to be $a/1000$ (3.5mm) while varied values are $a/3000$, $a/2000$ and $a/500$ (Fig. 6.2(c))

PVB shear modulus, G_{PVB} [mm]

The PVB interlayer is modelled as elastic material with variable shear modulus. The base parameter value for PVB shear modulus is chosen to be 0.5 N/mm² presenting the PVB stiffness under short-term wind load, while the other varied values are 0.1, 1.0 and 10 N/mm² (Figure 6.2(d)).

The summary of point supported glass panel parameters with their base and varied values are shown in Table 6.3. Underlined values symbolise the base parameter value.

Table 6.3 – Investigated parameters in point supported glass panel parametric study

Glass panel thickness t [mm]	Glass panel width b [mm]	Initial imperfection w_o [mm]	PVB shear modulus G_{PVB} [N/mm ²]
8/1.52/8	100	$a/3000$	0.1
12/1.52/12	<u>1200</u>	$a/2000$	<u>0.5</u>
15/1.52/15	1400	<u>$a/1000$</u>	1.0
19/1.52/19	1600	$a/500$	10.0

6.2.1 Parameter influences on V_{cr} values

The influences of geometrical/material glass panel parameters on the value of critical shear buckling force V_{cr} (§5.3.2) are presented in Figure 6.4. The glass panel thickness t , the glass panel width b , initial geometrical imperfections w_o and PVB shear modulus G_{PVB} are varied, analysed and their importance on V_{cr} is evaluated. The filled point (●) presents the V_{cr} for base value of the parameter, while the unfilled point (○) presents the varied values of the parameter.

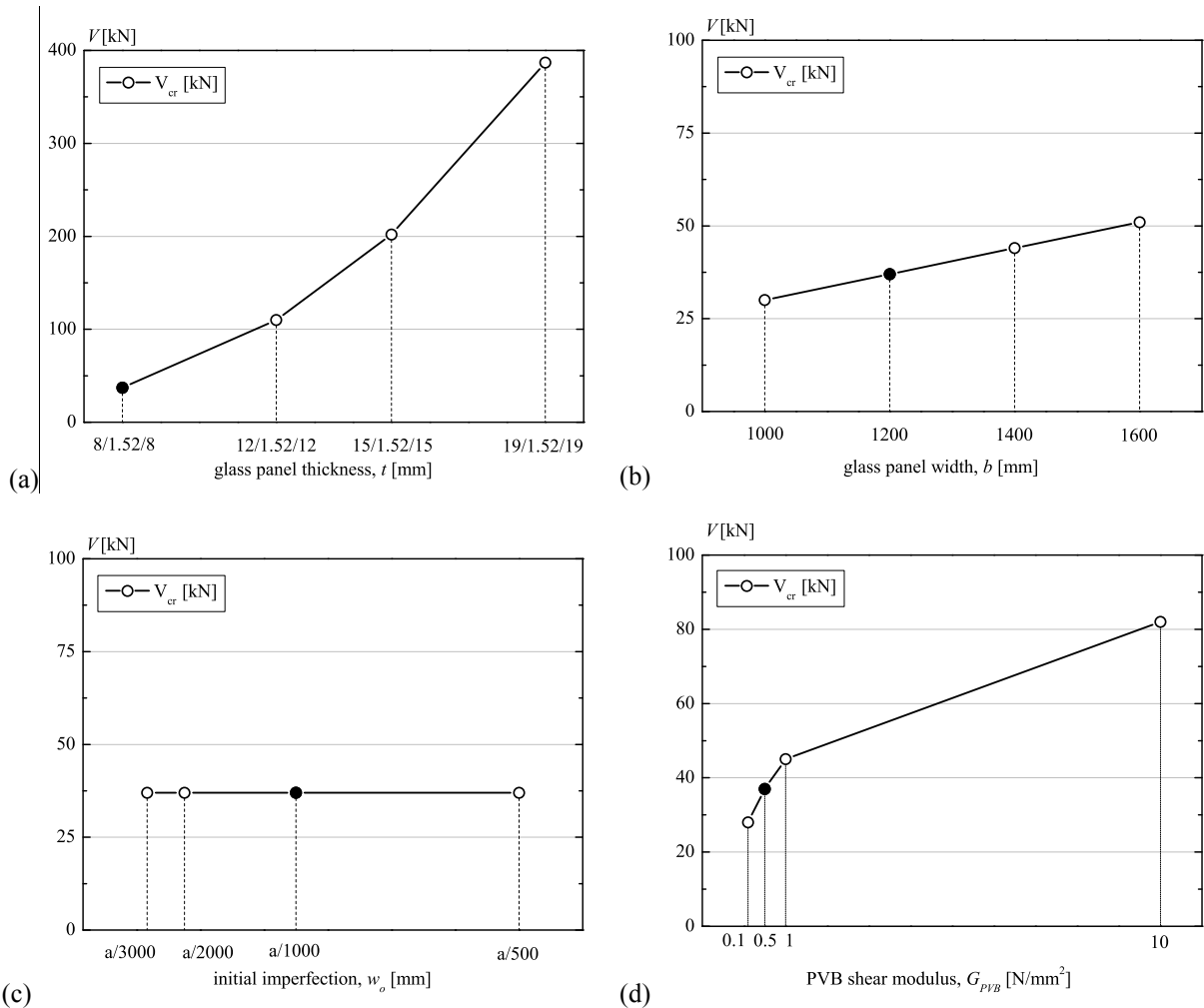


Figure 6.4 – Parameters influence on V_{cr} values

(a) glass panel thickness t (b) glass panel width b (c) initial imperfection w_o (d) PVB shear modulus G_{PVB}

From these results the following conclusion is drawn:

- By increasing the glass panel thickness t , the values of critical shear buckling force V_{cr} increases by geometrical progression with exponential growth. The glass panel thickness shows high influence on the value of V_{cr} (Fig. 6.4(a))
- The critical shear buckling force V_{cr} increases linearly with the increase of glass panel width b . The glass panel width has small influence on the value of V_{cr} (Fig. 6.4.(b))
- By increasing the initial imperfection w_o , the critical value remains constant. Therefore its influence on V_{cr} can be neglected. (Fig. 6.4(c)).
- By increasing the PVB shear modulus G_{PVB} in the laminated glass panel, the value V_{cr} increases by geometrical progression with exponential decay. The PVB shear modulus has medium influence on the value of V_{cr} (Fig. 6.4(d)).

6.2.2 Parameter influence on V - w_{max} behaviour

The influence of the geometrical/material glass panel parameters on the relation of in-plane shear force V vs. maximal out-of-plane deflection w_{max} (V - w_{max} behaviour, see Fig. 5.29) is presented in Figure 6.5. The full line symbolizes the base value of the parameter while the dotted lines symbolize the varied values of the parameter. The filled point (\bullet) presents the critical shear buckling force V_{cr} for base value of the parameter, while the unfilled point (\circ) presents the V_{cr} for varied parameter values.

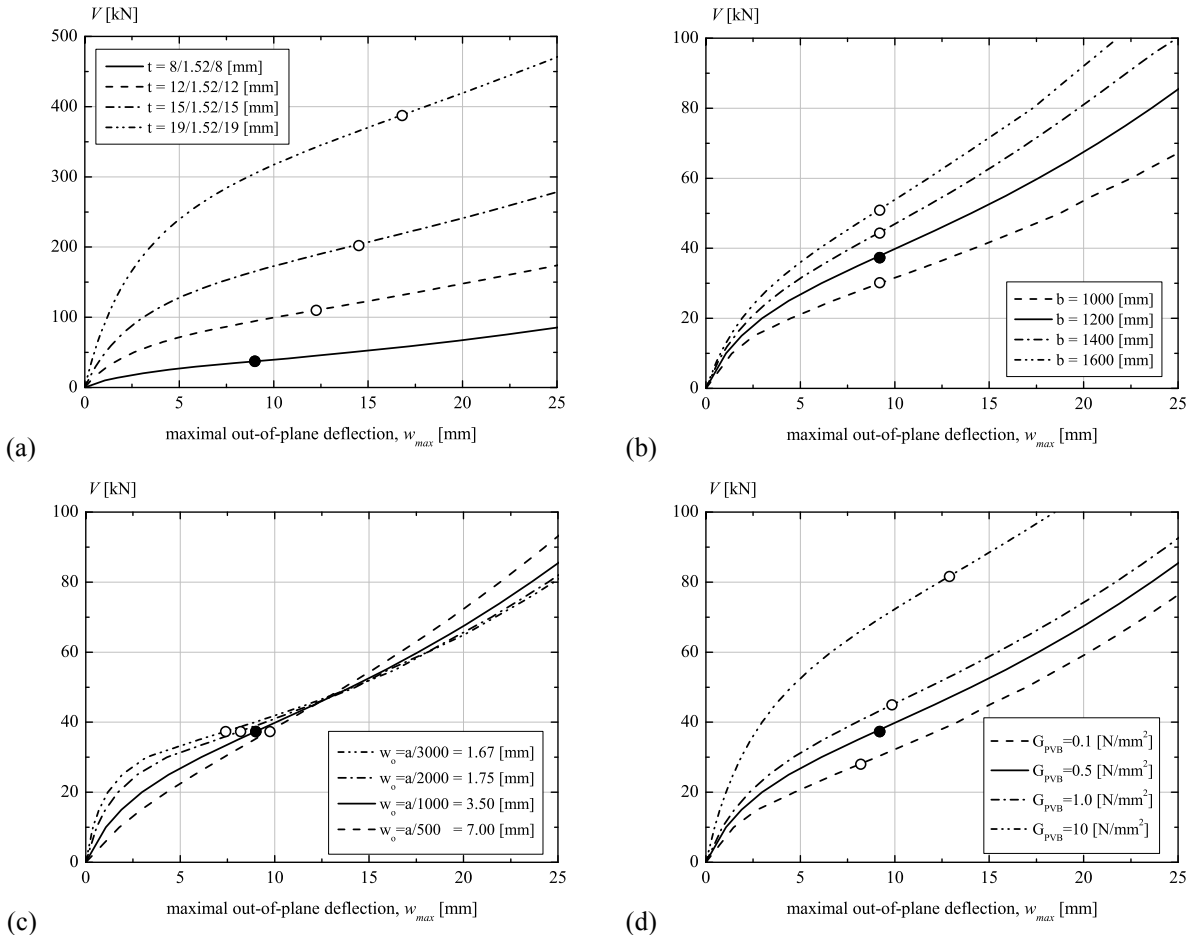


Figure 6.5 – Parameter influence on V - w behaviour

(a) glass panel thickness, t (b) glass panel width, b (c) initial imperfection, w_o (d) PVB shear modulus, G_{PVB}

From the results of parameter influence on V - w_{max} behaviour, the following conclusions are drawn:

- By increasing the glass panel thickness t , the stiffness of the glass panel increases proportionally for all values of in-planes shear force V . The w_{max} at critical point increases with increase of the glass panel thickness. The glass panel thickness has high influence on V - w_{max} (Fig. 6.5(a)).
- The stiffness increases proportionally for all values of in-plane shear force V when increasing the glass panel width b . The w_{max} at critical points remains constant for all values of b . The glass panel width has small influence on V - w_{max} behaviour (Fig. 6.5(b)).
- The initial geometrical imperfection influence on V - w_{max} behaviour can be divided in two parts. For the values smaller than about 120% of V_{cr} , the glass panel with bigger initial imperfection amplitude demonstrates less stiffness. By decreasing the initial imperfection amplitude, the stiffness grows, almost reaching the behaviour of an ideal plate for very small values ($a/3000$). For values higher than 120% of V_{cr} , the glass panel shows opposite behaviour from the one of smaller values. The initial imperfection has small influence on V - w_{max} behaviour (Fig. 6.5(c)).
- The V - w_{max} stiffness increases proportionally until the critical value V_{cr} is reached when increasing the PVB shear modulus G_{PVB} . After the critical values, the stiffness is equal for different PVB shear modulus – the curves are parallel. The w_{max} at critical points increase when the PVB stiffness increases. The PVB shear modulus has moderate influence on V - w_{max} behaviour (Fig. 6.5(d)).

6.2.3 Parameter influence on V - u behaviour

The behaviour of in-plane shear force V vs. in-plane displacement u (V - u behaviour, see Fig. 5.30) for different geometrical/material glass panel parameters is presented in Figure 6.6. Again, the full line symbolizes the base value of the parameter, the dotted lines symbolize the varied values of the parameter, the filled point (\bullet) presents the critical shear buckling force V_{cr} for base value of the parameter and the unfilled point (\circ) presents the V_{cr} for varied values of the investigated parameter.

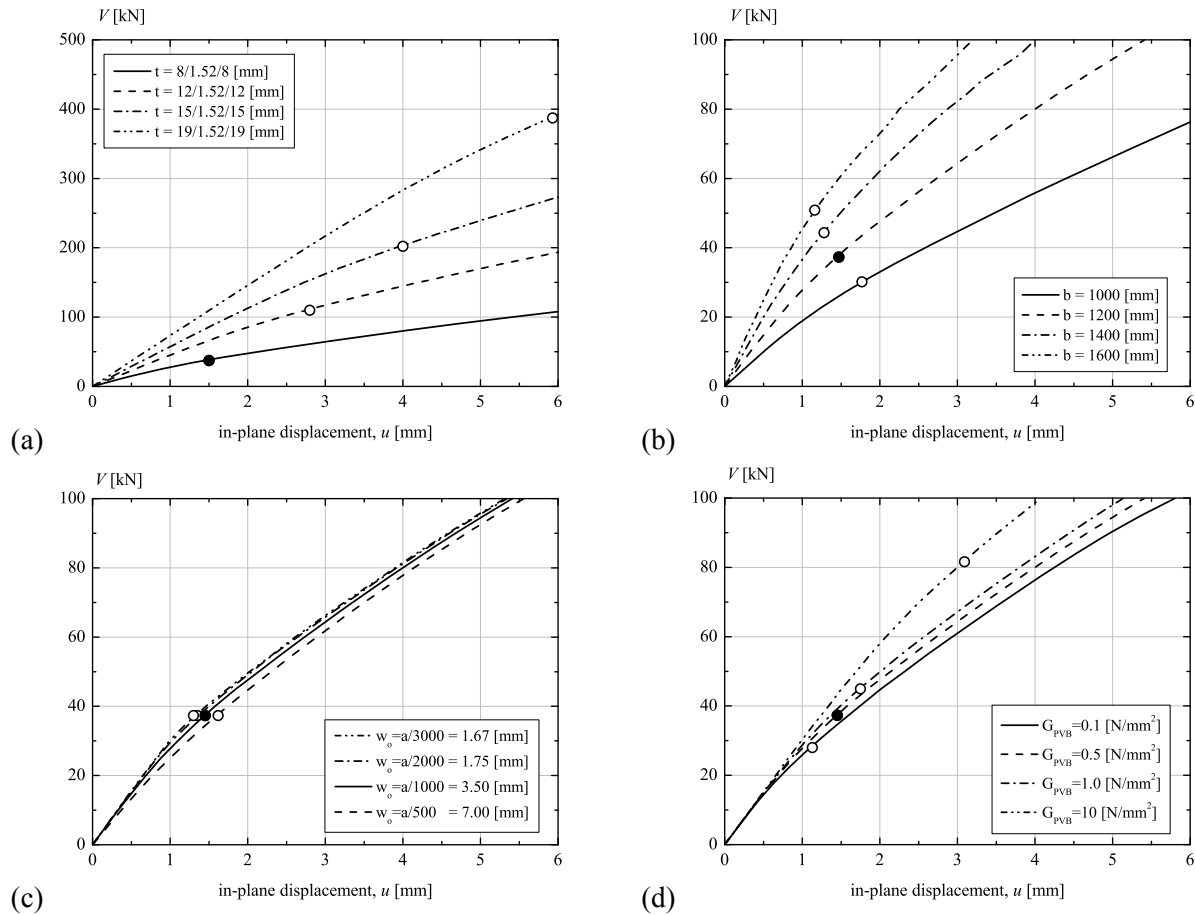


Figure 6.6 – Parametrical influence on V - u behaviour

(a) glass panel thickness, t (b) glass panel width, b (c) initial imperfection, w_o (d) PVB shear modulus, G_{PVB}

The results of influence of the parameters on V - u behaviour lead to the following conclusions:

- Thicker glass panel gives higher in-plane stiffness to the glass panel proportionally for all values of in-planes shear force V . The in-plane displacement u at critical points increases with the glass panel thickness. The glass panel thickness shows high influence on V - u behaviour (Fig. 6.6(a))
- By increasing the glass panel width b , the glass panel in-plane stiffness also increases for all values of in-plane shear force V . The u at critical points decreases with the increase of b . The glass panel width has moderate influence on V - u behaviour (Fig. 6.6(b))
- Glass panel initial geometrical imperfection w_o demonstrates a very small influence on V - u behaviour. The stiffness increases slightly with decrease of the initial imperfection. The initial imperfection w_o influences on V - u behaviour can be neglected (Fig. 6.6(c)).
- For the values smaller than the critical force V_{cr} , the in-plane glass panel stiffness increases proportionally with the increase of PVB shear modulus G_{PVB} . For the values higher than the critical force, the in-plane stiffness remains identical for all PVB shear module (the curves are parallel). The in-plane displacement u at critical points increase with increase of the PVB shear modulus. The PVB shear modulus has small influence on V - u behaviour (Fig. 6.6(d)).

6.2.4 Parameter influence on V - $\sigma_{1,max}$ behaviour

The behaviour of in-plane shear force V vs. maximal principal tensile stresses $\sigma_{1,max}$ (V - $\sigma_{1,max}$ behaviour, see Fig.5.32) influenced by different geometrical/material glass panel parameters, is shown in Figure 6.6. The maximal principal tensile stress $\sigma_{1,max}$ is measured at each load step and does not occur always at the same point of the glass panel. The full line symbolizes the base value of the parameter, the dotted lines the varied values of the parameter, the filled point (\bullet) presents V_{cr} for base value of the parameter and the unfilled point (\circ) presents V_{cr} for varied values.

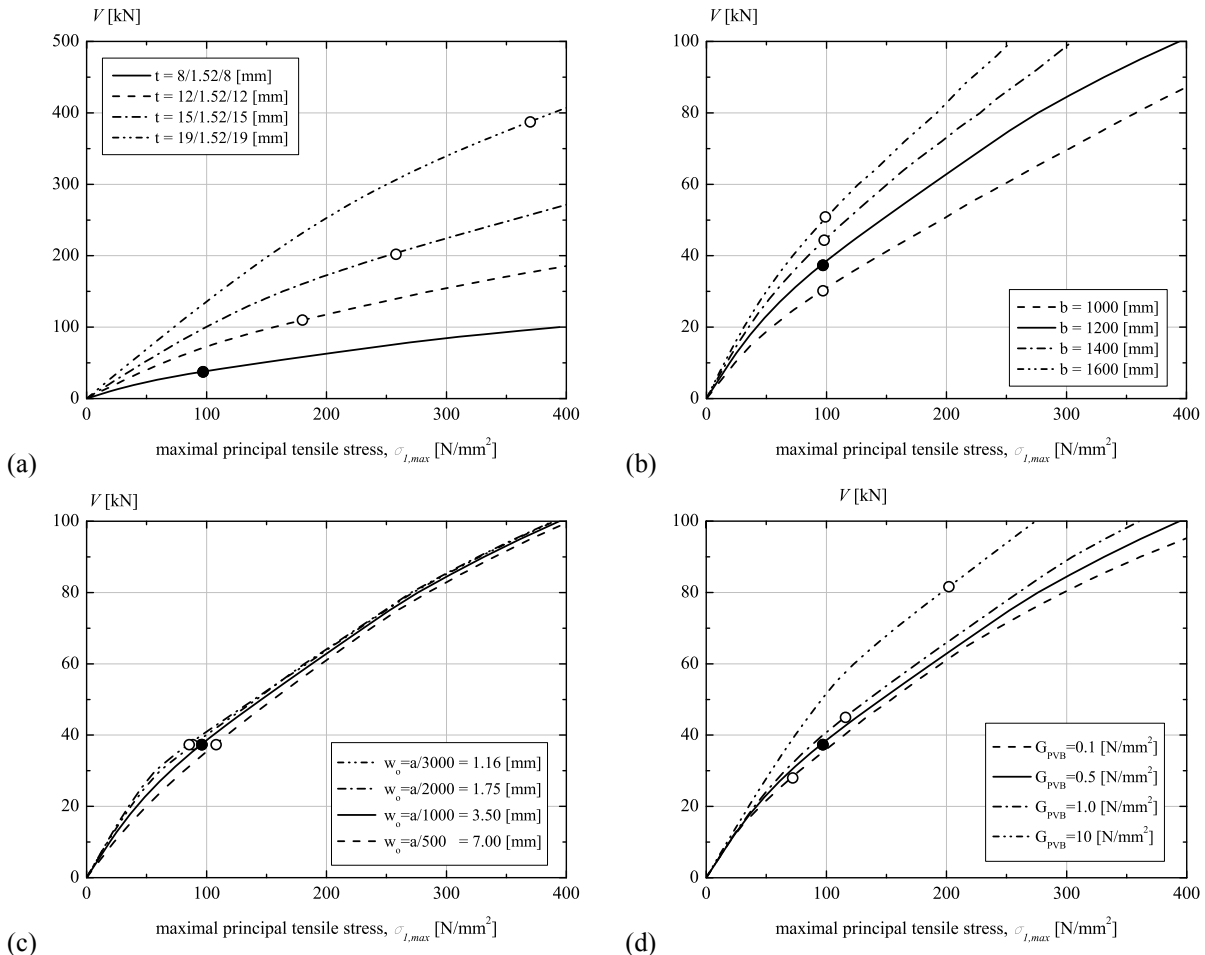


Figure 6.7 – Parametrical influence on V - $\sigma_{1,max}$ behaviour

(a) glass panel thickness, t (b) glass panel width, b (c) initial imperfection, w_o (d) PVB shear modulus, G_{PVB}

The parameter influence on V - $\sigma_{1,max}$ behaviour is similar to the parameter influence on V - u behaviour (§6.2.3) and consequently the similar conclusions can be drawn:

- By increasing the glass panel thickness t , the V - $\sigma_{1,max}$ curves increase proportionally for all values of in-planes shear force V . The $\sigma_{1,max}$ at critical points increases with the glass panel thickness. The glass panel thickness has high influence on V - $\sigma_{1,max}$ behaviour (Fig. 6.7(a))
- The V - $\sigma_{1,max}$ curves increase proportionally for all values of the in-plane shear force V , increasing the glass panel width b . The $\sigma_{1,max}$ at critical points remains constant for all values of b . The glass panel width demonstrates moderate influence on V - $\sigma_{1,max}$ behaviour (Fig. 6.7(b))
- The glass panel initial geometrical imperfection w_o has very small, negligible influence on V - $\sigma_{1,max}$ behaviour (Fig. 6.7(c))
- For the values smaller than the critical force V_{cr} , the V - $\sigma_{1,max}$ curves increase proportionally with the increase of PVB shear modulus G_{PVB} . For the values higher than V_{cr} , the V - $\sigma_{1,max}$ curves become parallel. The $\sigma_{1,max}$ at critical points increases with the increase of the PVB shear modulus. The PVB shear modulus shows small influence on V - σ behaviour (Fig. 6.7(d)).

6.2.5 Parameter influence on V - R behaviour

Figure 6.8 shows the influence of the geometrical/material glass panel parameters on behaviour of in-plane shear force V vs. support reactions R (V - R behaviour, see Fig. 31). Two support reaction results are shown in the graphs: tensile support reaction R_I at support 1 (+ x direction) and compressive support reaction R_3 at support 3 (- x direction). The full line symbolizes the base value of the parameter, the dotted lines the varied values of the parameter, the filled point (\bullet) presents V_{cr} for base value of the parameter and the unfilled point (\circ) presents V_{cr} for varied values.

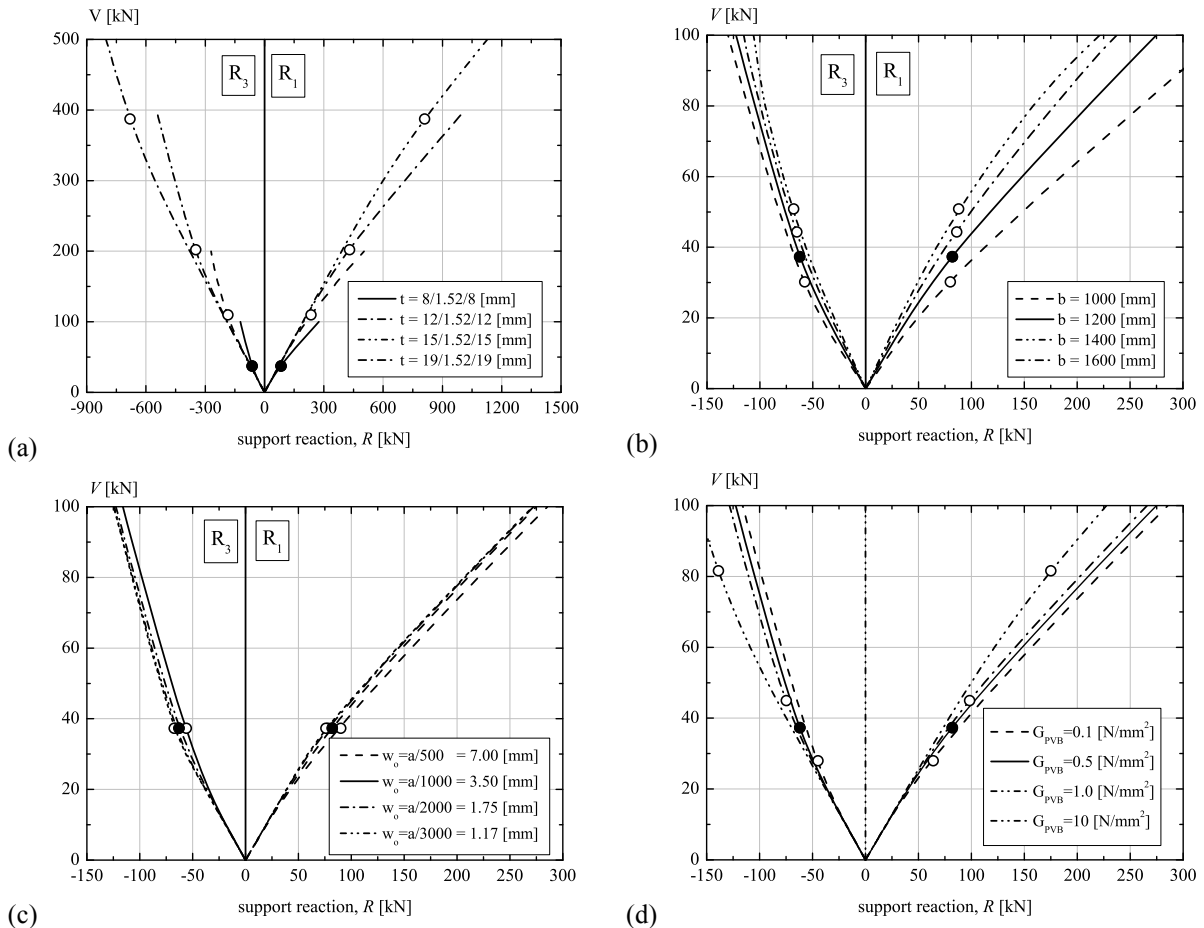


Figure 6.8 – Parametrical influence on V - R behaviour

(a) glass panel thickness, t (b) glass panel width, b (c) initial imperfection, w_0 (d) PVB shear modulus, G_{PVB}

From the parametric study on V - R behaviour, the following conclusions can be drawn:

- For the whole glass panel thickness t , the V - R curves (both R_I and R_3) are linear and identical, for the values smaller than the critical shear buckling force V_{cr} . Above V_{cr} the curves deviate: curves V - R_3 increase while curves V - R_I decrease. The glass panel thickness has high influence on V - R behaviour (Fig. 6.8(a))
- The curves V - R (both R_I and R_3) increase proportionally for all values of V when increasing the glass panel width b . A linear behaviour up to the point of critical values and later deviation is recognised. The glass panel width has small influence on V - R behaviour (Fig. 6.8(b))
- The influence of a different initial geometrical imperfection on V - R behaviour is very small, and therefore negligible (Fig. 6.8(c))
- The curves V - R_I increase while the curves V - R_3 decrease with the increase of PVB shear modulus G_{PVB} for values smaller than V_{cr} . For highest values of V_{cr} the curves becomes parallel. The PVB shear modulus has moderate influence on V - R behaviour (Fig. 6.8(d)).

6.3 LINEAR SUPPORTED PANEL PARAMETRIC STUDY

Two groups of parameters to study the linear supported glass panel behaviour are defined: the glass panel geometrical/material parameters and adhesive geometrical/material parameters. The base value of the parameters are taken from *standard linear supported glass panel* (Section 3.3), utilised also for experimental investigation and numerical modelling.

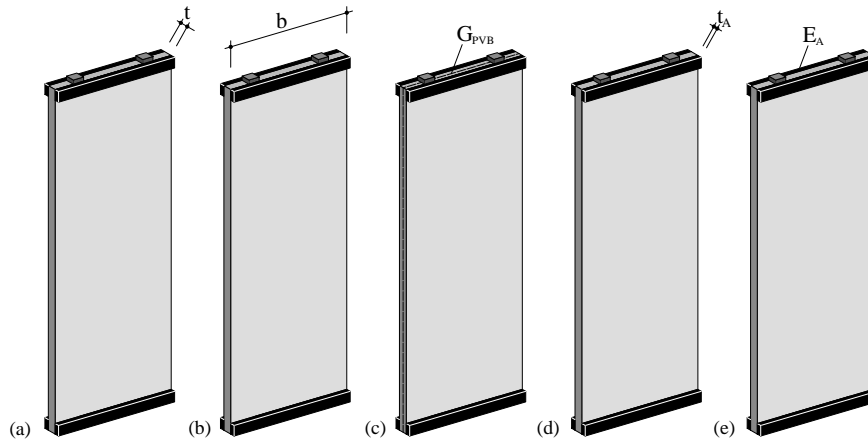


Figure 6.9 – Investigated parameters in linear supported glass panel parametric study (a) glass panel thickness t (b) glass panel width b (c) PVB shear modulus G_{PVB} (d) adhesive thickness t_A (e) adhesive stiffness E_A

Glass panel geometrical/material parameters are the same as in the point supported glass panel parametric study (Section 6.2). The same base values of the parameters are chosen. Exception is that the initial imperfection is not investigated due to reason that it demonstrates negligible influence:

Glass panel thickness, t (Fig. 6.9(a))
Glass panel width, b (Fig. 6.9(b))
PVB shear modulus, G_{PVB} (Fig. 6.9(c))

Additionally, following parameters of adhesive geometrical/material properties are investigated:

Adhesive thickness, t_A

The adhesive should resist elastic deformation due to temperature expansion difference between the glass and the substructure. Base value adhesive thickness t_A is 9.5 mm, while varied values of parameters are 4.0, 6.0 and 8.0 mm (Fig. 6.9(d))

Adhesive stiffness, E_A

The stiffness of the adhesive is defined with its modulus of elasticity. Base parameter corresponds to the adhesive material model defined Section 5.4, and has a value of 2.4 N/mm². Varied values of parameters are chosen to be 1.0, 5.0 and 10.0 N/mm² (Fig. 6.9(e))

The summary of linear supported glass panel parameters with base and varied values are shown in Table 6.10. Underlined values symbolise the base value of the parameters.

Table 6.10 – Investigated parameters in linear supported glass panel parametric study

Glass panel geometrical/material properties			Adhesive geometrical/material properties	
Glass panel thickness t [mm]	Glass panel width b [mm]	PVB shear modulus G_{PVB} [N/mm ²]	Adhesive thickness t_A [mm]	Adhesive stiffness E_A [N/mm ²]
8/1.52/8	100	0.1	4.0	1.0
12/1.52/12	<u>1200</u>	<u>0.5</u>	6.0	<u>2.4</u>
15/1.52/15	1400	1.0	8.0	5.0
19/1.52/19	1600	10.0	<u>9.5</u>	10.0

6.3.1 Parameter influence on V_{cr} values

Influence of glass panel geometrical/material and adhesive geometrical/material parameters on the values of critical shear buckling force V_{cr} are presented in the Figure 6.11. The filled point (●) presents the V_{cr} for base value of the parameter, while the unfilled point (○) represents varied values of the parameter. From these results, the following main conclusions are drawn:

- By increasing the glass panel thickness t , the values of critical shear buckling force V_{cr} increases by geometrical progression with exponential growth. The glass panel thickness shows very high influence on the value of V_{cr} (Fig. 6.11(a)).
- The critical shear buckling force V_{cr} increases linearly with the increase of glass panel width b . The glass panel width shows moderate influence on the V_{cr} values (Fig. 6.11(b)).
- Stiffer interlayer, meaning PVB with higher shear modulus G_{PVB} , gives the glass panel higher critical shear buckling force V_{cr} . It increases by geometrical progression with exponential decay. The PVB shear modulus demonstrates moderate influence on V_{cr} values (Fig. 6.11(c)).
- The adhesive thickness t_A has no influence on the value of critical in-plane shear force V_{cr} . It remains constant for all adhesive thickness (Fig. 6.11(a)).
- Increasing the stiffness of the adhesive by increasing its elasticity modulus E_A , the values of V_{cr} increase by geometrical progression with exponential growth. The adhesive stiffness demonstrates small influence on the V_{cr} value (Fig. 6.11(d)).

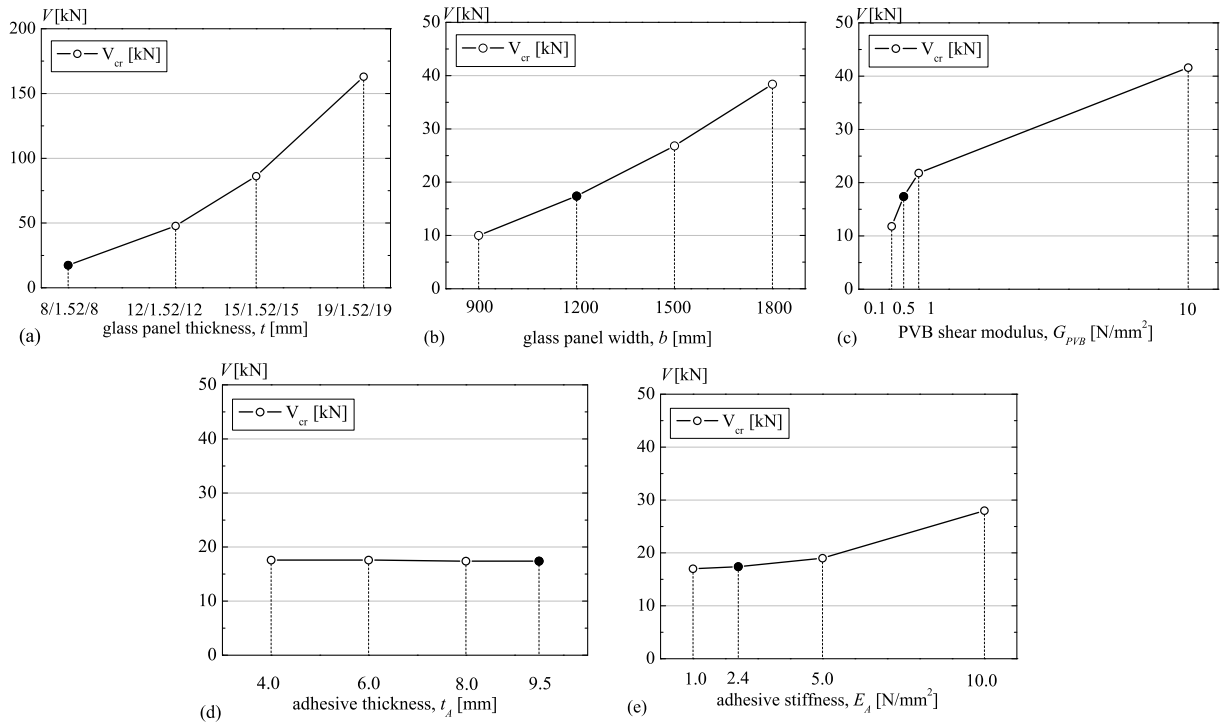


Figure 6.11 – Parameter influence on V_{cr} values (a) glass panel thickness t (b) glass panel width b (c) PVB shear modulus G_{PVB} (d) adhesive thickness t_A (e) adhesive stiffness E_A

6.3.2 Parameter influence on V - w_{max} behaviour

The glass panel geometrical/material and adhesive geometrical/material adhesive parameters influence the behaviour of in-plane shear force V vs. maximal out-of-plane deflection w_{max} (V - w behaviour, see Fig. 5.63) as shown in the Figure 6.12. The full line in the graphs presents the base parameter while the dotted lines present the varied parameters. The filled point (●) presents the critical shear buckling force V_{cr} for base value of the parameter, while the unfilled point (○) presents the V_{cr} for varied values of the investigated parameter. The filled triangle (▲) presents the in-plane shear force where the yielding of the adhesive occurs $V_{pl,A}$ for base value of the parameter, while the unfilled cube (Δ) presents the $V_{pl,A}$ for varied values of the parameters.

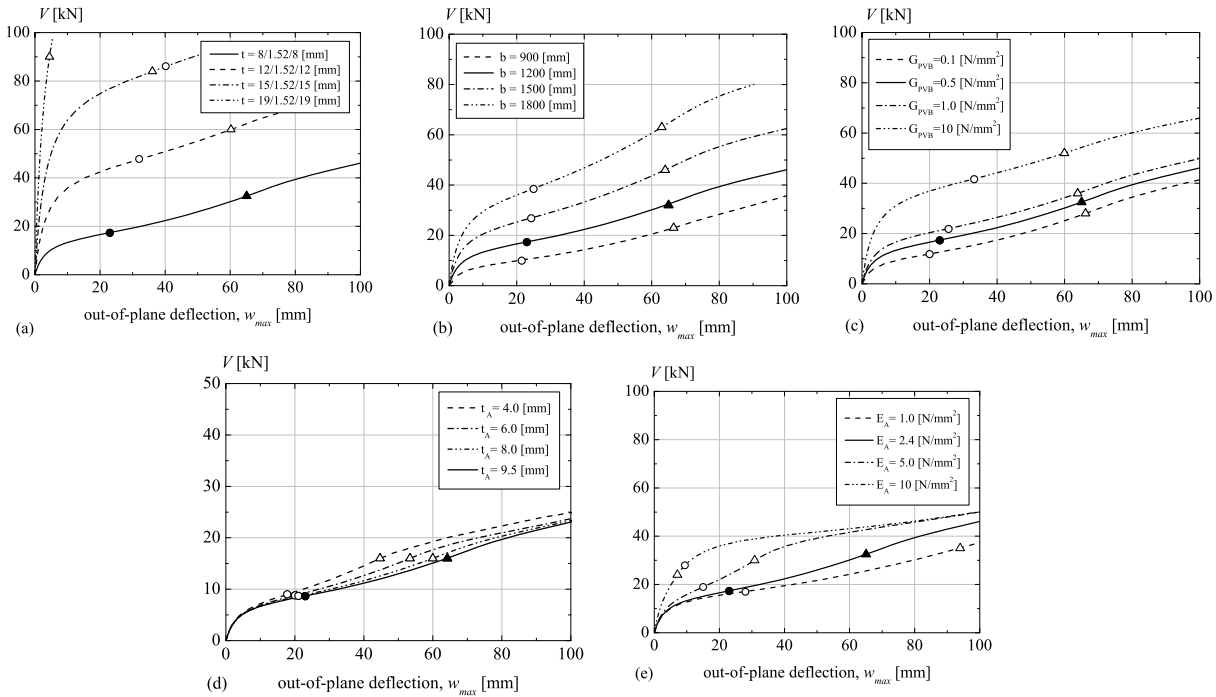


Figure 6.12 – Parametric study on V - w_{max} behaviour (a) glass panel thickness t (b) glass panel width b (c) PVB shear modulus G_{PVB} (d) adhesive thickness t_A (e) adhesive stiffness E_A

Main conclusions about the influence of the parameters on V - w_{max} behaviour are:

- By increasing the glass panel thickness t , the stiffness of the glass panel increases proportionally for all values of in-plane shear force V . Thinner glass panels reach their critical values before the yielding of the adhesive (8/1.52/8 and 12/1.52/12), on the other hand, for thicker glass panels the adhesive yielding occurs before reaching the critical values. The deflections w at critical points increase with the increase of the glass panel thickness, while the deflections w decrease at yielding point of the adhesive. The glass panel thickness has high influence on V - w_{max} behaviour (Fig. 6.12(a))
- Glass panel width b increases the glass panel stiffness proportionally for all values of in-plane shear force V . The deflections w at critical points increase with increase of the glass panel width, while deflections w at adhesive yielding point remain almost constant. The glass panel width has moderate influence on V - w_{max} behaviour (Fig. 6.12(b))
- The stiffness of the glass panel increases with the increase of PVB shear modulus proportionally until the critical value. For higher values, the curves are parallel and they have identical stiffness. The deflections w at critical points are higher for stiffer PVB modulus, while deflections at adhesive yielding points show the opposite behaviour. The glass panel width has small influence on V - w_{max} behaviour (Fig. 6.12(c))
- By increasing the adhesive thickness t_A , the stiffness of the glass panel decreases proportionally for the values of in-plane shear force V smaller than $V_{pl,A}$. After yielding of the adhesive, the stiffness of the glass panel decreases inversely proportionately. The deflections w at critical points and at adhesive yielding points increase with increase of the adhesive thickness. The adhesive thickness has small influence on V - w_{max} behaviour (Fig. 6.12(d)).
- Stiffer adhesive gives the glass panel higher stiffness when subjected to in-plane shear force V . The stiffness increases proportionally until the yielding of the adhesive $V_{pl,A}$. Afterwards the stiffness increases inversely proportionately. By utilising the stiffer adhesive, the yielding of the adhesive takes place before the critical shear buckling force V_{cr} is reached. The adhesive stiffness has moderate influence on V - w_{max} behaviour (Fig. 6.12(e)).

6.3.3 Parameter influence on V - u behaviour

Figure 6.13 shows the influence of glass panel geometrical/material and adhesive geometrical/material parameters on the behaviour of in-plane shear force V vs. in-plane panel displacement u (V - u behaviour, see Fig. 5.64). The following main conclusions on this parameters study are drawn:

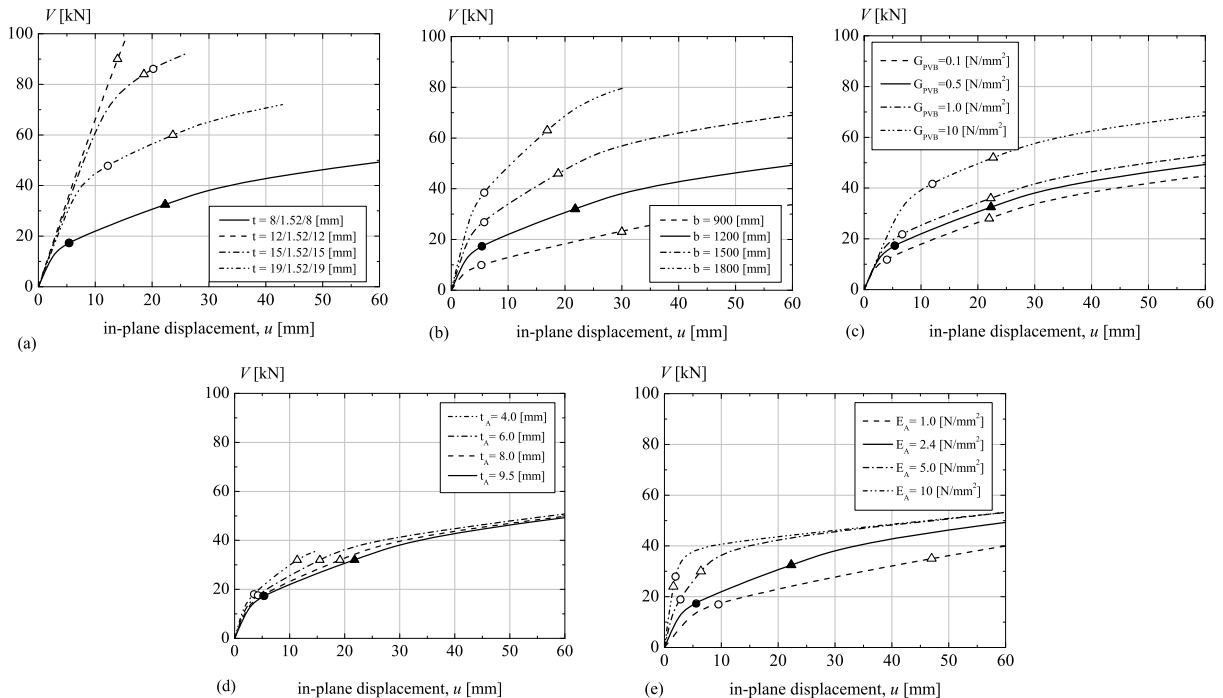


Figure 6.13 – Parametric study on V - u behaviour (a) glass panel thickness t (b) glass panel width b (c) PVB shear modulus G_{PVB} (d) adhesive thickness t_A (e) adhesive stiffness E_A

- The in-plane stiffness remains linear and constant until the approximate 80% of the value of critical shear buckling force V_{cr} for different glass panel thickness t . After this value, the in-plane stiffness increases proportionally with increase of the glass panel thickness. The displacements u at critical points increase with the increase of the glass panel thickness, while the displacements u at adhesive yielding decrease. The glass panel thickness has high influence on V - u behaviour (Fig. 6.13(a)).
- The in-plane stiffness increases when increasing the glass panel width b proportionally for all values of in-plane shear force V . The displacements u at critical points remain constant for all glass panel width, while displacements u at adhesive yielding points are decreasing. The glass panel width has moderate influence on V - u behaviour (Fig. 6.13(b)).
- The in-plane stiffness is linear and constant for all values of PVB shear modulus, up to 80% of the critical shear buckling force V_{cr} . After this value, the in-plane stiffness increases proportionally until the value of adhesive yielding $V_{pl,A}$. Afterwards the curvatures become parallel. The displacements u at critical points gets higher for stiffer PVB, while displacements u at adhesive yielding points are constant. The PVB has small influence on V - u behaviour (Fig. 6.13(c)).
- By increasing the adhesive thickness t_A , the in-plane stiffness decreases proportionally for a force smaller than the adhesive yielding force $V_{pl,A}$. After this point, the stiffness starts to decrease inversely proportionately. The displacements u at critical points and at adhesive yielding points increase with the increase of the adhesive thickness. The adhesive thickness has a negligible influence on V - u behaviour (Fig. 6.13(d)).
- The in-plane stiffness increases proportionally when stiffer adhesive (with higher modulus of elasticity E_A) is utilised until the force reaches the adhesive yielding force $V_{pl,A}$. Afterwards the stiffness increases inversely proportionately. Utilising the stiffer adhesive the yielding of the adhesive take place before glass plate reaches the critical shear buckling force V_{cr} . The adhesive stiffness has moderate influence on V - u behaviour (Fig. 6.13(e)).

6.3.4 Parameter influence on V - $\sigma_{1,max}$ behaviour

Influence of glass panel geometrical/material and adhesive geometrical/material parameters on behaviour of in-plane shear force V vs. maximal principal tensile stresses $\sigma_{1,max}$ (V - $\sigma_{1,max}$ behaviour, see Fig. 5.68) is shown in Figure 6.14. Regarding the parameter influence, the V - $\sigma_{1,max}$ behaviour demonstrates high similarity to the V - u behaviour. Therefore similar conclusions are drawn:

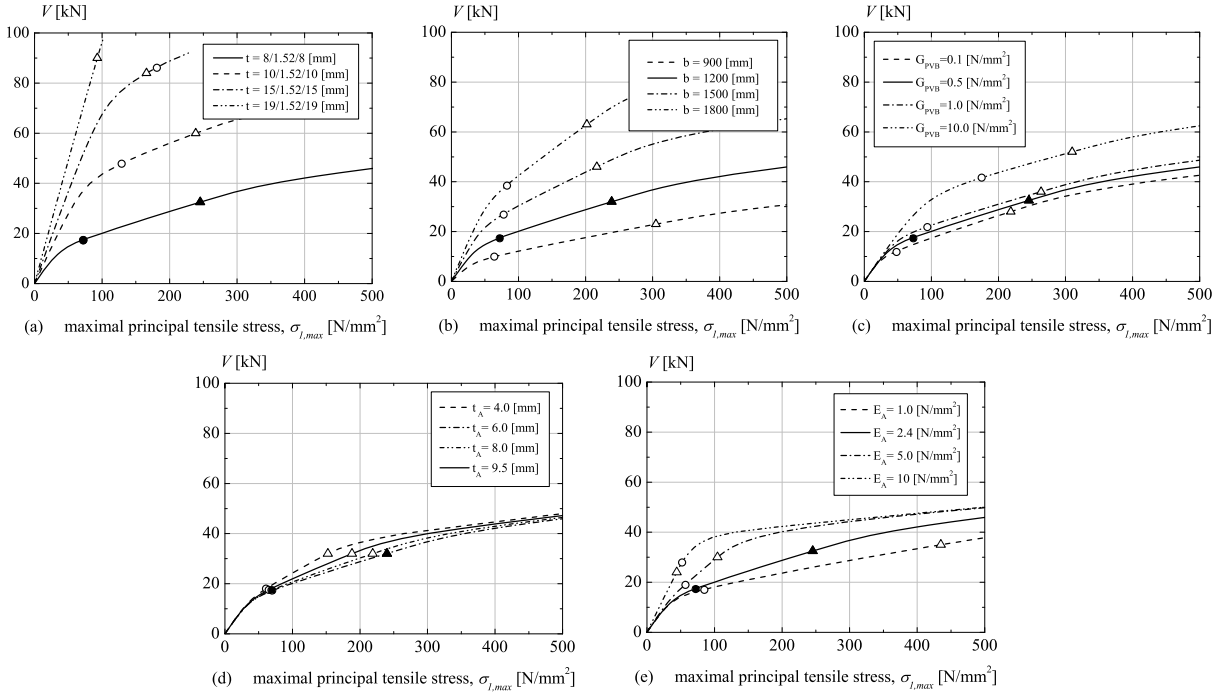


Figure 6.14 – Parametric study on V - σ behaviour (a) glass panel thickness t (b) glass panel width b (c) PVB shear modulus G_{PVB} (d) adhesive thickness t_A (e) adhesive stiffness E_A

- The V - $\sigma_{1,max}$ curves increase proportionally with increase of the glass panel thickness t for all values of in-plane shear force. The glass panel thickness has high influence on V - $\sigma_{1,max}$ behaviour (Fig. 6.14(a)).
- The V - $\sigma_{1,max}$ curves increase when increasing the glass panel width b , proportionally for all values of in-plane shear force. The glass panel width has moderate influence on V - $\sigma_{1,max}$ behaviour (Fig. 6.14(b)).
- The V - $\sigma_{1,max}$ curves are linear and constant for different values of PVB shear modulus, up to 80% of the critical shear buckling force V_{cr} . For higher values, curves increase proportionally until the critical values. Afterwards the curvatures become parallel. The PVB shear modulus has small influence on V - $\sigma_{1,max}$ behaviour (Fig. 6.14(c)).
- The V - $\sigma_{1,max}$ curves decrease proportionally to increasing the adhesive thickness t_A , for the value of the forces smaller than the adhesive yielding points $V_{pl,A}$. After this point, the curvatures start to decrease inversely proportionately. The adhesive thickness has a negligible influence on V - $\sigma_{1,max}$ behaviour (Fig. 6.14(d)).
- The V - $\sigma_{1,max}$ curves increase proportionally when stiffer adhesives are utilised, for the values smaller than the adhesive yielding force $V_{pl,A}$. Afterwards the curves increase inversely proportionately. The adhesive stiffness has moderate influence on V - $\sigma_{1,max}$ behaviour (Fig. 6.14(e)).

6.3.5 Parameter influence on V - R behaviour

Influence of glass panel geometrical/material and adhesive geometrical/material parameters on behaviour of in-plane shear force V vs. compressive support reaction at setting block 3 R_3 (V - R behaviour, see Fig. 5.65) is shown in the Figure 6.15. From the parametrical study the following main conclusions on V - R behaviour are drawn:

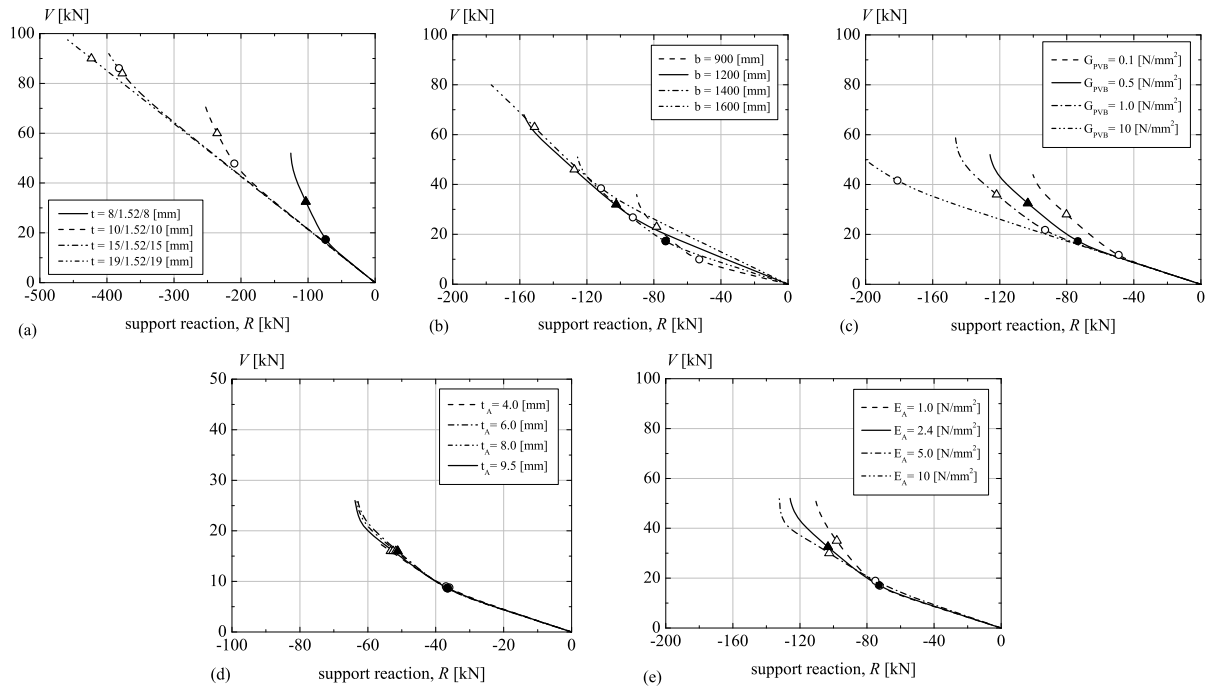


Figure 6.15 – Parameter influence on V - R behaviour (a) glass panel thickness t (b) glass panel width b (c) PVB shear modulus G_{PVB} (d) adhesive thickness t_A (e) adhesive stiffness E_A

- The V - R curves are linear and identical for different glass panel thickness t , until the value of critical force V_{cr} . For the higher values the curves deviated due to glass panel buckling and the nonlinear behaviour occurs. The support reactions R at critical points and at points of adhesive yielding increase with the increase of glass panel thickness. The glass panel thickness has high influence on V - R behaviour (Fig. 6.15(a)).
- The V - R curves increase with increases of glass panel width b , but the curves are not. After the critical force, the curves deviated crossing each others. The support reaction R at critical point and at adhesive yielding point increases with the increase of glass panel width. The glass panel width demonstrates small influence on V - R behaviour (Fig. 6.15(b)).
- For the values smaller than the critical shear buckling force V_{cr} the support reaction R is linear and identical for different PVB shear modulus. For values higher than the critical, curves deviate demonstrating non linear behaviour. The reactions at critical points and yielding adhesive points increase with the increase of PVB shear modulus. The PVB shear modulus shows moderate influence on V - R behaviour (Fig. 6.15(c)).
- For the whole adhesive thickness t_A the V - R curves show similar behaviour. The critical forces are the same for glass panels with different adhesive thickness. The curves deviate after the critical values and after yielding of the adhesive. The adhesive thickness has no influence on V - R behaviour (Fig. 6.15(d)).
- Although the values of the critical shear buckling forces V_{cr} are almost the same for different adhesive stiffness E_A , the V - R curves show different behaviour for the values higher than the critical ones. After the critical force, the V - R curves deviate but with different angles. The PVB shear modulus shows small influence on V - R behaviour (Fig. 6.15(e)).

6.4 SUMMARY AND CONCLUSIONS

Based on the numerical models developed in Chapter 5 and validated with the experimental investigation results from Chapter 4, the parametric study was done to recognise, analyse and evaluated the influences of different parameters. This study was divided in two parts:

- Point supported glass panel parametric study (Section 6.2)
- Linear supported glass panel parametric study (Section 6.3)

The objective of **Point supported panel parametric study** was to investigate the influence of different glass panel geometrical/material glass properties (glass panel thickness, glass panel width, initial geometrical imperfection of glass panel and the PVB shear modulus) on the global behaviour of point supported glass panel. The following conclusions can be drawn:

- The highest influence on the values of critical shear buckling force V_{cr} has the glass plate thickness t . The PVB shear modulus G_{PVB} has moderate influence; glass panel width b has small influence while initial imperfection w_o has no influence on the value of critical shear buckling force V_{cr} .
- The highest influence on the V - w_{max} behaviour (in-plane shear force V vs. maximal out-of-plane deflection w_{max}) has the glass panel thickness t . The PVB shear modulus G_{PVB} shows moderate influence, while the glass panel width b and the initial imperfection w_o show small influence.
- The highest influence on the V - u behaviour (in-plane shear force V vs. in-plane displacement u) has the glass panel thickness t , followed by glass panel width b with moderate influence, PVB shear modulus G_{PVB} with small influence and initial imperfection w_o with neglecting influence.
- The highest influence on the V - $\sigma_{l,max}$ behaviour (in-plane shear force V vs. maximal principal tensile stresses $\sigma_{l,max}$) has the glass panel thickness t followed by glass panel width b , PVB shear modulus G_{PVB} and initial imperfection w_o .
- The highest influence on the V - R behaviour (in-plane shear force V vs. support reactions R_1 and R_3) has the glass panel thickness t . The glass panel width b and PVB shear modulus G_{PVB} have small influence, while the initial imperfection w_o can be neglected.

The table 6.16 shows the summary of analysed parameters and their influence on the glass panel behaviour. Three arrows ($\uparrow\uparrow\uparrow$) means high influence, two arrows ($\uparrow\uparrow$) means moderate influence, one arrow (\uparrow) is small influence while (-) is for negligible influence. The final conclusion is that the highest influence on global behaviour of point supported glass panel subjected to in-plane shear force V , has the glass panel thickness t . The glass panel width b and the PVB shear modulus G_{PVB} have small to medium influence, while the initial imperfection w_o has very small and therefore negligible influence.

Table 6.16 – Parametric influences on point supported glass panel behaviour

Parameters	Investigated behaviour				
	V_{cr}	V - w_{max}	V - u	V - $\sigma_{l,max}$	V - R
Glass panel thickness, t	$\uparrow\uparrow\uparrow$	$\uparrow\uparrow\uparrow$	$\uparrow\uparrow\uparrow$	$\uparrow\uparrow\uparrow$	$\uparrow\uparrow\uparrow$
Glass panel width, b	\uparrow	\uparrow	$\uparrow\uparrow$	$\uparrow\uparrow$	\uparrow
Initial imperfection, w_o	-	\uparrow	-	-	-
PVB shear modulus, G_{PVB}	$\uparrow\uparrow$	$\uparrow\uparrow$	\uparrow	\uparrow	\uparrow

In **Linear supported panel parametric study** two parameter groups are investigated: the glass panel geometrical/material properties (glass panel thickness, glass panel width and the PVB shear modulus) and the adhesive geometrical/material properties (adhesive thickness and adhesive stiffness). The influence of these parameters on linear supported glass panel behaviour are analysed and evaluated, and the following conclusions can be drawn:

- The highest influences on the value of critical shear buckling force V_{cr} has the glass plate thickness t . The glass panel width b and PVB shear modulus G_{PVB} have moderate influence; the adhesive stiffness E_A has small influence while the adhesive thickness t_A has no influence on critical shear buckling force V_{cr} .
- The highest influence on the $V-w_{max}$ behaviour (in-plane shear force V vs. maximal out-of-plane deflection w_{max}) has the glass panel thickness t , the glass panel width b and the adhesive stiffness E_A , show medium influence while the PVB shear modulus G_{PVB} and the adhesive thickness t_A shows small influence.
- The highest influence on the $V-u$ behaviour (in-plane shear force V vs. in-plane displacement u) has the glass panel thickness t , followed by the glass panel width b and the adhesive stiffness E_A with moderate influence. The PVB shear modulus G_{PVB} has small influence, while the influence of adhesive thickness t_A influence is neglected.
- The highest influence on the $V-\sigma_{1,max}$ behaviour (in-plane shear force V vs. maximal principal tensile stresses $\sigma_{1,max}$) has the glass panel thickness t , followed by the glass panel width b and the adhesive stiffness E_A with moderate influence. The PVB shear modulus G_{PVB} has small influence, while the influence of adhesive thickness t_A influence is negligible.
- The highest influence on the $V-R$ behaviour (in-plane shear force V vs. support reactions R) has the glass panel thickness t , followed by the PVB shear modulus G_{PVB} with moderate influence, the glass panel width b and the adhesive stiffness E_A with small influence, while the adhesive thickness t_A has no influence.

Summary of the analysed parameters and the evaluation of their influence on the linear supported glass panel behaviour are presented in Table 6.17. Three arrows ($\uparrow\uparrow\uparrow$) means high influence, two arrows ($\uparrow\uparrow$) means moderate influence, one arrow (\uparrow) is small influence while (-) is for negligible influence. The final conclusion is that the highest influence on global behaviour of linear supported glass panel subjected to in-plane shear force V has the glass panel thickness t , followed by glass panel width b with moderate influence, the PVB shear modulus G_{PVB} and the adhesive thickness E_A from small to moderate influence, depending of the analysed behaviour, while the influence of adhesive thickness t_A is negligible.

Table 6.17 – Parametric influences on linear supported glass panel behaviour

Parameters	Investigated behaviour				
	V_{cr}	$V-w_{max}$	$V-u$	$V-\sigma_{1,max}$	$V-R$
Glass panel thickness, t	$\uparrow\uparrow\uparrow$	$\uparrow\uparrow\uparrow$	$\uparrow\uparrow\uparrow$	$\uparrow\uparrow\uparrow$	$\uparrow\uparrow\uparrow$
Glass panel width, b	$\uparrow\uparrow$	$\uparrow\uparrow$	$\uparrow\uparrow$	$\uparrow\uparrow$	\uparrow
PVB shear modulus, G_{PVB}	$\uparrow\uparrow$	\uparrow	\uparrow	\uparrow	$\uparrow\uparrow$
Adhesive thickness, t_A	-	\uparrow	-	-	-
Adhesive stiffness, E_A	\uparrow	$\uparrow\uparrow$	$\uparrow\uparrow$	$\uparrow\uparrow$	\uparrow

7 DESIGN PROPOSAL AND PRACTICAL RECOMMENDATIONS

7.1 INTRODUCTION

The results from experimental investigations (Chapter 4), the numerical modeling (Chapter 5) and the parametrical study (Chapter 6) are implemented by proposing the simplified method for preliminary design of point supported and linear supported glass panel subjected to in-plane shear force V . Practical recommendations for use of glass panel as a structural element in fully transparent pavilion are given. By following this design method and practical recommendations, the glass panel can be utilized as a structural element in fully transparent pavilions. Figure 7.1 shows the organization of Chapter 7.

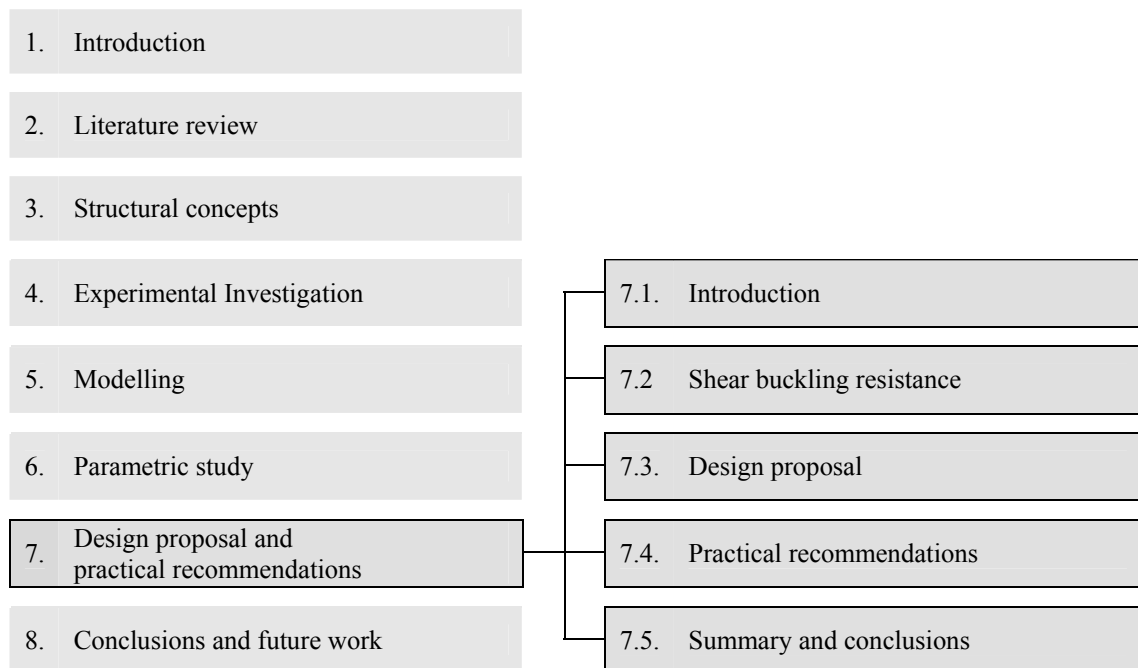


Figure 7.1 - Organization chart of Chapter 7

Shear buckling resistance. This section gives formulas and graphs for shear buckling coefficient k_τ and shear buckling reduction factor χ used to determine the shear buckling resistance $V_{b,Rk}$ for point supported and linear supported glass panels.

Design proposal. This section gives a step by step design method for the verification of the ultimate and serviceability limit state of glass panel under in-plane shear loading. This includes determination of loads and actions, structural analyses (determination of deformation, stresses and support reactions), determination of strength as well as verification of glass panel, point supported and linear supported connections.

Practical recommendations. This section gives practical recommendations on utilised materials (glass panels, mortar, bolts, adhesive, setting blocks and substructure), technical execution of the injection and gluing process, as well as erection of the fully transparent pavilion with point supported and linear supported glass panels.

At the end of this Chapter the summary and the main conclusions are given.

7.2 SHEAR BUCKLING RESISTANCE

The characteristic shear buckling resistance $V_{b,Rk}$ of the glass panel is the characteristic shear resistance of the glass panel V_{Rk} reduced by the shear buckling reduction factor χ :

$$V_{b,Rk} = \chi \cdot V_{Rk} \quad (7.1)$$

The shear buckling reduction factor χ determined in this section for point supported and linear supported glass panel is a function of non-dimensional shear plate slenderness $\bar{\lambda}$:

$$\bar{\lambda} = \sqrt{\frac{\tau_{Rk}}{\tau_{cr}}} \quad (7.2)$$

τ_{Rk} characteristic shear strength of the glass panel. By using the principal stress theory (commonly used for brittle materials like glass) it is assumed that shear stress resistance is the same as the bending stresses resistance [Wellershoff et al. 2005.1]:

$$\tau_{Rk} = \sigma_{Rk} \quad (7.3)$$

[prEN 13474-1] gives the value of bending stress resistance for heat strengthened glass ($\sigma_{Rk} = 70 \text{ N/mm}^2$) and for fully tempered glass ($\sigma_{Rk} = 120 \text{ N/mm}^2$). However, at the glass hole and edges (where the maximal stress occurs) the resistance is different than given in the standards due to distorted distribution of residual stress. It highly depends on the edge treatments (polishing and chamfering) [Schneider 2004].

τ_{cr} critical shear stress. For monolithic glass panel τ_{cr} is determined as in (see §5.3.2.1X):

$$\tau_{cr} = \frac{V_{cr}}{\sum t_g \cdot b} \quad (7.4)$$

V_{cr} being the critical shear buckling load of glass panel under in-plane shear force. For a monolithic glass panel it can be determined from the following formula:

$$V_{cr} = \frac{\pi^2 D}{b^2} \cdot k_\tau = \frac{\pi^2 E \cdot b \cdot t_g}{12(1-\nu^2)} \cdot \left(\frac{t_g}{b}\right)^2 \cdot k_\tau \quad (7.5)$$

For laminated glass panel the critical shear buckling load is:

$$V_{cr} = \frac{\pi^2 D_{lam}}{b^2} k_{\tau,lam} = \frac{\pi^2 E \cdot b \cdot t_g}{24(1-\nu^2)} \left(\frac{2t_g^2 + 6d^2}{b^2}\right)^2 k_{\tau,lam} \quad (7.6)$$

$k_\tau, k_{\tau,lam}$ the shear buckling coefficient for monolithic and laminated point supported (Figure 7.2) and linear supported (Fig. 7.3) glass panel. The shear buckling coefficient for linear supported glass panel should be multiplied by the adhesive coefficient β_A (Fig. 7.3(c)) which takes in account the adhesive stiffness ($\beta_A = 1$ for $E_A = 2.4 \text{ N/mm}^2$). The modified shear buckling coefficient k'_τ and $k'_{\tau,lam}$ becomes:

$$k'_\tau = \beta_A \cdot k_\tau \quad \text{for a monolithic glass panel} \quad (7.7)$$

$$k'_{\tau,lam} = \beta_A \cdot k_{\tau,lam} \quad \text{for a laminated glass panel} \quad (7.8)$$

D, D_{lam} flexural stiffness of monolithic and laminated glass [$\text{N}\cdot\text{mm}$]

E glass modulus of elasticity, $E = 70'000 \text{ [N/mm}^2\text{]}$

t_g glass thickness $t_g = 0.976 t_{nom}$ [Luible 2004]

t_{nom} nominal glass thickness given by the manufacturers

d distance between the glass sheet centre line axis in laminated glass [mm]

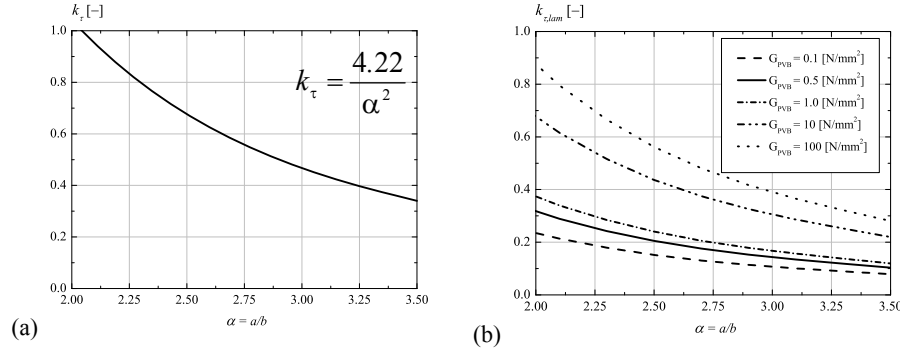


Figure 7.2 – Shear buckling coefficient for point supported glass panel (a) monolithic (b) laminated

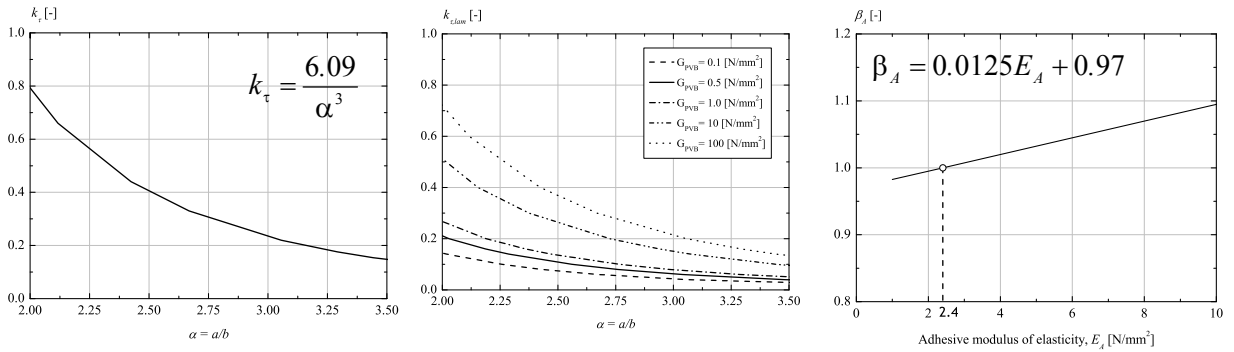


Figure 7.3 – Shear buckling coefficient for linear supported glass panel (a) monolithic (b) laminated (c) adhesive coefficient β_A

The shear reduction factor χ is a function of glass non-dimensional plate slenderness $\bar{\lambda}$. To determine their relation, the following procedure on models developed in Section 5.3 and 5.5 was conducted:

- The characteristic shear strength level was selected τ_{Rk} ($= \sigma_{Rk}$):
 $\tau_{Rk} = 10, 20, 30, 40, 50, 60, 70, 80, 90, 100, 110$ and 120 N/mm^2
- The elastic buckling analysis to determine the critical shear buckling force V_{cr} was solved
- The non-dimensional shear plate slenderness $\bar{\lambda}$ comparing the selected shear resistance τ_{Rk} and critical shear buckling stress τ_{cr} was determined using the Equation 7.2.
- By non linear buckling analysis the stress in the glass panel at each load step was calculated giving the characteristic shear buckling strength $V_{b,Rk}$
- Shear buckling reduction factor χ was determined by comparing the characteristic shear buckling resistance $V_{b,Rk}$ with characteristic shear resistance V_{Rk} utilizing Equation 7.1
- For corresponding level of shear strength τ_{Rk} the obtained results of shear reduction factor χ were related to non-dimensional shear plate slenderness $\bar{\lambda}$.

During the nonlinear buckling analysis of point supported glass panel the stresses in the glass panel are analysed. In the glass span, in addition to the normal stresses (caused by tensile and compressive diagonal) bending stresses occur due to buckling. At the compressive holes (supports 2 and 3), normal stresses (due to compressive diagonal) and bending stresses due to buckling, occur. On the other hand, near the tensile holes (supports 1 and 4), only normal stresses due to tensile diagonal take place (bending stress does not occur, because the tensile diagonal can not be buckle). Therefore, the stresses at the glass panel span and at the glass holes (both tensile and compressive) are accounted for and integrated in the shear buckling resistance of the point supported glass panel. Resistance at tensile glass hole is additionally verified by utilising stress concentration factor (§7.3.3.2).

During the nonlinear buckling analysis of linear supported glass panel, the maximum tensile stresses occur at glass panel span as well as near the setting blocks (supports). Therefore, the stresses at the glass panel span and at the edge near the supports are accounted for, and integrated in the shear buckling resistance of linear supported glass panel. Shear resistance of adhesive is separately determined in (§7.3.3.3).

To make the use of the relation between shear reduction factors χ and non-dimensional shear plate slenderness $\bar{\lambda}$ simple, design shear buckling curves are developed. The shear buckling curves in European Steel Design code [ENV 1991] are based on Ayrton-Perry format:

$$\left. \begin{aligned} \bar{\lambda} \leq \bar{\lambda}_o &\rightarrow \chi = 1 \\ \bar{\lambda} > \bar{\lambda}_o &\rightarrow \chi = \frac{1}{\phi + \sqrt{\phi^2 - \bar{\lambda}}} \end{aligned} \right\} \quad \phi = 0.5 \cdot (1 + \bar{\alpha}(\bar{\lambda} - \bar{\lambda}_o) + \bar{\lambda}) \quad (7.9)$$

Shear buckling curves for point supported and linear supported glass panel developed in this work are also based on the same format with the following coefficient $\bar{\lambda}_o$ and $\bar{\alpha}$:

Point supported glass panel

For values of the non-dimensional shear plate slenderness $\bar{\lambda}$ smaller than 3.75, the shear reduction factor χ should be taken as constant with the value of 0.04. For the value of $\bar{\lambda}$ greater than 3.75, χ should be determined using the Ayrton-Perry format with $\bar{\lambda}_o = 0.8$ and $\bar{\alpha} = 7$ (Fig. 7.4(a))

$$\left. \begin{aligned} \bar{\lambda} \leq 3.75 &\rightarrow \chi = 0.04 \\ \bar{\lambda} > 3.75 &\rightarrow \chi = \frac{1}{\phi + \sqrt{\phi^2 - \bar{\lambda}}} \end{aligned} \right\} \quad \phi = 4\bar{\lambda} - 2.3 \quad (7.10)$$

Linear supported glass panel

For $\bar{\lambda}$ smaller than 6.75, the shear reduction factor χ is constant with the value of 0.02. For $\bar{\lambda}$ greater than 6.75, χ should be determined if the coefficients are $\bar{\lambda}_o = 0.8$ and $\bar{\alpha} = 7$ (Fig. 7.4(b))

$$\left. \begin{aligned} \bar{\lambda} \leq 6.75 &\rightarrow \chi = 0.02 \\ \bar{\lambda} > 6.75 &\rightarrow \chi = \frac{1}{\phi + \sqrt{\phi^2 - \bar{\lambda}}} \end{aligned} \right\} \quad \phi = 4\bar{\lambda} - 2.3 \quad (7.11)$$

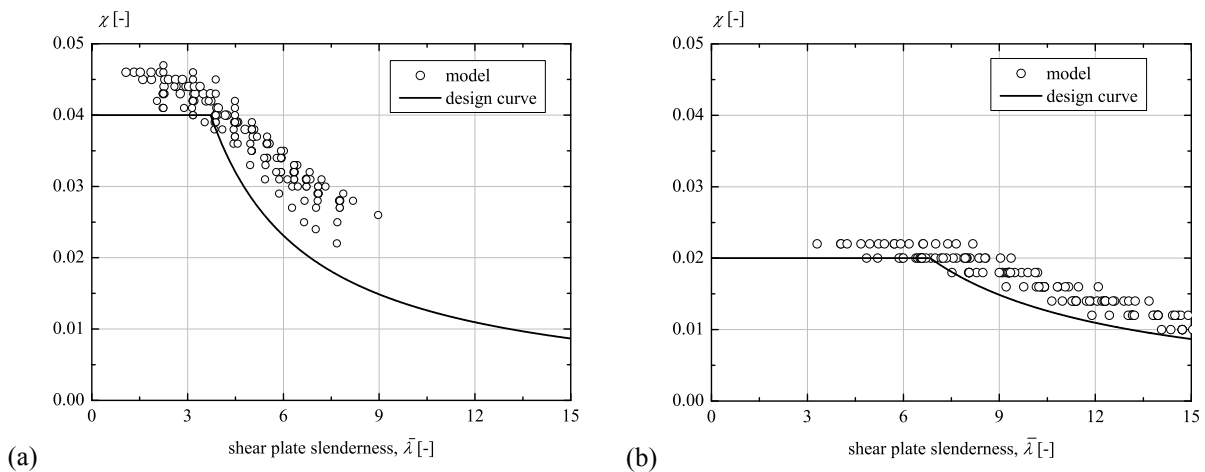


Figure 7.4 – Shear buckling reduction factor χ (a) point supported (b) linear supported glass panel

The point of $\chi - \bar{\lambda}$ relation is relatively small. Therefore, parametric study should be extended: more values for investigated parameters and new relevant parameters should be examined. Furthermore, a statistical method should be utilised to find good curve fitting. Consequently, curves of shear buckling reduction factors presented in Figure 7.4 can be used only for preliminary design. Further research is still required for the creation of a definitive design method.

7.3 DESIGN PROPOSAL

7.3.1 Determination of loads and actions

The actions on the fully transparent glass pavilion and the combination of actions are determined in accordance with [EN 1991] and [prEN 13474-1].

7.3.1.1 Permanent loads

The self-weight of the roof and other structural and non structural elements are classified as permanent loads and should be taken into account as a single action. Characteristic values of densities of materials should be specified. Mean values should be used as characteristic values [EN 1991]. For laminated glass, the self-weight should be calculated based on the nominal thickness and the density.

7.3.1.2 Snow load

Snow loads are defined according to [EN 1991] and classified as static actions. It acts vertically and refers to a horizontal projection of the roof (Fig. 7.5(a)). Characteristic snow load on a roof s is the product of the characteristic snow load on the ground s_k and appropriate coefficients:

$$s = \mu_i C_e C_t s_k \quad (7.12)$$

μ_i	roof snow load shape coefficient
s_k	characteristic value of snow load on the ground at the relevant site [kN/m ²]
C_e	exposure coefficient
C_t	thermal coefficient

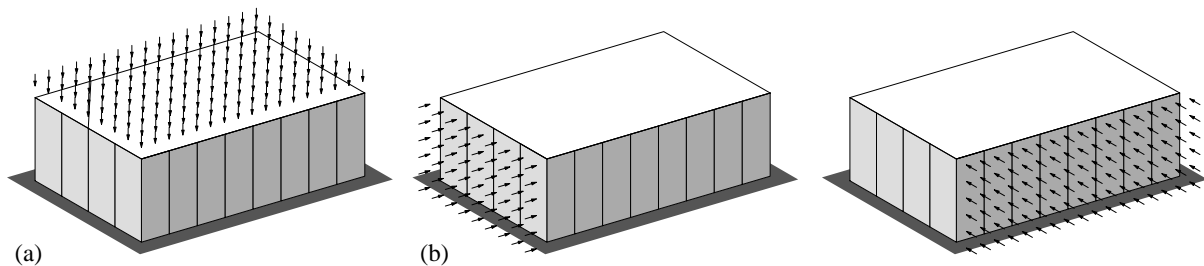


Figure 7.5 – Loads on fully transparent pavilion (a) snow load and self weight of the roof (b) wind load

7.3.1.3 Wind loads

Wind loads are defined according to the standard [EN 1991] and classified as a uniformly distributed pressure perpendicular to the surface of the glass panel (Fig. 7.5(b)). The wind pressure w_e acting on the outer surface of a structure is defined as:

$$w_e = c_{pe} q_k(z) \quad (7.13)$$

The wind pressure w_i acting on the inner surface of the structure is:

$$w_i = c_{pi} q_k(z) \quad (7.14)$$

The total pressure w_t acting on a structure is:

$$w_t = w_e - w_i \quad (7.15)$$

$q_k(z)$	the characteristic value of the wind load
c_{pe}	the aerodynamic factor for external pressure
c_{pi}	the aerodynamic factor for internal pressure

7.3.1.4 Other loads

Other loads that can act on the structure of fully transparent pavilions are defined in the standards [EN 1991] and [prEN 13474-1]:

- The imposed load from human impacts, furniture, movable objects, vehicle etc. They are modelled by distributed loads, line loads or concentrated loads or a combination of these loads.
- Maintenance load: 0.4 kN/m² or 1kN point load
- Thermal actions from unequal expansion between the glass and the structure if the movement is prevented or from internal temperature differentials within the glass panel.
- Accidental loads from disasters such as explosion, fire or earthquake.
- Internal loads from insulating glass units as the difference between the pressure in the cavity of the insulating glass unit and the pressure of the surrounding air due to difference of the altitude as well as climate actions from the variation of the temperature (summer and winter conditions) and the meteorological pressure between production and use.

7.3.1.5 Loads combination

For each load case, design value E_d for the effects of actions should be determined from combination rules involving design of actions according to the standard [EN 1991]. For combination of action for *the* ultimate limit state the design value is:

$$E_d = \sum \gamma_{G,j} G_{k,j} + \gamma_{Q,1} Q_{k,1} + \sum \gamma_{Q,i} \psi_{0,i} Q_{k,i} \quad (7.16)$$

The combinations of actions for serviceability limit states are defined as:

$$E_d = \sum G_{k,j} + Q_{k,1} + \sum \psi_{0,i} Q_{k,i} \quad (7.17)$$

The partial safety factor γ and the combination factors ψ for permanent and variable actions are given in the standard [EN 1991] for the ultimate limit state (ULS) and for serviceability (SLS)

7.3.2 Structural analyses

For linear supported glass panel with regular shape subjected to perpendicular distributed load the standard [prEN 13474-2] gives simple formulas and charts to determine the effective stress for the most unfavourable action combination and glass panel deflection to compare them with tolerable stresses and deflections. Such a simple structural analysis method for glass panels subjected to in-plane shear forces does not exist. Therefore, calculations using an appropriate numerical model involving all relevant variables and predicting the structural behaviour with an acceptable level of accuracy should be carried out.

The construction of a numerical model and the solution procedure should follow the method described in Section 5.3 for point supported and Section 5.5 for linear support glass panels. The boundary conditions applied to the model must represent those intended in the real structure. The characteristic values of loads and the load combination are determined as described in §7.3.1 in accordance with *the* standard [ENV 1991-1] an [prEN13474-1]. From the most unfavourable load combination, the following results of structural calculation (nonlinear buckling analysis) should be obtained:

- maximal glass panel out-of-plane deflection w_{max} ,
- in-plane displacement u ,
- maximal principal tensile stresses in the glass panel $\sigma_{I,max}$,
- support reaction forces R ,
- maximal shear stresses in the adhesive τ_A for linear supported model.

7.3.3 Determination of strength

7.3.3.1 Shear buckling strength

Strength property of glass products is presented by a characteristic value. Characteristic shear strength of the glass panel (buckling is not considered) is:

$$V_{Rk} = \tau_{Rk} \cdot b \cdot t \quad (7.18)$$

τ_{Rk}	characteristic shear strength of the glass panel [N/mm ²]
b	glass panel width [mm]
t	glass panel thickness ($t = 2t_g$) [mm]
t_g	glass thickness

Consequently, the design shear strength of the glass panel is:

$$V_{Rd} = \frac{V_{Rk}}{\gamma_M} \quad (7.19)$$

γ_M	shear resistance factor [$\gamma_M = 1.4$ proposed by Wellerhoff 2006]
------------	---

If shear buckling is considered, the design strength becomes:

$$V_{b,Rd} = \chi V_{Rd} \quad (7.20)$$

χ	shear buckling reduction factor developed in Section 7.2 for point supported and linear supported glass panel
--------	---

7.3.3.2 Point support connection (strength of glass hole under tensile)

The stress concentration factor K_t is the ratio of the peak stress to the nominal stress as a function of the ratio $(d/2c) \cdot \sin\beta$ (Fig. 7.6 and Fig. 7.7)

$$K_t = \frac{\sigma_{max}}{\sigma_{nom}} \quad (7.21)$$

σ_{max}	maximum stress at the edge of the hole perpendicular to the reaction force R
σ_{nom}	nominal stress

$$\sigma_{nom} = \frac{R}{A_{net}} \quad (7.22)$$

A_{net}	net area
-----------	----------

$$A_{net} = 2 \left(\frac{c}{\sin\beta} - \frac{d}{2} \right) \cdot \sum t_g = \left(\frac{2c-d}{\sin\beta} \right) \cdot \sum t_g \quad (7.23)$$

c	distance between glass hole and glass edge
d	diameter of the hole
β	angle at which reaction force R acts on the hole

$$\beta = \arctg \frac{b-2c}{a-2c} \tag{7.24}$$

a glass panel height
b glass panel width

From the Equation 7.2 the reaction force *R* is:

$$R = \frac{\sigma_{max} A_{netto}}{K_t} \tag{7.25}$$

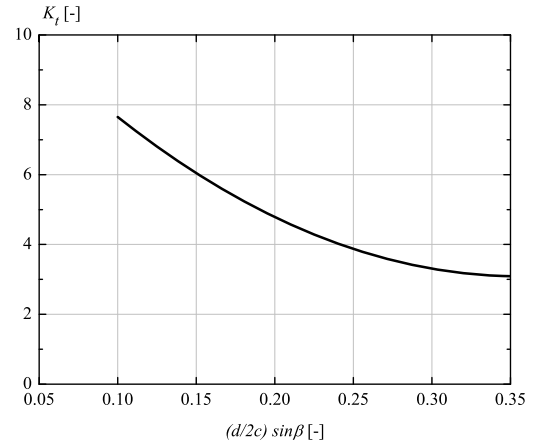
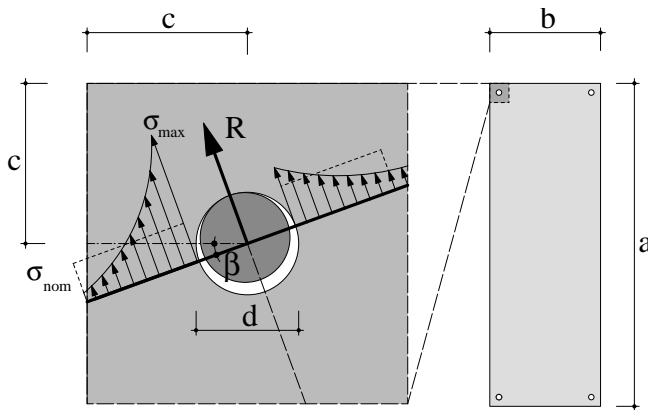


Figure 7.6 – Stress concentration at glass hole under tensile

Figure 7.7 – Stress concentration factor *K_t*

Changing the σ_{max} with the admissible stress at the edge of glass hole σ_{adm} (the fracture strength found in experiments, divided by a global safety factor that accounts for all uncertainties and variants associated with action, resistance and modelling), the design strength becomes:

$$R_{Rd} = \frac{\sigma_{adm} A_{netto}}{K_t} \tag{7.26}$$

Admissible stress at the edge of glass hole σ_{adm} is given by [Laufs 2002] as 33 N/mm² for heat-strengthened glass and 47 N/mm² for tempered glass.

7.3.3.3 Linear support connection (adhesive strength)

When glass panel is subjected to in-plane shear force *V*, in the adhesive interaction of longitudinal shear *R_l* and transversal shear *R_t*, shear stresses take place (Fig 7.8.)

Assuming uniform shear distribution in the bonded area between the adhesive and the glass/substructure, the longitudinal shear is:

$$R_l = 2\tau \cdot b \cdot c_A \tag{7.27}$$

and the maximal transversal shear (at the extreme of the adhesive) is:

$$R_t = \tau \cdot b \cdot c_A \tag{7.28}$$

c_A adhesive width

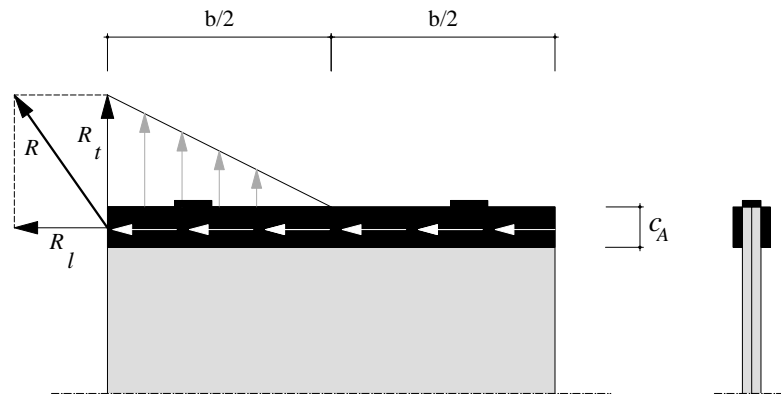


Figure 7.8 – Transversal and longitudinal shear in the adhesive

The resultant shear R is a vector sum of transversal and longitudinal shear:

$$R = \sqrt{R_l^2 + R_t^2} = \tau \cdot b \cdot c_A \cdot \sqrt{5} \quad (7.29)$$

In-plane shear force V is assumed to be caused by wind which is short-term load. Adhesive is not subjected to long-term stresses, because the self weight of the roof, and the glass weight itself are taken by setting blocks. The admissible stress and strain of the adhesive are given by the producer. For the structural silicon sealant DC993 utilised in this research the admissible shear stress under short-term loading τ_{adm}^{short} is [Dow Coning 2005]:

$$\tau_{adm}^{short} = 0.070 \text{ [N/mm}^2\text{]}$$

When introducing this value in the Equation 7.26 the design strength adhesive connection becomes:

$$R_{Rd} = (\tau_{adm}^{short}) \cdot b \cdot c_A \cdot \sqrt{5} \quad (7.30)$$

7.3.4 Verification

7.3.4.1 Ultimate limit state

Shear buckling verification

The design value of the shear force V_{Ed} shall satisfy:

$$V_{Ed} \leq V_{b,Rd} = \chi V_{Rd} \quad (7.31)$$

Point supported connection verification

The design value of the reaction force at tensile support R_{Ed} shall satisfy:

$$R_{Ed} \leq R_{Rd} = \frac{\sigma_{adm} A_{netto}}{K_t} \quad (7.32)$$

Linear support connection ULS verification

The design value of the resultant force in the adhesive R_{Ed} shall satisfy:

$$R_{Ed} \leq R_{Rd} = \sqrt{5} b h_A \tau_{adm}^{short} \quad (7.33)$$

7.3.5 Serviceability limit state

Out-of-plane deflection

The maximum glass panel out-of-plane deflection w_{max} calculated for the most unfavourable load conditions should not exceed the allowable deflection w_d

$$w_{max} \leq w_d = \frac{a}{c_w} \quad (7.34)$$

- a glass panel height
 c_w value specified for each project and agreed to by the client or specified by the National Annex in [ENV 1990]

In-plane displacement

The glass panel in-plane displacement u calculated for the most unfavourable load conditions should not exceed the allowable displacement u_d

$$u \leq u_d = \frac{a}{c_u} \quad (7.35)$$

- c_u value specified for each project and agreed to by the client or specified by the National Annex in [ENV 1990]

7.4 PRACTICAL RECOMMENDATION

7.4.1 Glass panel

Glass panel

When using the glass panel as a structural element in fully transparent pavilions, safety laminated glass with a minimum of the two sheets of glass must be utilized. Due to high stresses at load introduction places annealed glass is avoided and fully tempered or heat-strengthened glass must be used. The additional advantage of laminated glass is its residual resistance, where glass panel after the breakage of single or both glass sheets is still able to carry the load. Therefore, heat-strengthened glass should be utilised when ultimate resistance permits it, because it breaks in larger pieces and has a consequently higher residual resistance than the fully tempered glass.

The height of the glass panel is the same as the height of the building storey, while the width of the glass panel can vary. In this research the analysed height to width ratio $\alpha=a/b$ is in a range between 2 to 3.5 (the glass panel was keep constant $a=3500\text{mm}$, while glass panel width b varied from 1000mm and 1800mm wide. Consequently, the recommendations proposed here are valid only for this range.

In this application PVB is used as interlayer in the laminated glass (minimum thickness of 1.52mm). Other interlayer, as SentryGlas[®]Plus [DuPont 2003] [Pilkington 2005], can also be used.

Glass hole and glass edge

At the glass hole (in point supported glass panel) and glass edge (in linear supported glass panel) large stress concentration occurs due to load introduction. Therefore, special attention on the glass hole and glass edge should be paid: they must be polished and chamfered (Fig. 7.9). The glass holes are drilled before the tempering process and lamination of the glass sheets. Special attention should be paid on the precision of hole (position and diameter) to avoid intolerance once the glass layers are laminated. For better load transfer between the connection system and the glass, the cylindrical holes are preferred. The hole diameter and distance of the hole from the edge have a high influence on glass panel resistance when subjected to in-plane force. Minimum distance of the hole to the edge c is 100mm, and the minimum hole diameter d is 40mm. By increasing the ratio d/c , the stress concentration at glass hole subjected to tensile force decreases. By increasing the hole diameter d , the stress concentration at glass hole edge subjected to compressive force decreases. Therefore, the hole should be as large as possible, and situated as far as possible from the edge.

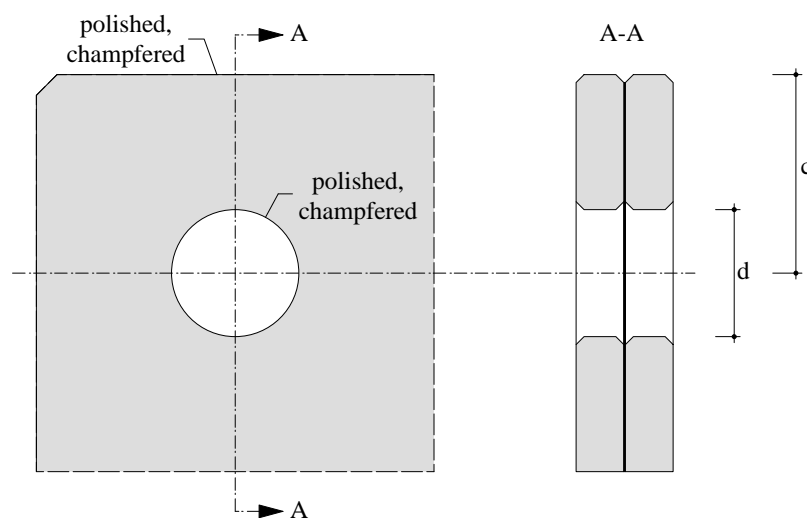


Figure 7.9 – Polished and chamfered glass hole and edge

7.4.2 Point supported connection devices

Connection devices

The two component mortar Hilti HIT HY70 [Hilti 2003] is proposed to fill the gap between the steel bolts and the glass, with the function of transferring the in-plane load (Fig.7.10). The injection should be done by using a special tool produced for this purpose. The load can be applied 24 hours after the injection, leaving the mortar enough time to dry and reach its maximum resistance.

It is recommended to use high strength bolts (8.8 or 10.9) with a minimum M20 diameter. Being in contact with the environment, stainless steel bolt is obligatory. The bolts must be accessible once the glass panel is in place, so the system can be easily removed and replaced in case the breakage of the glass panel occurs. It is advantageous if the bolt in the glass hole is directly connected to the glass by mortar avoiding an intermediate pin between the mortars and bolts. On one hand, eventual replacement of the glass panel gets harder, but the glass behaviour is improved avoiding the in-plane displacement due to fabrication tolerances between the pin and the bolt.

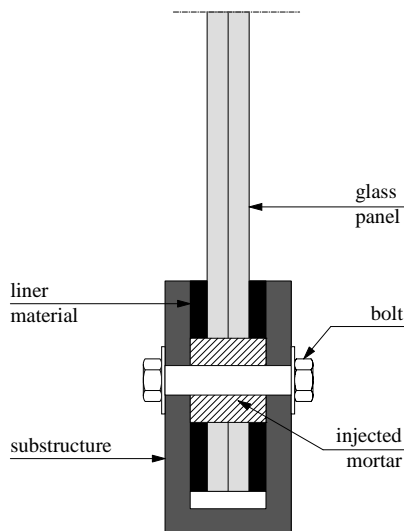


Figure 7.10 – Connection detail

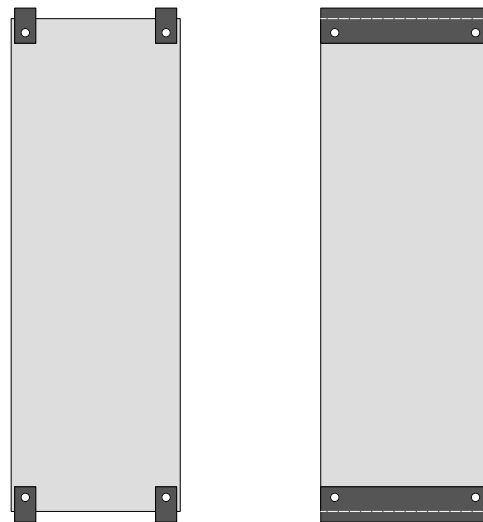


Figure 7.11 – Substructure (a) localised (b) edge long

Substructure

A substructure is the element connecting the glass panel and the roof/foundation. It must be made of stainless steel to resist the external environmental condition. The substructure can be an LNP profile, a UNP profile as well as a welded profile or bend sheets. The substructure can be localised near the connection devices (Fig. 7.11(a)) or can be placed along entire shortest edges of a glass panel (Fig. 7.11(b)). In such way, the out-of-plane deflections of the shortest edges are constrained and better behaviour (smaller deflection) can be expected. Between the glass panel and the substructure, a liner material (neoprene or POM) should be placed to avoid the direct contact between the glass and the substructure.

Execution technique

The assemblage of connection devices and the injection of the mortar are to be done by professionals in the workshop. In some cases, the injection of the mortar can be done directly on construction site, once the glass panel is positioned. The injection should dry for minimum 24 hours before the load is introduced. The substructure can be installed to the glass panel in the workshop or at construction site, depending on what is more convenient for the specified project. Installation of the glass panel on the construction site should be done by professionals. The connection devices should be easily accessible in case of replacement of glass panel due to a possible breakage.

7.4.3 Linear supported connection devices

Adhesive

The adhesive accepted by [EOTA 1999] for glazing is structural silicon and therefore only applicable for this kind of linear support connections. Structural silicon Dow Corning DC993 [Dow Corning 2003] and SG500 produced by SIKA are widely utilized. The recommendation given by the producers regarding surface preparation, cleaning procedure and adhesive application, should be followed. The gluing process must be done in the shop by professionals. The minimum thickness of the adhesive is 6 mm, and the recommended width to thickness ratios are provided by manufacturers. The width of the adhesive used for the present study is 40mm.

Setting block

At the contact surface of glass edge and setting block, high stresses occur. Therefore, high attention should be paid to the construction of the setting block. Instead of traditional material used for setting block as PVC, aluminium or wooden, the mortar is recommended in order to avoid the tolerance problem in laminated glass. The mortar HIT HY 70 produced by Hilti can be used. At each short edge (top and bottom) two setting blocks should be placed. The setting blocks are positioned at $b/5$ from the edges. The setting block width is 100 mm.

Substructure

Structural silicon sealant is not compatible with all metal surfaces and should be avoided in corrosive metals. In glazing, the adhesive is used mostly to glue glass with aluminium or stainless steel. In structural glass application, due to the high loads that the substructure has to transfer, the utilisation of a substructure of stainless steel is recommended (due to higher strength and stiffness than aluminium). In such a way, the good adherence between the substructure and the adhesive can be reached, as well as the adequate load transfer through the substructure avoiding premature failure of the substructure or high (plastic) deformation which can influence the glass panel behaviour. Stainless steel surface should be rough to permit better adherence with the adhesive.

Execution technique

The glass surface and the substructure surface to which the adhesive is applied should be first cleaned with the product recommended by the adhesive producer. Then, the spacer is attached to the glass panel, then the adhesive is applied and finally the substructure is glued. The injection of mortar as setting block should be done minimum 24 hours after the gluing. Due to required precision, the gluing process should be done by professionals in the workshop. The glass panel can be subjected to load only 7 days after the gluing process to assure that the adhesive has reached its final strength. The installation of the glass panel on the construction site should be done with care by professionals. The connection between the substructure and the roof/foundation should be easily accessible in case of glass breakage.

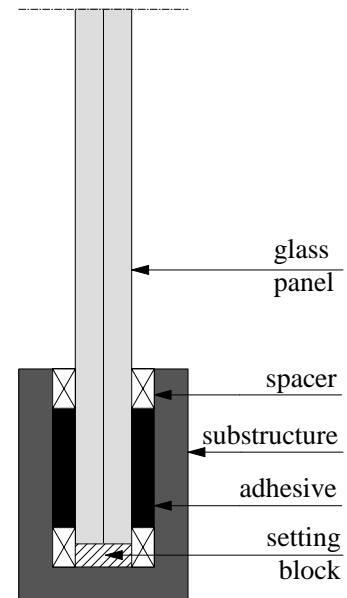


Figure 7.12 – connection detail

7.5 SUMMARY AND CONCLUSIONS

Chapter 7 proposes the simplified method for the preliminary design of point supported and linear supported glass panels subjected to in-plane shear force and practical recommendations for use of glass panel as structural element in fully transparent pavilions. The following conclusions are drawn:

Shear buckling resistance

- From experimental and numerical results the formulas and graphs are developed to determine the shear buckling resistance of point-supported and linear supported glass panels.
- Shear buckling reduction factor χ as a function of non-dimensional shear plate slenderness is defined by using the Ayrton-Perry Format.
- Stresses at the glass panel span and at the glass holes (both tensile and compressive) are accounted for and integrated in the shear buckling resistance of point supported glass panel.
- The developed simplified method can be utilised for the preliminary design.

Design proposal

- Step by step design method for a glass panel under in-plane shear loading is described: determination of loads and actions, structural analyses and verification.
- The ultimate resistance of shear buckling of glass panel can be verified by using the proposed design method.
- The ultimate resistance of the glass hole in tensile (point support connection) can be verified by using the stress concentration factor.
- Out-of-plane deflection and in-plane displacement serviceability limit should be verified by comparing it with tolerable values.

Practical recommendation

Due to the highest stresses occurring at the glass hole and the glass edge, those must be chamfered and polished. The connection devices should be arranged, the mortar injected and the adhesive glued by the professionals in a workshop with care. The substructure should be made of stainless steel to resist all environmental conditions. The connection between the substructure and the roof/foundation should be easily accessible in case of replacement of broken glass panel.

8 CONCLUSION AND FUTURE WORK

This Chapter summarises the results obtained in the previous chapters. The summary and principal results related to the objectives defined in the beginning of the thesis are given. Finally, suggestions for future work are proposed.

8.1 SUMMARY AND RESULTS RELATED TO THE OBJECTIVES

The main contributions of the thesis can be found in experimental investigation, numerical modelling and parametric study of shear buckling phenomena of developed glass panel concepts. These results have been used to develop a specific design method for glass panel under in-plane shear force. Moreover, this study leads to some practical recommendations for using glass panel as a structural element in fully transparent pavilions.

Objective 1: Evaluation of current knowledge and trends

Few researches about both plate buckling and shear buckling of the glass panel have recently been carried out dealing with simplest cases of circumferential (four sides) boundary conditions. No research on shear buckling behaviour of point supported glass panel or glass panel supported only on two sides exists. The shear buckling behaviour of such systems is still unknown.

The latest trends in contemporary architecture are increase of the building clearance and transparency by using glass as primary load carrying element. Fully transparent pavilions, as a single story building free of any steel or concrete frame, utilise glass panels as unique vertical structural elements. Few fully transparent pavilions have been built recently, but due to lack of knowledge in structural use of glass, the constructions were accompanied by expensive, full-scale prototype laboratory testing and time consuming numerical modelling.

Objective 2: Development of structural concepts

Based on the literature review on current structural glass knowledge and modern architectural trends, two structural concepts of glass panels with connection devices, potentially used in fully transparent pavilions, were developed. In the **point supported concept** the glass panel is attached to the substructure by bolted connections at the corners, while in the **linear supported concept** the glass panel is glued to the substructure on two shorter sides. The local behaviour of connection devices and global behaviour of glass panels should be analysed.

Objective 3.a: Analysis of structural concepts (experimental investigation)

The **point supported connection tests** was carried out to study the glass/substructure bolted connection behaviour and its influence on surrounding glass plate. The force eccentricity significantly decreases the specimen resistance and stiffness. The rigid connections offer higher stiffness with smaller deformation than the pinned connection. The bolt diameter influences specimen stiffness and resistance only in eccentric test but not in the axial test. Typical failure modes are tension in net section (specimen subjected to tensile force) and splitting tension (specimen under compressive force). Within bolted connections, the axial rigid connection proved itself to be the most suitable type.

Three **point supported panel tests** investigate the behaviour of full size glass panel joined to the substructure by means of an axial rigid connection and subjected to the in-plane shear force and to the interaction of in-plane shear force with out-of-plane distributed load and in-plane compression. In-plane glass panel stiffness does not depend on load cases. In-plane normal compressive force significantly decreases the shear buckling resistance. This is not the case for out-of-plane distributed

load. Glass panels fail due to splitting tension caused by stress concentration at the glass hole of compressive support where the higher stresses are measured. Specimens show relatively small in-plane displacements and out-of plane deflection.

Linear support connection tests studied the adhesive shear behaviour and utilization of the mortar as setting block. Three-side connection shows higher stiffness and resistance than two-side one under transversal shear, while under longitudinal shear the same stiffness with higher resistance is observed. Although showing higher resistance, two-side connection was chosen for further investigation due to its simpler application and better stress distribution. Mortar in compression demonstrated high resistance, and therefore suitable for load introduction.

Three **linear support panel tests** investigated the global behaviour of full size glass panel linearly supported by shortest edges, subjected to in-plane shear force only and to interaction of in-plane shear force with out-of-plane distributed load and in-plane compression. The adhesive significantly influences the glass panel deformation: high in-plane displacement and high out-of-plane deflection occur. Adhesive yielding influences the stress distribution in the glass panel. In-plane normal compressive force and out-of-plane distributed load significantly decreases the shear buckling resistance of the glass panel. Glass panels fail due to splitting tension caused by stress concentration at compressive setting blocks.

Objective 3.b: Analysis of structural concepts (numerical modelling)

By means of **point support connection model** the local behaviour of the axial rigid connection on the glass hole was studied. When tension force is applied, the maximal principal tensile stresses occur at the glass hole, perpendicular to the force direction. The stress concentration depends of d/c ratio. When compressive force is applied, the maximal principal tensile stresses occur on the glass hole in the force direction, in the contact area of connection devices and glass. The stress concentration depends on the hole diameter. The stress concentration has only local influence on small area around the hole; the stresses reach their nominal values at a certain distance from the hole.

The **point supported panel model** was developed to study the shear buckling behaviour of point supported glass panel. Elastic buckling analyses were used for determining the critical shear buckling force, the shear buckling coefficient and the shear buckling mode shapes. Nonlinear buckling analyses were used for analysing the glass panel global behaviour (deformation, stress distribution, reactions). Glass panel demonstrates post-buckling behaviour induced by a membrane effect. The out-of-plane deflection inflects at critical shear buckling force. The in-plane displacement is linear for the value smaller than critical shear buckling force when it deviates due to shear buckling, demonstrating nonlinear behaviour. Maximum tensile stresses occur due to stress concentration in glass hole at compressive supports. The first buckling mode shape has the most unfavourable influence on glass panel behaviour. The numerical model results are in good agreement with experimental results.

In order to define the adhesive material law, the adhesive behaviour under shear force was studied on developed **linear supported connection model**. The idealised elasto-plastic adhesive material model is in good agreement with the test results. Stress distribution in the adhesive bonding area is nonlinear (parabolic), with peak stresses at the overlap ends. The adhesive deformation highly influences the glass panel behaviour.

The shear buckling behaviour of linear supported glass panel was studied by means of **linear supported panel model**. Elastic buckling analyses were used for determining the critical shear buckling force, the shear buckling coefficient and the shear buckling mode shapes. Non linear buckling analyses were used for analysing the glass panel global behaviour (deformation, stress distribution, reactions). Although the tensile diagonal created by soft adhesive is not capable of keeping the buckle caused by compressive diagonal straight, it is strong enough to create the membrane effect in the panel and to give the post-buckling reserve to the system. When the critical shear buckling force occurs before the adhesive yielding, two inflection points in out-of-plane

deflection take place (at critical shear buckling point and at the yielding adhesive point). On the other hand, when adhesive yields before the glass panel reaches the critical shear buckling force, no inflection point occurs in glass panel out-of-plane deflection. The adhesive introduces high ductility in the glass panel. The first buckling mode shape has the most unfavourable influence on glass panel behaviour. The maximum tensile stresses occur due to the stress concentration at compressive setting block.

Objective 3.c: Analysis of structural concepts (parametric study)

The influence of glass panel geometrical/material parameters on shear buckling behaviour of **point supported panel** was investigated. The values of critical shear buckling force, the maximal out-of-plane deformation, the in-plane displacement, the reaction forces and the maximal principal tensile stresses were analysed. The glass panel thickness shows the highest influence; the glass panel width and PVB shear modulus have from small to moderate influence; while the initial imperfection has a negligible (slight) influence on global glass panel behaviour.

The influence of glass panel geometrical/material and adhesive geometrical /material parameters on the shear buckling behaviour of **linear supported panel** was investigated. Again, the values of critical shear buckling force, the maximal out-of-plane deformation, the in-plane displacement, the reaction forces and the maximal principal tensile stresses were analysed. The glass panel thickness shows the highest influence, the glass panel width has a moderate influence, the PVB shear modulus and adhesive stiffness have from small to moderate influence, while the adhesive thickness has negligible (slight) influence on global glass panel behaviour.

Objective 4: Providing design proposals and recommendations

A specific simple method for preliminary design of glass panel subjected to in-plane shear force is proposed. Formulas, graphs for shear buckling coefficient and curves of shear buckling reduction factors are developed in order to determine the shear buckling resistance of the glass panel. They evaluate the stress concentration at the supports induced by load introduction, together with the stresses in the glass span induced by buckling. Further research is still required for the creation of a definitive design method. Therefore, finite element modelling is necessary for detailed design.

This study leads to some recommendations for practical use of glass panel in fully-transparent pavilions as primary structural element. Necessary requirements for glass panel, connection devices, substructure and execution techniques are pointed out.

8.2 MAIN CONCLUSIONS

The main objective of this thesis was to understand the shear buckling behaviour of point supported and linear supported glass panel subjected to in-plane shear force, as well as to investigate their potential use as a structural element in fully transparent pavilions. For this reason, structural concepts were developed and analysed. Moreover, a specific design method was proposed. The main conclusions are as follows:

Point supported concept

The axial rigid connection is the most suitable connection type for in-plane load transfer between glass and substructure. Connection devices have high influence on local stress distribution around the glass hole (stress concentration). The stress concentration is decreased by increasing the d/c ratio (tension support) or the hole diameter (compression support). Consequently, the residual stresses on the surface of the glass hole (introduced by the tempering process) have significant influence on glass panel resistance.

Glass panel demonstrates post-buckling behaviour induced by membrane effect caused by crossing of compression and tension diagonal. Glass panel shows small in-plane displacement and small out-of-plane deflection. Shear buckling induces limited ductility to the system. The glass panel failed due to splitting tension along the compression diagonal. The crack appeared where the maximal tensile stresses occurred - at glass hole near the compressive supports.

Glass panel thickness strongly influences its global behaviour: by increasing the thickness the global deformation decreases and the resistance increases. Glass panel width and PVB shear modulus have small to moderate influence.

Point supported glass panel has a high potential as a load bearing structural member for in-plane shear transfer.

Linear supported concept

Two-side connection is chosen as the most suitable connection type for in-plane load transfer between glass and substructure. The idealised elasto-plastic material for structural silicon adhesive is in good agreement with the real behaviour. High adhesive deformability influences significantly the global deformation and stresses distribution in the glass panel. Mortar shows high compressive resistance, and it is therefore suitable for setting block application.

Linear supported glass panel shows large deformation and small resistance. Although the tensile diagonal created by the adhesive is not capable of keeping straight the buckle caused by compressive diagonal, the membrane effect on the glass panel takes place. This process gives the system a post-buckling reserve. The shear buckling behaviour changes considerably if the adhesive yielding occurs before or after the glass panel reaches its critical shear buckling force. The adhesive yielding introduces high ductility in the glass panel. The glass panel failed due to splitting tension along the compressive diagonal. The crack appeared where the maximal tensile stresses occur - at setting block compressive supports. The residual stresses in the glass panel strongly influence the glass panel resistance. Glass panel thickness shows a significant influence on its global behaviour. By increasing the thickness the global deformation decreases and the resistance increases. Glass panel width shows moderate influence, the PVB shear modulus and the adhesive stiffness have from small to moderate influence, while the influence of adhesive thickness can be neglected.

Due to large deformation and small resistance, linear supported glass panel has a limited potential as a load bearing structure member for in-plane shear transfer.

Design proposal and practical recommendations

The proposed design method for determining the shear buckling resistance can be used only for preliminary designs. It takes into account the stress concentration at the supports and the stresses in glass span induced by buckling. By following the proposed recommendations, the glass panel can be used as a structural element in fully transparent pavilions.

Point supported vs. linear supported concepts

Comparing the results from experimental, analytical and parametrical investigation, it is visible that point supported concept demonstrated higher stiffness, higher resistance and smallest deformation than the linear supported concept. As a conclusion, point supported concept is more suitable for application in fully-transparent pavilions than the linear supported concept.

8.3 FUTURE WORK

Due to complexity of mechanical glass behaviour and variety of glass/substructure connections, this thesis could not have analysed all the typologies and issues related to the shear buckling behaviour. However, in order to improve the above presented results, some suggestions for future work can be outlined as follows:

Splitting tension

High compressive stresses occur where the force is introduced, at compressive support in the glass hole (point supported concept) and at the edge in contact with setting blocks (linear support concept). Due to Poisson's ratio, perpendicular to this compressive field, tensile stresses originate trying to split the glass (splitting tension). This phenomenon is the main cause of glass panel failure. Related to this process, many researches were conducted in the past in concrete and rock mechanics fields, and a standardised Brazilian test was developed to determine the tensile resistance of both concrete and rock specimens. As far as glass is concerned, this problem has not been investigated yet. Since the standardised two rings test defines the tensile resistance and residual stresses in the glass span, it would be possible to determine the tensile resistance and residual stresses at glass panel edges and holes by developing a standardised splitting tension test.

Friction connections

In the above presented results, the stress concentration occurs at glass hole due to contact of connection devices and glass which causes glass failure. The stress concentration can be decreased by changing the force path between connection devices and glass and by avoiding the direct contact. The load transfer by friction between the connection devices and glass panel, introduced by pre-stressing the bolts, can be a solution. Due to creep, visco-elastic material should be avoided in friction connection, and therefore PVB interlayer and linear material between glass panel and connection devices should be locally replaced by, for instance, aluminium. In this way, a better shear buckling behaviour of the glass panel and a higher resistance at the connection points can be expected.

Adhesive

As far as the developed linear supported glass panel is concerned, the adhesive stiffness has a strong influence on shear buckling behaviour. Additionally, since structural silicon sealant can not support a permanent load, the setting block introduces high compressive stresses, which causes glass panel failure. By using a stiffer adhesive capable of carrying the permanent load, the glass panel deformation can be reduced as well as the necessity to have a setting block, avoiding the stress concentration at the edges. Nowadays, new adhesive with improved resistance, time durability and temperature stability are under development and many researches deal with their use and application in the glazing. Linear supported glass panel behaviour with such improved adhesive can be investigated in order to check whether high deformation and stress concentration may be avoided this way, and, moreover, the shear buckling behaviour can be improved.

Interlayer

Being a visco-elastic material whose stiffness depends of temperature and load duration, PVB interlayer has a significant influence on glass panel response. New interlayer materials with improved performance have recently been developed and their use in the lamination process has also spread to structural glass application. For example, SentryGlas[®]Plus [DuPont 2003] has a higher stiffness than PVB and using this interlayer the shear buckling behaviour of the glass panel can be improved. Indeed, due to the fact that two glass layers connected with stiff interlayer can act as a single element, the global deformation decreases while the resistance increases.

Load cases

The present work gives a detailed description of the behaviour of a glass panel subjected to an in-plane shear force. On the other hand, only a rough idea about shear buckling behaviour when in-plane shear force interacts with in-plane compressive force and out-of-plane distributed load could be given. Further research can be done in order to study deeper the influence of different load combination.

REFERENCES

- [Adams et al. 1979] ADAMS R.D., COPPENDALE J. *The Stress-Strain Behaviour of Axially-Loaded Butt Joints*, *Journal Adhesion*, Vol.10, No. 1, pp 49-62, 1979.
- [Allen 1969] ALLEN, H.G. *Analyses and design of structural sandwich panels*. Pergamon, Oxford, UK, Ch.8, 1969.
- [ANSYS 2005] ANSYS Release 10. SAS IP, Inc, 2005.
- [Belis et al. 2003] BELIS, J., VAN IMPE, R., LAGAE, G., VANLAERE, W. *Enhancement of the buckling strength of glass beams by means of lateral restraints*. *Structural Engineering and Mechanics*, Vol. 15, No. 5, pp. 495-511, 2003.
- [Bennison et al. 2002] BENNISON, S. J., SMITH, C. A., VAN DUSER, A., JAGOTA, A. *Structural Performance of Laminated Glass Made with a "Stiff" Interlayer*. In: *Glass in Buildings*, ASTM STP 1434, V. Block (editor), 2002.
- [Bernard et al. 2002] BERNARD, F., GY, R., DAUDEVILLE, L. *Finite Element Computation of Residual Stresses Near Holes in Tempered Glass Plates*. *Glass Technology*, Vol. 43C, 2002.
- [Blandini 2005] BLANDINI, L. *Structural use of adhesives in Glass Shells*. Ph.D. thesis, D 93 University of Stuttgart, Verlag Grauer, Stuttgart, 2005.
- [Bryan 1891] BRYAN, G. H. *On the Stability of a Plane Plate under Thrusts in its own Plane with Application on the "Buckling" of the Sides of a Ship*. *Proc. London Math. Soc.*, London, pp. 54, 1891.
- [Brush et. al 1975] BRUSH, D.O., ALMORTH O.B. *Buckling of bars, plates and shells*, McGraw-Hill, 1975.
- [Bruhns 2001] BRUHNS, O.T. *Advanced Mechanics of solids*, Institute of Mechanics, Ruhr-University Bochum, 2001.
- [Campagno 1995] CAMPAGNO, A., *Intelligent glass façades*. Buxuuser, Basel, 1995.
- [Crisinel et al. 2007] CRISINEL, M., EEKHOUT, M., HALDIMANN, M., VISSER, R., *EU COST C13, glass & interactive building envelopes (final report)*. *Research in Architectural Engineering Series*, Volume 1, IOS Press, Amsterdam, 2007.
- [Vollmar et al. 2006] VOLLMAR, T., CRISINEL, M., HALDIMANN, M., MOCIBOB, D. *Entwicklung eines Fassadenelements mit Flüssigkeitsschicht (COST/SBF Projekt C01.0037)*. *Rapport ICOM 562*, Ecole polytechnique fédérale de Lausanne (EPFL), 2006.
- [Crocombe 1989] CROCOMBE, A.D. *Global yielding as a failure criterion for bonded joints*. *International journal of Adhesion and Adhesives*, Vol. 9, No. 3, 1989.
- [Dawson 2001] DAWSON, S. *Glass at the cutting edge – glass used in building design*. *The Architectural review*, 2001.
- [Dawson 1999] DAWSON, S. *Working details*. Emap Cnstruct 1999.

- [Dorn et al. 1993] DORN, L., LIU, W. *Top stress state and failure properties of adhesive-bonded plastic/metal joints*. International journal of Adhesion and Adhesives, Vol. 13, No. 1, 1993.
- [Dow Corning 2003] DC 993 Structural glazing sealant. Product documentation, DOW CORNING, 2003.
- [Dow Corning 2007] DC 983 Silicon glazing & curtain wall C/A. Product documentation, DOW CORNING, 2007.
- [Duerr 2006] DUERR, D. *Pinned connection strength and behaviour*. Journal of structural Engineering, ASCE, Volume 132, Issue 2, pp. 182-194, February 2006.
- [DuPont 2008] SentryGlas Plus - *The Interlayer for Structural Laminated Glass*. DuPont, 2008.
- [Ekvall 1986] EKVALL, J. C. *Static strength analysis of pin-loaded lugs* Journal of Aircraft, Volume 23, Issue 5, pp. 438–443, 1986.
- [EN 1990] *Eurocode: Basis of Structural Design*. CEN, Brüssel, 2002.
- [EN 1991] *Eurocode 1: Actions on Structures*. CEN, Brüssel, 2002.
- [EN 1993] *Eurocode 3: Design of steel structures*. CEN, Brüssel, 2005.
- [Englhardt et al. 2005] ENGLHARDT, O., BERGMEISTER, K. *Structural Behaviour of Plane Glass Surface Structures Under Compression Stress Numerical and Experimental Investigation*. In: Proceedings of Glass Processing Days 2005, 17-20 June, Tampere, Finland, 2005.
- [Englhardt 2008] ENGLHARDT, O. *Transparent Surface Structures Engineering to Architecture*. In: Proceedings of Conference on Architectural and Structural Application of Glass, Delft, Netherlands, 2008.
- [EOTA 1999] ETAG Nr.002, *Guideline for European technical approval for structural sealant glazing systems (SSGS) - part 1: supported and unsupported systems*. EOTA - European Organisation for Technical Approvals, Brüssel, 1999.
- [Frocht et al. 1940] FROCHT, M.M. AND HILL, H.N. *Stress-Concentration Factors Around a Central Circular Hole in a Plate Loaded Through Pin in the Hole*. Journal of Applied Mechanics, March 1940.
- [Hart-Smith 1973] HART-SMITH L.J., *Adhesive-bonded Double Lap Joints*, NASA CR-112235, United States of America, 1973.
- [Haldimann 2006] HALDIMANN, M. *Fracture Strength of Structural Glass Elements - Analytical and numerical modelling, testing and design*. Thèse EPFL No 3671, Ecole polytechnique fédérale de Lausanne (EPFL), 2006.

- [Haldimann 2007] HALDIMANN, M. *Design of Glass Members - A Critical Review of the Present Knowledge*. Research in Architectural Engineering Series, Volume 1, IOS Press, Amsterdam, 2007.
- [Haldimann et al. 2008] HALDIMANN, M., LUIBLE, A., OVEREND, M. *Structural use of Glass*. Structural Engineering Document SED, International Association for Bridge and Structural Engineering IABSE, Zürich, 2008.
- [Harris et al. 1984] HARRIS, J.A., ADAMS, R.D. *Strength prediction of bonde sinle lap joints by non-linear finite element methods*. International journal of Adhesion and Adhesives, Vol. 4, No. 2, pp 65-78, 1984.
- [Heywood 1952] HEYWOOD, B. *Designing by Photoelasticity*. Chapman and Hall, London, 1952.
- [Hilti 2003] HIT-HY 50, Product documentation, HILTI, 2003.
- [Hilti 2007] HIT-HY 70, Product documentation, HILTI, 2007.
- [Hirt 2006] HIRT, M. A., BEZ, R., NUSSBAUMER, A. *Construction métallique – Notions fondamentales et méthodes de dimensionnement*, Traité de Génie Civil volume 10, Presses polytechniques universitaires romandes (PPUR), 2006.
- [Hirt 2006.1] HIRT, M. A., CRISINEL, M. *Charpentes métalliques*, Traité de Génie Civil volume 11, Presses polytechniques universitaires romandes (PPUR), 2005.
- [Huveners et al. 2003] HUVENERS, E. M. P., VAN HERWIJNEN, F., SOETENS, F. *Load Sharing in Insulated Double Glass Units*. Heron, Vol. 48, No. 2, pp. 99-122, TNO / Netherlands School for Advanced Studies in Construction, 2003.
- [Huveners et al. 2005] HUVENERS, E., VAN HERWIJNEN, F., SOETENS, F., HOFMEYER, H. *In plane loaded glass panes in facades, temperature loads in fixed bonded glass panes*. In: Proceedings of Glass Processing Days 2005, 17-20 June, Tampere, Finland, 2005.
- [Huveners et al. 2007] HUVENERS, E. M. P., VAN HERWIJNEN, F., SOETENS, F. *Glass panes acting as shear wall*. Heron, Vol. 52, No. 1/2, pp. 5-29, TNO / Netherlands School for Advanced Studies in Construction, 2007.
- [IStrucE 1999] *Structural Use of Glass in Buildings*, The Institute of Structural Engineers, 1999.
- [Keck 1998] KECK, J. *Zur Beschreibung finiter Deformationen von Polymeren: Experimente, Modellbildung, Parameteridentifikation und Finite-Elemente-Formulierung*. PhD Thesis, Institute of Mechanics, University of Stuttgart, 1998.
- [Kuenzi et al. 1975] KUENZI, E.W., ERICKSEN, W. S., ZAHN J.J. *Shear stability of flat panels of sandwich construction*, Armed services technical information agency, Virginia 1975.

- [Laufs 2000] LAUFS, W. *Ein Bemessungskonzept zur Festigkeit thermisch vorgespannter Gläser*. Ph.D. thesis, RWTH Aachen / Shaker Verlag, 2000. ISBN 3-8265-8044-3.
- [Laufs2001] LAUFS,W., LUIBLE,A., MOHREN, R. *Étude préliminaire sur le verre comme élément de construction dans le bâtiment*. Rapport ICOM 403F, Ecole polytechnique fédérale de Lausanne (EPFL), 2001.
- [Liess 2001] LIESS, J. *Bemessung druckbelasteter Bauteile aus Glas*. Ph.D. thesis, BoD GmbH, Norderstedt, 2001.
- [Laufs et al. 2003] LAUFS, W., LUIBLE, A. *Introduction on Use of Glass in Modern Buildings*. Rapport ICOM 462, Ecole polytechnique fédérale de Lausanne (EPFL), 2003.
- [Lotz 1995] LOTZ, S. *Untersuchung zur Festigkeit und Langzeitbeständigkeit adhäsiver Verbindungen zwischen Fügepartnern aus Floatglas*. Ph.D. thesis, Universität Kaiserslautern, Fachbereich Maschinenwesen, 1995.
- [Luiblé 2004] LUIBLE, A. *Stabilität von Tragelementen aus Glas*. Thèse EPFL 3014, Ecole polytechnique fédérale de Lausanne (EPFL), 2004.
- [Luiblé et al. 2005] LUIBLE, A., CRISINEL, M. *Plate Buckling of Glass Panels*. In: Proceedings of Glass Processing Days 2005, 17-20 June, Tampere, Finland, pp. 476-479, 2005.
- [Luiblé et al. 2006] LUIBLE, A., CRISINEL, M. *Design of Glass Beams Subjected to Lateral Torsional Buckling*. In: Proceedings of the IABSE Symposium 2006 "Responding to Tomorrow's Challenges in Structural Engineering", 13-15 Sept., Budapest, Hungary, 2006.
- [Maniatis 2006] MANIATIS, I. *Numerical and Experimental Investigations on the Stress Distribution of Bolted Glass Connections under In-Plane Loads*. Ph.D. thesis, Technische Universität München (TUM), 2006.
- [Matthews et al. 1982] MATTHEWS F.L., KILTY P.F., GODWIN E.W. *A Review of the Strength of Fiber-Reinforced Plastics, Part 2: Adhesively Bonded Joints*, Composites, Vol. 13, No. 1, pp 29-37, 1982.
- [Mocibob et al. 2007] MOCIBOB, D., CRISINEL M. *Glass panel under in-plane shear loading – experimental investigation on structural glass panel point support*. In: Proceedings of Glass Performance Days 2007, Tampere, Finland, 2007.
- [Mocibob et al. 2007.1] MOCIBOB, D., CRISINEL M. *Structural behaviour of glass panel in fully-transparent pavilion*. In: Proceedings of International Conference on Shell and Spatial structures (IASS), Venice, Italy, 2007.
- [Mocibob et al. 2008] MOCIBOB, D., CRISINEL M. *Linear connection system for structural application of glass panels in fully-transparent pavilions*. In: Proceedings of Conference on Architectural and Structural Application of Glass "Challenging glass", Delft, Netherlands, 2008.
- [Nijssse 2003] NIJSSE, R. *Glass in Structures*, Birkhäuser, 2003.

- [Overend 2002] OVEREND, M. *The Appraisal of Structural Glass Assemblies*. Ph.D. thesis, University of Surrey, March 2002.
- [Peterson 1953] PETERSON, R.E. *Stress Concentration Design Factors*. John Wiley & Sons, Inc. 1953.
- [Pilkey 1997] PILKEY, W. D. *Peterson's Stress Concentration Factors*. 2nd Edition, Wiley, New York, 1997. ISBN 0471538493.
- [Pilkington 2005] *Pilkington Planar*. Product documentation, W&W Glass, USA, 2005.
- [prEN 13474-1] *Glass in building - Design of glass panes - Part 1: General basis of design*. CEN, Brussels, 1999.
- [prEN 13474-2] *Glass in building - Design of glass panes - Part 2: Design for uniformly distributed load*. CEN, Brussels, 2000.
- [Renton et al. 1975] RENTON W.J., VINSON J.R. *On the Behaviour of Bonded Joints in Composite Material Structures*, Engineering Fracture Mechanics, Vol. 7, No. 1, pp 41-60, 1975.
- [Rice et al. 1995] RICE, P., DUTTON, H. *Structural glass*, E&FN Spon, Imprint of Chapman & Hall, 1995.
- [Schneider 2001] SCHNEIDER, J. *Festigkeit und Bemessung punktgelagerter Gläser und stossbeanspruchter Gläser*. Ph.D. thesis, TU Darmstadt, Institut für Statik, 2001.
- [Sedlacek et al. 1999] SEDLACEK, G., BLANK, K., LAUFS, W., GÜSGEN, J. *Glas im Konstruktiven Ingenieurbau*. Ernst & Sohn, Berlin, 1999.
- [Schittich et al. 2001] Schittich, C., Staib, G., Balkow, D., Schuler, M., Sobek, W. *Construire en verre*. Presses polytechniques et universitaires Romandes (PPUR), 2001.
- [Schneider 2001] SCHNEIDER, J. *Festigkeit und Bemessung punktgelagerter Gläser und stossbeanspruchter Gläser*. Ph.D. thesis, TU Darmstadt, Institut für Statik, 2001.
- [Schneider 2004] SCHNEIDER, J. *Glass strength in the borehole area of annealed float glass and tempered float glass*. International journal of forming, 2004.
- [Scott et al. 1982] SCOTT, R. G., STONE, J. C. *The effects of design variables on the critical stresses of eye bars under load: An evaluation by photoelastic modelling*, Proc., Joint Conf. on Experimental Mechanics of the Society for Experimental Stress Analysis, Honolulu, 1982.
- [Slessor 1998] SLESSOR, C. *Glass evolution - use of glass in architecture*. The Architectural review, 1998.
- [Smith 2007] SMITH, K.M., FLANNERY, J.A. *Library design*, Neues Publishing Company 2007.
- [Southwell et al. 1924] SOUTHWELL, R., SKAN, S. *On the stability under shearing forces of a flat elastic strip*. In: Proceeding of Royal Society of London, Series A, 1924.

- [Timoshenko et al. 1961] TIMOSHENKO, S. P., GERE, J. M. *Theory of elastic Stability*. Second Edition, McGraw-Hill, New York, 1961.
- [Timoshenko 1966] TIMOSHENKO, S. P. *Théorie de la stabilité élastique*. Dunod, Paris, 1966.
- [Timoshenko et al. 1970] TIMOSHENKO, S.O., GOODIER, J.N. *Theory of Elasticity*, McGraw-Hill, New York 1970.
- [Volkersen 1965] VOLKERSEN, O. *Recherches sur la théorie des assemblages collés. Construction métallique*, No. 4, pp. 3-13, CTICM, France, 1965.
- [Weller 2001] WELLER, B., THOMAS, S. *Designing of bonded joints in glass structures* In: Proceedings of Glass Processing Days 2007, Tampere, Finland, 2003.
- [Wellershoff et al. 2002] WELLERSHOFF, F., SEDLACEK, G., KASPER, R. *Design of joints, members and hybrid elements for glass structures*. 2002.
- [Wellershoff et al. 2003] WELLERSHOFF, F., SEDLACEK, G. *Glass pavilion Rheinbach – stability of glass columns*. In: Proceedings of Glass Processing Days 2005, 17-20 June, Tampere, Finland, 2003.
- [Wellershoff et al. 2005] WELLERSHOFF, F., SEDLACEK, G. *Glued Connections for New Steel Glass Structures*. In: Proceedings of Glass Processing Days 2005, 17-20 June, Tampere, Finland, 2005.
- [Wellershoff et al. 2005.1] WELLERSHOFF, F., SEDLACEK, G. *Stabilisation of Building Envelopes with the use of the glazing*. In: Proceedings of Glass Processing Days 2005, 17-20 June, Tampere, Finland, 2005.
- [Wellershoff 2006] WELLERSHOFF, F. *Nutzung der Verglasung zur Aussteifung von Gebäudehüllen*. Ph.D. thesis, RWTH Aachen / Shaker Verlag, 2006. ISBN 978-3-8322-5046-1.
- [Wigginton 1996] WIGGINTON, M. *Glass in architecture*. Phaidon, London 1996.
- [Zenkert 1997] ZENKERT, D. *The Handbook of Sandwich Construction*. Engineering Materials Advisory Service Ltd., United Kingdom, 1997.

Curriculum Vitae

Name Danijel Močibob
Date of birth 4th February 1977, Koper (Slovenia)
Nationality Croatian

EDUCATION

10.2005 – present PhD candidate
 Swiss Federal Institute of Technology (EPFL), Lausanne, Switzerland
 Doctoral Thesis: Glass panel under shear loading - use of glass envelope for building stabilization
 Supervisor: Dr. J.P. Lebet

10.2002 – 9.2004 MSc in computational engineering – Structural mechanics
 Ruhr Universität Bochum, Germany (RUB), Bochum, Germany
 Master thesis: Design of Composite Railway Bridge according to the EN
 Supervisor: Prof. Dr.-Ing. R. Kindmann

10.1995 – 10.2000 Diploma in civil engineering
 University of Rijeka, Rijeka, Croatia
 Diploma thesis: Design of steel hale with movable crane
 Supervisor: Prof. Dr. M. Čaušević

PROFESSIONAL EXPERIENCE

10.2004 – present Research Engineer
 Steel Structures Laboratory (ICOM)
 Swiss Federal Institute of Technology (EPFL), Lausanne, Switzerland

9.2001 – 9.2002 Structural Engineer
 Arhetip 21, Poreč, Croatia

07.1999 – 08.1999 Student Engineer
 Takigami Steel Construction Co. Ltd., Handa, Japan

07.1998 – 08.1998 Student Engineer
 Karayollari Genel Mudurlugu, Ankara and Bahce, Turska

PUBLICATIONS

Vollmar, T., Crisinel, M., Haldimann, M., and Močibob, D., *Entwicklung eines Fassadenelements mit Flüssigkeitsschicht*. COST/SBF Project 01.0037, EPFL, ICOM, Lausanne, 2006.

Močibob, D. and Crisinel, M. *Glass panel under in-plane shear loading: experimental investigation on structural glass panel point support*. In: Proceedings of Glass Performance Days (GPD 2007), Tampere, Finland 2007

Močibob, D. and Crisinel, M., *Structural behaviour of glass panel in fully-transparent pavilion*. In: Proceedings of International Conference on Shell and Spatial structure (IASS 2007), Venice, Italy, 2007.

Močibob, D. and Crisinel, M., *Linear connection system for structural application of glass panels in fully-transparent pavilions*. In: Proceedings of Conference on Architectural and Structural Application of Glass (Challenging glass 2008), Delft, Netherlands, 2008.

Močibob, D. and Crisinel, M., *Influence of boundary conditions on shear buckling behaviour of glass panels*. In: Proceedings of International Symposium of the Application of Architectural Glass (ISAAG 2008), Munich, Germany, 2008.

Močibob, D. and Belis, J., *Coupled experimental and numerical investigation of structural glass panels with small slenderness subjected to locally introduced axial compression*. Engineering Structure (submitted).

PROFESSIONAL AFFILIATIONS

Member of International Association for Bridge and Structural Engineering (IABSE)